The Impact of Real-world Constraints on Tidal Stream Energy Resource Assessments

Misha Dilipkumar Patel

St Catherine's College

University of Oxford

A thesis submitted for the degree of

Doctor of Philosophy

May 2024

Abstract

The potential of tidal stream energy in the UK is widely acknowledged to be significant, however, real-world constraints greatly limit the viable extraction of energy. Multiple lease sites for development have been withdrawn or remain in testing phases since their agreement, due to financial and technical challenges. This evidences the need to strategically define new areas for development based on refined assessments and inform the development of arrays at sites by identifying and overcoming the challenges and constraints.

To investigate the challenges of quantifying the tidal stream energy resource and examine a range of parameters affecting the resource, a low order idealised channel model is adopted. Different channel characteristics are applied to consider multiple case studies and blockage-corrected blade element momentum theory is used to represent turbine performance, also adopted in higher order modelling. The investigation highlights the inter-dependence of key parameters affecting tidal stream energy resource assessments, much like the constraints limiting the resource. Findings from the low order model inform the impact of modelling assumptions necessary for higher order modelling.

The use of a 2-D model enabled the investigation of bathymetry as a limiting practical constraint and the implication of the spatial variability of tidal stream energy at a site, which informed the development of a novel framework for designing arrays of homogeneous and heterogeneous turbine specifications (diameter and rated speed). Comparison of homogeneous and heterogeneous arrays in the Inner Sound highlights that adopting heterogeneous designs (with diameters of 5 – 20 m and rated speeds of 1.5 – 2.5 m/s) can increase power per turbine, while deploying significantly fewer turbines. The approach maximises usage of a site, whilst allowing the maximum allowable diameter of turbine to be deployed in areas, and exploits the spatial variation of the resource across a site by tailoring turbines to operate at appropriate rated speeds for a target capacity factor.

Finally, the framework is extended to identify multiple, independent, heterogeneous arrays across the Pentland Firth. The successive identification of arrays presents a feasible incremental development strategy for the Pentland Firth and minimises interference between arrays by accounting for how the resource responds to presence of arrays. A range of development options are proposed, based on different priorities. The tidal stream energy resource is assessed to be within 1 – 1.8 GW in the Pentland Firth with the consideration of real-world constraints, based on different development strategies and priorities.

Acknowledgments

I would like to acknowledge Professor Thomas Adcock, Dr Amanda Smyth and Dr Athanasios Angeloudis for their excellent supervision and insightful discussions, which have helped me develop my research. Tom, Amanda and Than, I am grateful to have had you as such supportive supervisors and appreciate your guidance and wisdom. I am thankful for the support from the Leathersellers' Company and St Catherine's College to undertake this research, both of which championed the work I have done during my time at Oxford.

It has been a honour to work with dedicated and passionate individuals and groups across the university on equality, diversity and inclusion initiatives. I would like to thank the students, and academic and professional services staff who have made such initiatives and their continuation possible.

I am thankful for the community of people that have become my friends at Oxford, including members of Room 11, the Penthouse, St Catz, BIPOC STEM, GJCC and WiE.

The support of my mum and dad has been invaluable and I am grateful to them for nurturing my passions and being my inspiration. My sister, Riah, has been a constant support and friend and her visits to explore the best food places in Oxford have always been a welcome break. I would also like to thank my partner, Aidan, for his unwavering support and encouragement.

Contents

Nomenclature

α	Angle of attack
α_{WD}	Wetting and drying parameter
β	Blade pitch angle
ΔU_{max}	Wake Centre-line velocity deficit
δ_0	Dimensional form of λ_0
δ_1	Dimensional form of λ_1
δ_2	Dimensional drag parameter representing thrust due to the support structure
δ_D	Sectional drag
δ_L	Sectional lift
δ_T	Sectional axial thrust
δ_τ	Sectional tangential torque
η	Free surface elevation
λ_0	Non-dimensional drag term representing dynamic balance of the channel
λ_1	Non-dimensional drag term representing drag due to turbines
ν	Kinematic viscosity
Ω	Angular velocity
ω	Frequency
$\psi_{p,r}$	Bump function, p and r are the centre and support radius of the function
ρ	Water density
σ_{S_2}	Angular speed, example given for S_2 constituent
τ_b	Seabed friction

a'_{2i} Tangential induction factor

a Amplitude

A_C Channel cross sectional area

A_S Frontal area of the support structure

a_{2i} Axial induction factor

ADCP Acoustic Doppler Current Profiler

ADT Actuator disc theory

AEP Annual Energy Production

B Blockage

B_L Local blockage

BC-BEMT Blockage-corrected blade element momentum theory

BEMT Blade element momentum theory

C_d Channel drag coefficient

c_i Chord length

C_P Coefficient of power

C_T Coefficient of thrust

c_t Turbine drag coefficient

$C_{D,S}$ Support structure drag coefficient

C_{Di} Drag coefficient of force on blade

C_{Li} Lift coefficient of force on blade

C_{T1} Coefficient of friction of one row of turbines

D Turbine rotor diameter

D_S Support structure diameter

DG Discontinuous Galerkin

EIA Environmental Impact Assessment

f Coriolis force parameter

F_i Tip loss correction factor

F_S Support structure thrust

f_{S_2} Nodal factor, example given for S_2 constituent

FE Finite Element

FEM Finite Element Methods

FF Form factor

g Acceleration due to gravity (9.81 m/s)

g_{S_2} Phase lag, example given for S_2 constituent

$\tilde{h}$ Modified bathymetry

H Total water depth (sum of free surface water elevation and depth at rest)

h Depth of channel

l Length of channel

L_S Support structure length (hub height)

l_s Array area dimension, side length

l_T Length of channel occupied by turbines

l_{min} Minimum distance to the mainland

LES Large Eddy simulations

M_Z bending moment

n	Manning coefficient
N_R	Number of rows of turbines
PDE	Partial differential equation
Q	Flow rate
R	Turbine radius or blade length
r_3	Wake induction factor
r_i	Ratio between the velocity u_i and the free-stream velocity ($= u_i/u$)
RANS	Reynolds-averaged Navier-Stokes
s	Spacing between turbines
SIF	Significant impact factor
SWE	Shallow water equations
T	Thrust
TSR	Tip Speed Ratio - the ratio between inflow speed and turbine rotational speed
$\mathbf{u}$	Depth averaged velocity vector made of horizontal components (u, v)
$\mathbf{u}^{\perp}$	Velocity vector rotated 90°counter-clockwise
u	Free stream velocity
u_1	Turbine through-flow velocity
u_3	Flow velocity in the near wake of the turbine
u_4	Bypass flow velocity
u_r	Rated speed
u_{S_2}	Nodal angle, example given for S_2 constituent
V_{S_2}	Equilibrium phase, example given for S_2 constituent

W	Inflow velocity to turbine
w	Channel width
$\mathbf{x}$	Position coordinate
x	Distance along the length of the channel
Z_e	Sectional modulus

Chapter 1

Introduction

More than 70% of the Earth's surface is covered in water with 97% in oceans, which is a huge potential resource for harnessing energy (NASA, 2021). One source of renewable energy from the oceans is tidal energy, harnessed from tides caused by the gravitational pull of the Moon and Sun on the Earth's sea water (Pugh, 1987). Energy can be extracted from energetic tidal streams using turbines or by constructing barrages to harness energy from the tidal range. This thesis focuses on the potential contribution of tidal stream energy to renewable energy generation in the UK, by considering real-world constraints on the resource to assess the amount of energy that can be harnessed.

The UK has a legal commitment to reach net zero carbon emissions by 2050 (Department for Energy Security and Net Zero, 2022). The Climate Change Committee's (2020) sixth carbon budget predicts an increase in electricity demand to 550 – 680 TWh/year by 2050, from approximately 320 TWh/year in 2022 (Martin, 2023). The increase in electricity demand will be primarily due to the electrification of heating and transport to replace the reliance on oil and gas. Wind and solar energy are estimated to contribute a combined total of 515 TWh/year by 2050. To make up the remaining proportion of supply and meet projected demands, complementary sources of renewable energy will be required. The UK currently has an installed operational capacity of 10.4 MW of tidal stream energy with a projection of 11.5 GW to be installed by 2050, contributing 34 TWh/year (Coles et al., 2021). In order to achieve this ambitious installed capacity, it is crucial to understand the tidal stream resource so that informed investment and development decisions can be made.

1.1 A Case for Tidal Stream Energy

The energy trilemma describes the three challenges that need to be balanced regarding energy supply: security, environmental sustainability and affordability/equity. The

World Energy Council publishes a World Energy Trilemma Index Report annually to measure the progress of each challenge globally. The UK ranked eighth amongst the 126 countries included in the 2024 report (World Energy Council, 2024). However, the report highlights that despite Europe's urge to diversify energy supply, the energy crisis has called to attention the issues surrounding affordability of energy and recommends investments in renewable energy generation to achieve affordability in the long term.

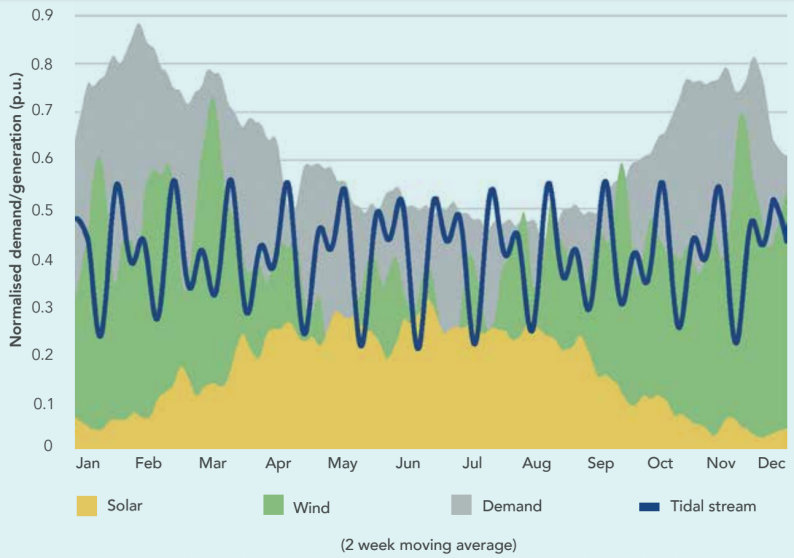

Figure 1.1: Energy demand (normalised to annual hourly peak) and generation, backcast from 2019 weather data in Great Britain (Policy and Innovation Group, University of Edinburgh, 2023).

National Grid ESO (2022) has identified a key challenge of maintaining the resilience of energy systems during high electricity demand with low wind and solar production periods. The cyclic nature and predictability of tides makes tidal stream energy well-suited for contributing to electricity base loads and balancing the grid (Ocean Energy Europe, 2023, National Grid ESO, 2022). This predictability over long time periods, in the order of hundreds of years, allows for forecasting of tidal stream energy generation, which could be key for ensuring energy security (Policy and Innovation Group, University of Edinburgh, 2023). The consistent cyclic production of tidal stream energy is a key benefit of the resource that makes it unique compared to any other form of renewable energy. The resource is not correlated to other renewable sources and is independent of seasonal weather patterns. Therefore, tidal stream energy can potentially be harnessed during periods of low wind or solar energy, which are the primary sources of renewable

power generation in the UK, contributing 28.8% of total electricity generation in 2022 (Department for Energy Security and Net Zero, 2023). Figure 1.1 demonstrates the advantage of tidal stream energy's reliability in supplying energy during wind droughts and outside summer months, when solar supply is low (Policy and Innovation Group, University of Edinburgh, 2023).

1.2 Tidal Stream Energy Resource

1.2.1 Tides

Tides, characterised by the rise and fall of sea levels, are long waves influenced by various factors. Coastal features, such as constrictions in channels, can lead to increased flow velocity, while enclosed sea areas can lead to seiching (oscillations). Coriolis forces impact the pattern of tides and lead to the formation of amphidromic points, where the tidal amplitude of a given frequency is zero (i.e., there is no vertical displacement and hence no tide), around which high and low amplitude tides rotate.

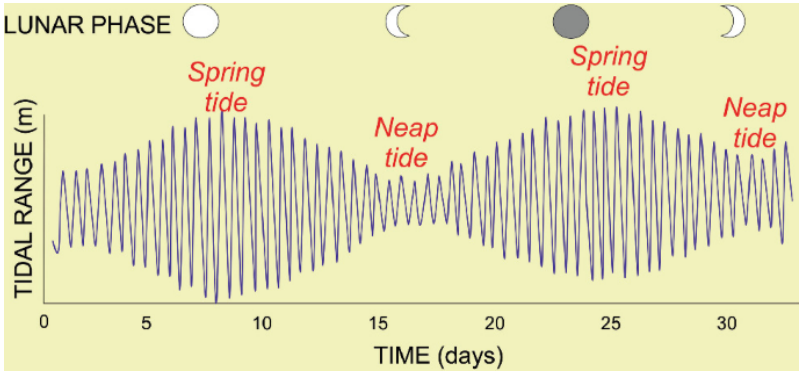

Figure 1.2: Spring-neap cycle of tides over a month with two high and low waters a day (Morales, 2022).

The classification of tides is dependent on the positions of the Sun, Moon and Earth. When the Moon is aligned with the Sun and Earth, the superimposed forces due to the Sun and Moon create solar and lunar bulges, resulting in a large amplitude spring tide (Pugh, 1987). Neap tides, characterised by lower amplitudes, occur when the Sun and Moon are at a 90° angle relative to the Earth, leading to counterbalancing forces. The spring-neap cycle lasts approximately 14 days (Figure 1.2), with high and low tides occurring twice in a lunar day (24 hours and 50 minutes) at the equator. Consequently,

high tides shift by approximately an hour each day.

1.2.2 Potential UK Sites for Tidal Stream Energy Extraction

The UK is at the forefront of marine energy exploration, with insights into offshore projects from expertise in oil and gas (Department for Energy Security and Net Zero and Department for Business, Energy and Industrial Strategy, 2013). The Crown Estate and Crown Estate Scotland have previously identified lease sites across the UK, which have the potential to be developed for commercially viable tidal stream energy extraction. The UK also has the world's largest marine testing facility, the European Marine Energy Centre, and a number of companies that are working to develop tidal sites. Significant work has been undertaken in developing and testing devices for extracting tidal stream energy. The European Marine Energy Centre (2020) identifies 97 companies developing tidal devices of varying types and configurations across 16 countries, including the UK, USA, Canada and Germany.

The Sustainable Development Commission's report (Metoc, 2007) identifies 20 areas in the UK with the potential to harness tidal stream energy, shown in Figure 1.3, alongside the peak flows at mean spring tide (Department of Trade and Industry, 2008). Within the 20 potential areas identified by Metoc (2007), 30 lease sites were agreed by the Crown Estate from 2010 for UK tidal stream energy development (RenewableUK, 2015). Up to 2015, 7 were in planning, 13 were in development, 2 pre-construction, 4 under construction and 4 operational (test sites) (Appendix A). However, since 2015 multiple sites have returned their leases to the Crown Estate and as of 2017 the Crown Estate devolved, establishing the additional Crown Estate Scotland. Across England, Wales, Northern Ireland and Scotland, there are now fewer than 20 sites leased or agreed to lease for tidal stream energy development. This demonstrates the evolving definition of lease sites for tidal stream energy development and their likelihood to be redefined or expanded based on updated modelling of the resource and seabed priorities for the Crown Estate and Crown Estate Scotland.

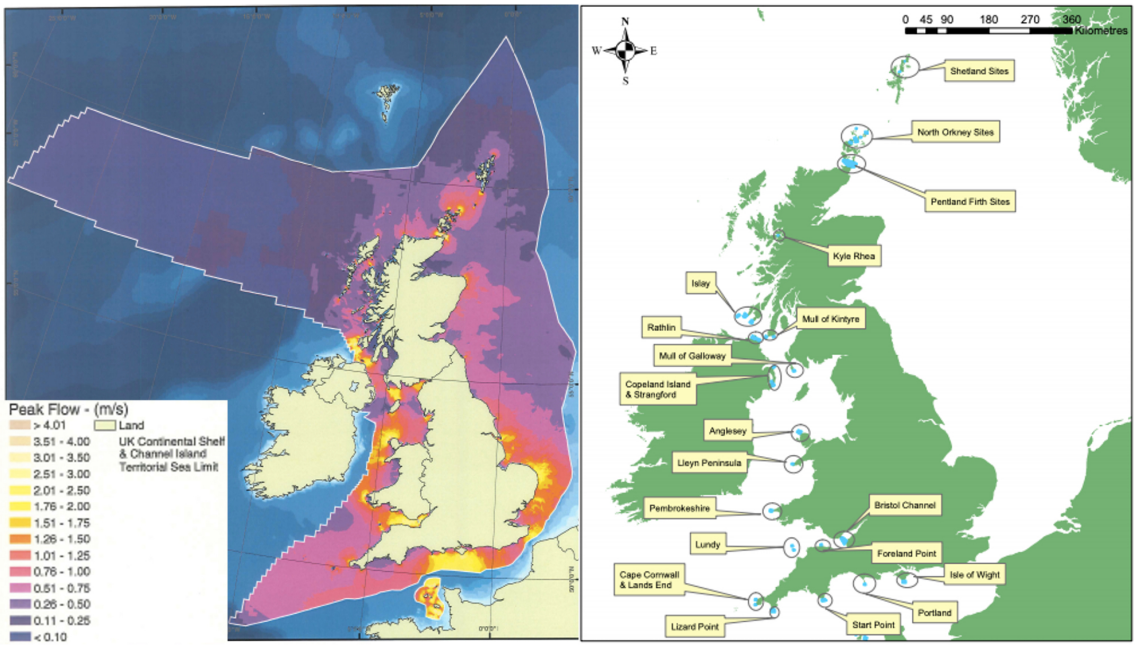

Figure 1.3: Peak spring tide flow (left, Department of Trade and Industry 2008) and location of tidal stream resource (right, Metoc 2007).

The potential for tidal stream energy has driven the investment in lease sites, which has been supported by the UK Government through Contract for Difference (CfD) funding rounds. Four tidal stream development projects gained support from CfDs in 2022 for over 40 MW of capacity to be installed between 2025 – 2027, and funding for another 53 MW was awarded across 11 projects in 2023 (Garanovic, 2023). The protection for developers from volatile electricity wholesale prices that CfDs provide is key for the future of tidal stream energy. Up until 2021, no tidal stream energy projects had won support through CfDs (Coles et al., 2021). Therefore, the contracts awarded in recent years demonstrate promising signs of progress in the industry.

1.3 Motivation

Quantifying the magnitude of the resource is vital for deciding whether to invest in tidal energy and understanding its contribution to reducing dependence on fossil fuels. A key issue, however, is that site-based resource assessments can vary by orders of magnitude, with national and world resource figures being equally variable. This is partly due to the complexity of understanding the fluid mechanics of the tidal flow and how turbines interact with it, but also due to the consideration of constraints limiting the viable

extraction of the resource. Cartwright et al. (1980) estimate the total power from tidal waves coming in to the UK from the continental shelf is approximately 250 GW, but only a fraction of this can be extracted (MacKay, 2016). The technical potential of the resource has been estimated up to 22.5 GW (HM Government, 2010), although this amount of power could not be extracted. A number of studies assess the UK's average tidal stream resource to be 1.5 – 22.5 GW (Black and Veach, 2005, Metoc, 2007, Carbon Trust, 2011). Carbon Trust (2011) states that re-prioritising the use of offshore sites could increase their assessment of the practical resource to 3.3 GW. The assessments are wide-ranging and the range conflicts with more detailed site-based resource assessments. Site-based assessments are also wide-ranging due to the use of different models and assumptions, which prevents them from being used as part of an overall UK resource assessment. Resource assessments can also assist with turbine design by providing data to characterise hydrodynamic effects, identifying appropriate sites for tidal stream developments and assessing the overall production of energy from an array over the lifetime of a project (Thiébot et al., 2022). Therefore, a refined resource assessment is necessary to inform investment decisions and for the development of technology and array implementations to continue.

1.4 Research Objectives

This thesis aims to consider a number of limiting real-world constraints on tidal stream energy extraction to refine existing resource assessments and propose a method that incorporates these constraints into models, to be replicated across multiple sites. The research scope encompasses technical, practical, and some accessible constraints on the resource. However, the constraints on the viable resource are not included in the scope of this thesis because it is critical to establish a better understanding of incorporating the foundational layers of the pyramid (Figure 2.4) before expanding work to include the final tier. The intention for providing a more refined assessment of the resource is to inform future developments for tidal stream energy, considering The Crown Estate and

Crown Estate Scotland's evolving allocation of the seabed to different usages and the increasing investment in tidal stream energy.

The research objectives are:

1. To investigate the impact of the inclusion and exclusion of modelling parameters on the assessment of tidal stream energy resource in a low order model.
2. To explore how spatial variability of the resource at a site can inform array design by developing and applying a heterogeneous array design framework.
3. To refine the assessment of tidal stream energy at the Pentland Firth by considering practical and accessible constraints.

1.5 Thesis Outline

This chapter has presented the background of tidal stream energy, motivation for the research and the objectives that have guided the research.

Chapter 2 provides context of the research area. The many scales of tidal energy, from blade scale to regional scale (Adcock et al., 2015) are outlined, including a discussion of how these scales interact, and how they may be separated to be assessed individually for simplicity. Methods for assessing tidal stream energy resource and for modelling and implementing turbines in existing studies have been reviewed and appraised. The uncertainties and assumptions made in each of these methods are considered to inform the methods used in this thesis. Reviewing previous studies of site-based resource assessments acknowledges existing work in this area and identified research gaps, which emphasise the motivation of this research.

The remainder of the thesis is categorised into two parts; Part I: Idealised Channel Study and Part II: Pentland Firth Case Study, each consisting of two chapters. Exploring parameters affecting resource assessments in idealised channels, modelled in 0-D and 2-D, allowed the consideration of a greater number of parameters, and the opportunity to validate the 2-D modelling software used in the thesis before moving to a more

complex domain. Thus the work from Part I informs Part II.

Chapter 3 (Part I) presents an investigation of how low order parameters affect tidal stream energy resource assessments. This work considers two idealised channels defined by Vennell (2010) and incorporates the Blockage Corrected Blade Element Momentum Theory (BC-BEMT) to represent turbines, a method which is carried forward for the 2-D modelling work. The effects of modelling with multiple constituents over the 18.6 year nodal cycle, capping strategies and turbine performance curve characteristics are explored. The work presented in this chapter allowed key parameters affecting tidal stream energy resource assessments to be identified, and quantified the uncertainties of including or excluding specific parameters.

Chapter 4 (Part I) replicates the idealised channels, modelled in Chapter 3, in 2-D modelling software *Thetis*. Comparing results with the literature (Vennell, 2010) provided confidence in the 2-D software and how it represents turbines in models, which is identified as a key difficulty in the literature review. Continuous and discrete methods for implementing turbines in *Thetis* and how they meet the needs of different applications (e.g., regional scale vs. array scale) were considered. Array layout is investigated using the discrete method to explore staggered and aligned rows of turbines and the impact of row spacing in an idealised channel. The impact of boundary effects on capacity factor and power was also investigated to highlight the effect on analysis when they are not accounted for and the importance of placing boundaries far from the place of interest when modelling a real site. The exploration of 2-D parameters and modelling options informed the 2-D modelling of a real site.

Chapter 5 (Part II) presents the development of a heterogeneous array design framework to explore the compromise in energy when array design is constrained by homogeneous turbine specifications. The framework considers the practical limitations of bathymetry and the spatially variable resource across a site, to define the diameter and rated speed of turbines, and is designed to be applied at any tidal stream site. The difference in

performance between homogeneous and heterogeneous arrays is investigated, using the Inner Sound of the Pentland Firth as a case study to demonstrate the framework.

Chapter 6 (Part II) brings together work from previous chapters to conduct a refined resource assessment of the Pentland Firth by considering additional levels of the pyramid of constraints (practical and accessible), which have not previously been considered in existing studies. The heterogeneous array design framework is extended and applied beyond the Inner Sound (used as a case study in Chapter 5) to identify further areas for tidal stream energy development. A study is undertaken to assess the impact of developing multiple sites in the Pentland Firth, beyond the Inner Sound.

Each chapter of the thesis progressively introduces greater complexity to the resource assessment modelling, beginning with a 0-dimensional analytical model applied to idealised channels. The study then advances to a numerical depth-averaged shallow water equation model of the idealised channels, providing a more realistic representation. Moving from idealised channels to a real site requires consideration of a complex bathymetry and site geometry, and the impact on hydrodynamics. Finally, the study is expanded to a larger scale by exploring the entire Pentland Firth. This entails investigating the interaction of multiple independent arrays in close proximity and assessing their impact on the tidal stream energy resource.

Chapter 7 concludes the findings of the thesis, outlines the impact and novelty of the research, and proposes future work.

Chapter 2

Tidal Stream Energy Resource Assessment

Resource assessments of tidal stream energy have been the subject of a number of studies, employing a range of methods to model site hydrodynamics and extraction of energy through different representations of turbines. Accurately quantifying the resource of tidal stream energy requires an understanding of the interactions between turbines and the flow across various scales inherent in tidal energy investigations. To manage the complexity of this multi-scale problem, the scales are often approximated as decoupled, resulting in a number of simplifying assumptions and necessary compromises. Additionally, tidal energy can be modelled across different dimensional orders, presenting a trade-off between computational efficiency and accurately representing the inherently 3-D nature of the problem. High order modelling refers to models with higher orders in terms of dimension, such as a 2-D depth-averaged model, a layered 2-D model or a 3-D model. Low order modelling refers to a 0-D model, which is a depth-averaged model integrated over two dimensional lengths, which can also be considered as a 1-D model.

In Section 2.1, tidal stream energy resource assessment methods are presented along with the scales of tidal energy. The associated effects of modelling large arrays, used for resource assessments, are also discussed. The methods for modelling and implementing turbines in hydrodynamic models are outlined in Section 2.2. In Section 2.3 the limitations and compromises between different dimensional models are discussed. The limiting constraints on tidal stream energy are discussed in Section 2.4. A review of previous resource assessments of the Pentland Firth is presented in Section 2.5 to appraise methods and investigate the reasons for ranging assessments of the resource.

2.1 Tidal Stream Energy Resource Assessment Methods

Resource assessments require modelling at different scales to incorporate the design, specification and operation of tidal devices, array interactions and the effect of an

array on the hydrodynamics of a site (Serhadlıoğlu, 2014). Adcock et al. (2021) describe three scales involved in tidal energy resource assessments, and highlight interactions occurring both ways between them. To assess the resource, scales may need to be uncoupled and evaluated individually. The turbine-scale involves individual turbines and focuses on the hydrodynamic interactions between a limited number of turbines, either a countable amount or down to the scale of an individual turbine (e.g., considering the hydrodynamics of turbine blades or effects of the support structure) (Adcock et al., 2021). The field-scale focuses on hydrodynamic effects of large numbers of turbines (Goward Brown et al., 2017). At this scale, the array comprises a vast number of turbines (countless) and the analysis would be dominated by interactions between devices, addressing the hydrodynamic effects of the flow interacting with the array as a whole (Goward Brown et al., 2017). Large-scale tidal dynamics are the focus of regional scale modelling and require a more simplified approach to modelling the thrust applied by the turbines in an array on the flow, in comparison to the other scales. Figure 2.1 illustrates the scales, sub-scales and order of magnitude of each (Adcock et al., 2015, Jie et al., 2016). Goward Brown et al. (2017) notes that the length-scale of investigation and applicability of methods is dependent on the focus of the study and the research objectives.

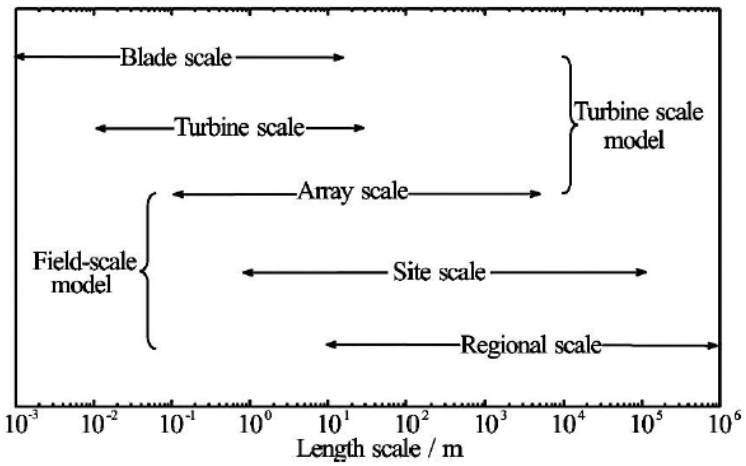

Figure 2.1: Tidal energy scales (Jie et al. 2016 adapted from Adcock et al. 2015).

Analytical and numerical models can been used to assess the resource of tidal stream energy. Predicting power available to a turbine as a portion of the kinetic energy flux

has been used in the wind industry and early attempts to quantify tidal stream energy resource have adopted this approach (Fraenkel, 2002, Black and Veach, 2005, Blunden and Bahaj, 2007). However, the method does not consider the presence of turbines and their impact on the flow, nor does it consider the configuration of closely arranged turbines in rows, which can theoretically extract more power than the undisturbed kinetic energy in the channel (Vennell, 2013, Adcock et al., 2014). Garrett and Cummins (2005) demonstrated, through a simplified model, that the overall drag coefficient of a channel increases when turbines extract power, slowing down the flow in the channel. Acknowledging the impact of turbines on the resource, Black and Veach (2005) introduced a 'Significant Impact Factor'(SIF) to calculate extractable power without significant environmental and economic impact. In their Phase I study, a 20% SIF was uniformly applied across all sites, while Phase II classified tidal sites into five types, each associated with different SIF. Blunden and Bahaj (2006) produced a time-series of tidal velocity data at Portland Bill and gave an example of how to use the data to predict power outputs by assuming the power as a fraction of kinetic energy. However, Garrett and Cummins (2005) demonstrated that the effect of tidal stream turbines on the flow is not directly related to the undisturbed kinetic flux.

Garrett and Cummins (2005) considered a model of a channel, with flow driven by the head difference between two large basins of water, to assess the upper bound extractable power averaged over a tidal cycle. Turbines were modelled as a fence spanning the width of a channel and it is assumed the free surface of the channel is volume constrained. Utilising a 2-D, depth-integrated model, Draper et al. (2014a) calculated the maximum extractable power from the Pentland Firth to be 4.19 GW. The assessment of the resource surpasses that calculated with Garrett and Cummins' method, attributed to the increase in head difference due to the presence of turbines and the subsequent change in phase of the tidal elevation at each end of the channel.

In reality, a fence of turbines will not span the entire width of a channel. Therefore,

Garrett and Cummins (2007) extended the model to allow turbines to occupy a fraction of the channel, uniformly spaced across the width. Tidal turbine efficiency is the ratio between power available to turbines and power removed from the channel, which includes losses due to friction and mixing. Garrett and Cummins (2007) demonstrate that if the wake induction factor is, $r_3 = \frac{1}{3}$ (using the terminology of Vennell 2010), the available power to turbines increases but the turbine efficiency decreases because more energy is lost through mixing, dependent on blockage. Vennell (2010) further extended the model to investigate hydrodynamic interactions at array scale and the effect on turbine efficiency. He notes that optimal 'tuning' allows large farms to realise the majority of a channel's potential, contingent on the number of turbines, channel geometry, bed friction and tidal forcing.

Tidal dynamics can be analogously modeled as an electrical circuit. Change in voltage represents the head difference across a channel, electrical currents correspond to volumetric flux and loss of energy due to turbines is related to electrical resistance. Maximum extractable power can be estimated by optimising the power dissipated across the resistors. Turbine resistance and the natural impedance of a channel can be equated through impedance matching (Rainey, 2009). Draper et al. (2014b) extended the analogy for multiple connected channels in the Pentland Firth.

It is difficult to capture the tidal dynamics and complex geometry of a real site using analytical models. Therefore, numerical 2-D and 3-D models are often employed to undertake studies of this kind. In regions where the water depth is much shallower than the tidal wavelength, the flow can be well approximated as having small vertical acceleration, with the assumption of hydrostatic pressure, relative to the horizontal direction. Consequently, the 2-D version of the Reynolds-averaged Navier Stokes (RANS) equations, obtained through the integration of Reynolds-averaged, incompressible continuity and conservation of momentum equations in the vertical (depth) direction, can be used to describe the flow, also known as the 2-D Shallow Water Equations (SWE)

(Falconer, 1993). Neglecting the third dimension, through depth-integration, can reduce computational costs.

Whilst 2-D SWE can approximate flow dynamics at a real site, higher-order modelling is necessary to capture 3-D processes. 3-D Computational Fluid Dynamics (CFD) models can offer improved accuracy in assessing the power available to turbines by resolving hydrodynamic phenomena at the device scale. However, the computational cost and challenges associated with using CFD to model a large array makes it impractical to do so. At regional-scale, the SWE can be solved with discrete vertical layers throughout the water column, referred to as a 3-D model in this thesis but is a model made up of 2-D layers Layered models have been applied to the Pentland Firth by O'Hara Murray and Gallego (2017), De Dominicis et al. (2017) and Goward Brown et al. (2017), and by Thiébot et al. (2020a) at the Alderney Race.

2.1.1 Large Array Effects

Vennell et al. (2015) discussed the design of large arrays of turbines and presented eight key array effects due to the dynamics of turbines that are significant for understanding power production. Four of the effects have been introduced in the previous section. The first is the impact of power extraction from large arrays on the free stream velocity of the flow (Garrett and Cummins, 2005, Vennell, 2010). The second effect is the idea that there is a maximum power that can be extracted from a channel, which is achieved through a balance of the farm's thrust coefficient to maximise power and the correlated reduction in velocity (as per the previous effect). The tuning of individual turbines based on the channel, array size and arrangement of turbines is another key effect and it is noted that this comes at a high computational cost. Performance of turbines in large arrays with optimal tuning in comparison to isolated turbines and the exceedance of the Betz limit is another effect, outlined previously (Vennell, 2010).

An effect presented by Vennell et al. (2015) that is not previously discussed relates to the power return from increasing the number of turbines in a row for a large array and

how that might lead to an increase or decrease in power return based on the channel's characteristics. The increase in power of an individual turbine also relates to greater structural loads that the turbine needs to be able to withstand, which leads to increased construction costs. The micro-siting of turbines in an array to exploit hydrodynamic effects (e.g., positive interaction of turbine wakes) is another effect. Funke et al. (2014) propose an automated optimisation method for array layouts, considering the position and tuning of turbines for extracting maximum power. The optimisation method considers non-linear interactions between turbines, channel geometry and flow, using a gradient based algorithm to model flow realistically with a large array. The computational cost of the method is feasible and was applied to an array with up to 256 turbines in the Inner Sound of the Pentland Firth with steady state conditions.

Finally, the inclusion of more turbines through additional rows is a key effect presented by Vennell et al. (2015) and refers to the diminishing returns of adding rows that can lead to decreased power for individual turbines despite potential increase in overall array output. Adcock et al. (2013) highlight that the total extractable power is not accessible without an unrealistically large array because the cost of additional rows will exceed the value of additional power, due to diminishing returns. Available power is defined as a fraction of the extractable power that is available to turbines for power generation. Goss et al. (2021) use break even power (BEP) to optimise the number of turbines in an array by accounting for the profit per unit of generated power and the cost per device. BEP provides a threshold beyond which additional turbines that do not generate enough power are not considered economically viable in an array. Therefore, incremental power is a useful metric for assessing the viability of additional rows of turbines (Adcock and Draper, 2014b). The cost benefit of additional rows based on incremental power is a vital consideration in tidal stream energy resource assessments because in theory, many additional turbines can be deployed, increasing the assessed resource, especially if the impact of turbines on the flow velocity is not accurately considered. However, the benefit of an accurate and refined resource assessment is to inform investment

decisions for tidal stream energy development; therefore, economically viable arrays should be considered. Accurately representing turbines and their physical impact on flow is vital to ensure an accurate resource assessment that does not consider additional rows, without considering the diminishing returns in incremental power.

2.2 Modelling and Implementation of Turbines

The choice of turbine modelling is a critical part of a resource assessment. A balance between simplicity and modelling fidelity must be achieved for a reliable and feasible resource assessment method.

Actuator Disc Theory (ADT) can be used to evaluate the head loss across a turbine. The wind industry has used unconstrained ADT to represent rotors of axial flow turbines in a simplified way: a uniform, porous, circular disc of the same swept area as the rotor, which exerts a uniform resistance on the flow. The model predicts an upper limit for turbine efficiency whereby the extractable power from the actuator disc cannot be greater than $\frac{16}{27}$ of the kinetic flux passing through the disc, defining the upper Lanchester-Betz limit. The limit is a conservative upper bound for wind energy, acknowledging that actual turbine power production is further diminished by factors like turbine efficiencies and wake rotation (Sørensen, 2011).

ADT can be applied to tidal turbines, however, in tidal energy extraction the flow is constrained by the seabed, free surface and channel sidewalls, as opposed to an unconstrained and incompressible flow in wind (Bryden et al., 2007). Given the proximity of tidal turbines to finite flow boundaries, the assumptions underlying unconstrained linear momentum ADT become inappropriate in this scenario.

Garrett and Cummins (2007) extended the theory for a narrow channel, low Froude number scenario with a negligible free surface (rigid lid) to replace the unbounded scenario with a volume-flux constrained flow. They demonstrate that there is an 'extra efficiency' for an isolated tidal turbine compared to the Lanchester-Betz limit due to

the confining boundaries of a tidal channel. The maximum coefficient of power, $C_{P_{max}}$, is given in Equation 2.1,

$$C_{P_{max}} = \frac{16}{27}(1-B)^{-2}, \tag{2.1}$$

where B refers to blockage, defined as the proportion of the channel's cross sectional area occupied by the swept area of turbines in the same plane, also known as global blockage. Array blockage describes the ratio between the representative array area and the cross-sectional area of the channel and local blockage is the ratio of the single device area to the cross-sectional area of the local passage of flow (Nishino and Willden, 2012).

Houlsby et al. (2008) argued the assumption regarding the free surface was incorrect because pressure varies along the channel, resulting in a change in water level. Changes in pressure and the free surface are more significant in high blockage scenarios (Whelan et al., 2009). Therefore, Whelan et al. (2009) introduced a free surface variable to consider finite upstream Froude numbers in a model. Houlsby et al. (2008) incorporated downstream mixing to account for non-uniform flow once it has passed through and bypassed the turbine. They also combined the volume (Garrett and Cummins, 2005) and pressure (Whelan et al., 2009) constrained models to approximate flow in an open channel. The model is valid under the assumptions of constant upstream velocity and cross-sectional area, inviscid flow and hydrostatic pressure at points 1, 4 and 5 in Figure 2.2.

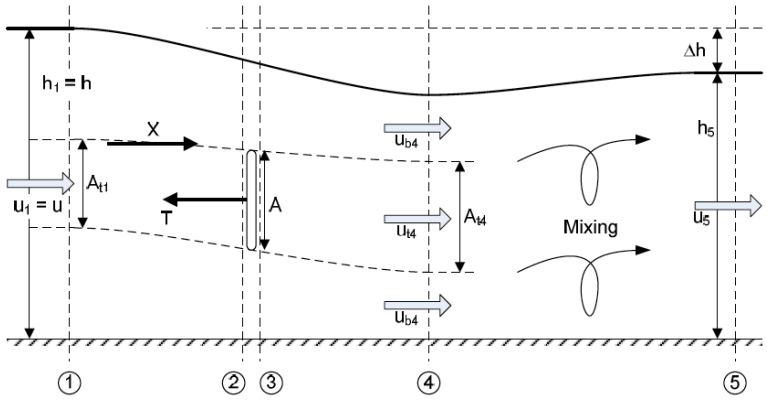

Figure 2.2: Linear momentum actuator disc theory in an open channel (Houlsby et al., 2008).

Representing a turbine as an actuator disc does not rely on assumptions about spe-

cific blade designs. The approach makes a distinction between the power available to turbines and the total power extracted from the channel. However, it is a simplified representation and does not realistically capture device-flow interactions or how real turbines operate under different operating conditions. Therefore, it can only provide an upper bound limit for a resource assessment (Chen et al., 2019).

Adcock et al. (2013) utilised ADT to consider the available power and obtain an upper bound assessment of the resource at the Pentland Firth, accepting the theory overestimates the resource. The study did not account for losses related to the support structure, mechanical inefficiencies, and electrical inefficiencies, which would likely reduce the assessment. ADT was also adopted to define upper bound resource assessments at Anglesey Skerries and Portland Bill (Serhadlıoğlu et al., 2013, Adcock and Draper, 2014b).

Blade element momentum theory (BEMT) is an extension of ADT that can also be used to model the performance of turbines. The method provides insights into the effect of turbine operation, specification, and blade designs based on knowledge of blade properties, such as lift and drag coefficients of the aerofoil and twist and solidity profiles of the blade. Therefore, the extension offers advantages compared to ADT. BEMT has been used in wind energy applications but, as previously highlighted, tidal turbines experience a change in performance due to blockage effects. The constrained flow field that results in blockage effects has been previously accounted for by embedding BEMT in CFD simulations (adopted by Masters et al. 2011 and Edmunds et al. 2014) or by adjusting the momentum equations in the theory according to Garrett and Cummins (2007) and Whelan et al. (2009).

Vogel et al. (2018) presents BC-BEMT as a semi-analytical tool for investigating the effect of blockage and tip speed ratio (TSR) on the performance of a turbine. The method relies on the rigid lid momentum model (Garrett and Cummins, 2007) and is validated by boundary layer resolved simulations of a blade (Vogel et al., 2018). BC-BEMT has been implemented by Chen et al. (2019) and Vogel et al. (2018) to model the performance of a

turbine. Figure 2.3, adapted from Chen et al. (2019), demonstrates the overestimation of turbine performance using ADT compared to BC-BEMT. The difference is attributed to the consideration of the discrete number of blades and the constituent hydrofoil experiencing lift and drag.

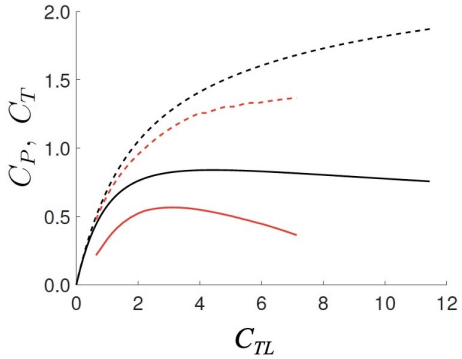

Figure 2.3: C_P (solid) and C_T (dashed) against local thrust coefficient, C_{TL}, which is described as the ratio between C_T and the turbine kinetic pressure in Houlsby et al. (2008), for ADT (black) and fixed pitch BC-BEMT, blockage=0.16 (red) (adapted from Chen et al. 2019).

The actuator line method is another technique for modelling turbines and their effects on the flow field (Sørensen and Shen, 2002). Similar to BEM, it involves discretising the blade in the spanwise direction. The overall blade force (lift and drag) is modelled as a momentum source term along the rotating actuator lines (Wimshurst and Willden, 2016b). The method is well-suited for studies of the near-wake flow field because it can solve time-varying phenomena like tip vortices (Chen, 2019). However, as the method enhances accuracy in representing turbine performance, it also introduces additional demands for parameters and computational time. Therefore, the objective of the research should dictate the choice of modelling and is considered too computationally expensive for resource modelling, compared to ADT and BC-BEMT.

Experimental coefficients of power and thrust (C_P and C_T) versus tip speed ratio (TSR) curves can be used to describe the performance of turbines as an alternative to analytical models. However, it must be noted that experimental data comes with limitations, particularly in terms of exploring various turbine operations and channel scenarios. It is also challenging to replicate realistic operating conditions in an experiment with a scaled model due to insufficient Reynolds number scaling. While experimental data

provides valuable insights, especially when available for comparison with numerical and analytical results, it may not cover the entire spectrum of possible conditions and configurations. Data from real turbine testing sites is also limited and often protected.

In addition to modelling turbine performance, turbines must be implemented in resource assessment models to capture the interaction between turbines, energy extraction and channel dynamics. Turbines can be implemented in depth-averaged models in a number of ways. However, there are challenges with applying the correct force on the flow due to turbines extracting energy in a depth-averaged model because of the 3-D nature of the problem. Turbines interact with flow in a 3-D manner and generate wakes, which affects the flow around them. Consequently, a 3-D model is required to capture the flow physics. However, due to their complexity, layered models are often employed as an alternative (Adcock et al., 2021).

The impact of resistance on the flow, induced by the presence of tidal turbines, can be accounted for by introducing an additional bed roughness term, enabling the computation of dissipated power (Sutherland et al., 2007). The maximum power averaged over a tidal period can be calculated using a depth-averaged value for bed roughness, which represents tidal turbines across a specified area of the seabed. The force can be included as an additional momentum sink that adopts the form of the bed shear term. Serhadlıoğlu (2014) emphasises that the method predicts the power extracted, which is a combination of the power available to turbines and the power lost due to mixing. The method has been adopted by Sutherland et al. (2007), Blunden and Bahaj (2007) and Yates et al. (2013) to assess the resource in the Johnstone Strait in Canada, Portland Bill in the UK and sites on the west coast of the UK.

The presence of turbines can be also accounted for by calculating the head loss across turbines as line discontinuities. Draper et al. (2010) used linear momentum actuator disc theory to represent the operation of tidal turbines in a sub-grid model whereby the head loss is calculated by modifying the flow conditions upstream and downstream of the line

discontinuity according to Houlsby et al. (2008). The method relies on turbines being uniformly modelled as a fence, thus the interactions between devices are simplified (Djama et al., 2022). Adcock et al. (2013) assessed the upper bound resource in the Pentland Firth and Serhadlıoğlu et al. (2013) quantified the resource at the Anglesey Skerries using ADT to calculate head loss across turbines and implemented the turbines into their models as line discontinuities.

3-D CFD RANS and Large Eddy Simulations (LES) can be integrated with low order representations of turbines (e.g., ADT, BEM). These methods are suitable for modelling turbulence and challenges surrounding turbulence closure are solved with the Boussinesq assumption (Vogel, 2014). They are most appropriate for studies on blade loading, turbine performance and wake interactions, although their computational costs are a consideration (Chen, 2019).

2.3 Modelling Limitations and Compromises

Resource assessments have been undertaken using 0-D, 2-D and 3-D models. A comparison of 2-D and 3-D hydrodynamic modelling software is presented in Appendix B. Each model has its limitations and compromises. Low order analytical channel models are a useful first insight into the tidal dynamics and interactions with turbines. The simplicity and low computational cost of such models allows the investigation of a large parameter space. However, the models rely on limiting assumptions that may not be applicable in real scenarios and the flow behaviour is simplified. The limited dimensions of the model do not allow for accurate representation of real sites and therefore, restrict their use for resource assessments.

According to O'Hara Murray and Gallego (2017), lower order models can be used to assess the exploitable resource and environmental impact. However, they are restricted in modelling key 3-D processes. The shearing of flow in the horizontal plane, due to the turbulence in the wake of coastal features such as headlands and islands, is

not captured in depth-averaged models (Adcock et al., 2013). The in-depth velocity variations due to secondary flows that similarly occur around coastal features or due to flow separation in the vertical plane by steep changes in bathymetry are also omitted in depth-averaged models. The flow effects described by Adcock et al. (2013) lead to differences between the predicted and actual depth-averaged velocities and affect large-scale mixing. Despite the difficulties in accurately depicting the physics, studies that adopt 2-D models can provide valuable insights and can be validated against field-measurements to ensure the model is able to reasonably predict the velocity in the primary area of interest within the model's domain.

Whilst 2-D models provide a reasonable representation of tidal dynamics, Stansby (2006) highlights the limitations of depth-averaged models for shallow wakes. Stansby (2003) adopts a 3-D boundary layer model with a two mixing length eddy-viscosity turbulence model: a vertical mixing length of classic Prandtl form and a horizontal mixing length of a multiple of the vertical length that gave good predictions. Stansby (2006) compares the 3-D model with a 2-D model. When reduced to a depth-averaged form, the horizontal mixing length is approximately half the water depth. For the 2-D model, Stansby (2006) found that whilst the prediction of stable wakes and their size was poor, the wake structures were similar for both models when vortex shedding was prominent. The increase in the bed friction coefficient as a result of horizontal strain rates is not captured in a 2-D model, which is likely what results in the poor prediction of wakes.

In depth-averaged models, the impact of tidal turbines is imposed over the whole water column (De Dominicis et al., 2017). O'Hara Murray and Gallego (2017) state the representation of tidal stream turbines in 2-D models is unrealistic because devices will only partially occupy the water column. The impact on the flow due to the energy extraction of an array of turbines is important to consider in resource assessments. Goward Brown et al. (2017) suggest the depth-averaging of velocity in a 2-D model can

lead to a potential misrepresentation of these effects and consequently overestimate the resource. In reality, velocity varies in-depth and has been demonstrated, through field-measurements, to display a vertically sheared velocity profile (Greenwood et al., 2019), which is a function of the bed roughness. Goward Brown et al. (2017) emphasise the importance of the vertical structure of flow in minimising the uncertainty in velocity and therefore, assessments of power. They suggest that 2-D models are useful for initial assessments of the resource but the use of 3-D models will allow a more accurate representation of the interaction between the resource and turbines. Goward Brown et al. (2017) found that 3-D modelling is necessary for determining the vertical flow bypass around the turbine and also suggest 2-D modelling can lead to an underestimation of the levels of sediment transport and uncertainties in environmental impact assessments.

When modelling multiple rows of turbines, there will be a velocity deficit and region of increased turbulence in the wake of an upstream row that will have an effect on the row downstream. Adcock et al. (2021) highlights that whilst depth-averaged methods can apply the reasonably correct amount of thrust to the model, the 3-D mixing behind the turbine and associated energy dissipation are not captured as easily. Therefore, they suggest that at a large-scale it is not sensible to resolve individual wakes with 2-D models because there is an uncertainty in representing the physics correctly in the near-wake region. However, the overall effect of wake losses due to an array may be accounted for using constant eddy-viscosity models to represent mixing effects or an analytical correction (Zhang et al., 2022, Vogel and Willden, 2017, Adcock et al., 2021).

2.4 Limiting Constraints on the Resource

There is a hierarchy of constraints that play a fundamental role in limiting the tidal stream resource, presented in Figure 2.4. The categorisation of the resource was introduced by Sustainable Energy Ireland (2004), and adopted by O'Rourke et al. (2010) and Segura et al. (2017). The technical and socio-economic constraints presented in Figure 2.4 are interrelated and challenging to deal with. Therefore, many past assessments of

the resource have not accounted for them.

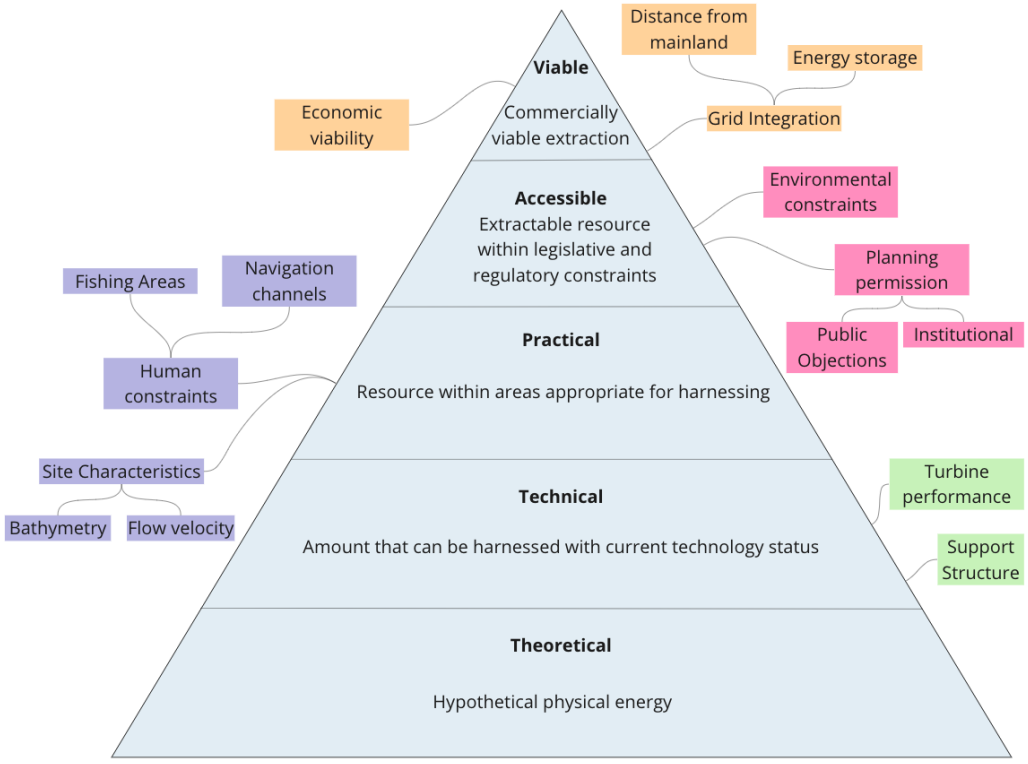

Figure 2.4: Pyramid of constraints on the useful energy available from a resource.

The theoretical resource can be considered as the amount of energy physically available at a site and requires an understanding of a site's hydrodynamics through measurements of tidal elevations, current speeds and hydrographic survey data (Segura et al., 2017). Sustainable Energy Ireland (2004) conducted a resource assessment of the Irish Sea based on the categorisation of the resource and considered the theoretical resource as the mean tidal-current power in a cross-section of flow, calculated by Fraenkel (2002) as,

$$P_{\text{mean}} = \frac{1}{2}\rho K_s K_n U_{\text{peak}}^3 \quad [\text{Wm}^{-2}], \tag{2.2}$$

where U_{peak} is the peak spring-tide velocity, K_s is the velocity shape factor that describes the variation of velocity over a tidal cycle (0.424 for sinusoidal flow) and K_n is a factor that describes the ratio of neap to spring tides (assumed to be 0.6).

Technical constraints on the theoretical resource will reduce a resource assessment due to limitations of the current status of technology (U.S Department of Energy). Therefore,

Sustainable Energy Ireland (2004) incorporated a turbine efficiency of 0.39 to their resource assessment and excluded any areas with peak flow velocities lower than 1.5 m/s based on the feasibility of early-stage technology.

Practical limitations include site characteristics (e.g., bathymetry and flow velocities) and human constraints that dictate the usage of a site (e.g., navigation channels and fishing areas). For the Sustainable Energy Ireland (2004) study, this limited the resource assessment to areas with bathymetry between 20 and 40 m and flow velocities greater than 1.5 m/s. Areas used for shipping, military, and existing pipelines and cabling were also excluded.

The accessible resource is limited by legislative and regulatory requirements, often designed to preserve the natural environment. Despite the vast areas of ocean covering the Earth's surface, only 13% is not affected by human activities (directly or indirectly) (Jones et al., 2018). There is growing concern about the impact of offshore activities on marine wilderness and potential for public objection to tidal developments due to a required redistribution and re-prioritisation of the seabed. This will impact recreational and fishing areas, and navigation channels. There is also potential for public objection to visibility of mooring structures above sea level, although the visual impact is much less significant than offshore wind because turbines are submerged (Haggett, 2011). Extracting tidal stream energy can have environmental impacts, and the risk to marine animals must be considered. When energy is extracted from an energetic tidal strait, the velocity of the flow reduces compared to its ambient state and significant reduction of flow velocity can lead to sediment accumulation and deposition, resulting in negative impacts on the ecosystem (Haverson et al., 2018). However, limitations can be placed so the maximum permissible change in velocity due to the presence of turbines is not exceeded, which will mainly impact the number of turbines deployed at a site. Collision risk between turbines and marine animals needs to be monitored, however, there have been no collisions detected to date (Coles et al., 2021). Shared usage of the seabed also

ensures turbines do not occupy the entire width of the channel, allowing animals to navigate around the developed area, which is also necessary for navigation channels.

Sustainable Energy Ireland (2004) found the areas of primary importance for accessibility were preservation of the benthic environment, marine mammals and fishing grounds as well as minimising the impact on coastal aesthetics and recreational activities. They emphasise that environmental constraints will vary between sites, requiring individual environmental impact assessments. Therefore, they do not incorporate accessibility constraints in their resource assessment.

The viable resource is limited by the constraints of the previous categories and considers additional commercial and techno-economic limitations (e.g., cost, grid integration and the scale of array deployments) (O'Rourke et al., 2010). Sustainable Energy Ireland (2004) adopted the Marine Current Turbines Ltd techno-economic model to incorporate viable constraints in their resource assessment.

O'Rourke et al. (2010) highlighted the need to update resource assessments based on developments in the tidal stream energy field, including the installation of a 1.2 MW Seagen turbine developed by Marine Current Turbines Ltd. at Strangford Lough (Power Technology, 2020). The performance of the turbine in practice highlighted the underestimation of the resource presented by Sustainable Energy Ireland (2004). O'Rourke et al. (2010) suggested a detailed 2-D model, with a finer mesh and over a smaller area, could provide a more accurate assessment of the theoretical resource. In addition, technical and practical limitations should be continually revised based on new developments of technology and better understanding of sites to ensure an up to date resource assessment. The revised site-based study of Strangford Lough by O'Rourke et al. (2010) led to a 15% increase in the assessment of the viable resource in comparison to Sustainable Energy Ireland (2004).

2.5 Pentland Firth Resource Assessments

Whilst a number of UK resource assessments have been undertaken, assessments of the practical and technical resource range between 1.5 – 22.5 GW (Metoc, 2007, Black and Veach, 2005, Carbon Trust, 2011, HM Government, 2010). A number of site-based studies have been carried out to quantify the UK's tidal stream resource (Appendix C). However, methods have not been consistent so it is not suitable to make a direct comparison between studies or combine assessments of different sites to calculate the UK's overall resource.

The Pentland Firth is potentially the single largest contributor to the UK's tidal stream resource. Site-based assessments range between 1 – 17.7 GW (Table 2.1, 2.2). The large range highlights the inconsistency in resource assessments and the need for a refined method to quantify the resource.

Black and Veach (2005) applied the kinetic flux method to quantify tidal stream energy in the Pentland Firth, critiqued in Section 2.1. Salter and Taylor (2007) suggest that studies based on the kinetic flux under-predict the Pentland Firth's resource. Salter (2009) further argued that estimates based on open flow field equations, used for predicting the output of wind turbines, and incorrect turbine design can lead to the potential resource of tidal stream energy to be underestimated by up to two orders of magnitude. Salter and Taylor (2007) used the electrical circuit analogy to describe channel impedance in the Pentland Firth. The assessment was based on the assumption that energy lost to bed friction will be similar to the energy extracted by turbines. Salter (2009) highlights the uncertainty of bed friction losses in the Pentland Firth. The method is highly dependent on the value of bed friction and the uncertainty in the parameter impacts the overall assessment greatly. Salter (2009) assumes that flux in the channel is unchanged by the presence of turbines. However, the current changes when resistance is added to the flow, which is a significant omission from Salter's method and indicates why the assessment is much greater in comparison to other assessments presented in Tables

Table 2.1: (Part 1) Pentland Firth resource assessments.

Reference	**Method**	**Resource Assessment**
Black and Veach (2005)	• Kinetic flux method • Significant impact factor (SIF) to represent fraction of resource available for extraction Data Sources • Department for Trade and Industry (DTI) Renewable Atlas • Admiralty Charts	• 1 GW Without significantly reducing natural flow
Carbon Trust (2011)	• 2-D model • Turbines modelled as additional drag terms in momentum equation Data Sources • Marine Energy Atlas Software •Flow Development-2D (TFD-2D)	• 0.9 GW Practical resource • 2.0 GW with relaxed environmental and economic constraints
Salter and Taylor (2007), Salter (2009)	• Electrical circuit analogy to calculate channel impedance Data Sources • Bed friction value of Menai Strait (Campbell et al., 1998)	• 17.7 GW at peak flow, 1/3 of 53 GW dissipated by seabed
Easton et al (2012)	• 2-D model • Smagorinsky method dissipating energy Data Sources • Validated with TOPEX/POSEIDON altimeter data • British Oceanographic Data Centre (BODC) Software • MIKE21 Flow Model Flexible Mesh	• 8.97 GW Mean energy flux, 80% dissipated through bed friction
Adcock et al (2013)	• 2-D model • Three rows of turbines occupying width of Pentland Firth • ADT - included as line discontinuity Data Sources • Validated with ADCP gauge data Software • Discontinuous Galerkin ADCIRC	• 1.9 GW Upper bound available power averaged over spring-neap cycle, 0.4 blockage
Draper et al (2014a)	• 2-D model • Sub-channels: Stroma, Swona and Pentland Skerries Data Sources • Bathymetry data interpolated from Seazone Ltd. Software • Discontinuous Galerkin ADCIRC	• 4.19 GW (M_2 and S_2) • 3.75 GW (M_2 only) Power potential

Table 2.2: (Part 2) Pentland Firth resource assessments.

Reference	**Method**	**Resource Assessment**
O'Hara Murray and Gallego (2017)	• 3-D model • Turbines incorporated as momentum sink Data Sources • UK Hydrographic Office • Marine Scotland Science • Admiralty Chart Software • FVCOM	Upper bound mean extractable power: • 5.3 GW (M_2 and S_2) • 4.9 GW (M_2 only) • 1.4 GW Moderate environmental impact
De Dominicis et al (2017)	• 3-D model • 8 tidal constituents • Varying thrust coefficient • Smagorinsky (horizontal), $\kappa - \epsilon$ (vertical) Data Sources • Global self-consistent, hierarchical, high resolution shoreline data • TOPEX/POSEIDON and Jason altimeter data Software • FVCOM	• 1.64 GW Average annual available power

2.1, 2.2. The assessment by Salter and Taylor (2007) is based on peak flow, therefore the power averaged over the tidal cycle will be significantly lower.

Carbon Trust (2011) assessed the practical resource potential of the Pentland Firth as part of a national study, using a depth-averaged SWE model. They revised an initial estimate of 0.9 GW by relaxing the constraints based on environmental and economic considerations, recognising the cost-benefits of economies of volume for large scale development at the Pentland Firth and acknowledging the fact that the model did not accurately represent environmental impacts. The updated assessment increased by 120%, highlighting the sensitivity of resource assessments to assumptions on limitations to the resource (Coles et al., 2021).

Easton et al. (2012) calculated the mean energy flux into the Pentland Firth but did not consider the practically extractable resource, stating that it was unlikely a maximum of 10 GW flux could be extracted. Meteorological forcing and additional flow sources were

excluded from the study. Only the astronomical and Coriolis forcing were incorporated, as they were considered to be more significant. Easton et al. (2012) noted the limited availability of *in-situ* data for modelling. Numerical models are useful, however, lack of comparable field data makes verifying results difficult. This highlights a significant challenge of carrying out a validated and accurate resource assessment.

Adcock et al. (2013) assessed the upper bound power available to three rows of turbines occupying the width of the Pentland Firth. They found that for a given number of rows, the power available is greater with a larger blockage but as more rows are added, the increase in power shows diminishing returns. Therefore, a minimum incremental power per swept area of 1 kW/m^2 was implemented as a crude equivalent to offshore wind. They suggest a refined assessment will unlikely exceed their upper bound assessment because the model overestimates power available compared to a turbine that will generate an equivalent opposing force on the flow. An assumption of the model is that the maximum reduction in peak flow rate at the site must be no greater than 30%, which is likely to exceed environmental impact restrictions. It is unlikely that a row of turbines would be deployed across the entire width of the Firth due to other seabed usage priorities, such as shipping channels.

Draper et al. (2014a) assessed potential power from sub-channels in the Pentland Firth, highlighting that it cannot be described by a single value. They acknowledge the power potential of channels are dependent on the deployment and operation of arrays in parallel or series channels. They found that developments of parallel sites increased power extraction but sites developed in series experienced losses in power extraction. This is crucial because the original lease sites in the Pentland Firth were leased to different developers, therefore developments should be regulated, (Appendix A). Their assessment does not consider power available to turbines.

O'Hara Murray and Gallego (2017) applied a 3-D model to the Pentland Firth. The model assumes turbine performance is the same regardless of flow direction. This

would require a yawing mechanism and could have an impact on flow dynamics near turbines. The assessment is a theoretical upper bound, not a viable resource assessment (Figure 2.4) because the power extraction refers to power removed from the flow due to turbines exerting thrust on the flow rather than electrical power. Their assessment requires a large array (up to 31,420 turbines) to be deployed across the entire width of the Pentland Firth, causing a 38% volume transport reduction and changes up to 2 ms^{-1} in flow velocity. The scenario they modelled would likely exceed environmental and leasing regulations. The study does also present a more realistic scenario (5636 turbines) with less environmental impact, reducing the assessment by 72%.

De Dominicis et al. (2017) used a 3-D model to assess the ocean's response to energy extraction from a large array, environmental impact and power available for electricity generation. They estimate the resource to be of the same order of magnitude as that assessed by O'Hara Murray and Gallego (2017) (moderate environmental impact scenario). This site-based study does consider lease site area restrictions making it a more refined assessment.

2.6 Conclusion

This chapter offers a comprehensive review of the literature pertaining to resource assessments in the context of this thesis. Methods for modelling tidal flow characteristics and turbines have been identified and evaluated to inform the development of a refined model for conducting site-based resource assessments. The limitations associated with the choice of dimensional models are acknowledged and discussed. Appraisal of methods for modelling tidal dynamics, turbine performance and implementation of turbines has highlighted the need to choose a model based on the objective of the research and when compromises due to modelling choices are made, it is necessary to acknowledge and understand the impact on the results. The review of site-based resource assessments has highlighted the necessity for a more refined and updated resource assessment of tidal stream energy, acknowledging the substantial work already

conducted in this area. The observed variation in resource assessments arises from inconsistent methods, assumptions, and the consideration of constraints limiting the resource. This makes direct comparison between assessments and potential combination of site-based studies to assess the UK's overall resource untenable (Metoc, 2007).

The methods and assumptions from previous site-based assessments inform the modeling decisions made in this thesis and highlight existing research gaps. The significant range in site-based resource assessments underscores the need for an assessment that considers additional practical and accessible constraints, aspects often omitted or approximated in existing studies. O'Rourke et al. (2010) emphasised the need to revise resource assessments based on advances in the field, especially concerning technical and practical limitations for extracting the viable resource. A refined resource assessment is sought in subsequent Chapters by considering technical, practical and accessible limitations to the resource.

Part I

Idealised Channel Study

Chapter 3

Investigation of Parameters Affecting Resource Assessments through Analytical Modelling

The need for a high order standardised model to refine assessments of the tidal stream energy resource is highlighted in Chapter 2. Various models have been employed in the study of tidal stream energy. However, to establish a robust and validated model, which is applicable to a wide range of sites, a thorough analysis of key parameters affecting the resource must be undertaken. Using a low-order model can inform the development of a refined high order model by identifying how parameters affect a resource assessment, allowing the examination of challenges in quantifying tidal stream energy.

Section 3.1 presents existing studies that utilise lower order modelling techniques and how the work undertaken in this chapter combines extensions of low order models to extend the work further. An overview of the parameters investigated in this chapter is presented alongside. Details of the model for representing the channels adopted in the study, a shallow channel and tidal strait, and the extensions of including multiple tidal constituents and nodal cycle variability are presented in Section 3.2. In Section 3.3, the theory and implementation of BC-BEMT are outlined. The turbine performance curve is described along with an explanation of the turbine control strategy adopted in this thesis. The results and discussion are presented in Section 3.4.

3.1 Overview of Parameters and Low Order Modelling Extensions

A number of studies have utilised low order channel models with adaptations, summarised in Table 3.1. ADT and BC-BEMT have been used to model turbines across the studies. The number of constituents, consideration of support structures, capping strategies, wake deficits and velocity reduction criteria are presented. This study is the first to encompass all modelling parameters, as illustrated in Table 3.1.

Table 3.1: Channel model adaptations.

Study	Turbine model	Constituents	Support structure	Power capping	Combined capping	Wakes	Velocity reduction
This study	BC-BEMT	8	✓	✓	✓	✓	✓
Vennell (2010)	ADT	-	✗	✗	✗	✗	✗
Adcock and Draper (2014b)	ADT	2+	✗	✗	✗	✗	✗
Muchala and Willden (2017)	ADT	-	✓	✓	✗	✗	✓
Wang and Adcock (2019)	ADT	2	✓	✓	✓	✗	✗
Chen et al. (2019)	BC-BEMT, ADT	2	✗	✗	✗	✗	✗

Low order parameters affecting resource assessments were identified through a literature review of UK site-based resource assessments (Section 2.5 and Appendix C). Parameters are categorised into site-based channel characteristics, array and turbine design, and simulation settings (Figure 3.1). Key dependencies and relations between parameters and metrics are illustrated in Figure 3.1 but the connections are not exhaustive. The parameters form the basis of case scenarios modelled for assessing the importance of key parameters affecting the resource. Figure 3.1 presents economic and power analysis metrics and links between parameters are illustrated. Economic metrics are excluded from the scope of this study because the thesis focuses on the practical and accessible constraints on the resource and does not explicitly consider the viable resource (Figure 2.4).

The geometry and dynamic balance of two channels, a shallow channel and a deep tidal strait, characterised by Vennell (2010), are used as generic idealised channels for the study. The shallow channel is drag dominated and the tidal strait is inertia dominated (Garrett and Cummins, 2005). The depth of the shallow channel was doubled (to 40 m) for this study to ensure the placement of turbine rotors and support structures complied with minimum blade tip to seabed and blade tip to sea surface clearances outlined in Meygen (2012). The dynamic balance, which defines the dominating force (inertia or drag) acting on the channel, was maintained.

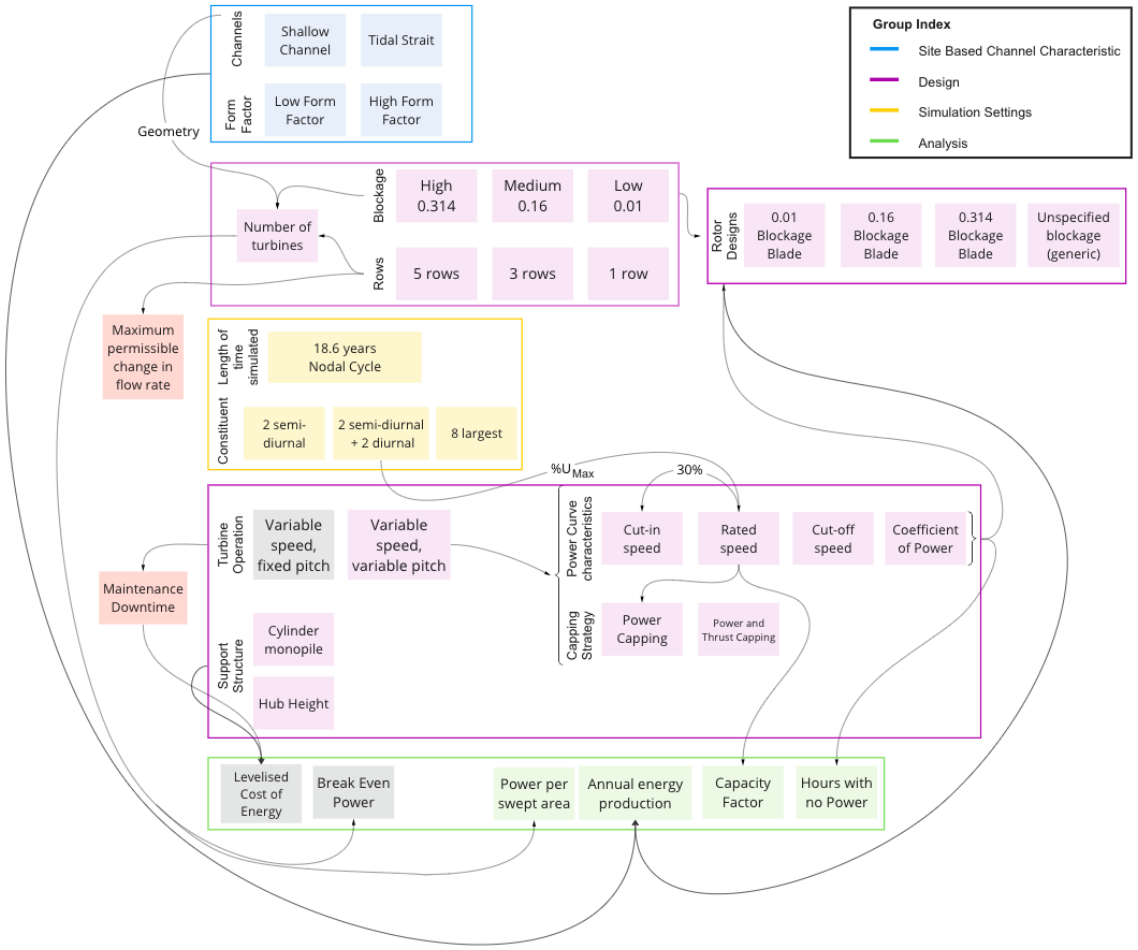

Figure 3.1: Organogram of low order parameters and analysis metrics.

Four blade geometry designs are considered; three designs optimised for a given blockage, and one unblocked design (Figure 3.1). Other design choices relating to turbines were cut-in, cut-out and rated speeds. These characterise the performance curve of a variable-speed variable-pitch (VSVP) operated turbine, which were defined following a standardised approach proposed by Lewis et al. (2021). Two capping strategies, power capping and combined power and thrust capping, were adopted.

3.2 0-D Model of Tidal Dynamics

3.2.1 Simple Channel Model

The analytical model proposed by Garrett and Cummins (2005) applies the 1-D approximation of the conservation of momentum shallow water equation,

$$\frac{\partial u}{\partial t} + u\frac{\partial u}{\partial x} + g\frac{\partial \eta}{\partial x} = -F \tag{3.1}$$

where u is the flow speed, which is a function of time t and position x along the length of the channel in the streamwise direction, with cross sectional area $A_C(x)$ (Figure 3.2). Acceleration due to gravity is given by g and η represents the free surface water elevation that creates a pressure gradient to drive the flow through the channel. The opposing forces on the flow are represented by F and consists of the resistance due to turbines and bed friction. The model assumes the flow velocity through the channel and the turbine drag are independent of transverse positioning of turbines that occupy the entire width of the channel.

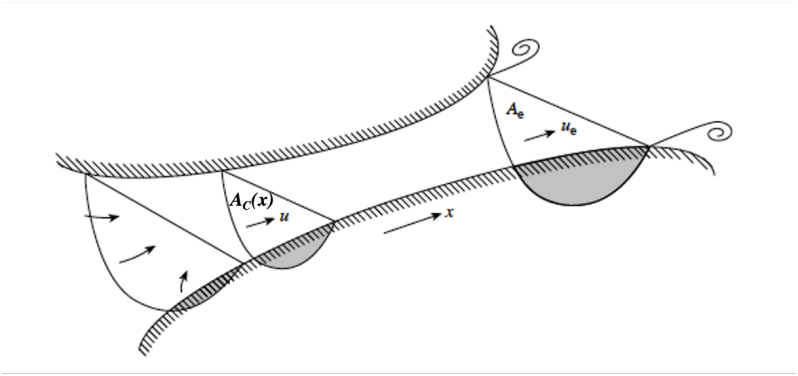

Figure 3.2: Depiction of a channel connecting two basins with area, A_C, along the x-direction of the channel and flow velocity, u, (adapted from Garrett and Cummins 2005).

The constricted channel joins two large bodies of water and the head difference between either end of the channel drives the current through it. The simplifying assumptions of this model are that the changes in elevation due to the rising and falling of the tide are negligible. The conservation of volume principle dictates that flow rate through the channel is $Q = A_C u$, and independent of the position x if the length of the channel is sufficiently short compared to the tide's wavelength, which tends to be in the order of hundreds of kilometres (Garrett and Cummins, 2005). The tides either end of the channel are assumed to be unaffected by the currents. The channel must also be characterised by a low Froude number to ensure that the first order approximations of depth and velocity are functions of position only.

Equation 3.1 can be integrated along the length of the channel (x-direction, Figure 3.2)

to give

$$c\frac{dQ}{dt} - g\eta_0 = -\delta_1 Q|Q| - \delta_0 Q|Q| \tag{3.2}$$

where,

$$\delta_0 = \int_0^l C_d \left(hA_C^2\right)^{-1} dx + \frac{1}{2}A_e^{-2}. \tag{3.3}$$

The parameter c is described by $c = \int_0^l A_C^{-1} dx$, where l is the length of the channel. The water level difference between the tidal basins on either end of the channel is assumed to be independent of both the flow through the channel and the changes in F when turbines are deployed. The elevation varies with time and can be described by the amplitude, a_o, and frequency, ω_0, of the forcing by $\eta_0 = a_0 \cos(\omega_0 t)$. The drag term $\delta_1 Q|Q|$ represents the force on the flow due to turbines, also written as $\int_0^l F_t dx$. The drag coefficient of the channel is represented by C_d in Equation 3.3 and A_e is the cross sectional area at the exit of the channel where the flow jets, with velocity u_e, into a comparatively stagnant tidal basin and is associated as an energy loss (Figure 3.2).

Equation 3.2 can be non-dimensionalised with the following terms, if the turbine drag is assumed to be proportional to the velocity squared and the drag due to support structure is excluded, to give Equation 3.4,

$$Q' = \frac{\omega_0 c}{g a_0} Q, \lambda_0 = \frac{g a_0}{(\omega_0 c)^2}\delta_0, \lambda_1 = \frac{g a_0}{(\omega_0 c)^2}\delta_1, \text{ and } t' = \omega_0 t,$$
$$\frac{\mathrm{d}Q'}{\mathrm{d}t'} + (\lambda_0 + \lambda_1) Q' \left|Q'\right| = \cos\left(t'\right). \tag{3.4}$$

The bed friction and exit losses are represented by λ_0 and the drag due to turbines is represented by λ_1. The parameter λ_0 is also considered as the dynamic balance of the channel, and when no turbine are present it describes the balance between drag and inertia forces in the channel. The dominant physics is indicated by the value of λ_0 bounded by the inertial ($\lambda_0 = 0$) and quasi steady ($\lambda_0 \to \infty$) limits. A value of $\lambda_0 >> 1$ implies a drag dominated channel and $\lambda_0 < 1$ characterises a channel dominated by inertia.

For a real site, with channel length, l, and depth, h, λ_0 can be described by

$$\lambda_0 = \frac{g a_0}{\omega_0^2 l h} C_d. \tag{3.5}$$

Equation 3.5 implies that channels with large dimensions, l and h, tend to have lower dynamic balance and are therefore, inertia dominated (e.g., Cook Strait in New Zealand is a large, deep strait with $\lambda_0 \approx 0.1$, Vennell et al. 2015). The Tory Channel in New Zealand is a shallow channel with $\lambda_0 \approx 5$ (Vennell et al., 2015). In reality, sites will have variable currents, bathymetry and width across the channel, which makes the characterisation of the dynamic balance with simple non-dimensional parameters difficult. However, it is a good initial approximation of a channel's dynamics (Adcock and Draper, 2014b).

The maximum average power can be assessed, if data on the pressure head and flux of a channel in natural state can be obtained, through an analytical calculation by $\gamma \rho g a Q_{max}$ (Garrett and Cummins, 2005). If $\gamma = 0.22$, the maximum average power available can be assessed, within 10% accuracy, because $0.21 < \gamma < 0.24$ at the inertial and quasi-steady limit respectively.

The Garrett and Cummins (2005) model is suitable for capturing leading order physics of the effects from extracting energy on the dynamics of the channel and calculating upper bound energy extraction at a low computational cost.

3.2.2 Combined Model

The tidal dynamics of the channels used in this chapter are represented with a channel model proposed by Vennell (2010), which is an extension of the model proposed by Garrett and Cummins (2005). The model considers the Garrett and Cummins (2007) volume-flux constrained actuator disc theory to represent rows of turbines occupying the entire width of a channel.

To comply with the assumptions of the Garrett and Cummins (2005, 2007) models, Vennell (2010) assumes the array of turbines only occupies a short section of the channel's length so the flow can be considered in a quasi-steady state. Additional simplifying

assumptions of the model are that the channel has a rectangular cross-sectional area, which is uniform along the channel length, and turbines are arranged in a grid (Figure 3.3, adapted from Vennell 2010). Furthermore, the model assumes that the downstream spacing between rows is adequate for the flow in the near-wake of the turbine, u_3, and the bypass flow, u_4, to fully mix and recover to the free stream velocity, u, before encountering the subsequent downstream row of turbines, because $u_4 \geq u > u_3$. In blockage affected flow scenarios, turbine loads increase because of the streamwise pressure gradient that develops due to the confined wake expansion (McNaughton et al., 2022). This is what causes the bypass flow to accelerate relative to the free stream flow.

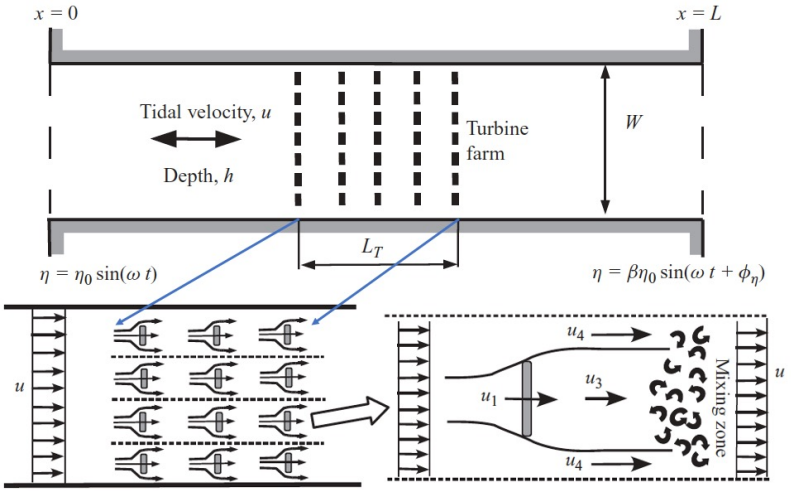

Figure 3.3: Channel and array schematic with flow velocities demonstrated ($u_4 \gg u_1 > u_3$) (adapted from Vennell 2010, Garrett and Cummins 2007).

The Vennell (2010) model explores how tuning the turbine through-flow, with velocity u_1, and density of an array interacts with the flow at a larger scale and how that affects the maximum available power from a channel. Garrett and Cummins (2005) study demonstrated the turbine-flow interaction leads to a decrease in flow speed along the channel due to an increase in overall drag and assessed the channel's power potential through that. Whilst the potential estimated by the Garrett and Cummins (2005) model assumes turbines occupy the entire cross-section of the channel, Garrett and Cummins (2007) considered a more realistic scenario that allows mixing behind turbines that dissipates energy flow. They demonstrate that there is a difference between the chan-

nel's potential (i.e., maximum power dissipated due to turbines, P_{lost}), and the power available, P_{avail} for electricity generation due to wake dissipation (Vennell, 2010). The power available is lower than the power lost and can be written as,

$$P_{lost} = Fu = \rho N_R C_{T1} A_c u^3 \tag{3.6}$$

$$P_{avail} = Fu_1 = \rho N_R C_{T1} A_c u^3 r_1 \tag{3.7}$$

where F is the force on the turbines and r_1, which is the multiplying factor between P_{avail} and P_{loss}, is the turbine flow velocity coefficient based on the definition $r_i = u_i/u$. The number of turbines in each row is represented by N_R. The force on the turbines is $F = \rho N_R C_{T1} A_C u^2$, where C_{T1} is the drag coefficient for one row of turbines expressed as $C_{T1} = \frac{B}{2}(r_4^2 - r_3^2)$. The ratios between the bypass flow and the free-stream flow, and the through-turbine flow and the free-stream flow can be expressed as

$$r_4 = \frac{1 - r_3 + \sqrt{B - 2Br_3 + \left(1 - B + B^2\right) r_3^2}}{1 - B} \tag{3.8}$$

and

$$r_1 = \frac{r_3 \left(r_4 + r_3\right)}{r_4 + 2r_3 - 1}. \tag{3.9}$$

The parameter r_3 is the turbine wake flow velocity coefficient and is used as a turbine tuning parameter by adjusting the turbine pitch. The Lanchester-Betz limit dictates the optimal tuning of a isolated turbine in a constant free-stream velocity is $r_3 = 1/3$. Garrett and Cummins (2007) also found the optimal tuning to be $r_3 = 1/3$ for a turbine in a channel. However, Vennell (2010) demonstrated that when you consider an array of turbines in a channel this value for optimal tuning does not maximise the power output of an entire array. For optimal tuning, r_3 should be dependent on the number of rows and the blockage, instead.

The 0-D hydrodynamic model is useful to study parameters affecting the resource at a low computational cost despite the limiting assumptions of the model. Therefore, in this chapter, the flow rate in the channel is found by solving the governing equation,

$$\frac{1}{c}\frac{dQ}{dt} = g\eta - (\delta_0 + \delta_1 + \delta_2) Q|Q|. \tag{3.10}$$

Equation 3.4 is the non-dimensional form of equation 3.10, with the inclusion of a drag parameter to represent the support structure thrust, δ_2, in addition to δ_0 and δ_1, which represent the channel bed friction and turbine thrust. The non-dimensional form is solved using the Runge Kutta 4^{th} order method and initial conditions are calculated from the approximate analytic solution for velocity given in Appendix A3 in Vennell (2010). To ensure the model had been implemented correctly, the results in Table 1 of Vennell (2010) were reproduced as a method of validation. Vennell (2010) uses ADT to represent turbines, therefore assumptions about the design, specification or operation of the turbine are not considered.

3.2.3 Nodal Cycle and Constituents

Tidal power varies across multiple time-scales from seconds to decades. Many studies examine the tidal resource over a shorter time-scale, like the spring-neap cycle, because simulating longer time scales requires significantly more computational time and resources (Adcock et al., 2014). The variability of tides in the order of hourly, daily and weekly timescales are mostly dependent on the semi-diurnal, diurnal and shallow water (for shallow or coastal areas) constituent interactions. Examples of this variability are the asymmetry between ebb and flood, variability in high or low tides over a 24-hour period and variation of the spring-neap cycle over a fortnight (Thiébot et al., 2022). However, there is a longer time-scale that needs to be considered, the nodal cycle, which affects tides over scales of years to decades. Due to the orbital path of the Moon, the amplitudes and phases of harmonic tidal constituents vary over 18.6-years resulting in a small modulation in tides. Therefore, the 18.6-year nodal cycle contributes to a variation in the resource annually. Investigating the variability of the resource over the nodal cycle is beneficial for developers who require long term projections of tidal stream developments for feasibility and investment decisions. If the variation is significant, it is also necessary for turbine developers to consider the maximum loads that occur over the nodal cycle (Thiébot et al., 2022).

Thiébot et al. (2020b) conducted a study of the Alderney Race to consider the influence of the nodal cycle on the tidal resource from 2014 to 2034. The study indicated the nodal cycle affects predictions of annual power density up to an order of 10%. The study also considered turbines with a rated power of 1.3 MW to assess the annual energy production over the nodal cycle, which led to a 7% modulation. In an extension of the work, Thiébot et al. (2022) broadened the investigation to other sites, the Fromveur Strait and Ramsey Sound, to consider the variability of tidal stream energy resource in North Western Europe. The modulation in annual power density for the additional two sites was found to be comparable. Their study suggests that the variation in annual maximum velocity across the nodal cycle could have a noticeable impact on turbine loads, such that the difference in maximum turbine loads is up to 7–10% between the top and bottom of the cycle. While the effect on tidal asymmetry was found to be minor, the spring-neap variability demonstrated a more consistent pattern at the peak of the nodal cycle (Thiébot et al., 2022). The findings of Thiébot et al. (2020b, 2022) emphasise the importance of analysing and quantifying the effect of the nodal cycle and the technical specification IEC TS 62600-2015 (2015) recommends investigating the resource across different time-scales.

In this chapter, a low order model is used to study the potential annual variation in average power production over the nodal cycle. The insights gained from the low-order modelling will inform higher-order models, where a balance between the number of cases run and the length of simulated time is critical. The channel model is extended to model the variation of the resource over the nodal cycle and include additional harmonic constituents. To incorporate multiple harmonic constituents, the elevation is expressed as,

$$\eta = a_0 \cos(\omega_0 t) + a_1 \cos(\omega_1 t) + ... + a_N \cos(\omega_N t). \tag{3.11}$$

To consider the variation of the nodal cycle, the nodal adjustments are accounted for as a sum of harmonics of each constituent. An example of the harmonic expansion for the

S_2 constituent is given as,

$$a_{S_2} f_{S_2} \cos(\sigma_{S_2} t - g_{S_2} + (V_{S_2} + u_{S_2})) \tag{3.12}$$

where a_{S_2} is amplitude, f_{S_2} is the nodal factor, σ_{S_2} is angular speed, g_{S_2} is phase lag at the time zone, u_{S_2} is the nodal angle and V_{S_2} is the equilibrium phase (Pugh, 1987). Figure 3.4 presents the variation of the nodal factor for 8 constituents.

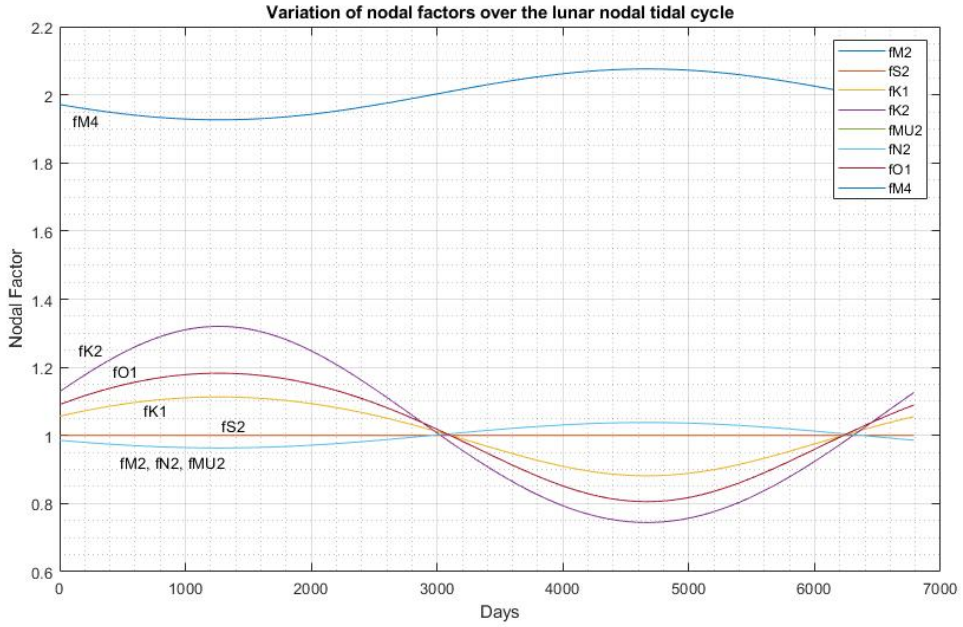

Figure 3.4: Nodal Factor Variations of 8 constituents over 18.6 years (6,789 days).

Tides can be classified into three main tidal regimes (Table 3.2), which describe the number of high and low tides each day. The regimes are defined based on the form factor (FF), also known as the Formzahl number, which classifies tides based on the ratio of the diurnal (O_1 and K_1) and semi-diurnal (M_2 and S_2) constituent amplitudes (Pugh, 1987),

$$FF = \frac{a_{K_1} + a_{O_1}}{a_{M_2} + a_{S_2}}. \tag{3.13}$$

Figure 3.5 presents the classifications of tides worldwide and demonstrates the majority of areas are classified as semi-diurnal, this includes sites across the UK, which means they are dominated by the M_2 and S_2 constituents. In this chapter, two sites spanning the semi-diurnal range were chosen to investigate the effect of FF among semi-diurnal

Table 3.2: Classification of different tidal regimes based on Form Factor.

Tidal Regime	Definition	Form Factor (FF)
Semi-diurnal	Two high and low tides per day	$0 \leq FF \leq 0.25$
Mixed semi-diurnal	Two high and low tides per day with the second high and low tide at a different height to the first	$0.25 \leq FF \leq 1.5$
Mixed diurnal	One high and low tide per day with an additional small high and low tide during the fortnightly tidal cycle	$1.5 \leq FF \leq 3$
Diurnal	One high and low tide per day	$3 \leq FF$

sites. The effect of the number of constituents included in the model on the resource assessment was also considered. Availability of amplitude and phase constituent data highly influenced the choice of sites.

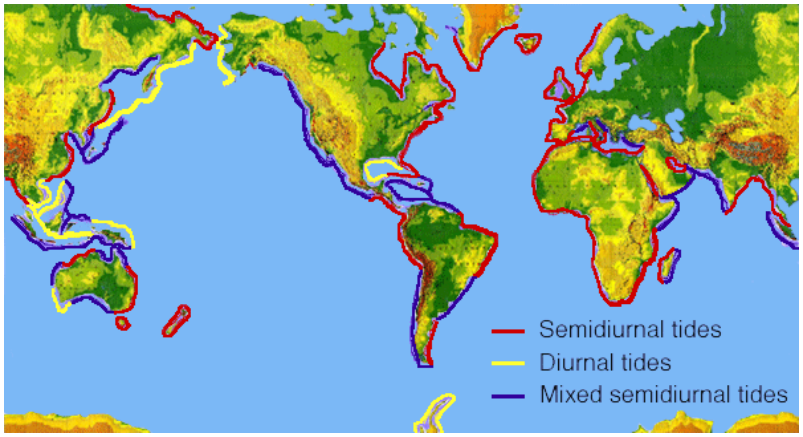

Figure 3.5: World map indicating the tidal regimes along coastlines (US Department of Commerce, National Oceanic and Atmospheric Administration, 2013).

To calculate the head difference in Equation 3.10, the difference between harmonic expansions for each constituent at two geographical points near the studied locations were taken from published data. Three constituent scenarios were modelled: 2 semi-diurnal constituents (M_2 and S_2), 2 semi-diurnal and 2 diurnal constituents (additional O_1 and K_1) and the 8 largest constituents (additional K_2, M_4, MU_2 and N_2). Admiralty Tide Tables (Hydrographic Office, 2017) provide phase and amplitude data for M_2, S_2, O_1 and K_1 constituents at sites across the UK. However, published data for other constituents is more limited. The data for sites with higher FFs were from tidal gauges at Weymouth (FF=0.15) and Bournemouth (FF=0.22), presented in Table 3.3 (Blunden

and Bahaj, 2006). The data for low FF sites were from tidal gauges in Coverack (FF=0.05) and Lizard Point (FF=0.06) and modelled with up to 4 constituents only, due to the availability of data (Table 3.4, Hydrographic Office 2017). Note that all sites considered are semi-diurnal, however, the constituent data from Weymouth and Bournemouth are at the higher end of the semi-diurnal FF range, while Lizard Point and Coverack are at the lower end.

Table 3.3: Amplitude and phase constituent data for Weymouth and Bournemouth (Blunden and Bahaj, 2006).

Constituent	Weymouth		Bournemouth	
	Amplitude [m]	Phase [°]	Amplitude [m]	Phase [°]
M_2	0.591	190	0.408	373
S_2	0.309	242	0.183	292
O_1	0.048	350	0.041	348
K_1	0.090	111	0.091	112
K_2	0.086	238	0.05	291
M_4	0.149	24	0.194	75
MU_2	0.110	194	0.071	193
N_2	0.133	183	0.105	247

Table 3.4: Amplitude and phase constituent data for Lizard Point and Coverack (Hydrographic Office, 2017).

Constituent	Lizard Point		Coverack	
	Amplitude [m]	Phase [°]	Amplitude [m]	Phase [°]
M_2	1.69	138	1.72	144
S_2	0.55	186	0.57	192
O_1	0.07	97	0.07	99
K_1	0.06	328	0.05	336

3.3 Turbine Model

ADT can be used to represent turbines as uniform discs and their performance can be analysed by estimating the pressure drop and reduction in average velocity through the

rotor of a turbine (Section 2.2). However, the theory does not consider the geometry of blades, which leads to an oversimplification of real turbine behaviour because uniform discs only remove the axial momentum from the flow, thus overestimating the performance of a turbine. As highlighted in Section 2.2, its application in a resource assessment is constrained to providing only an upper bound value, which limits the refinement of quantifying the resource. The advantages and disadvantages of using CFD to resolve turbine performance has also been discussed in Section 2.2. CFD can provide a high level of accuracy by considering turbulence and wake effects in addition to blade design but is computationally demanding and is not feasible to implement in large-scale resource assessment models.

To account for the design of blades and introduce a more realistic low order model of a turbine, BC-BEMT is implemented in this thesis. BC-BEMT is proposed by Vogel et al. (2018) as a more realistic representation of turbine performance compared to ADT and offers a balance by being more computationally efficient than CFD. The theory behind BC-BEMT and its implementation are outlined.

3.3.1 Blade Element Momentum Theory

The traditional blade element momentum theory (BEMT) is an established method in the wind industry. It combines the linear momentum and blade element theories by equating the axial thrust forces calculated in each theory. BEMT considers a turbine with n number of blades that rotate with angular velocity, Ω. Each blade can be discretised into blade elements from the rotor to the blade tip (along the blade length, R) with annual rings δ_r apart (Figure 3.6a). Figure 3.6b presents the aerofoil of a representative blade element, from which the lift and drag forces on each blade element can be calculated based on the angle of attack, α, blade pitch angle, β_i, the inflow velocity, W, and the axial and tangential inductions factors, a_{2i} and a'_{2i}, for i blade elements. Summing the angle of attack and blade pitch angle gives, $\phi = \alpha + \beta_i$, which is the angle that the relative inflow velocity, W_i, approaches the blade elements.

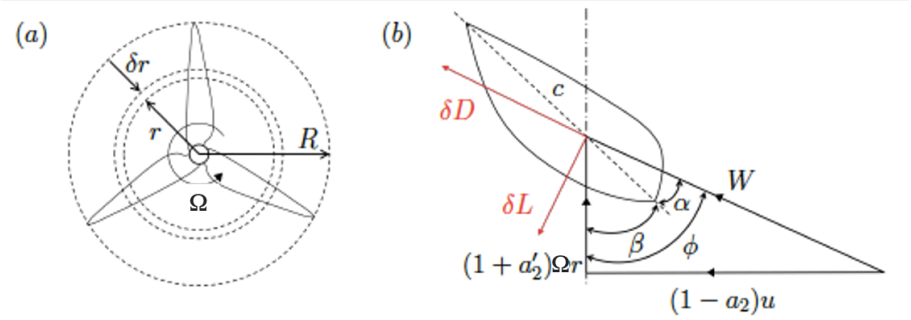

Figure 3.6: Schematic of (a) a turbine rotor discretised into blade elements via an annular ring and (b) schematic of the blade section section demonstrating the lift and drag forces (Adapted from Chen 2019, Burton et al. 2011).

The axial and tangential velocities for each blade element are calculated as $(1-a_{2i})u$ and $(1+a'_{2i})\Omega r$, based on the assumption that spanwise velocities and 3D flow phenomena are neglected. The axial inflow velocity is represented by u and the distance from the centre of the rotor along the blade length is r.

As demonstrated in Figure 3.6, the sectional drag, δD, acts in the direction of the relative inflow velocity, and the sectional lift, δL, acts at a normal to the sectional drag and the relative inflow velocity,

$$\delta D = \frac{1}{2}\rho W_i^2 c_i C_{Di} \delta r, \tag{3.14}$$

$$\delta L = \frac{1}{2}\rho W_i^2 c_i C_{Li} \delta r, \tag{3.15}$$

where, c_i is the chord length of the section and C_{Di} and C_{Li} are the coefficients of lift and drag of the forces of the blade.

BEMT is underpinned by the assumptions that there is no radial interaction between each blade element and the change of momentum of the fluid passing through the swept annulus, created by the element, is due to each element independently (Chen et al., 2019).

A tip loss correction factor is adopted to account for the reduction in momentum change that occurs at the blade tip. The tip loss correction factor, F_i, proposed by Glauert (1983) is adopted. The correction is implemented by multiplying the axial and tangential

induction factors, a_{2i} and a'_{2i}, by the dimensionless factor given as,

$$F_i = \frac{2}{\pi}\cos^{-1}\left[\exp\left[\frac{n(1-(R/r))}{2\sin\phi_i}\right]\right]. \tag{3.16}$$

The tip loss correction factor varies along the length of the blade with a value of 1 along the majority of the blade. However, towards the tip of the blade, the factor decreases to 0 where the correction is necessary. Therefore, the correction reduces the axial and tangential induction factors as the radial flow approaches the tip (Burton et al., 2011, Chen, 2019).

The thrust and power of the rotor can be calculated by integrating the sectional axial thrust and tangential torque, δ_T and δ_τ, over all the blade elements, which are given as,

$$\delta T = \frac{1}{2}\rho W_i^2 n c_i \left(C_{Li}\cos\phi_i + C_{Di}\sin\phi_i\right)\delta r = 4\pi r\rho u^2\left(1-a_{2i}F_i\right)a_{2i}F_i\delta r, \tag{3.17}$$

$$\delta\tau = \frac{1}{2}\rho W_i^2 n c_i \left(C_{Li}\sin\phi_i - C_{Di}\cos\phi_i\right) r\delta r = 4\pi r^3\rho u\left(1-a_{2i}F_i\right)a'_{2i}F_i\omega\delta r. \tag{3.18}$$

3.3.2 Blockage Corrected Blade Element Momentum Theory

In tidal scenarios, the flow is confined, whereas in wind scenarios the flow is considered unconfined due to wind turbines occupying a comparatively small part of the atmospheric boundary layer. Therefore, tidal turbines experience blockage effects that are considered to be influential on the performance of turbines and must be accounted for (Garrett and Cummins, 2007). Vogel et al. (2018) extended BEMT to account for the volume-flux constraints on the flow field in tidal scenarios thus proposing BC-BEMT. In the unbounded linear momentum theory, the static pressure in the near-wake of the turbine is assumed to recover to levels of the upstream value in the far-wake, leading to a velocity deficit that is twice as large in the far-wake compared to at the turbine plane. However, the volume-flux constraints in tidal streams cause a streamwise static pressure difference due to the accelerated bypass flow, which allows the turbine to achieve a higher maximum power coefficient by applying a greater thrust coefficient. BC-BEMT equates the axial thrust calculated by the blade element and volume-flux constrained linear momentum theories to account for the pressure difference (Vogel et al., 2018,

Chen, 2019).

In BC-BEMT, the rotor is similarly separated by annular rings of width δ_r, which creates annular streamtubes, where mass, momentum and energy are conserved, and surrounded by a bypass flow. Figure 3.7 presents the BC-BEMT model of the flow passing a rotor. The model's upstream boundary is determined by the macroscopic flow around the turbine and the downstream boundary is located at a point where the static pressure is equalised across the annular streamtubes and the bypass flow (Vogel et al., 2018).

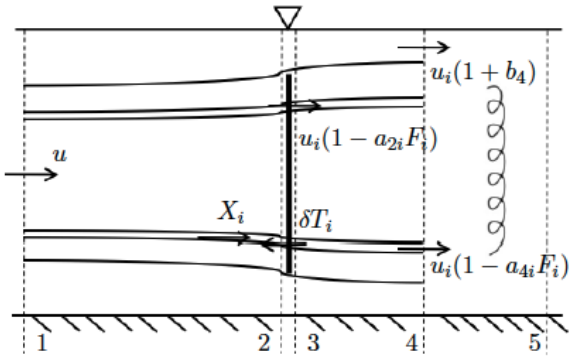

Figure 3.7: Diagram of the BC-BEMT model demonstrating the five stations across which the flow past the rotor is analysed (Chen 2019 adapted from Vogel et al. 2018).

In Figure 3.7, station one exists far upstream of the rotor such that the flow velocity is assumed to be independent of the turbine's operation. Stations two and three are immediately upstream and downstream of the rotor and the fourth station is far downstream such that the static pressure between the core and bypass streamtubes will have equalised. The energy removed from the flow due to mixing of the core and bypass flow, is assumed to be between station four and five and the flow is assumed to return to a uniform state with the same speed as far upstream (Garrett and Cummins, 2007, Vogel et al., 2018).

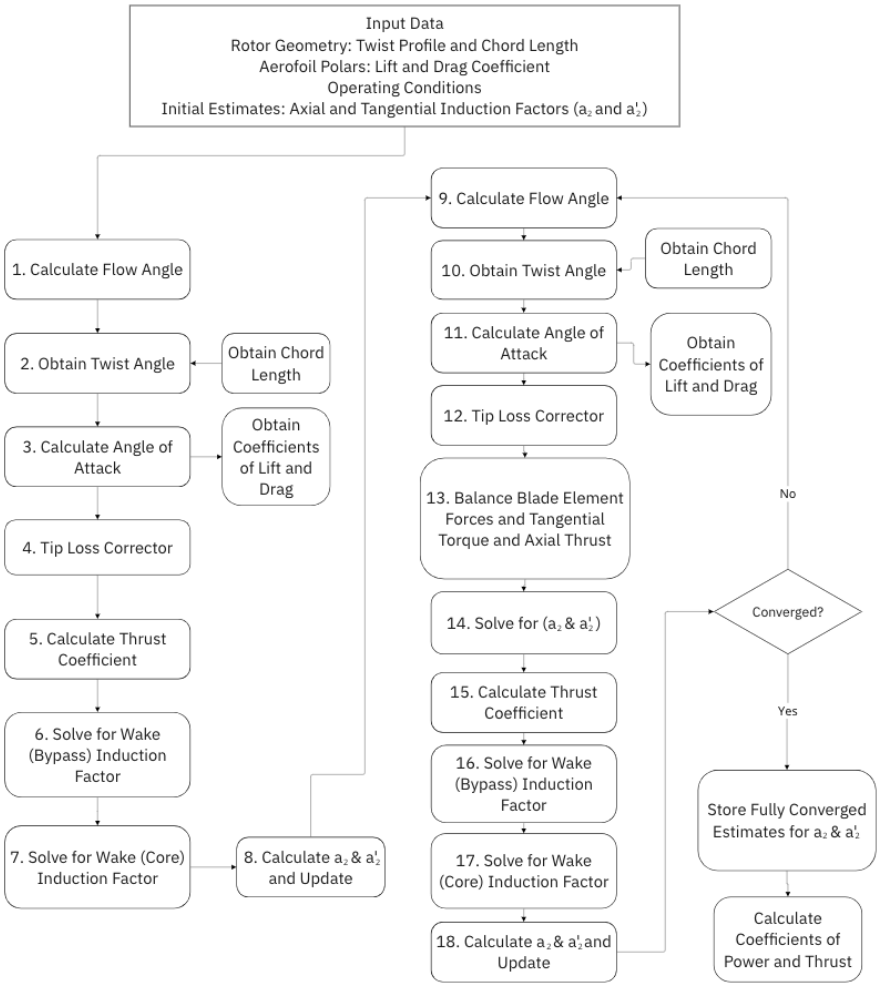

Figure 3.8: Blockage-corrected blade element momentum theory calculation sequence, adapted from Chen (2019).

Figure 3.8, adapted from Chen (2019), presents the calculation sequence for BC-BEMT to obtain the coefficients of power and thrust, C_P and C_T, used to characterise the performance of a turbine. Initial estimates for axial and tangential induction factors are set to $a_{2i} = 0.3$ and $a'_{2i} = 0.01$ to calculate the inflow angle. The relative twist angle and cord length are interpolated and the angle of attack is calculated to interpolate the coefficients of lift and drag. A tip loss correction is applied to account for the gaps between the finite number of blades (Equation 3.16, Glauert 1983). The sectional axial thrust for each element is calculated and the total axial thrust on the blade is obtained through integration. This gives an initial estimate for C_T, which can be used to solve the quartic function for bypass wake induction factor, b_4, and the cubic function for wake induction factor, a_4, presented in Vogel et al. (2018). The axial and tangential induction

factors are calculated and updated using Equation 3.19 and Equation 3.20 (Chen, 2019).

$$a_{2i} = \frac{(2\sigma_i \mu i(1 - a_{4i}F_i) - F_i\gamma_i) - \sqrt{\gamma_i(F_i^2\gamma_i + 4\frac{\sigma_i\mu_i}{\sin^2\phi}(1 - a_{4i}F_i(1 - F_i))}}{2\frac{\sigma_i\mu_i}{\sin^2\phi}(1 - a_{4i}F_i)} \tag{3.19}$$

$$a'_{2i} = \frac{\sigma_i(C_{Li}\sin\phi_i - C_{Di}\cos\phi_i(1 - a_{2i}))}{4\sin\phi_i\cos\phi_i F_i(1 - a_{2i}F_i) - \sigma_i(C_{Li}\sin\phi_i - C_{Di}\cos\phi_i)(1 - a_{2i})} \tag{3.20}$$

The blade solidity, σ_i, and γ_i and μ_i are given by,

$$\sigma_i = nc_i/2\pi r_i, \tag{3.21}$$

$$\gamma_i = \left(b_4^2 + 2\left(b_4 + a_{4i}F_i\right) - 2a_{4i}^2F_i^2\right), \tag{3.22}$$

$$\mu_i = C_{Li}\cos\phi_i + C_{Di}\sin\phi_i. \tag{3.23}$$

Steps 1 – 4 of the calculation sequence, outlined in Figure 3.8, are repeated. The blade element forces and axial thrust and tangential torque equations are balanced and the axial and tangential induction factors are solved before recalculating the thrust coefficient and induction factors. The axial and tangential induction factors are recalculated and checked for convergence within a relative error of 10^{-6}. A relaxation parameter of 20% old value and 80% new value is implemented when updating the solution. Once the solutions have fully converged, the total axial thrust and tangential torque on the blade can be used to calculate C_P and C_T.

Three rotors designed for blockages of 0.01, 0.16 and 0.314 by Cao et al. (2018) (low and medium) and Schluntz and Willden (2015) (high) were used and one unblocked rotor designed for variable-speed operation (Burton et al., 2011). The hydrofoil used for all blades was the Risø-A1-24 (Wimshurst and Willden, 2016a), with adapted lift/drag coefficient and angle of attack data in Chen et al. (2019). A 20 m diameter rotor was used for all turbines in this chapter.

3.3.3 Turbine Performance Curve and Control Strategy

Using BC-BEMT to solve the blockage-designed blades provides C_P and C_T−TSR curves to characterise the performance of the turbine. At TSR = 0, the rotor is not rotating and therefore, power is not extracted. At very high values of TSR, the rotor is rotating with such a high speed that it acts like a solid disc with no mass transport through the rotor, which leads to no energy extraction. However, there is an optimal Tip Speed Ratio (TSR) the rotor can be operated at. For the 0.01, 0.16 and 0.314 blockage designed blades the optimal operation is at TSR = 5.5, 5.5, and 5 respectively.

The performance of a turbine is dependent on the control strategy, which is an important power limiting operational aspect of turbines. The three main strategies for turbine control are stall regulation (fixed-speed, fixed-pitch (FSFP)), fixed-speed, variable pitch (FSVP), or variable-speed, variable-pitch (VSVP), where the speed refers to rotational speed and pitch refers to the blade pitch angle (Anderson, 2020). FSFP turbines are mechanically simpler compared to variable operations, however, they compromise on optimum hydrodynamic performance. VSVP operation offers a greater hydrodynamic performance and has been widely adopted for large diameter wind turbines. VSVP operation is applied for the turbines modelled in this thesis because they are also commonly used in practice for large diameter tidal turbines (13 m – 21 m) (Adcock et al., 2021). A power curve, that describes the power a turbine generates at different flow speeds, can be derived from the C_P−TSR data. For variable speed operation, the rotor speed, Ω, must vary with the inflow speed, leading to the cubic relationship presented in Figure 3.9.

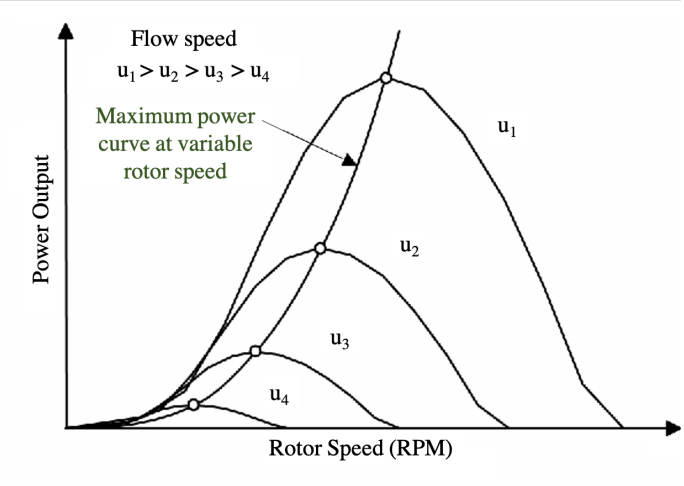

Figure 3.9: Power output against rotor speed for various flow speeds demonstrating the maximum power for variable speed operation (adapted from Zhang et al. 2008).

When operating at a constant TSR, the ratio between inflow speed and rotor speed is fixed, so the cubic relationship presented in Figure 3.9 is the same for power against inflow speed. Therefore, part of the performance curve of the VSVP turbine can be defined using this relationship. Figure 3.10 presents the performance curves of a VSVP turbine under two capping strategies: power capping and combined power and thrust capping. The power capped performance curve (black, solid) is characterised by the cut-in speed, cut-out speed and rated speed. Below the cut-in speed no power is generated. Between the cut-in and rated speed, the performance curve can be defined according to the 'maximum power' curve illustrated in Figure 3.9. Above rated speed and below cut-off speed, the turbine operates at a rated power and so power production is constant (i.e., power is being capped). Above cut-off speed the turbine shuts down and no power is produced.

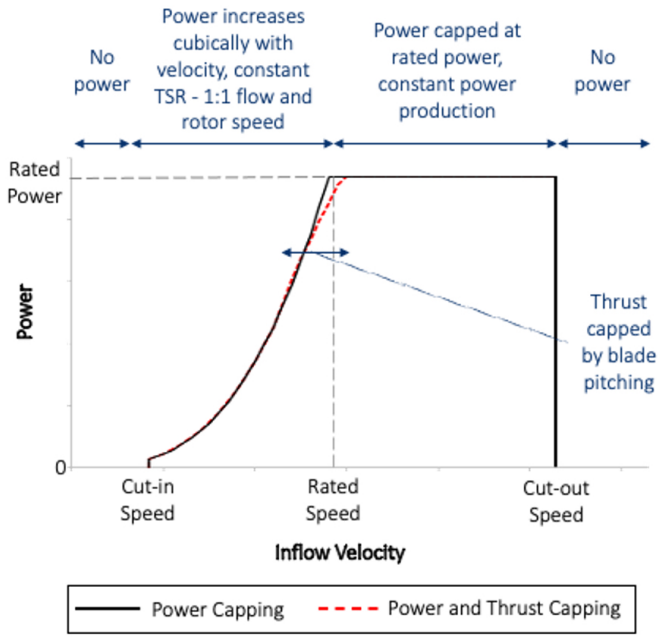

Figure 3.10: Performance curve of a variable-speed, variable-pitch operated turbine with power capping (black, solid) and combined power and thrust capping (red, dashed).

The cut-in, cut-out and rated speeds are usually defined by manufacturers. The cut-in speed is chosen on the basis that the turbine should not operate at very low flow velocities because the turbine will turn slowly for long periods of time without producing much power whilst contributing to the wearing of turbine mechanisms, which is not economically beneficial. The cut-out speed is usually a protective strategy for the turbine in periods of high velocities and extreme loading. The rated speed is chosen to cap power and ensure that an energy storage system is not oversized to accommodate peak spring-tide velocities that lead to spikes in power over short-periods of time, resulting in cost savings. Capacity factor is related to the rated speed of a turbine and is defined as the ratio between the actual power produced by an array to the power that could be produced if turbines constantly operated at rated power. The choice of rated speed for turbines in an array will impact the capacity factor of an array.

A study of 14 horizontal-axis tidal turbines provides a range of values to define a standardised performance curve, proposing the cut-in and rated speeds as a percentage of the maximum flow velocity (% of U_{max}) (Lewis et al., 2021). Figure 3.11a presents the

power and thrust coefficient of the standardised performance curves demonstrating the study's proposal that the cut-in speed should be 30% of rated speed. The rated speed is defined as 46% of U_{max} at the site, based on 4 constituents (M_2, S_2, O_1 and K_1). Rated speed is defined for a low intermittency scenario based on studies of European sites to enable more consistent power with fewer hours of no power.

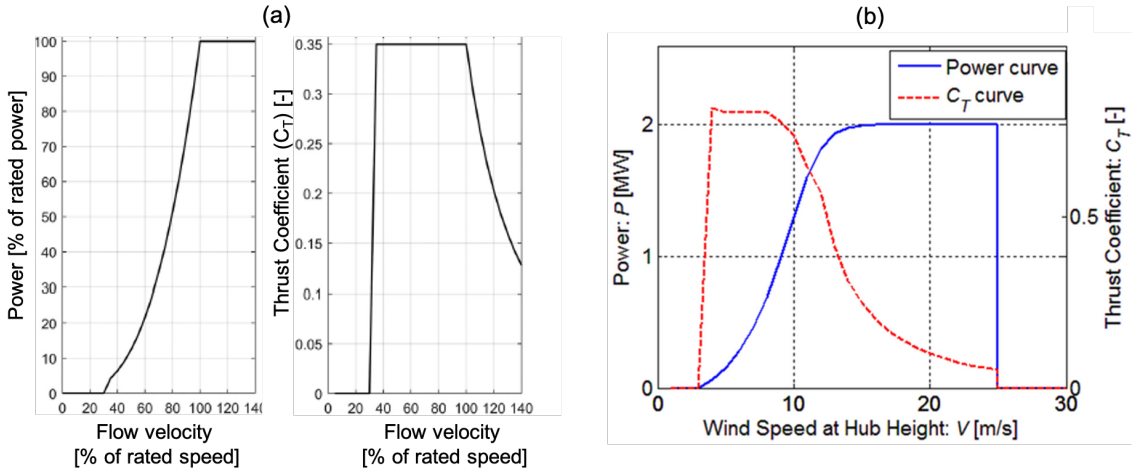

Figure 3.11: Power and thrust coefficient performance curves for (a) a standardised turbine representation, adapted from Lewis et al. (2021), and (b) a real Vestas V80 wind turbine, adapted from Feng and Shen (2015).

In reality, the shape of a performance curve is not as simple as those presented in Figures 3.10 and 3.11a. The graphs presented in Figure 3.11b demonstrate the power and thrust coefficient curves for the Vestas-V80 wind turbine, incorporating the complexities of a real performance curve. However, due to the lack of open-source empirical industrial data available for the performance of tidal turbines in practice, the simplified performance curves outlined in Figures 3.10 and 3.11a are used.

Wang and Adcock (2019) proposed a combined power and thrust capping strategy for bottom-fixed turbines to limit peak thrust and peak power. The size of the support structure diameter, resistance on the flow due to the support structure and the channel's flow velocity are inter-dependent. Therefore, adopting the combined capping strategy can lead to a reduction in support structure diameter and a lower thrust on the flow. For the power and thrust capping performance curve (Figure 3.10 red, dashed line), there is a region where the thrust is capped by pitching the turbine blades at a fixed rotational

speed, reducing the axial induction factor and generating less power at each velocity with respect to power capping (Buck and Garvey, 2015). Once rated power is reached, the performance curve behaves in the same way as the power capping strategy curve because the blades pitch to cap power rather than thrust.

The algorithm for converging the required diameter of a support structure of the turbine based on a combined power and thrust capping strategy is outlined in Figure 3.12. The initial conditions for the combined capping strategy are the conditions outlined in Vennell (2010) Appendix A3. The governing equation (Equation 3.1) is then solved without any capping strategy or consideration of support structure to obtain data for flow rate, power and thrust. From the peak power and thrust data, the capped threshold values are calculated. Thrust was capped at 80% of uncapped peak thrust, as in Wang and Adcock (2018, 2019), and power was capped at the rated power, determined by rated speed. A two-part iteration to converge the diameter of the support structure follows.

For the first iteration, the thrust of the turbine is calculated based on the velocity data and an initial estimate for the support structure diameter. The bending moment and required diameter for the estimated turbine thrust is calculated. The drag due to the support structure is then added to the total thrust at every iteration and the diameter of the support structure is recalculated, leading to a small increase with each iteration. Once the increase in support structure diameter is within 0.001 m, the first iteration converges. The support structure diameter is then incorporated into the channel model and run until steady state without capping.

The second iteration considers the effect of the support structure on the flow, which is not accounted for in the first iteration. The power at each Runge-Kutta 4^{th} order method step is evaluated against the threshold value and if the threshold is exceeded, power is capped to the threshold value (P_{cap}). The thrust is calculated and evaluated against the threshold value and similarly if the threshold is exceeded, thrust is capped to the threshold value (T_{cap}). The velocity data is then fed back into the first iteration

and the process continues from there until the flow rate between each of the iteration processes is within 0.1%. At that point, the process is considered converged and the final calculation of the support structure diameter from iteration 1 is the fully converged size of the support structure.

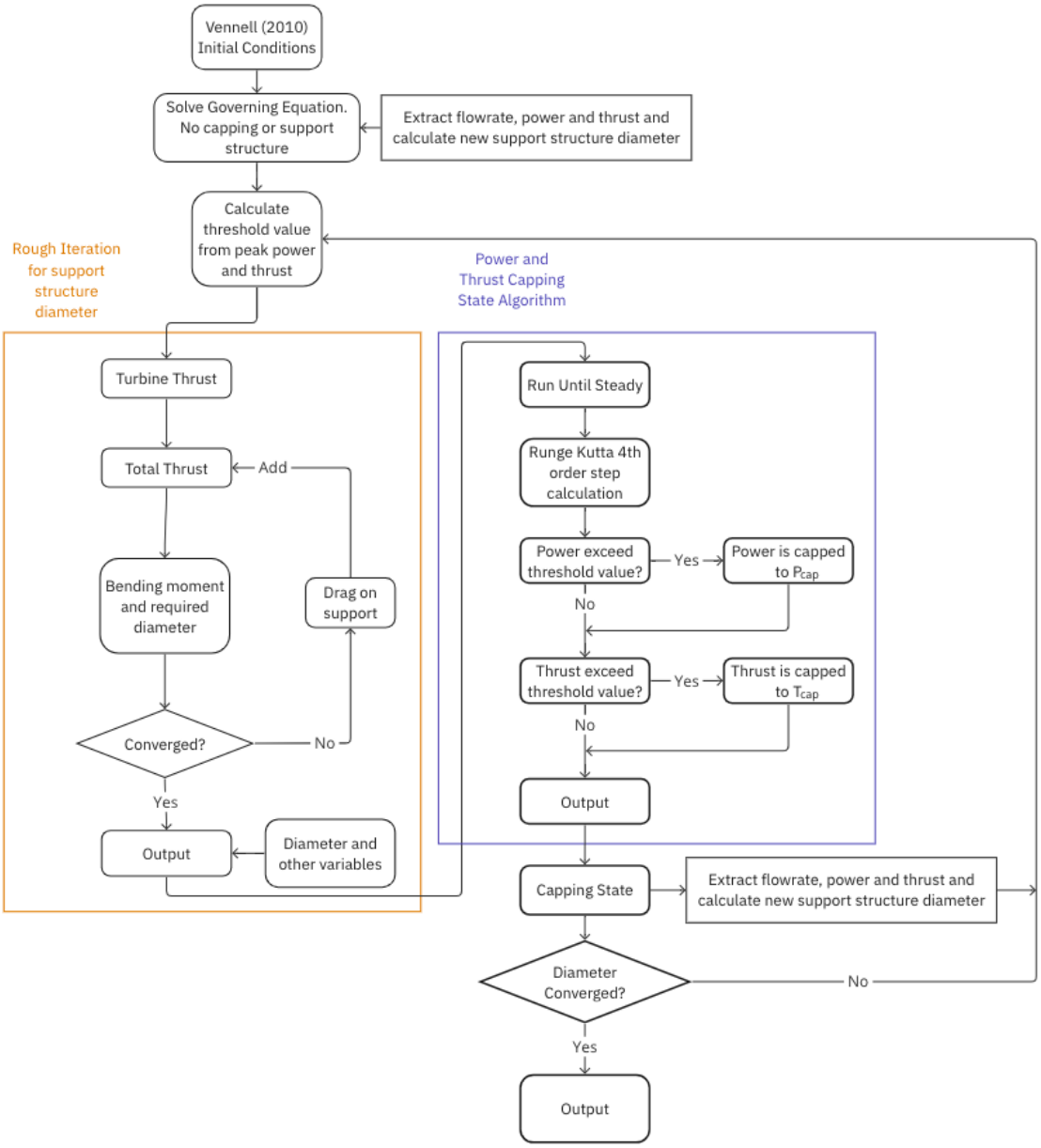

Figure 3.12: Combined power and thrust capping calculation sequence, adapted from (Wang and Adcock, 2018).

The support structure thrust, F_S, is calculated by,

$$F_S = \frac{1}{2}\rho C_{D,S} L_S D_S u^2, \tag{3.24}$$

where the drag coefficient of the support structure is $C_{D,S} = 1.2$, proposed by Muchala and Willden (2017) for a cylindrical support structure over a wide range of Reynold's numbers, length of the support structure is $L_S = 15$ m to allow for reasonable clearance and the initial estimate for diameter is $D_S = 3$ m. The converging support structure diameter is calculated by assuming the maximum allowable stress, σ_{max}, of the support structure is 250 MPa (based on an estimation for tensile strength of steel) (Wang and Adcock, 2018, 2019). The maximum allowable stress is related to the bending moment applied to the support, M_Z, and the sectional modulus, Z_e, as

$$\sigma_{max} = \frac{M_Z}{Z_e}. \tag{3.25}$$

The sectional modulus is calculated on the assumption of a hollow cylinder with thickness of 5% of the column diameter and the bending moment is assumed to act perpendicularly at the top of the beam, as per Wang and Adcock (2018, 2019).

Both capping strategies are investigated in this chapter. For the combined capping strategy the support structure diameter is optimised to withstand the capped thrust and for the power capping strategy, cases are modelled without a support structure.

3.3.4 Wakes

The theoretical studies on the effect of blockage on the flow through the turbine and the bypass flow have been outlined in Section 2.1. In some instances the local flow accelerates due to turbines being closely spaced in the lateral direction and confinement of flow due to the shallow depth (i.e., local blockage), which leads to individual turbine power increasing (Ouro and Nishino, 2021). Stallard et al. (2013) and Noble et al. (2020) have conducted experiments demonstrating this effect.

Due to the extraction of axial momentum across the rotor plane of a tidal stream turbine a wake develops downstream of the turbine that can be categorised into near-wake and far-wake regions. There is a velocity reduction induced by the extraction of momentum behind the turbine compared to the upstream flow, which is defined as a velocity deficit (Jump et al., 2020). In instances where turbines are positioned at a sufficient

distance downstream of their upstream counterparts, mixing of the flow in the wake of the upstream turbine and accelerating by-passing flow will occur and velocity will return to the uniform value upstream of the turbine. Tip vortices form on rotating turbine blades and can shed into the downstream wake of the turbines, adding further complexity to characterising the wake. The turbulence characteristics of flow can be described in terms of turbulence intensity, defined as the root-mean-square of the standard deviation of the flow velocity divided by the mean, and the turbulence length scale, which describes the size of eddies. Turbulence also affects wake generation and characterisation, and can aid wake recovery.

The combined channel model proposed by Vennell (2010), adopted in this chapter, does not account for turbulence in wake mixing and assumes the distance between rows is large enough for mixing to have occurred and the velocity onset to the downstream row to have returned to the free stream velocity. However, the space required for wake recovery between longitudinal rows of turbines is not practical for a real array because tidal stream developments are constrained to areas of strong current and sites leased by the The Crown Estate and The Crown Estate Scotland. Applying a full wake-recovery assumption to real tidal array designs poses challenges, making the ideal spacing for wake recovery less feasible. Myers et al. (2011) highlight the negative wake interactions and increased velocity deficits of closely packed turbines, which underscores a concern for developers aiming to maximise lease sites through densely arranged rows in the longitudinal direction. Consequently, if the velocity deficit in the wake of a turbine, which has not fully recovered before the next downstream row, is not considered when assessing the power produced by an array then the resource will be overestimated because wakes can detrimentally affect the performance of turbines.

The inclusion of wakes of adjacent turbines, and being bounded by the free surface and seabed, increases the velocity of the bypass flow around a turbine and will also impact the velocity deficit compared to a turbine in unbounded flow (Stallard et al., 2013). The

rate of mixing and length scales of the wake-recovery process will be impacted due to the effects on the bypass and wake flow velocities. This affects the performance of a tidal turbine (i.e., power produced) at the micro-scale (turbine-to-turbine) (Ouro and Nishino, 2021). Multiple experimental studies have been conducted to investigate the downstream flow of an individual turbine, modelled either as a mechanical rotor (Myers and Bahaj, 2009, Maganga et al., 2010) or a static porous disc (Bahaj et al., 2007, Sun et al., 2008). The interaction of wakes between multiple tidal turbines was experimentally investigated by Stallard et al. (2013, 2015). Stallard et al. (2015) demonstrated the velocity deficit in the wake of an individual turbine in shallow turbulent flow becomes self-similar and 2-D at 8 rotor diameters or greater downstream. The study only considers a few rows of turbines and might not be accurate for large arrays.

Stansby and Stallard (2016) suggest a superimposition method of velocity deficits, similar to what has been applied to wind turbine wakes with self-similar flow (Larsen, 2009). They give Equation 3.26 to calculate centre-line velocity deficit, ΔU_{max}, from the upstream uniform velocity, U_0, for a turbine with diameter, D, at a specified downstream distance, x. The equation shows good agreement with results in Stallard et al. (2015) within 4 to 8 rotor diameters downstream.

$$\frac{\Delta U_{max}}{U_0} = -0.216 + 0.8639/\sqrt{x/D}. \tag{3.26}$$

Stansby and Stallard (2016) proposed blockage correction factors to correct the velocity at each row of turbines and velocity deficits are superimposed to account for wake superimposition. The method can be demonstrated on three rows of turbines where the upstream turbine is row 1 and the furthest downstream turbine is row 3. The velocity of the flow onset to turbines in row 1 is denoted as U_0 with a volume flux of q_0 through the row. The flux downstream of row 1, q_1, is calculated based on the velocity deficit (Equation 3.26). The blockage correction factor is defined as q_0/q_1, where $q_1 < q_0$, and applied to give the velocity onset to row 2 as $U_0 q_0/q_1$. Velocity deficits are superimposed to give the flux q_2 at row 3 and the velocity onset to row 2 is multiplied by the blockage

correction factor q_0/q_2, where $q_2 < q_0$, to give the onset velocity to row 3.

Understanding the structure, expansion and recovery of wakes is important to ensure an accurate resource assessment. Wakes are dependent on turbulence intensity, alignment, blockage, row spacing and array layouts and their complexity is difficult to capture with the method presented by Stansby and Stallard (2016). They state studies of single turbines, in wind and tidal streams, indicate velocity deficit in the wake of a turbine is highly dependent on turbine thrust. Despite the drawbacks of the method, it is necessary to consider wake effects on the flow velocity, and subsequently on power, in some way because they will have a significant impact on a resource assessment and it is a simple and effective method to implement at this stage.

3.4 Results and Discussion

For the two idealised channels modelled in this chapter, a shallow channel and tidal strait, the head difference was calculated with constituent data from four UK sites with FF = 0.06 and 0.05 (low) and FF = 0.22 and 0.15 (high) to span the semi-diurnal classification range (Table 3.13). For the high FF cases, 2, 4 and 8 constituents were modelled and for the low FF cases, 2 and 4 constituents were modelled due to the availability of data from the literature. Four rotor designs were simulated for each case: three designed for 0.01, 0.16 and 0.314 blockages and one designed for unblocked conditions. Turbines were operated at the TSR corresponding to optimum C_P from BC-BEMT C_P vs TSR derived curves. Three blockage cases were defined based on the rotors designed for specific blockages. For each blockage, 1, 3 and 5 row arrays were simulated. The channel geometry, blockage and number of rows defined the number of turbines in each case. For each case, power capping and combined power and thrust capping were simulated. The initial simulations were run without wake effects. Wake effects were accounted for by applying a blockage correction factor and deficit to the velocity onset to each row of turbines, spaced 8 rotor diameters downstream for comparison.

3.4.1 Nodal Cycle, Form Factor and Constituents

To investigate long-term variability of tidal stream energy due to the nodal cycle, an analysis of average annual energy production (AEP) spanning 18.6 years was conducted. Figure 3.13 presents the percentage change in AEP with respect to the mean over 18.6 years of a 5 row array, with 0.314 blockage in a shallow channel, modelled with 2, 4 and 8 high FF constituents. The maximum variation is up to 6.42% with 8 constituents. In the year with the lowest AEP (2005) the array generates 88% of the energy produced in 2016, which is the year with the highest AEP. This accounts for a substantial difference of 1.36 GWh/year. The variation when modelling with 2 and 4 constituents is up to 5.37% and 5.61%, respectively. The maximum variation decreases with decreasing numbers of constituents because, when multiple constituents are in phase, there is a peak in velocity, and the maximum velocity is greater with 8 constituents than with 2 constituents.

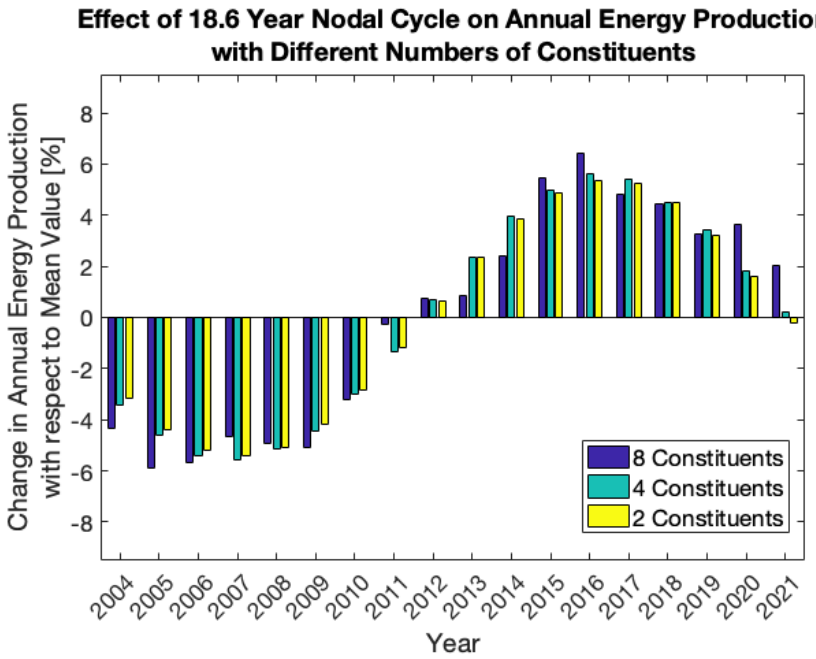

Figure 3.13: Annual energy production over the nodal cycle with 2, 4 or 8 high form factor constituents for an array with 5 rows and 0.314 blockage in a drag dominated shallow channel.

The maximum variation diminishes with a decrease in the number of turbines, observed in both high and low FF constituent data scenarios within the shallow channel. Figure 3.14 illustrates this trend for 1, 3, and 5 rows of turbines in a shallow channel, modelled

with 4 low FF constituents and 0.16 blockage. Given that the shallow channel is drag-dominated, a smaller number of turbines, relative to the friction in the channel, exerts a less significant impact on the flow, and consequently the power.

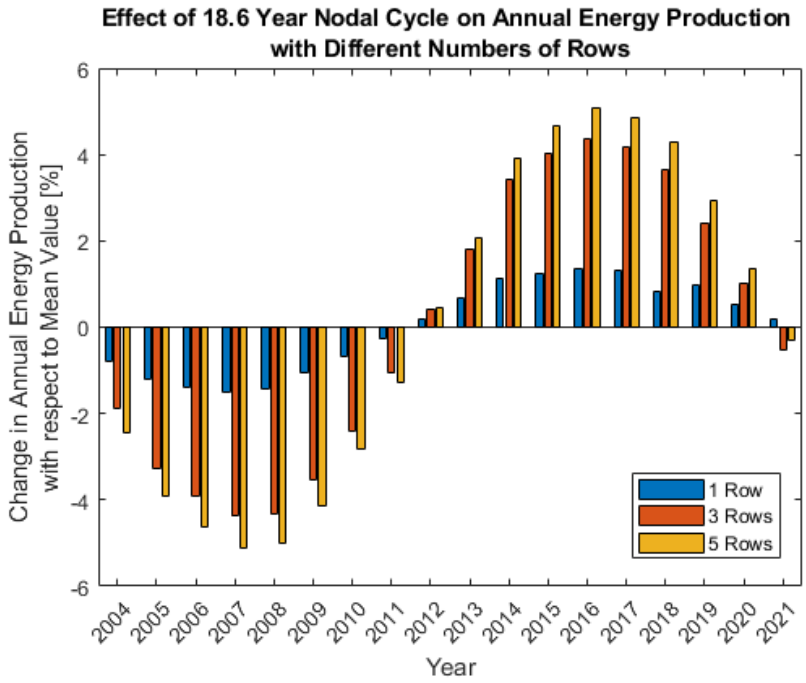

Figure 3.14: Annual energy production over the nodal cycle with 4 low form factor constituents for an array with 1, 3 or 5 rows and 0.16 blockage in a drag dominated shallow channel.

Figure 3.15 demonstrates the variation in AEP for a 5 row array with the three different blockages in a tidal strait, modelled with 8 high FF constituents. The change in AEP from the mean value over 18.6 years is less significant than the shallow channel case (Figure 3.13), with a maximum of 1.97% greater than the mean in 2016 and 2.39% less than the mean in 2005. For a blockage of 0.01, which has fewer turbines per row than the higher blockage case, the maximum variation from the mean increases to 3.83%, demonstrating the opposite effect on power variation over the nodal cycle with decreasing number of turbines as in the shallow channel (Figure 3.14). Figure 3.16 presents the same 5-row array in a tidal strait, but modelled with low FF constituents. The graph illustrates a notable reduction in variation with increasing blockage, aligning with observations from high FF tidal strait results. For 0.01 blockage, AEP exhibits variations of up to 8.77% from the mean, which diminish to 5.41% for 0.314 blockage in the same year, 2016. In

each blockage scenario in the tidal strait, the maximum percentage change from the mean AEP increases with fewer rows or decreasing blockage, which both relate to fewer turbines. The relative change between cases with different numbers of turbines (based on rows or blockage) is less significant in the inertia-dominated tidal strait compared to the drag-dominated shallow channel. The drag-dominated channel experiences more significant relative changes with more turbines present due to the large background resistance present in the channel.

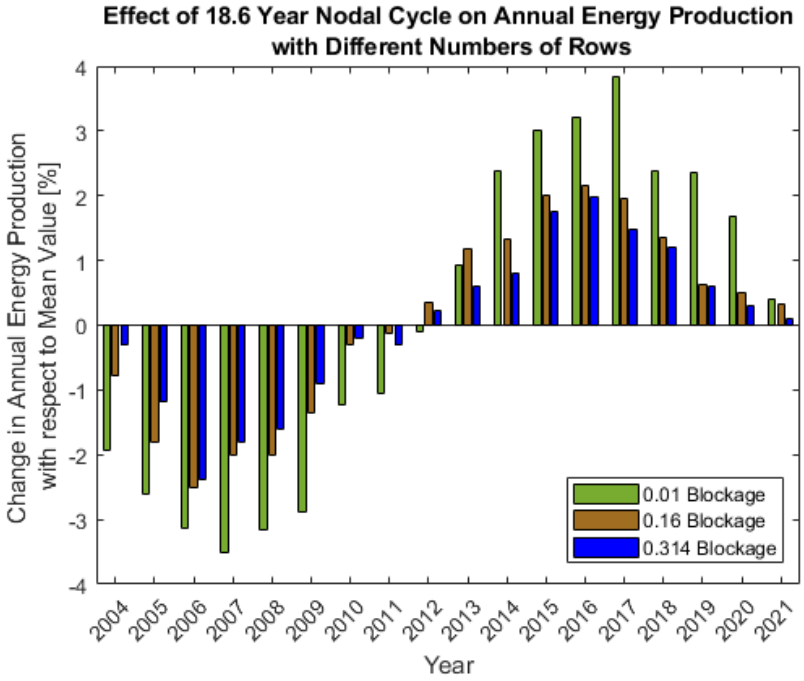

Figure 3.15: Annual energy production over the nodal cycle for an array with 5 rows, 4 high form factor constituents with 0.01, 0.16 or 0.314 blockage in an inertia dominated tidal strait.

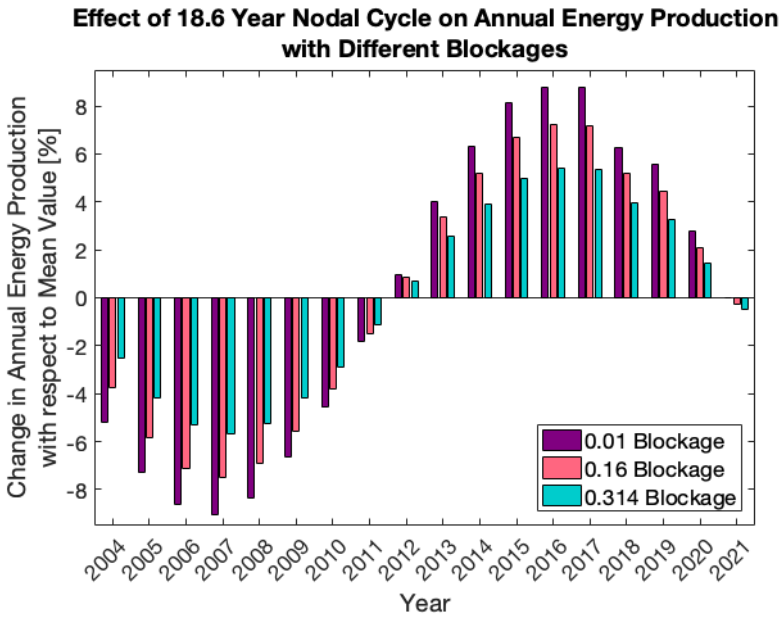

Figure 3.16: Annual energy production over the nodal cycle for an array with 5 rows, 4 low form factor constituents with 0.01, 0.16 or 0.314 blockage in an inertia dominated tidal strait.

The results indicate that assessing the resource in one particular year could lead to a significant overestimation or underestimation, if the whole nodal cycle is not considered. The dynamic balance is shown to be an important parameter for indicating how the maximum variation from the mean increases or decreases with additional turbines. Understanding the trend over the 18.6-year cycle and recognising the years in which the resource deviates greatest from the mean (2005 – 2007 below, 2016 – 17 above) in a low order model can inform findings from higher order models to ensure they do not have to be run for the full nodal cycle.

The prevalence of semi-diurnal sites in the UK and study of sites at each end of the semi-diurnal FF range emphasises the importance of understanding how quantifying the resource is affected by the number of constituents used for modelling. For high FF data, the number of constituents modelled has a more significant impact on the velocity than the low FF site. Peak velocity is up to 0.32 m/s and 0.19 m/s greater with 8 high FF constituents than with 2 constituents for the tidal strait and shallow channel across all arrays. However, the difference between 4 and 2 constituents is only up to 0.01 m/s. The high FF constituent data, presented in Table 3.3, indicates that whilst M_2 and S_2

constituents dominate, K_2, M_4, MU_2 and N_2 constituents are also significant and there is a larger difference in amplitude and phase for constituents between the two high FF sites. The K_1 and O_1 constituents are diurnal constituents, therefore, they are smaller at semi-diurnal classified sites and there is very little amplitude or phase difference between the two sites, therefore the difference between the 2 and 4 constituent results do not vary as significantly for the high FF data. The peak velocity occurs when constituents are in phase and adding more constituents, with greater phase difference, leads to a greater difference in velocity. The low FF sites are dominated by the M_2 and S_2 constituents, therefore, the difference between peak velocity for 2 or 4 constituents is only 0.01 m/s because the K_1 and O_1 constituents are much smaller in comparison (Table 3.4).

Modelling sites on the lower end of the semi-diurnal FF range with 2 additional diurnal constituents does not have a great impact on the resource assessment because they have a relatively small effect on velocity and subsequent power output. However, when modelling with higher FF data, additional constituents impact velocity, power output and variability over the nodal cycle. Constituents with greater amplitude and phase differences for calculating the head difference are critical for accurately representing the channel.

3.4.2 Maximum Permissible Change in Velocity

The presence of turbines in a channel can lead to a reduction in peak flow velocity compared to an ambient case with no turbines. The reduced flow velocity from the peak value, in the absence of an array, can be constrained in an effort to minimise the environmental impact of tidal arrays. A study of the hydrodynamic impact on the morphology at Ramsey Sound indicated the reduction in velocity and subsequent reduction of bed shear stress, which is proportional to the square of velocity, leads to sediment accumulation and deposition up to 16 km away from the array (Haverson et al., 2018). Significant changes in sediment transport can make benthic habitats unfavourable for native species, leading to their burial or displacement.

Tables 3.5 and 3.6 present the percentage change in maximum velocity for cases with different blockages, rows, constituents (high FF) and channel geometries with respect to the ambient case. Permissible reductions of 10% and 20% from the peak velocities in an ambient case were considered and red cells indicate exceeded conditions.

Table 3.5: Percentage change in maximum velocity for high form factor constituent scenarios with respect to the ambient case. Values exceeding 10% reduction in peak flow velocity in red and permissible cases in green.

		Change in Maximum Velocity [%]					
		Tidal Strait			Shallow Channel		
10% Permissible Change		2 Constituents	4 Constituents	8 Constituents	2 Constituents	4 Constituents	8 Constituents
Blockage = 0.01	1 Row	0.2	0.2	0.2	0.6	0.6	0.6
	3 Rows	0.5	0.5	0.5	1.9	1.9	1.9
	5 Rows	0.8	0.8	3.1	3.1	3.1	3.1
Blockage = 0.16	1 Row	3.4	3.4	3.2	11.4	11.3	11.4
	3 Rows	9.3	9.4	9.3	25.9	25.8	25.9
	5 Rows	14.2	14.2	14.0	35.1	34.8	35.0
Blockage = 0.314	1 Row	9.6	9.7	9.6	26.6	26.4	26.5
	3 Rows	22.4	22.7	22.0	47.0	46.7	47.0
	5 Rows	30.9	31.2	30.3	56.4	56.2	56.4

Based on the results outlined in Tables 3.5 and 3.6, the maximum permissible change is much less restrictive for the tidal strait, with 67% of proposed layouts not reducing the maximum velocity in the channel by more than 10% and 85% for 20% permissible change. Note that the number of turbines in the 0.16 blockage, 5 row array is greater than 1 row at 0.314 blockage. Therefore, the former exceeds the 10% limit while the latter does not. For the shallow channel, more than 50% of the proposed arrays are not within the permissible change in flow rate restrictions. The tidal strait is inertia dominated, therefore the flow can withstand more turbines without affecting the peak

velocity substantially, compared to the shallow channel, which already has significant background friction because it is drag dominated. The results outlined in Vennell (2010) corroborate this, with 1 row of turbines in the shallow channel reducing flow velocity by 26% compared to a 5% reduction in the tidal strait with 0.25 blockage.

Table 3.6: Percentage change in maximum velocity for high form factor constituent scenarios with respect to the ambient case. Values exceeding 20% reduction in peak flow velocity in red and permissible cases in green.

		Change in Maximum Velocity [%]					
		Tidal Strait			Shallow Channel		
20% Permissible Change		2 Constituents	4 Constituents	8 Constituents	2 Constituents	4 Constituents	8 Constituents
Blockage = 0.01	1 Row	0.2	0.2	0.2	0.6	0.6	0.6
	3 Rows	0.5	0.5	0.5	1.9	1.9	1.9
	5 Rows	0.8	0.8	3.1	3.1	3.1	3.1
Blockage = 0.16	1 Row	3.4	3.4	3.2	11.4	11.3	11.4
	3 Rows	9.3	9.4	9.3	25.9	25.8	25.9
	5 Rows	14.2	14.2	14.0	35.1	34.8	35.0
Blockage = 0.314	1 Row	9.6	9.7	9.6	26.6	26.4	26.5
	3 Rows	22.4	22.7	22.0	47.0	46.7	47.0
	5 Rows	30.9	31.2	30.3	56.4	56.2	56.4

Tables 3.7 and 3.8 present the percentage change in maximum velocities but for cases modelled with low FF constituents, with red cells indicating exceeded conditions for 10% and 20% reduction in peak velocity, respectively. The feasibility of sites for both channels are similar with high or low FF data. For the shallow channel with low FF data, (Tables 3.7 and 3.8), 78% and 67% of arrays are unfeasible for 10% and 20% permissible change, which is one case scenario extra for each, compared to the high FF cases (Tables 3.5 and 3.6). The feasibility of sites remains the same for the tidal strait regardless of FF.

Table 3.7: Percentage change in maximum velocity for low form factor constituent scenarios with respect to the ambient case. Values exceeding 10% reduction in peak flow velocity in red and permissible cases in green.

		Change in Maximum Velocity [%]			
		Tidal Strait		Shallow Channel	
10% Permissible Change		2 Constituents	4 Constituents	2 Constituents	4 Constituents
Blockage = 0.01	1 Row	0.2	0.2	2.6	2.1
	3 Rows	0.5	0.5	6.6	6.6
	5 Rows	0.9	0.9	10.3	10.3
Blockage = 0.16	1 Row	3.5	3.5	29.9	29.7
	3 Rows	9.4	9.4	50.6	50.3
	5 Rows	14.3	14.3	59.8	59.4
Blockage = 0.314	1 Row	9.7	9.7	51.4	51.1
	3 Rows	22.5	22.9	69.6	68.9
	5 Rows	30.6	30.8	76.0	75.3

These cases demonstrate that a maximum permissible change in velocity could significantly restrict array developments due to environmental impact, particularly for high blockage arrays. The restriction of maximum permissible change in velocity will be a limiting factor on the accessible resource, although, currently there is no regulatory basis for the limitation (Coles et al., 2021). In reality, the leased areas for development will be a greater limiting factor on the number of rows in an array due to space constraints, which affects the reduction of peak flow rate.

Table 3.8: Percentage change in maximum velocity for low form factor constituent scenarios with respect to the ambient case. Values exceeding 20% reduction in peak flow velocity in red and permissible cases in green.

		Change in Maximum Velocity [%]			
		Tidal Strait		Shallow Channel	
20% Permissible Change		2 Constituents	4 Constituents	2 Constituents	4 Constituents
Blockage = 0.01	1 Row	0.2	0.2	2.6	2.1
	3 Rows	0.5	0.5	6.6	6.6
	5 Rows	0.9	0.9	10.3	10.3
Blockage = 0.16	1 Row	3.5	3.5	29.9	29.7
	3 Rows	9.4	9.4	50.6	50.3
	5 Rows	14.3	14.3	59.8	59.4
Blockage = 0.314	1 Row	9.7	9.7	51.4	51.1
	3 Rows	22.5	22.9	69.6	68.9
	5 Rows	30.6	30.8	76.0	75.3

There are other factors that may have a greater environmental impact that need to be considered for tidal development. An example across the cases presented in this chapter is the high blockage scenario ($B = 0.314$), which increases the risk of collisions with marine life due to such a large fraction of the channel's CSA being occupied by rotors (Polagye et al., 2011). Additionally, development of low turbulence sites is more desirable for tidal energy because it reduces unsteady loads. Turbulence intensity indicates the magnitude of flow velocity fluctuations. Typically, turbulence intensity in the boundary layer of a tidal stream (5 m from the seabed) is 12 – 13% streamwise and 7 – 8% transverse/vertically (Milne et al., 2013). An increase in turbulence intensity can reduce the velocity deficit in the near-wake region of a turbine and reduce the evolution of vortices in high turbulent intensity environments. However, it can also have a significant effect on the loading and performance of turbines (Nuernberg and Tao, 2018).

Therefore, the impact of array deployments on turbulence intensity could be considered as a limiting factor on the size of arrays for environmental reasons. Environmental impact assessments (EIA) are beyond the scope of this thesis, but the potential negative impact on the environment from tidal stream energy extraction is important to consider and has been the focus of other studies (Polagye et al., 2011, Goward Brown et al., 2017, De Dominicis et al., 2018, Haverson et al., 2018). Future research has the potential to systematically incorporate restrictions that limit environmental impacts into resource assessments, once regulatory guidance is clearer.

3.4.3 Rotor Design

An unblocked rotor design was compared to the performance of blockage designed blades. For the highest blockage ($B = 0.314$) the average annual energy density, defined as the average annual energy over the nodal cycle divided by the rotor swept area, increased by up to 41% in the tidal strait and 34% in the shallow channel, when using a blockage designed blade. At a low blockage ($B = 0.01$) the percentage increase in energy density is much less significant with up to 3% increase in the tidal strait and up to 4% for the shallow channel.

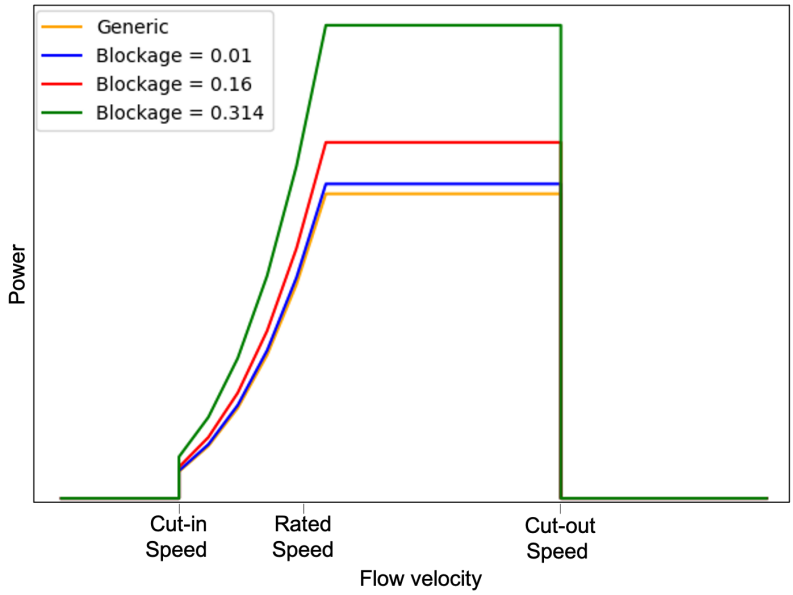

Figure 3.17: Performance curves of the 0.01, 0.16, 0.314 blockage designed blades and an unblocked blade design for the same rated, cut-in and cut-out speeds.

Rotors designed with blockage considerations can enhance the power output of arrays compared to rotors without blockage considerations, operating under the same conditions. Figure 3.17 presents an example of performance curves for the four blade designs, C_P values according to BC-BEMT, in agreement with Chen (2019) for the blockage-designed blades. The increase in performance is significant in higher blockage scenarios because the percentage difference in the coefficient of power between the 0.314 blockage designed blade compared to the unblocked blade is 35%. For 0.01 blockage, the coefficients of power have a percentage difference of 3%. Blockage is significant in tidal streams compared to wind, where flow is effectively unconstrained. Therefore, designing blades for specific blockages in tidal stream energy is an advantage for harnessing the resource.

BC-BEMT allows the performance of rotor designs to be studied but it has limitations. The incorporation of Glauert's (Glauert, 1983) tip correction does not account for all losses near the blade tip due to spanwise flows, and empirical corrections to the flow are dependent on blockage and rotor design. BC-BEMT cannot predict the performance of turbines in extreme operating conditions, high TSR and high and low pitch angles, because it does not consider stall delay, and propeller and turbulent wake states of turbines. However, BC-BEMT is a more realistic alternative to ADT, allowing turbine specifications and operation to be studied (Chen et al., 2019).

3.4.4 Performance Curve Characteristics

The use of a VSVP power curve for turbine performance representation necessitates the definition cut-in, cut-out and rated speeds. Investigating the effect of defining these points, based on a study of a standardised power curve by Lewis et al. (2021), on the resource is important to consider.

A Random Forest (RF) model was employed to evaluate the significance of cut-in, cut-out, rated speeds, and the number of turbines on an array's AEP. In RF modeling, the outcomes (in this instance, AEP) are predicted based on a set of inputs, and the im-

portance of each input is determined by measuring the error between the prediction and the true outcome after permuting the inputs, as described in Molnar (2021). If the error increases after permutation, it indicates the model relied on that input for its predictions, therefore it is important to the outcome and will have a higher importance estimate. The importance estimates have been normalised to range between 0 and 1, where 0 is least important and 1 is most.

To work well, the RF Model requires continuous input data and a realistic range. The input range of performance curve characteristics were defined as percentages of the maximum velocity at the modelled sites, based on 4 constituents (M_2, S_2, K_1, O_1), following the standardised power curve method (Lewis et al., 2021). For Figure 3.18, the range of each speed was kept the same size, 25%. The number of turbines as a predictor is not strictly a continuous data set. However, the number of turbines is defined by the number of rows and blockage, giving a non-uniform and wide enough range to be compatible.

In Figure 3.18, the number of turbines has the highest importance estimate, because the model heavily relies on this predictor to predict the AEP of the array. The indication that the number of turbines is an important parameter affecting the output of an array is realistic and provides confidence in the model. Rated speed has the second highest importance estimate. It dictates the rated power of a turbine and changing its value would have a large impact on the AEP of an array because it affects a wide range of velocities onset to the turbine and the subsequent power produced. The cut-in and cut-out speeds have relatively low importance estimates suggesting they are not important when predicting the AEP of an array.

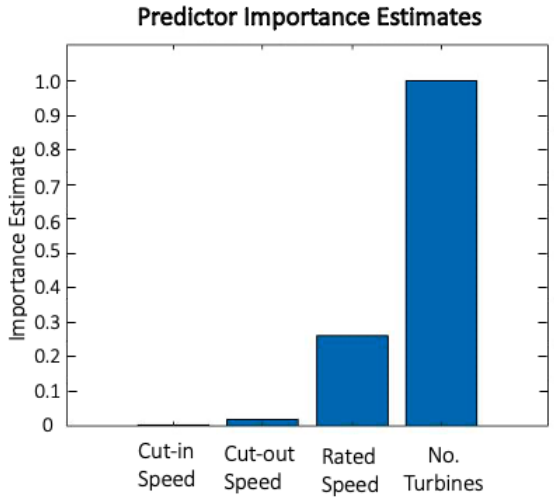

Figure 3.18: Random Forest model importance estimates for cut-in speed (5-30% of U_{max}), cut-out speed (65-90% of U_{max}), rated speed (35-60% of U_{max}) and number of turbines (1-50).

The same inputs were used to test the effect of range size on the results (Figure 3.19). The ranges were kept the same except for the rated speed, which was reduced to a 5% range.

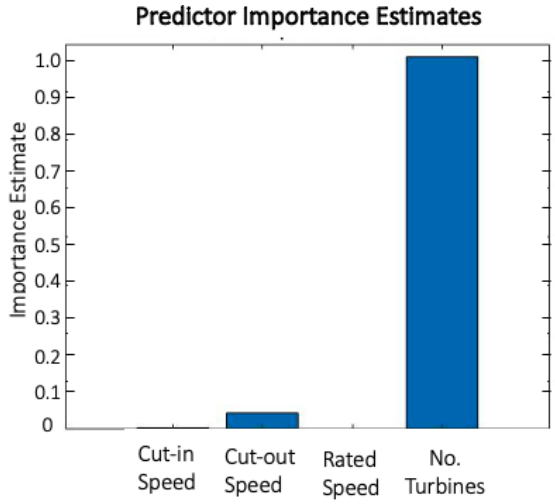

Figure 3.19: Random Forest model importance estimates for cut-in speed (5-30% of U_{max}), cut-out speed (65-90% of U_{max}), rated speed (45-50% of U_{max}) and number of turbines (1-50).

The reduced range for rated speed resulted in a significant reduction in the importance estimate, to almost zero. This is realistic because it is unlikely that any choice of rated speed within a small range will change the overall array output at this scale. The range provided for rated speed for the case presented in Figure 3.18 is a more reasonable choice for turbine specifications. Hence the indication that rated speed is the most

important performance curve characteristic is valid.

To ensure the observations predicted by the RF model were accurate, the correlation coefficient between the models predicted and actual outcomes was calculated, giving a 90% correlation. A regression method was also used to determine the importance of the same parameters affecting the resource to compare with the Random Forest model results. The order of importance estimates of the predictors were in agreement for both methods. A RF model is most appropriate to use to study importance estimates, instead of a regression model, when a large number of inputs (four or more) are considered or inputs are interrelated.

The outcome of the RF modelling indicated the choice of cut-in and cut-out speeds did not significantly affect the resource, as measured by AEP. However, careful consideration of an appropriate rated speed should be taken. Lewis et al. (2021) provides different values for the definition of rated speed, as a proportion U_{max}, based on energy yield scenarios and sites.

3.4.5 Power Capping and Combined Power and Thrust Capping

Thrust capping has a detrimental effect on power output over a small range of velocities compared to power capping, as illustrated in Figure 3.10, where the combined capping curve exhibits a slight deviation from the power capping curve. However, thrust capping offers the advantage of optimising support structure diameter according to the maximum thrust the turbine will withstand, which only occurs over small periods of time, resulting in cost savings in material usage (Wang and Adcock, 2019). In this study, the support structure diameter is reduced by up to 63% in the shallow channel and up to 23% in the tidal strait.

In this thesis, it is assumed that turbines are always aligned to face the oncoming flow, which is realistic for horizontal axis turbines with the adoption of a yaw mechanism (De Dominicis et al., 2017). However, the effect of yawing and fluctuations in turbulent

velocity are not considered. The effects could increase the peak thrust, which requires blade pitching to cap, thereby affecting turbine performance during thrust capping. Additionally, the model does not consider the sheared velocity profile and subsequent effect of loading on the support structure. Despite these assumptions, the low order model offers valuable insights into the two capping strategies and their impact on resource assessments.

The average annual energy density for 1 row arrays, at all blockages, were within 0.01 MWh/m^2 for power capping and, power and thrust capping scenarios. With the exception of the tidal strait at 0.16 and 0.314 blockages, where the average annual energy density was 0.09 and 0.06 MWh/m^2 greater with the combined capping strategy. However, power capping cases do not include support structure drag. To investigate the impact of the support structure, a case was run where the support structure is modelled with power capping and the initial estimate for the diameter of the support structure (3 m) is assumed. With support structure drag included in power capping, the average annual energy density of power capped cases decreases by 16% compared to the combined capping strategy and 8% compared to the power capping strategy without the inclusion of support structure in the shallow channel, and minimal difference in the tidal strait. Therefore, the annual energy density is greatest for an array that adopts a combined capping strategy (with support structure). Power capping strategies lead to a lower annual energy density and when a support structure is modelled with power capping, the lowest annual energy density is achieved due to the additional drag due to the support structure. The capacity factor decreases up to 2% when power capping compared with combined capping strategies, with the inclusion of the support structure in both.

Whilst combined capping can offer a reduction in material cost, the results demonstrate that the impact on the resource is relatively small. Considering the additional calculations required for thrust capping, when higher order models are being used the

additional computational expense is disproportionately large compared to the impact on assessing the resource (Wang and Adcock, 2019). Additionally, economic limitations on the viable tidal resource are not within the scope of this thesis, thus, the primary advantage of thrust capping is not captured.

The results presented in Section 3.4.1, demonstrating the variation of the resource of the nodal cycle, all include power capping. Capping reduces variability across the nodal cycle because it caps power over short periods of time when velocity peaks due to constituents being in-phase. Without power capping the variation across the nodal cycle would be greater. For combined capping, the optimisation of the support structure diameter through thrust capping limits the reduction of the flow, therefore, the maximum variation in AEP from the mean, over the nodal cycle, decreased when combined capping was adopted.

3.4.6 Wake Effects and Velocity Deficits

The inclusion of wake effects as a velocity deficit to downstream rows decreases capacity factor and energy per swept area of multi-row arrays. The change in average annual energy per swept area for 1 and 5 row arrays decreases by 5%, when flow downstream of each row is assumed to fully mix and recover to the free stream velocity before the next row, and 28% when flow velocity recovery between rows does not take place, for a high FF tidal strait scenario at 0.314 blockage. An 8 diameter separation between rows is assumed for Equation 3.26. In the shallow channel, the change in energy per swept area for 1 and 5 row arrays is 52% (without wakes) and 64% (with wakes). The change in annual energy per swept area for 1 to 5 rows decreases as blockage decreases. This highlights that additional rows in the drag dominated shallow channel has a significant impact on the resource and the inclusion of wake effects enhances this.

Stansby and Stallard (2016) compared the blockage correction and velocity deficit superposition method with experimental results from Stallard et al. (2015) and found root-mean-square errors in the velocity deficit up to 0.0682. Turbulence length scales

and wake interactions are complex, and whilst the method proposed gives an initial insight into the effect of wakes in a low order model, higher order modelling is required to more accurately capture the effects.

3.5 Conclusion

In this chapter, the study of idealised channels in a 0-D model was undertaken to determine how channel characteristics and operational parameters impact the assessment of the resource. The findings indicate dynamic balance is a key parameter affecting tidal dynamics when turbines are present in a channel and therefore, key to resource assessments. The influence of the nodal cycle on the variability of AEP was found to be most significant in a drag dominated channel with increasing blockage, but in an inertia dominated channel the variation from the mean decreased with increasing blockage. Constraints on the maximum permissible reduction in peak flow velocity are more limiting for a drag dominated channel and indicate that high blockage arrays are likely to be unfeasible under such restrictions, which should be carefully considered in array designs. Using turbine blades optimised for a given blockage results in substantial increase in energy yield, compared to using unblocked turbine designs, especially at high blockages. Despite UK sites being characterised as semi-diurnal, the FF within the semi-diurnal range has an effect on the number of constituents that should be modelled. For the calculation of head difference, it is important to consider the amplitude and phase difference of each constituent at the two locations chosen to characterise the site. When constituents have large amplitude and phase differences they have a greater impact on the variability of the resource across the nodal cycle. The modelling of high FF sites with limited constituents, cannot fully capture the variation of the resource as constituents move in and out of phase. This highlights the importance of differentiating sites within the semi-diurnal FF range to determine the appropriate number of constituents for modelling.

The specification of turbines is vital to harness the optimum resource, and rated speed is

the most important performance curve characteristic. The use of an RF model provided confidence in the standardised performance curve method because it gives sufficient consideration for rated speed (Lewis et al., 2021). The choice of cut-in and cut-out speeds can also impact the assessment of resource, although not as much as rated speed according to RF modelling. Adopting the same method for defining the performance curve across all the cases presented in this chapter allows for conclusions from the comparative analysis to be useful, despite the influence of the choice of the characteristic points.

Combined power and thrust capping is a beneficial strategy for savings in support structure and foundation material costs and increases energy per swept area compared to power capping alone, but it is computationally expensive for higher order modelling. Adopting capping strategies decreases the variability of the resource across the nodal cycle. An initial investigation of velocity deficit on multiple row arrays indicated that change in energy per swept area from 1 to 5 rows is significantly increased when accounting for wakes. However, a more detailed study on turbulence and wake effects would need to be undertaken in a higher order model, to ensure a more accurate evaluation of wake effect on the resource.

The use of the 0-D channel model in this chapter has provided valuable insights into how parameters affect the resource. One takeaway is the interrelated nature of these parameters, making the identification of the key individual parameters affecting the resource difficult, whilst highlighting the complexity of resource assessments. As the thesis progresses into 2-D numerical modelling, it acknowledges the introduction of additional complexities necessitating modeling compromises and assumptions. However, the foundational understanding derived from low order modeling allows informed modelling decisions to be made.

Chapter 4

Implications of 2-D Numerical Modelling

Low order modelling has provided useful insights into key parameters affecting resource assessments in Chapter 3, but limits the accurate representation of tidal dynamics and the exploration of real-world constraints on the resource. Transitioning from low order modelling to 2-D modelling of an idealised channel allows the opportunity to explore 2-D modelling techniques and validate the modelling software as an intermediate step between 0-D models of idealised channels and 2-D modelling of a real site.

In this chapter, the idealised channels proposed by Vennell (2010), and modelled in Chapter 3, are replicated using the 2-D shallow water equation model, *Thetis* (Kärnä et al., 2018). The extensions (e.g., combined capping, multiple constituents, nodal-cycle) implemented in Chapter 3 are not modelled in this chapter due to the computational limitations of higher order modelling and the need to explore other parameters that were not possible to investigate in the 0-D model. The details of the 2-D hydrodynamic model, and turbine implementation and representation are outlined in Section 4.1. In Section 4.2, results from the 2-D modelling of the Vennell (2010) idealised channels, with continuous and discrete implementations of turbines, are compared to the literature. Different array layouts are considered in Section 4.3, using the discrete representation of turbines to investigate the impact of row spacing and arrangement of turbines. In Section 4.4, the impact of boundary effects for different domains is highlighted and discussed for an idealised channel.

4.1 2-D Modelling

4.1.1 The *Thetis* Shallow Water Equation Model

The SWE (Saint-Venant equations) describe flow beneath a free surface in a domain where the horizontal scale and wavelength are much greater than the vertical scale (Vallis, 2019). The 2-D SWE are commonly used to capture the leading order physics of

tidal energy sites (Blunden and Bahaj, 2006, O'Rourke et al., 2010, Easton et al., 2012, Adcock et al., 2013). The use of a 2-D depth-averaged model necessitates the assumption of homogeneity in the vertical, in-depth, direction. It requires the shallow fluid layer, described by the equations, to have a constant density and be in a state of hydrostatic equilibrium. These equations are derived by depth-averaging the Navier-Stokes equations, with the flow's motion fully described by the continuity (mass conservation) and conservation of momentum equations.

The non-conservative form of the 2-D non-linear SWE are solved in *Thetis* to account for velocity and elevation variation, which are important when considering large-scale oceanic flows, and the Coriolis effect when modelling real sites. The discretisation approach of the non-conservative form allows terms to be rearranged outside of the derivatives. For coastal applications, this is appropriate due to the moving control volume in the domain (Mackie, 2022).

The coupled partial differential equations that form the set of 2-D SWE are;

$$\frac{\partial \eta}{\partial t} + \nabla \cdot (H\mathbf{u}) = 0, \tag{4.1}$$

$$\frac{\partial \mathbf{u}}{\partial t} + \mathbf{u} \cdot \nabla \mathbf{u} - \nu \nabla^2 \mathbf{u} + f\mathbf{u}^{\perp} + g\nabla\eta = -\frac{\tau_b}{\rho H}, \tag{4.2}$$

where η is the free surface elevation, t is time, H is the sum of the free surface elevation and depth at rest (i.e., total water depth) and the vector $\mathbf{u}$ represents the components of depth-averaged velocity (Kärnä et al., 2018). In Equation 4.2, ν is effective kinematic viscosity, $f\mathbf{u}^{\perp}$ represents the force of the Coriolis effect, g is acceleration due to gravity, τ_b is the bed friction and ρ is the water density (Kärnä et al., 2018, OpenTidalFarm, 2016, Goss et al., 2020). For the idealised cases modelled in this chapter, the Coriolis force is neglected but incorporated in subsequent Chapters of the thesis where modelling of real sites is undertaken.

The bed friction, τ_b, is represented using a quadratic drag term (Equation 4.3), where

the bed friction coefficient of drag is, C_d.

$$\frac{\tau_b}{\rho} = C_d|\mathbf{u}|\mathbf{u}. \tag{4.3}$$

The kinematic viscosity, ν, is made up of the molecular viscosity and eddy viscosity (turbulent viscosity) (Vouriot et al., 2019). Molecular viscosity is the measure of a fluid's ability to deform and is in the order of 10^{-6} $m^2 s^{-1}$, therefore, considered negligible. Eddy viscosity is similar to molecular viscosity in terms of diffusing momentum, however, it acts at a larger scale and arises from the momentum transport through a flow field due to turbulent velocity fluctuations (Du Feu, 2019).

A viscosity sponge, which is a layer of increased viscosity and friction, is applied at the open boundaries of the model to assist uniform mixing and dampen numerical instabilities or re-circulation at the boundary (Vouriot et al., 2019). The viscosity at the open boundary is set to 1000 m^2 s^{-1} and decreases linearly with distance away from the boundary to the end of the viscosity sponge. The viscosity sponge increases the model's stability and is applied only at the open boundaries. Ensuring the sponge does not extend to areas of interest (i.e., areas of the domain occupied by turbines) minimises the effect on the results. The viscosity is set to 1 m^2 s^{-1} outside of the viscosity sponge (as used in Zhang et al. 2022 and Jordan et al. 2022) serving as a constant eddy viscosity turbulence model. The constant eddy viscosity approach avoids excessive dissipation of hydrodynamic structures in areas of the region with finer resolution mesh whilst ensuring model stability (Vouriot et al., 2019).

The adoption of numerical modelling in this chapter, allows the partial derivatives presented in Equations 4.1 and 4.2 to be approximated through discretisation, bypassing the need for analytical solutions. This can be achieved through finite element methods (FEM) or finite volume methods. *Thetis* is an unstructured grid modelling software that simulates coastal flows using *Firedrake*'s finite element (FE) partial differential equation (PDE) solver (Rathgeber et al., 2016, Kärnä et al., 2018). In this thesis, the discontinuous Galerkin finite element (DG-FE) method is adopted to discretise SWE

spatially, and solved iteratively by the PETSc's Newton method (Balay et al., 2016). DG-FE is well suited to applications dominated by advection with unstructured meshes, such as coastal domains. The domain is discretised into a finite set of elements and the variables that are being solved for are approximated and typically continuous within each element. The unknown variables in this application are depth-averaged velocity and free-surface elevation. They are discretised by a velocity-pressure finite element pair ($P_1^{DG} - P_1^{DG}$), which are represented by piecewise-linear discontinuous basis functions (Kärnä et al., 2018, Goss et al., 2019).

The velocity and elevation are defined across each element of the mesh individually and the value at the node is the same between connecting elements. The model is forced at the boundaries: open boundaries are forced by tidal elevation functions with Dirichlet boundary conditions, that differ for idealised and real site applications in this thesis, and a free-slip boundary condition is applied for the closed (coastal) boundaries. The shared adjoining nodal values and boundary values are used to solve the SWE across the domain (Du Feu, 2019).

The unstructured triangular meshes used in this thesis were created in *qmesh*, which uses Geographical Information Systems software to define the domain and interfaces it with the mesh generation tool *Gmsh* (Avdis and Hill, 2017, Geuzaine and Remacle, 2017). The resolution for each mesh is dependent on the individual application and will be described for each study in this thesis.

The semi-implicit Crank-Nicolson time marching scheme is used for temporal discretisation. This scheme takes the average of the forward and backward Euler methods and is advantageous because it is unconditionally stable for linear systems and has good second-order accuracy in time and space. A constant timestep of $\Delta t = 50$ s was applied in this chapter.

All simulations were conducted on an Intel(R) Core(TM) i7-7700 workstation with 8

CPUs, 32GB RAM and an Ubuntu 21.04 operating system.

4.1.2 Turbine Implementation

Turbines can be implemented in depth-averaged models in a number of ways, as outlined in Section 2.2. In *Thetis*, turbines are represented as an additional sink term in the momentum equation (Equation 4.2), to include the force on the flow due to turbines (Kärnä et al., 2018). In this chapter, linear momentum actuator disc theory is used to represent the performance of turbine rotors, keeping in line with Vennell (2010) for comparison purposes. The turbine drag coefficient, c_t is applied in addition to the bed friction (Equation 4.3) in the area that turbines are placed such that arrays are characterised by areas of enhanced bottom friction (Zhang et al., 2022). Equation 4.4 presents the sink term that is included in the momentum equation to represent the inclusion of turbines (Goss et al., 2020).

$$\frac{c_t}{\rho H}|\mathbf{u}|\mathbf{u} \tag{4.4}$$

The non-dimensional and spatially varying drag coefficient, c_t, is set to zero in areas where turbines are not deployed. The force on the flow due to the array is

$$F_{array} = \int_{\Omega_{array}} \rho c_t d(\mathbf{x})|\mathbf{u}|\mathbf{u} d\mathbf{x}. \tag{4.5}$$

The thrust force exerted by 'N' number of turbines in an array is approximated by Equation 4.6, where C_T is the thrust coefficient and A_T is the swept area of an individual turbine rotor.

$$F_{array} = \sum_{i=1}^{N} \frac{1}{2}\rho C_T A_T |\mathbf{u}_i|\mathbf{u}_i \tag{4.6}$$

The free stream velocity at the coordinate of the i^{th} turbine is represented by $\mathbf{u}_i$. The thrust coefficient is dependent on the velocity according to a performance curve and individual turbine rotor area in the array, described in Equation 4.6, is assumed to be homogeneous. The equivalent continuous version of Equation 4.6 is

$$F_{array} = \int_{\Omega_{array}} \frac{1}{2}\rho C_T A_T d(\mathbf{x})|\mathbf{u}(\mathbf{x})|\mathbf{u}(\mathbf{x}) d\mathbf{x}. \tag{4.7}$$

The drag coefficient, c_t, can be related to the turbine's thrust coefficient, C_T, swept area of the turbine, A_T and the turbine density, $d(\mathbf{x})$, as $c_t(d(\mathbf{x})) = \frac{1}{2}C_T A_T d(\mathbf{x})$, by equating Equations 4.5 and 4.7. In *Thetis*, the combined turbine density can be calculated from individual turbine densities, $d_i(\mathbf{x})$, as $d(\mathbf{x}) = \sum_{i=1}^{N} d_i(\mathbf{x})$.

The instantaneous power produced by the array is given by Equation 4.8, where, $c_p(\mathbf{x})$ is the power coefficient function defined as, $c_p(\mathbf{x}) = C_P(\mathbf{u}(\mathbf{x}))A_t d(\mathbf{x})$,

$$P_{array} = \int_{\Omega_{array}} \frac{1}{2}\rho c_p(\mathbf{x})|\mathbf{u}(\mathbf{x})|^3 d\mathbf{x}. \tag{4.8}$$

Turbines can be implemented using two approaches in *Thetis*; continuous or discrete. The continuous method, also known as the distributed drag method (Coles et al., 2016), applies the drag (Equation 4.7) over the representative array area to parameterise groups of turbines, used by Kramer et al. (2015) and Funke et al. (2016). The continuous method is better suited for regional scale modelling. For the discrete implementation of turbines, the turbine drag (Equation 4.9) is applied over the representative area of an individual turbine, used by Funke et al. (2014, 2016) and Jordan et al. (2022). This approach requires the resolution of the mesh, in the location of turbines, to be finer than the diameter of the turbine being represented so they can be resolved individually. This method is best applied for micro-siting turbines or the modelling of arrays containing a small number of turbines, otherwise it is computationally demanding and limits the exploration of other parameters.

$$F_{\text{turbine}} = \frac{1}{2}\rho C_T A_T ||\mathbf{u}||\mathbf{u}. \tag{4.9}$$

Figure 4.1 demonstrates the concepts of turbine density and blockage for a simplified channel by looking at the channel in two different planes. The representative planform areas, used to calculate the turbine density (Equation 4.10), for discrete and continuous approaches are presented. In idealised channels, the number of turbines used to calculate the turbine density is defined by Vennell (2010) as $N = N_R B \frac{A_C}{A_T}$, where N_R is the number of rows of turbines uniformly arranged in an array across the entire width

of a channel. The concept of blockage focuses on the proportion of the in-depth cross-sectional area occupied by turbines, compared to turbine density, which is based on the perpendicular plane.

$$\text{Turbine Density, } d(\mathbf{x}) = \frac{\text{Number of Turbines, N}}{\text{Representative Planform Area}}. \tag{4.10}$$

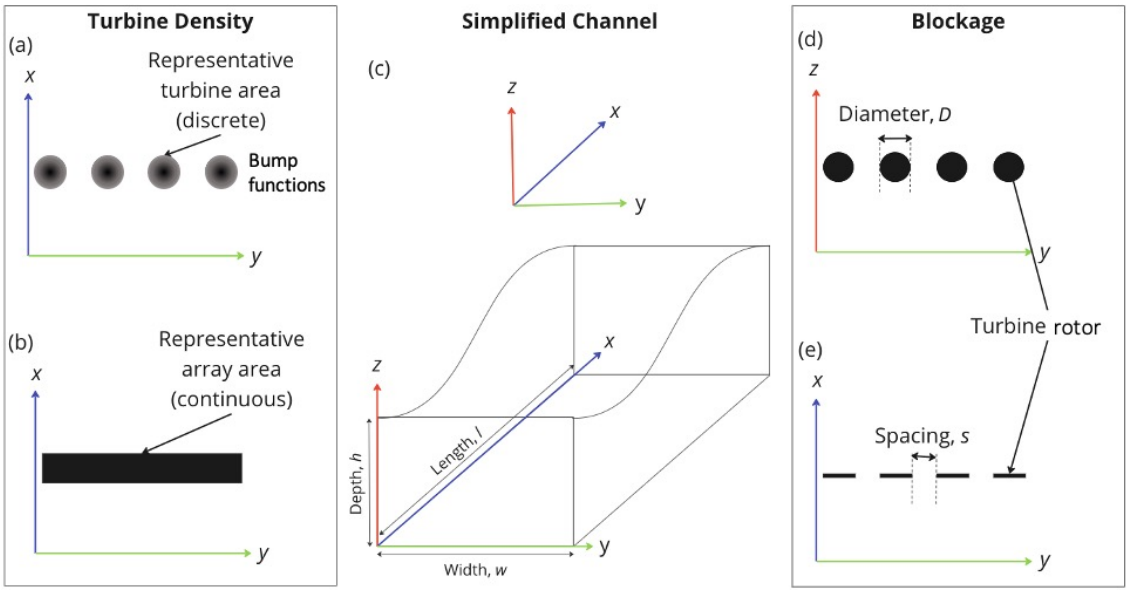

Figure 4.1: Diagram demonstrating key features of turbine density, for continuous and discrete implementations, and blockage in a simple channel.

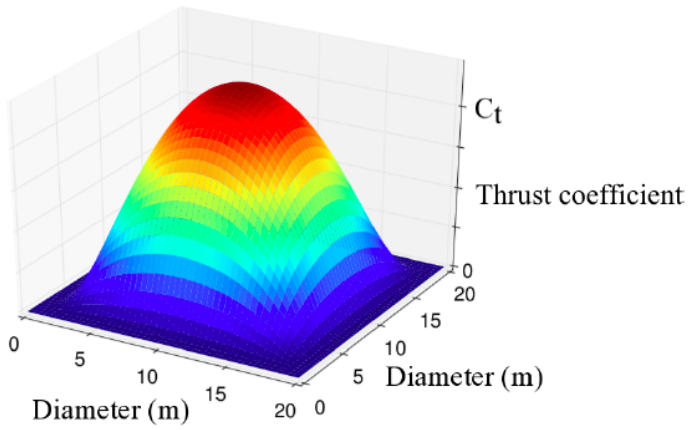

Figure 4.2: Bump function for a 20 m diameter turbine with thrust coefficient, C_T, (Du Feu 2019 adapted from Funke et al. 2014).

A bump function, which is a smooth function with finite support, is adopted in the discrete turbine implementation so that the friction value smoothly increases at the position of each turbine. The 1-D bump function is described by Funke et al. (2014) as,

$$\psi_{p,r}(x) \equiv \begin{cases} e^{1-1/\left(1-\left|\frac{x-p}{r}\right|^2\right)} & \text{for } \left|\frac{x-p}{r}\right| < 1 \\ 0 & \text{otherwise} \end{cases}, \tag{4.11}$$

where p and r are the centre and support radius of the function. Figure 4.2 illustrates the bump function (Funke et al., 2014, Du Feu, 2019).

Funke et al. (2014) compared the two methods of representing turbines, continuous and discrete, through an optimisation study for conducting a resource assessment in the Pentland Firth. Although their study identified that the discrete method provides a more detailed depiction of the flow pattern within the array area compared to the continuous method, the overall array wake and bypass patterns align closely between the two methods. They propose that the continuous approach is suitable for optimising turbine arrays because it approximates large scale flow patterns well.

By equating Equations 4.5 and 4.7 it is assumed that the local velocity, $\mathbf{u}(\mathbf{x})$, which averaged across the depth of the water column and laterally between through-turbine and bypassing flows, can be approximated as the free stream velocity at the turbine location. This leads to the assumption that the calculated power is the total power extracted from the hydrodynamics and incorporates unresolved mixing losses, because assessing the power available to a turbine requires the velocity through the turbine to be known (Zhang et al., 2022). In regional-scale studies, where turbines are continuously represented and, therefore, a coarser mesh is used compared to micro-siting studies employing discrete turbine implementation, this approximation is justifiable. As the turbine density becomes more distributed across a coarse mesh, the local velocity approaches the free-stream velocity (Schwedes et al., 2017). When the mesh resolution becomes smaller than the wake recovery length scale, the approximation that the free-stream velocity can represent the local velocity is no longer valid (Kramer and Piggott, 2016). A correction for the velocity at the turbine is presented by Kramer and Piggott

(2016),

$$U_{\infty}(\mathbf{x}) = \frac{1}{1 + \frac{1}{4}\frac{A_t}{\hat{A}_t} C_{\mathrm{t}}(|\mathbf{u}(\mathbf{x})|)} |\mathbf{u}(\mathbf{x})|, \tag{4.12}$$

where the numerical cross-section of the turbine is represented by $\hat{A}_t = HD$. Equation 4.12 is derived from 1-D linear momentum ADT and based on the principles of Bernoulli, conservation of momentum and the continuity equation (Jordan et al., 2022). By correcting the velocity to consider the impact of introducing turbines, the correct C_T and C_P values can also be applied to turbines. The local blockage and shear effects are assumed to be negligible (Garrett and Cummins, 2007).

4.2 Idealised Channel - Validation

To investigate the hydrodynamic and turbine modelling capabilities of *Thetis*, the idealised channels outlined in Vennell (2010) are replicated in the 2-D software to compare outcomes. The tidal amplitude and surface phase difference, from Vennell (2010), are outlined in Table 4.1, a value of $C_d = 0.005$ is applied to the domain, and the elevation at each end of the channel for the 2-D *Thetis* model is presented in Figure 4.3.

Table 4.1: Channel data from Vennell (2010).

	Shallow Channel	Tidal Strait
Tidal amplitude, a [m]	1.0	0.7
Surface phase difference, ϕ_g [°]	10	180

As proposed by Vennell (2010), the head difference between either end of the idealised channel drives the current through it. The open boundaries at x = 0 and x = l (according to Figure 4.1) are forced by sinusoidal tidal elevation functions,

$$\begin{aligned} \mathrm{x} = 0: &\quad a\sin\omega t, \\ \mathrm{x} = \mathrm{l}: &\quad a\sin\omega t + \phi_g. \end{aligned} \tag{4.13}$$

Table 4.2 summarises the results from Vennell (2010) for the shallow channel and tidal strait. Three cases are presented for each channel; an ambient case with no turbines, 1

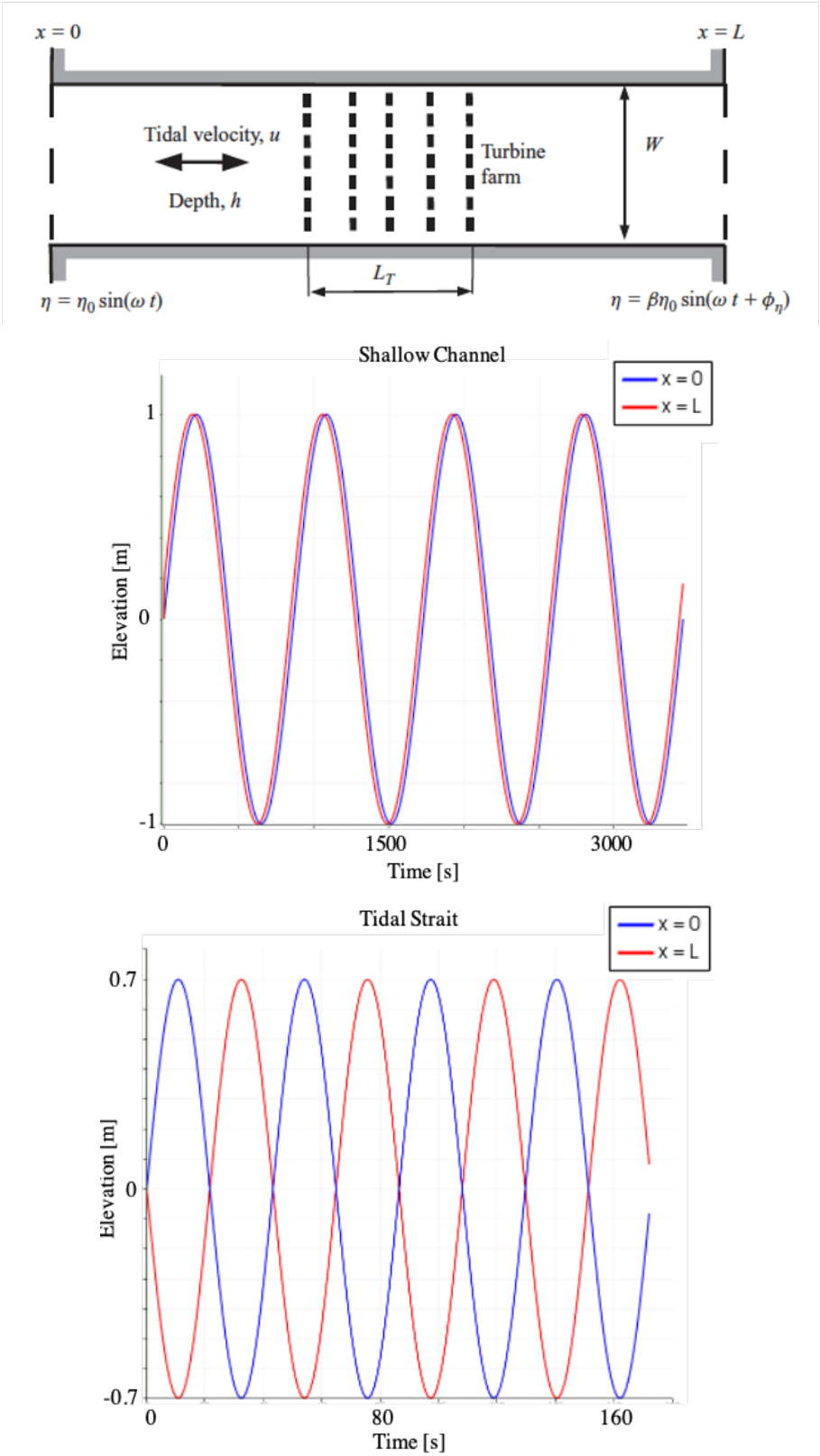

Figure 4.3: Diagram of the simple channel from Vennell (2010) and the elevation from the 2-D models demonstrating the forcing at either end of the channel in accordance to the values in Table 4.1.

row of turbines and 10 rows of turbines. In the cases where turbines are implemented, blockage is 0.25 and the power available is presented. The shallow channel accommodates 30 turbines per row and the tidal strait accommodates 800 turbines per row at this blockage. The current amplitude is presented for all cases.

Table 4.2: Replication of results for shallow channel and tidal strait modelled in 0-D analytical model, from Vennell (2010).

			Shallow Channel	Tidal Strait
Vennell (2010)	0 rows	Current amplitude [m/s]	2.7	1.9
	1 row	Average power available	4.8 MW	0.4 GW
		Current amplitude [m/s]	2.0	1.8
	10 rows	Average power available	8.2 MW	2.3 GW
		Current amplitude [m/s]	1.6	1.6

Table 4.3: Results for the shallow channel and tidal strait represented in 2-D numerical model, *Thetis*.

			Shallow Channel	Tidal Strait
	0 rows	Current amplitude [m/s]	2.7	1.8
Continuous	1 row	Average power available	4.4 MW	0.32 GW
		Current amplitude [m/s]	2.1	1.8
	10 rows	Average power available	7.8 MW	2.2 GW
		Current amplitude [m/s]	1.4	1.6
Discrete	1 row	Average power available	3.9 MW	0.26 GW
		Current amplitude [m/s]	2.3	1.8
	10 rows	Average power available	7.7 MW	2.04 GW
		Current amplitude [m/s]	1.5	1.6

Percentage difference from Vennell (2010) results [%]

+15 +10 +5 0 -5 -10 -15 -20 -25 -30 -35

The power available and current amplitude for each case and channel, when modelled in 2-D, are presented in Table 4.3. The percentage difference for each result, compared

to the literature, is presented by colour. Continuous and discrete methods for turbine representation are implemented. For the cases presented in Tables 4.3, the array areas have been modelled such that the length of the channel occupied by the array (l_T) is large enough to allow enough mixing for the velocity to recover to the free stream value between rows, in line with the assumption made in Vennell (2010).

For the ambient case, the current amplitude remains consistent in the shallow channel, and only a 5% difference is observed in the tidal strait. To verify that the horizontal viscosity value had no impact on the undisturbed channel in the ambient case, considering the absence of turbulent mixing, the horizontal viscosity value was systematically altered and the current amplitude remained the same.

There are two competing effects in a channel, the thrust applied to the flow due to turbines and the available power from the turbines. The introduction of resistance due to the presence of turbines results in a decrease in flow velocity. When the flow velocity through the turbine decreases as the faster flow bypasses it, both the applied thrust, and consequently, the available power decrease. The tidal strait is characterised as an inertia dominated channel and experiences minimal change in maximum velocity when turbines are present, therefore, these effects are easier to balance because there is less impact on the current. This is demonstrated in the Vennell (2010) results, reproduced in Table 4.2, and corroborated through the examination of maximum change in peak velocity in Section 3.4.2. With the inclusion of turbines in the 2-D model of the tidal strait case, the current amplitude is in agreement with the 0-D model in Vennell (2010) for both discrete and continuous methods. Conversely, the current amplitude in the shallow channel, governed by drag, demonstrates a greater sensitivity to the presence of turbines in the literature, and when comparing the 2-D model to the 0-D model results, the current amplitude differs from the Vennell (2010) 0-D model by up to 15%. Across all scenarios, the available power in the 2-D model is reduced compared to the 0-D model. A lower value in power availability and greater current amplitude compared to

the literature indicates less resistance in the flow due to turbines as per the description of the competing effects, and is observed in the shallow channel with 1 row of turbines. For the 10 row discrete implementation of turbines in the shallow channel, both the power and the current amplitude are lower than the results in the literature by 5%. For the continuous implementation of the same case, the power is 5% lower and the current amplitude is 13% lower. Although row spacing in the discrete implementation and the array area for the continuous implementation were great enough to fulfill the mixing requirements between rows of Vennell (2010) it is possible that the decrease in both current amplitude and power is due to interactions between rows. This would also be applicable to the tidal strait where a decrease in power is observed compared to the literature despite no change in current amplitude, indicating the 2-D model captures more intricate turbine interactions and tidal dynamics.

The agreement between continuous and discrete implementation of turbines is important for assessing how well the continuous approach approximates the discrete modelling of individual turbines, which is why turbines were modelled with both approaches. Better agreement between the different turbine implementations is observed in cases with a greater number of turbines (10 rows), resulting in a 7% difference in available power for the tidal strait and 1% difference for the shallow channel. This aligns with expectations that as the number of turbines increases the more similar the methods become in their implementation. This convergence occurs because as the number of turbines or the turbine diameter increases for the discrete method, the total representative turbine area becomes more similar to the representative array area used in the continuous method. The case that deviates the most from results in the literature is the discrete 1 row case for both the shallow channel and tidal strait.

The mesh resolution in each channel was determined based on the application of continuous and discrete approaches for modelling turbines. In the shallow channel, the continuous implementation utilised a mesh with 2600 nodes, while the discrete

approach required a more detailed mesh of 33359 nodes. Similarly, in the tidal strait, the continuous implementation employed a mesh with 3658 nodes, and the discrete approach necessitated a higher resolution with 135768 nodes. Simulations were conducted on four nodes in parallel. As an example of the computational cost of a simulation in *Thetis*, for the tidal strait simulations conducted on four nodes in parallel, the discrete case with 135768 nodes took 27 hours to simulate 14 days and the continuous case with 3658 nodes took approximately an hour to simulate 14 days. The discrete approach is computationally more intensive, due to its requirement for a mesh finer than the diameter of an individual turbine in areas where the turbines are modelled. The minimum element size was 5 m in the discrete cases and 50 m in the continuous cases. Moving to regional-scale modelling for resource assessments introduces increasing challenges in discretely modeling turbines, due to mesh resolution requirements.

In a transient simulation, where flow is varying with time, numerical stability and accuracy of the simulations needs to be ensured, which requires a balance between spatial and temporal discretisation. Therefore, a sensitivity analysis is undertaken to test timesteps of 5 s, 50 s and 100 s for the idealised cases simulated in *Thetis*. Table 4.4 presents the maximum percentage change in instantaneous and average power for the 50 s and 100 s timestep simulations, with respect to the 5 s timestep simulation. The results demonstrate there is negligible impact on the calculated power output from the modelled arrays when different timesteps are used (< 1% change in average power and < 1.5% change in instantaneous power). Figure 4.4 presents an example of power over time for the tidal strait case with 10 rows of turbines modelled discretely to demonstrate the agreement between the cases using different timesteps. In this chapter, a timestep of 50 s was used in all cases. The choice of a 50 s timestep is considered reasonable relative to the mesh size for all cases in this chapter, including the discrete application where the mesh is required to be finest. Mackie (2022) modelled the Ramsey Sound in *Thetis* using a mesh with minimum element size of 8 m and, having conducted a sensitivity analysis for timesteps of 50 s and 100 s, considered a temporal discretisation

of 100 s as appropriate.

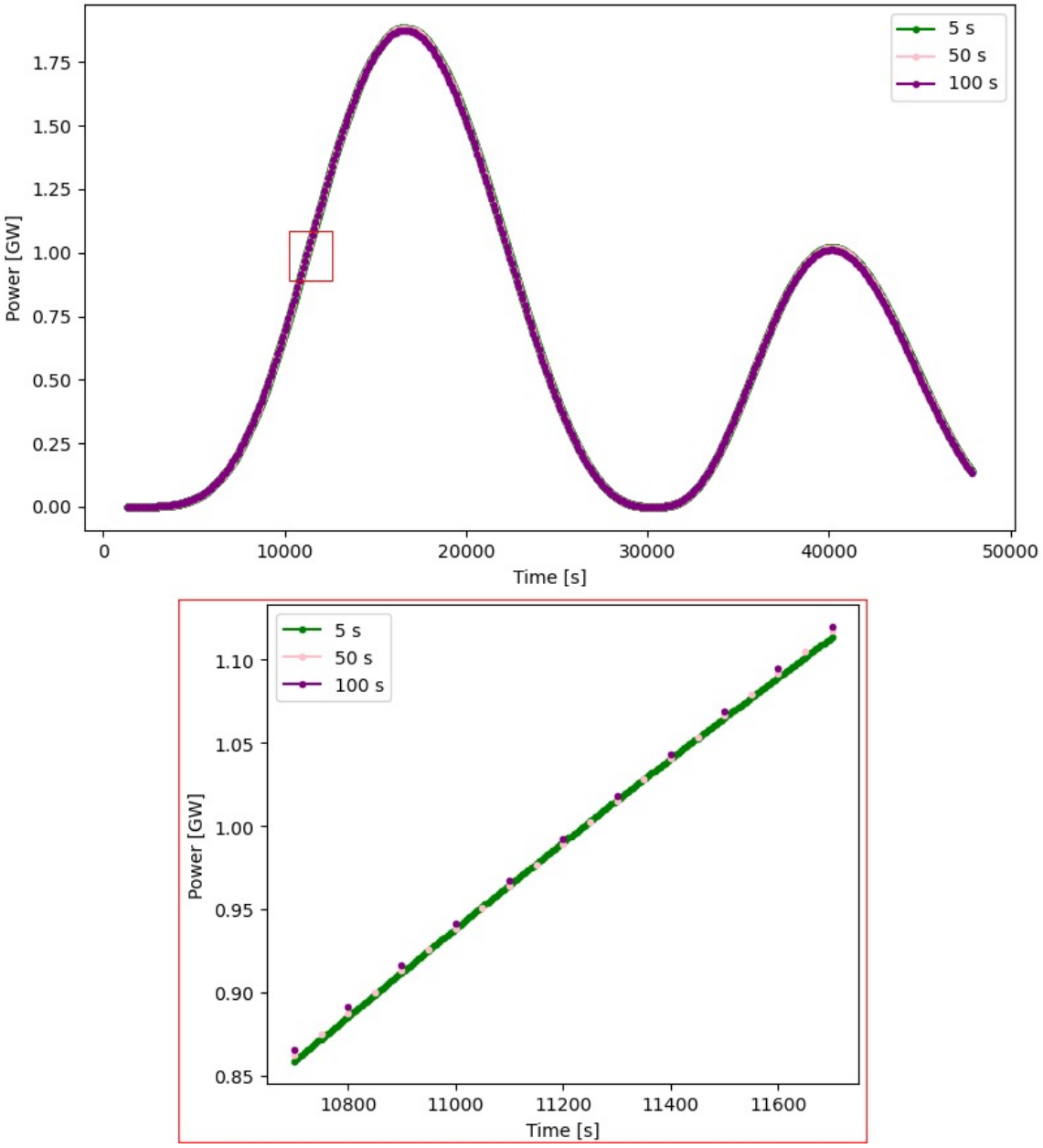

Figure 4.4: Power for the discrete, 10 row, tidal strait case simulated with 5 s, 50 s and 100 s timesteps over a high and low tide cycle and a detailed view of a subset of data.

Table 4.4: Maximum percentage difference in instantaneous and average power for cases using 50 s and 100 s timesteps with respect to cases using a 5 s timestep

Timestep	Maximum difference in Instantaneous Power [%]	Maximum difference in Average Power [%]
5 s	-	-
50 s	0.88	0.62
100 s	1.16	0.97

4.3 Array Layout

Designing the layout of turbines in an array is an important aspect of developing a site for tidal stream energy extraction, due to the interaction between turbines and the flow. It will involve a balance between maximising energy extraction and minimising alterations to the flow (De Dominicis et al., 2018). In the development of future tidal arrays, the incorporation of multiple turbine rows necessitates careful consideration of both micro-scale (turbine-to-turbine) and macro-scale interactions (array-to-tidal channel) (Ouro and Nishino, 2021). Early development stages of tidal stream energy sites focus on the performance of a small number of turbines (e.g., four 1.5 MW turbines tested at the Meygen lease site for Phase 1 of developments). Further development of the site will require the deployment of larger arrays of turbines (Zhang et al., 2022). The micro-siting of turbines is driven by the dynamics of the accelerating bypass flow between turbines and the turbulent mixing of wakes to leverage positive interactions for power generation (Ouro and Nishino, 2021). The macro-scale effects are discussed in Section 2.1.1.

The performance of turbines in a channel has been investigated with the adoption of analytical models. Garrett and Cummins (2007) demonstrated that placing turbines in a row to create a tidal fence enhances the power generated by each turbine in uniform flow when compared to an isolated turbine (corroborated by experimental results by Stallard et al. 2013, Noble et al. 2020), and Nishino and Willden (2012) further considered a fence of turbines that partially occupies the width of a channel. A study by Draper and Nishino (2014) focused more specifically on two rows of turbines and their arrangement by extending LMADT in an analytical model to consider two types of turbine arrangements, aligned and staggered (demonstrated in Figure 4.5). Their study on turbine arrangement is important for applications where tidal channels are not sufficiently long or wide to allow for wake recovery or avoid wake interactions. They place conditions on longitudinal row spacing such that the distance is large enough for pressure to equalise

but not for significant wake mixing before the second row of turbines. The findings from these studies indicate that, two rows of turbines in a staggered arrangement outperform two rows that are aligned. However, the efficiency of a single row containing the same total number of turbines and equivalent array width is greater than the two row arrangements.

Numerical modelling has also been undertaken to study array layouts. Bai et al. (2013) similarly demonstrated that a staggered arrangement of turbines yielded greater power than an aligned arrangement. They find a lateral spacing of 2.5 rotor diameters to be most appropriate, whilst longitudinal spacing should be as great as possible. Funke et al. (2014) used lease area and minimum turbine spacing constraints at the Pentland Firth to micro-site 256 turbines and applied an efficient gradient-based optimisation, computing the gradient of power extraction with respect to turbine positions and tuning parameters. This approach expands away from a structured row format in order to optimise the performance of turbines.

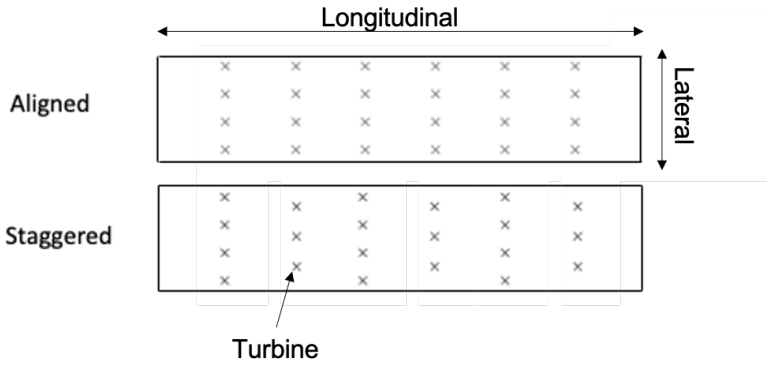

Figure 4.5: Aligned and staggered row arrangements in an idealised channel.

The adoption of a 2-D channel model in this chapter, allows the effect of longitudinal spacing and array layout on the power output of the array and current amplitude of the idealised channel scenarios, proposed by Vennell (2010), to be investigated. Aligned and staggered turbine arrangements are considered. Table 4.5 presents the results of 10 rows of turbines, modelled discretely, spaced 5 and 10 rotor diameters apart in the longitudinal direction and with 0.25 blockage.

Table 4.5: Average power available for 10 rows of turbines, implemented with the discrete approach, with row spacing constraints and array layouts in the tidal strait and shallow channel proposed by Vennell (2010).

	Layout	Array Length, l_T, [m]	Longitudinal Row Spacing [Rotor Diameter]	Average Power Available	Average Power per Turbine	Current Amplitude [m/s]
Shallow Channel	Staggered	900	10	7.08 MW	22.48 kW/turbine	1.44
		450	5	6.69 MW	21.22 kW/turbine	1.42
	Aligned	900	10	6.97 MW	21.78 kW/turbine	1.44
		450	5	6.63 MW	20.72 kW/turbine	1.42
Tidal Strait	Staggered	1800	10	1.34 GW	0.155 MW/turbine	1.56
		900	5	1.01 GW	0.117 MW/turbine	1.55
	Aligned	1800	10	1.19 GW	0.137 MW/turbine	1.56
		900	5	0.97 GW	0.111 MW/turbine	1.55

Comparing the power for each scenario in Table 4.5 to the 10-row, discrete implementation in Table 4.3, demonstrates that the power decreases by up to 7% in the shallow channel and up to 52% in the tidal strait when rows are arranged such that full mixing between rows does not occur. The most significant decrease in power for both idealised channels is observed in the scenario with aligned arrangement of turbines and the shortest longitudinal row spacing (5 rotor diameters), which is observed in other studies (Bai et al., 2013, Draper and Nishino, 2014). For the shallow channel, the power per turbine increases by 7% when turbines are arranged in a staggered layout and rows are spaced 10 rotor diameters apart. For the tidal strait there is a 38% increase in power per turbine between the same scenarios. The increase in power per turbine through doubling longitudinal row spacing is up to 6% in the shallow channel and 32% in the tidal strait. The change in array layout, from aligned to staggered, leads to an increase of up to 3% for the shallow channel and 13% for the tidal strait, which is at least half the impact of changes to row spacing for each channel. The current amplitude between cases are similar, but the 5 rotor diameter spacing leads to a greater decrease compared to the 10 rotor diameter spacing.

The results illustrate the impact of relaxing the limiting assumption made for the Vennell (2010) channel model (Section 3.2.2), that the longitudinal spacing between rows is adequate for the full mixing of the near-wake flow and the bypass flow such that it to returns to the free stream velocity. At real sites, there will be a constrained lease site for turbine deployment, making the Vennell (2010) assumption unrealistic to maintain. In order to exploit the resource it is necessary to balance the spacing between rows to minimise negative wake-turbine interactions, whilst maximising the number of rows at each site. In *Thetis*, the mixing is controlled by the horizontal viscosity, which was set to a relatively low value to ensure full mixing does not occur at an unrealistically short horizontal length scale. It is noted in Vennell (2010) that deploying 10 rows of turbines in the 0-D channel model, whilst maintaining row spacing to allow full recovery of the velocity between rows, is in conflict with the assumption that the length of the channel occupied by turbine rows, l_T (Figure 4.1), is much smaller than the length of the channel, l, ($l_T \ll l$). In the shallow channel, turbines with rotor diameter of 10 m are deployed and 20 m rotor diameter turbines are deployed in the tidal strait, with the array length for each scenario presented in Table 4.5.

4.4 Boundary Effects

Transitioning from a 0-D analytical model to a 2-D numerical model necessitates careful consideration of the placement and influence of open boundaries. The introduction of turbines in a model and changes in the hydrodynamic model domain have implications at the open boundaries. Therefore, it is important to understand how these affect results and analysis.

To assess the influence of boundary conditions on power and capacity factor, a row of 20 m diameter turbines, simulated using the continuous approach, is studied across 15 idealised channels with distinct uniform channel depth (ranging from 35 m to 50 m) and seabed drag coefficients (C_d = 0.002 – 0.003 to reflect values in the Pentland Firth) (Equation 4.2). The rated speed was incorporated as a turbine design parameter (rang-

ing from 1.6 – 2.0 m/s), in addition to the channel characteristics. Capacity factor is dependent on the rated speed and it was demonstrated in Chapter 3 that rated speed is the most important characteristic point of the turbine performance curve for predicting the power output of an array.

Figure 4.6 presents the capacity factor and power normalised by the kinetic flux at the boundary for the cases. The peak capacity factor of the array is observed in the channel characterised with lowest drag coefficient (0.002) and deepest bathymetry (50 m). This channel has the least resistance, due to the low drag coefficient of the seabed, and the greater depth results in a smaller drag effect and the least dissipation compared to a shallower channel. The effect of depth on dissipation is observed between the deep tidal strait and shallow channel when examining the impact on current amplitude with the introduction of turbine resistance. In contrast, when considering power normalised by kinetic flux at the boundary, the peak occurs in the channel with the shallowest bathymetry and greatest drag coefficient, presenting an inverse relationship to the capacity factor results. The rated speed was found to have no impact on this trend across different channels, although it can be observed that as the rated speed increases, normalised power decreases while capacity factor increases (illustrated in Figure 4.7).

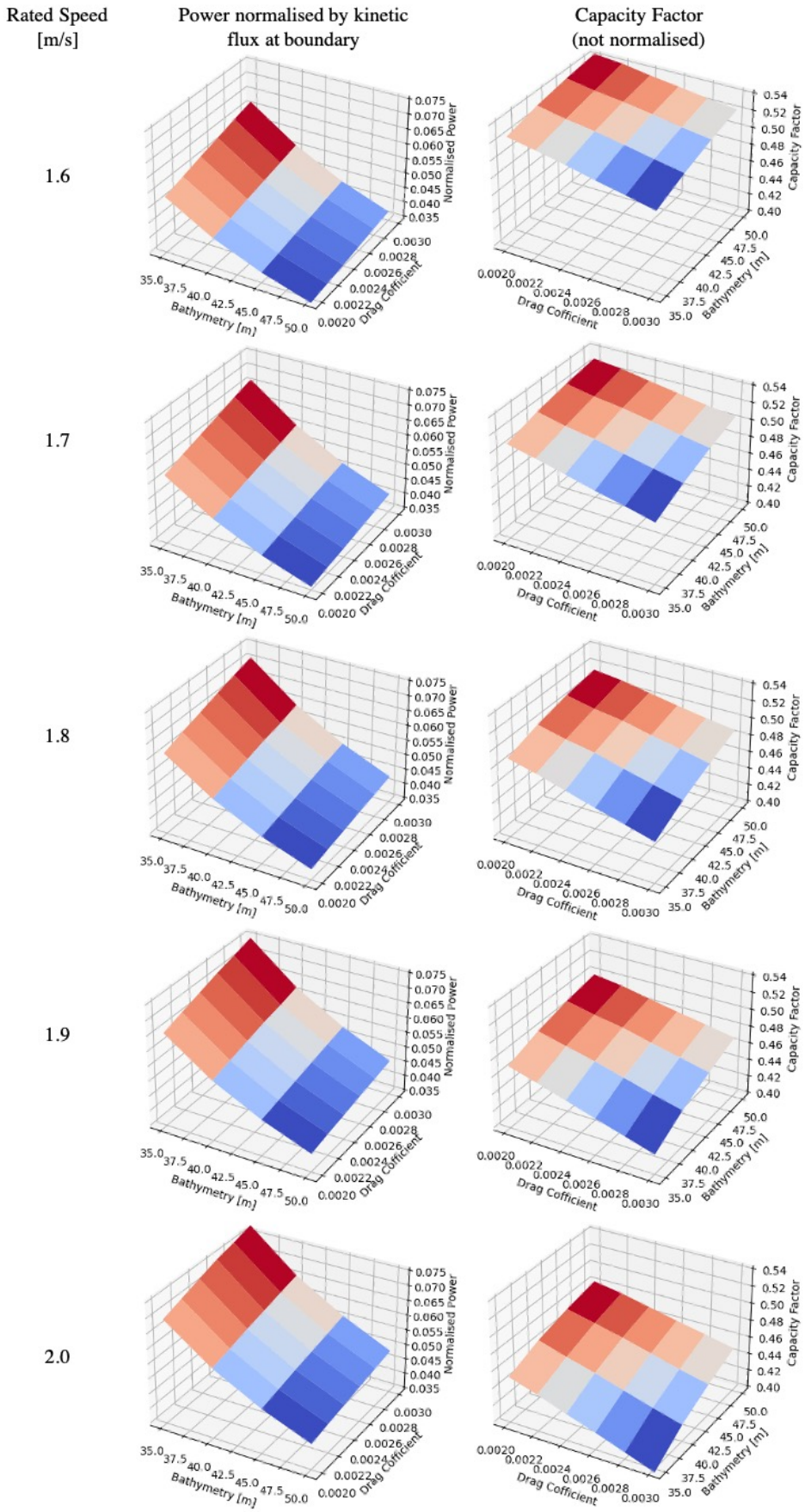

Figure 4.6: Surface plots for normalised power and capacity factor of turbines in 15 channels with different depth and seabed drag coefficients, operating with different rated speeds.

Notably, the capacity factor results do not account for changes in boundary effects. However, since power is normalised by the kinetic flux at the boundary, these results account for different boundary effects in each domain, allowing for an assessment of how effectively the resource is extracted in each channel. When comparing channels with different characteristics in a 2-D numerical model, if the power is not normalised or the capacity factor is being considered, the results can be misinterpreted because they do not account for boundary effects in the changing domains. The normalised power for cases outlined in Section 4.5 are not presented because normalising by the kinetic flux does not affect the trends in power. Only channels with the same characteristics are compared, therefore, the flux into the domain is unchanged because the same number of turbines and channel characteristics are implemented in each domain that is compared, as opposed to comparing the power output of the shallow channel to the tidal strait.

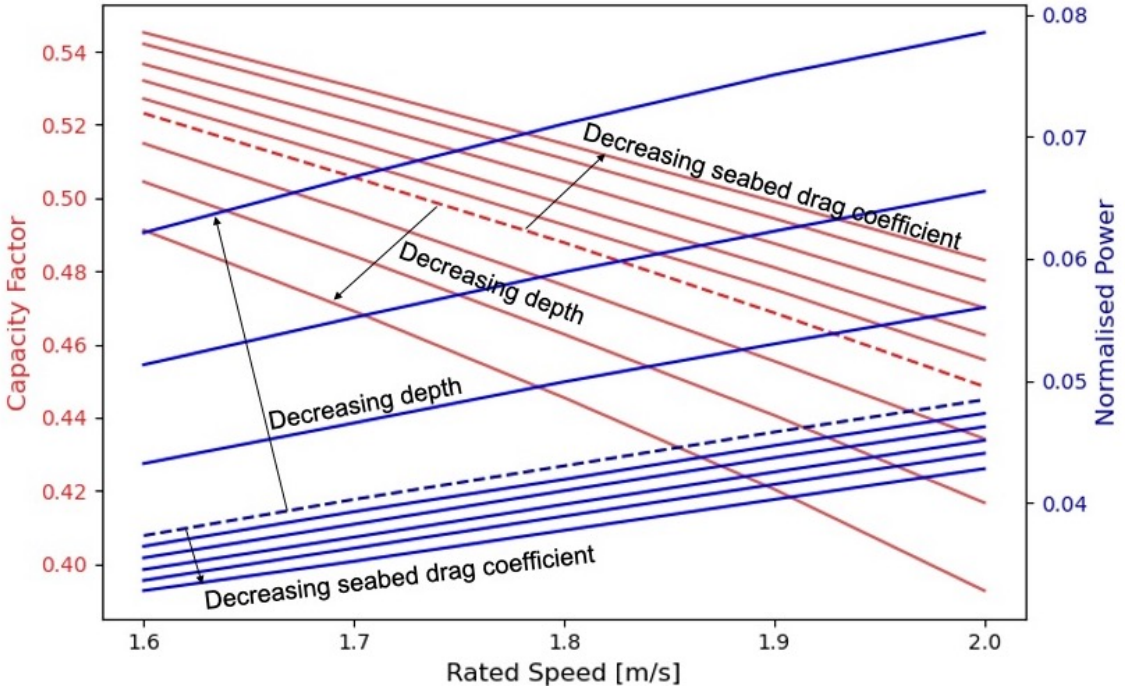

Figure 4.7: Capacity Factor and normalised power for turbines operating at rated speed in the range of 1.6 – 2.0 m/s, in channels with depth ranging from 35 m – 50 m and seabed drag coefficient ranging from 0.002 – 0.003. Dashed lines demonstrate the case of a channel with 50 m depth and 0.003 seabed drag coefficient.

In this Section, the physical parameters of the idealised channels have been chosen

to create hypothetical cases, which is not applicable to real sites where the physical parameters of a channel are predetermined. However, the results demonstrate the importance of incorporating boundary effects in analysis of results from a hydrodynamic model. When modelling a real site, it is important to place open boundaries far away from areas of interest and avoid shallow water areas to ensure their effects are negligible (Garrett and Greenberg, 1977, Venugopal et al., 2010, Adcock et al., 2011). Placing open boundaries beyond the continental shelf decreases the influence of boundary conditions.

4.5 Conclusion

In this chapter, the transition from a 0-D analytical model to a 2-D numerical model of a channel has been explored and allows the investigation of 2-D modelling implications in an idealised channel before more complicated domains are introduced. Comparing results of idealised channels, proposed by Vennell (2010) and studied in Chapter 3, with the literature presented the opportunity to validate the 2-D software and how it represents turbines in models, which is identified as a key difficulty in the literature review. The agreement of results with the literature provided confidence in the model and exploration of 2-D parameters and techniques informs the 2-D modelling of a real site. Demonstrating consistency between 0-D and 2-D models results allows applicability of the insights from the study undertaken in Chapter 3, whilst acknowledging their differences.

The continuous and discrete approaches for implementing turbines in *Thetis*, and how they meet the needs of different applications (e.g., resource scale vs. array scale) are considered. It is found that the discrete implementation is more similar to the continuous implementation, in terms of power outputs, for a greater number of turbines due to the representative array and turbine areas being more similar. The computational expense of discrete modelling is demonstrated through the number of nodes required in the mesh for each application. The transition to real-site modelling will require large

arrays to implemented, thus requiring the adoption of the continuous approach for modelling turbines.

For the simple domains adopted in this chapter, it is reasonable to explore array layouts through the use of discrete turbine implementation. Array layouts are considered with cases of staggered and aligned rows of turbines spaced at different longitudinal distances apart. This investigation extends the study of the idealised sites by not assuming rows are spaced to allow full mixing before the next downstream row to emulate more realistic space constraints of lease areas at real sites. The results indicated that the longitudinal distance between rows has a greater effect on the power than the arrangement of turbines and that the staggered layout and greater longitudinal row spacing cases yield the greatest power.

The impact of boundary effects on capacity factor and power is also investigated to highlight the effect on analysis when they are not accounted for and the importance of placing boundaries far from the place of interest when modelling a real site. The study of real sites will require open boundaries to be placed far from the area of interest and will typically be in much deeper areas of water than the cases modelled in this chapter.

Part II

Pentland Firth Case Study

Chapter 5

Heterogeneous Array Design Framework: Inner Sound Case Study

The study of a real site introduces new constraints on the resource. In this chapter, a heterogeneous array design framework is proposed to specify the diameter and rated speed of turbines based on the bathymetry and flow velocity across a site. The motivation for exploring array design in the context of spatial variability is presented in Section 5.1 through the review of other studies that have considered array design and resource extraction. The Inner Sound of the Pentland Firth is used as a case study to represent the variability of a real site, outlined in Section 5.2. However, the intention is to draw general, rather than site specific conclusions. In Section 5.3, details of the 2-D model of the Pentland Firth are presented and model validation is presented in Section 5.4. The heterogeneous array design framework is presented in Section 5.5, which implements heterogeneity of turbine specifications across a site as a whole, but maintains homogeneity within smaller array areas. This allows a compromise between uniformity of turbines, for ease of manufacturing, operation and maintenance, and heterogeneous turbine specifications to maximise utilisation of site area and power extraction. Cases that were homogeneous in diameter, homogeneous in diameter and control, and heterogeneous in diameter and control were defined and the results are presented in Section 5.6. The impact of site variability and design compromises on the power and capacity factor of arrays are discussed in Section 5.7. The performance of homogeneous and heterogeneous arrays are compared and further impacts of arrays on the flow at the site are also discussed.

5.1 Array Design and Practical Constraints

The investigation of low order parameters affecting tidal stream energy resource assessments in Chapter 3 considers some of the constraints on the resource (Figure 2.4) but

limitations of the model did not allow many of them to be explored (Patel et al., 2023). The study of a real site, in a 2-D model introduces the opportunity to explore additional constraints limiting the tidal stream resource.

There are a number of key challenges that need to be addressed to develop technology for extracting tidal stream energy. Two of these challenges are evaluating the magnitude of the resource and considering how to develop arrays at specific sites. Many prior studies have focused on arranging turbines to maximise positive hydrodynamic interaction (Draper and Nishino, 2014, Funke et al., 2016, O'Hara Murray and Gallego, 2017) with other work looking at optimising economic factors (Goss et al., 2020). Phoenix and Nash (2019) explored array layouts to minimise hydro-environmental effects and Du Feu et al. (2017) considered the trade-off between maximising the power yield of an array and the impact on the flow. The positive and negative hydrodynamic interactions are investigated by González-Gorbeña et al. (2015) for different array densities and thrust coefficients to conduct a resource assessment and the findings suggest the need for optimising complex array layouts to maximise power and reduce negative interference.

However, perhaps the biggest issue is the variable conditions across a typical tidal site. The flow at tidal sites is constrained by coastline and bathymetry, which is what causes the fast flow, and typically varies significantly over length scales of the order of the water depth. This means turbines in a farm may experience very different flow patterns and will be installed in varying water depths, which merit alternate turbine sizes. Thus, ideally a tidal farm would be designed so that each turbine was optimised for its local water depth and flow regime. However, homogeneity of turbines is typically preferred for array design because the uniformity offers ease of operations and maintenance, and reduces manufacturing costs by exploiting economies of volume. For large arrays, a degree of heterogeneity is expected, either due to incremental advances at the site or significant variations in the marine environment. There are limited and relatively few sites suitable for tidal energy extraction, in comparison to wind energy, therefore it is

important to maximise tidal sites.

The need to consider turbines of different specifications to accommodate spatial variation across a site is also recognised and investigated at the Alderney Race (Bahaj and Myers, 2004, Coles et al., 2020). Coles et al. (2020) expand on a notable early study of the site (Bahaj and Myers, 2004), demonstrating the need to update and refine site-based estimates. Bahaj and Myers (2004), use data from Admiralty Charts and Publications (1999) to define sub-arrays of 'first generation' devices, with different rotor diameter and rated power to assess the resource. The work is extended further in Coles et al. (2020) by using 2-D hydrodynamic modelling to improve data resolution, incorporate blockage effects and improve performance through power coefficient, array capacity, rotor diameter and device micro-siting enhancements. However, the consideration of heterogeneous arrays at the Alderney Race is site-specific.

A more systematic framework for defining and implementing heterogeneous arrays at any tidal site is presented in this chapter. The tidal resource of the Inner Sound is modelled and includes the parameterisation of turbines for different rotor size (diameter) and control (rated speed) to explore the impact on the resource when keeping these as uniform as possible. The framework enables the compromise between uniformity of turbine specifications and maximising energy yield from a site to be explored and can be used as a basis for defining what specifications of devices can be applied at a site for further micro-siting of turbines. Implementing homogeneous turbines is often the first step in quantifying the resource. This study looks at how array design can be prescribed by bathymetry and how much energy is sacrificed by implementing homogeneous arrays, rather than heterogeneous arrays at a site.

5.2 The Inner Sound and Meygen Lease Site

The Inner Sound is chosen as a case study because it is a significant site of interest, hosting the largest tidal energy plant in the world (Meygen), which has a lease area

covering 3.5 km. It is located north of the UK, between the Scottish mainland and the island of Stroma. The Inner Sound has characteristics that are typical of many tidal sites, including significant variation in bathymetry across the site and high flow velocities. Additionally, like the majority of tidal sites globally (Figure 3.5), the Inner Sound is characterised by semi-diurnal tides (Egbert and Ray, 2001, Martin-Short et al., 2015).

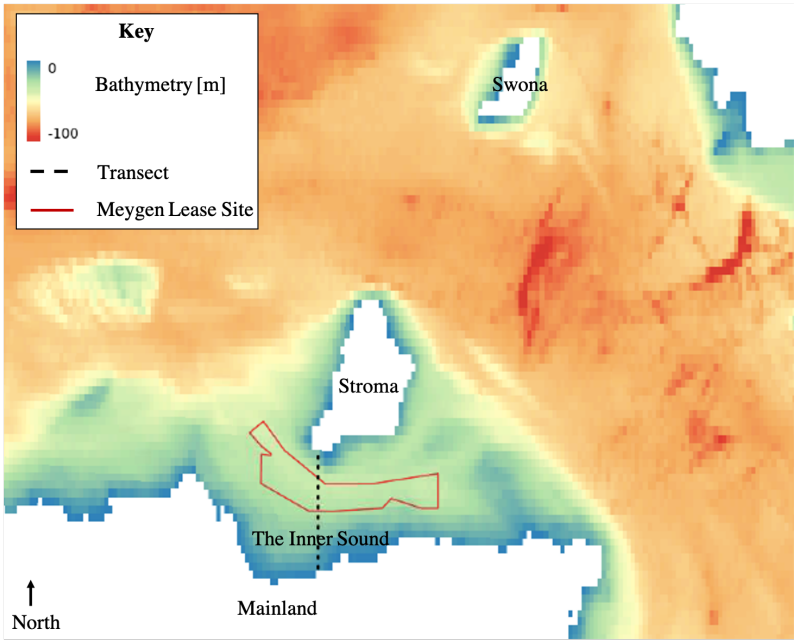

Figure 5.1: Map of the Pentland Firth with bathymetry data obtained from Edina Digimap Service (2020). The Meygen lease site and a transect used to evaluate the flow rate through the Inner Sound are presented.

The bathymetry for the Inner Sound is illustrated in Figure 5.1. As with most tidal stream energy sites, the Inner Sound, and the area occupied by the MeyGen lease site, has limited areas where the bathymetry is deep enough for large turbines to be deployed. The site was agreed for lease based on a 398 MW potential installed capacity. Figure 5.2 presents the planned development phases for the project to achieve this installed capacity.

Figure 5.2: Development phases of the Meygen lease site.

Phase 1 is operational and involved the deployment of four 1.5 MW turbines, which have produced 51 GWh in their 6 years of generating to grid (0.97 MW annual average power), as of March 2023 (SAE Renewables, 2023). The 18 m diameter turbines are bottom-fixed and horizontal-axis, with three blades each. Meygen has identified troughs across the site that are deep enough to deploy four turbines of this diameter. In initial stages of development, this is feasible, however, Phases 2 and 3 will require an increased installed capacity of 50 MW, necessitating more areas for turbines to be deployed by a target of 2028. The remaining 342 MW of installed capacity intended at the site are in planning stages.

5.3 Model Details

The 2-D modelling software, *Thetis*, utilised in Chapter 4 is used to model the Pentland Firth to undertake the study of the Inner Sound. The non-conservative form of the 2-D non-linear shallow water equations (Equation 4.1 and 4.2) are solved in *Thetis* (Kärnä et al., 2018, OpenTidalFarm, 2016, Goss et al., 2020). The 2-D shallow water equations are commonly used to capture leading order physics of tidal energy sites (Blunden and Bahaj, 2006, O'Rourke et al., 2010, Easton et al., 2012, Adcock et al., 2013).

The model has been adapted from Jordan et al. (2022) and modified for this study. The drag on the flow due to bed friction is applied to the seabed area using a spatially

variable Manning coefficient in this chapter, therefore, the bed friction in Equation 4.2 is represented as,

$$\frac{\tau_b}{\rho} = g n^2 \frac{|\mathbf{u}|\mathbf{u}}{H^{\frac{1}{3}}}, \tag{5.1}$$

where n is the Manning coefficient (Mackie, 2022, Jordan et al., 2022). The Manning coefficient was defined by Jordan et al. (2022) according to the classification of the seabed composition based on British Geological Survey data, with the method described by Mackie et al. (2021).

For large coastal domains, it is necessary to include the advection forces due to the Earth's rotation. The term that represents the Coriolis force in Equation 4.2 is made up of the Coriolis forcing parameter f and $\mathbf{u}^{\perp}$, which is the velocity vector rotated such that the components $(-v, u)$ are the transverse and longitudinal components of $\mathbf{u}$ (anti-clockwise over 90°).

Bathymetry data was obtained from Edina Digimap, with a resolution of 1 arc-second (approximately 30 m), and tidal constituent data from TPXO8-atlas (Edina Digimap Service, 2020, Egbert and Erofeeva, 2002). The model is forced with M_2 and S_2 constituent data for 14 days, representative of the spring-neap cycle, once fully evolved flow conditions were established from an initial state of equilibrium. The open boundaries are specified far away from the Pentland Firth (approximately 85 km east and west and 130 km north and south of the site) so that results are independent of the open boundary locations (Venugopal et al., 2010, Adcock et al., 2011). This is critical to avoid boundary effects impacting the analysis of results, as emphasised in Section 4.4. In Chapter 3 and previous studies it has been demonstrated that using two constituents to model a semi-diurnal site leads to up to 9% difference in power, in comparison to modelling with 8 constituents, and has been shown to capture the leading order physics of the site (Adcock et al., 2014, Patel et al., 2023). In this study, the relative changes between cases are being considered, therefore, modelling with 2 constituents is sufficient to capture the variability over the spring-neap cycle as a minimum requirement.

Prescribing the elevation at the boundary is theoretically incorrect because the free-surface at the open boundaries should be allowed to change due to changes in tidal dynamics within a model. However, according to Rainey (2009), the error in the free-surface elevation at the boundary will be negligible if the changes to the tidal dynamics at the boundary are small and the boundary does not induce any resonance due to the principal constituents of harmonics. Adcock et al. (2013) found that deploying a significant number of turbines, which would lead to a 25% decrease in flow rate through the Pentland Firth, would only cause up to 3% change in flow rate at the boundary demonstrating the insignificance of the error that is introduced by the forcing and locations of the open boundaries.

The unstructured triangular mesh used to model the Pentland Firth in this chapter is presented in Figure 5.3. The domain is discretised with the discontinuous Galerkin piecewise linear velocity-pressure finite element pair. The final unstructured mesh has 20,710 nodes, with a minimum element size of 60 m in the area where turbines are placed. A timestep of 50 s was used.

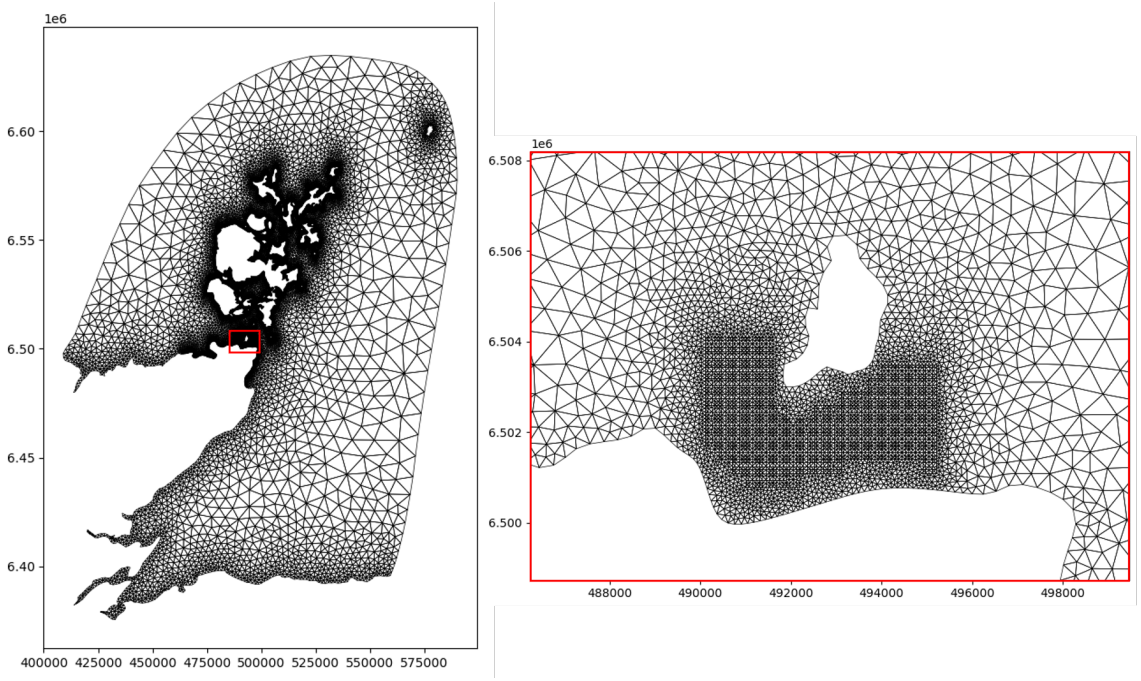

Figure 5.3: Mesh used in the study to model homogeneous and heterogeneous arrays in the Inner Sound.

Between high and low tides, inter-tidal zones can be observed at coastal areas. During high tides, zones are submerged and during low tides they are exposed, leading to wetting and drying of the coastal areas during the tidal cycle. Wetting and drying is most significant in areas with a large tidal range and gently sloping bathymetry. The wetting and drying process is represented by the modified bathymetry formulation, presented by Kärnä et al. (2011),

$$\tilde{h} = h + \frac{1}{2}\left(\sqrt{H^2 + {\alpha_{WD}}^2} - H\right), \tag{5.2}$$

where h is the bathymetry and $\tilde{h}$ is the modified bathymetry, which is used to ensure the total water depth, H, is always positive. The wetting and drying parameter is denoted by α_{WD} and dictates the size of the transition zone between wet and dry areas. The value of α_{WD} is set to 0.5 m, as used in other studies (Kärnä et al., 2011, Mackie, 2022, Jordan et al., 2022).

5.3.1 Turbine Implementation

Turbines are modelled as a momentum sink, as in Chapter 4, which is an approximation and cannot fully capture the 3D interaction between the turbine and the flow. The thrust generated by a turbine is also not applied uniformly across the water column in reality, which is what is imposed in a depth-averaged model (discussed in Section 2.2). The continuous approach for implementing turbines is used in this chapter because the focus is on the resource across a site and how it responds to different turbine specifications in arrays, rather than the micro-siting of turbines. Therefore, individual turbines do not need to be resolved discretely. The number of turbines is applied as a turbine density to the relevant subdomain (Equation 4.10).

Blockage is an important effect to be accounted for in models because it allows greater energy to be extracted from tidal turbines (Garrett and Cummins, 2007, Whelan et al., 2009, Dehtyriov et al., 2021). When modelling a real site it is difficult to assess the blockage that turbines experience because the depth and width of a channel at a real site varies and blockage is dependent on the cross sectional area of flow. There is no

formally robust method for incorporating the effect of blockage into models given the different methods and assumptions of including turbines and their interaction with the flow between different models. In this chapter, blockage-corrected blade element momentum theory (BC-BEMT) is used to calculate the coefficients of power and thrust of turbines included in this study (Vogel et al., 2018, Chen, 2019), despite the difficulty in calculating blockage for a real site. Performance curves are defined based on the assumption that all turbines adopt VSVP control in this study. Although a VSVP control strategy is prevalent for large diameter turbines, whilst smaller turbines typically operate with fixed pitch (Adcock et al., 2021), VSVP operation is assumed for all turbines to allow a more uniform approach.

The number of turbines implemented in each array area, to calculate and assign the turbine density, was based on a spacing between turbines to allow for approximately 0.16 blockage. The blade designed by Cao et al. (2018) for optimal performance in 0.16 blockage, that was adopted in Chapter 3, was used as the closest relevant blade design. The thrust applied by the cylindrical, bottom-fixed, support structure is calculated as,

$$F_S = 0.5\rho C_{D,S} A_S u^2, \tag{5.3}$$

with drag coefficient $C_{D,S} = 1.2$ over a wide range of Reynolds numbers (Muchala and Willden, 2017). The frontal area of the support structure, A_S, is the product of the support structure diameter D_S and the length of the support structure L_S. The length of the support structure is the sum of turbine radius and the seabed to blade-tip clearance. The diameter of the support structure is based on a 0.2 ratio between A_S and the rotor area, A_T, as proposed by Muchala and Willden (2017) for a 20 m diameter turbine. This method is simpler and more conservative compared to the thrust-capping approach suggested by Wang and Adcock (2018). When turbines are deployed in areas with greater depth than the minimum clearance requirements, the diameter of the support structure is increased according to the increased length of the support structure.

Individual turbine wakes and associated turbulence cannot be explicitly represented

in this work due to the resolution of the mesh required, which is unfeasible in large domains. However, turbulent mixing cannot be excluded and the horizontal viscosity approach adopted in Chapter 4 is reasonable for the objectives of this thesis because of the scale of modelling undertaken.

5.4 Model Validation

The model of the Pentland Firth used in this study has undergone validation in the study it was adopted from (Jordan et al., 2022) through comparison of amplitude and phase of M_2 and S_2 constituents and correlation of vector components of velocity between observed data from ADCP and data predicted by the model and the comparison of elevation data at Wick tidal gauge to the model. Given the minor modifications made to the model further validation checks have been carried out to ensure there is no substantial change in the natural flow considerations. Comparing the model to observed data from *in-situ* measurements is important for modelling real sites due to the necessary simplifications in the model and the assumptions regarding boundary conditions, seabed characterisation and accuracy of bathymetry data. Adcock et al. (2021) suggests the phase difference is most important to examine in the validation of currents. The phase is primarily dependent on accurate characterisation of the dynamic balance, emphasised as a critical parameter in Chapter 3. Therefore, it is less dependent on local factors that are affected by measurement and post-processing errors due to *in-situ* measurements susceptibility to noise.

The modelled and observed data for harmonic products of the M_2 and S_2 constituents (amplitude and phase) are presented for velocity in Table 5.1 and for elevation in Table 5.2. Figure 5.4 presents the three acoustic Doppler current profilers (ADCPs) (green) that were used to validate velocity and the tidal gauges (red) that were used to validate elevation.

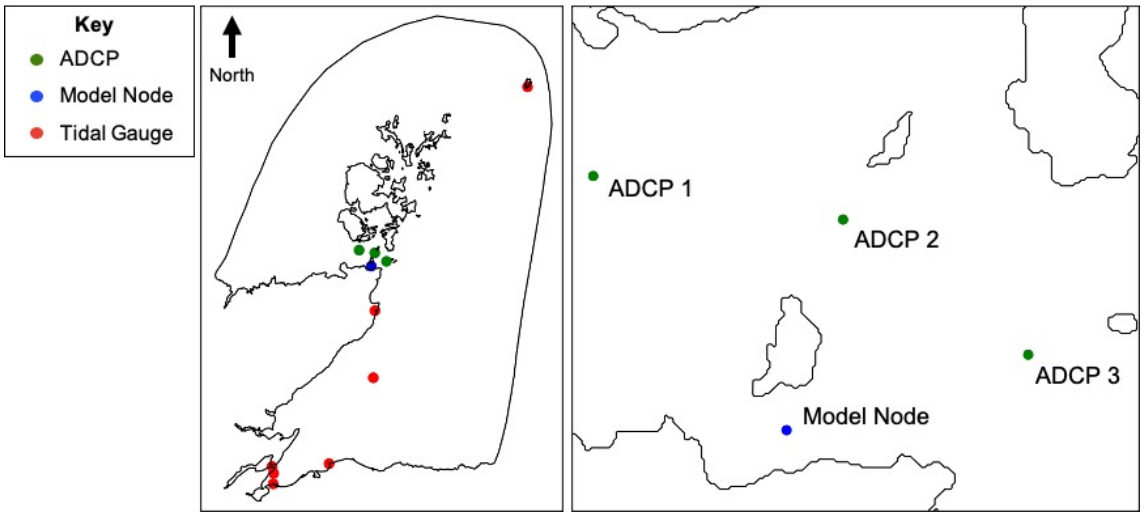

Figure 5.4: Points across the model's domain where observed and modelled data were compared for validation.

Table 5.1: Validation of model velocity against observed data from ADCPs.

	Constituent	Observed amplitude [m/s]	Modelled amplitude [m/s]	Amplitude difference [m/s]	Observed phase [°]	Modelled phase [°]	Phase difference [°]
ADCP 1	M_2	1.70	1.68	0.02	248	240	8
	S_2	0.59	0.62	0.03	281	279	2
ADCP 2	M_2	2.53	2.78	0.26	244	250	6
	S_2	0.98	0.94	0.04	291	293	2
ADCP 3	M_2	2.35	2.31	0.04	251	256	5
	S_2	0.67	0.86	0.19	296	291	5

The observed velocity data from ADCPs was obtained from the literature, published in Adcock et al. (2013). The comparison of observed and modelled data for harmonic analysis of velocity are more sensitive to bed friction, as indicated in Garrett and Cummins (2005). Modelling with a spatially variable Manning coefficient for bed friction across the model's domain aligns well with the observed data.

For the elevation comparisons, the results demonstrate good agreement and changes in bed friction values across the domain, modelling with quadratic drag and spatially variable Manning coefficients, show little to no difference in results. The co-tidal chart

for the M_2 constituent is presented in Figure 5.5.

Table 5.2: Validation of model elevation against observed data from tidal gauges.

	Constituent	Observed amplitude [m]	Modelled amplitude [m]	Amplitude difference [m]	Observed phase [°]	Modelled phase [°]	Phase difference [°]
Wick	M_2	1.02	1.03	0.01	322	321	1
	S_2	0.35	0.35	0	0.30	357	3
Burghead	M_2	1.16	1.22	0.06	340	336	4
	S_2	0.39	0.43	0.04	18	12.9	5
Cromarty	M_2	1.29	1.21	0.08	335	335	0
	S_2	0.46	0.43	0.03	12.2	10.9	1.3
Fair	M_2	0.61	0.57	0.04	300	305	5
	S_2	0.21	0.21	0	331	336	5
Moray Firth	M_2	1.30	1.27	0.03	337	336	1
	S_2	0.45	0.45	0	15.1	11.7	3
Nigg	M_2	1.29	1.27	0.02	335	335	0
	S_2	0.46	0.45	0.01	12.2	11	1
Penrod	M_2	1.09	1.11	0.02	331	332	1
	S_2	0.40	0.39	0.011	6	7.89	1.9

For each mesh used to model the Pentland Firth in the thesis, mesh independence was examined to ensure the elevation and velocity were unaffected by changes. The resolution of each mesh was highly dependent on the use of the mesh and representation of turbines. Therefore, the balance between computational expense and accurate representation of flow, particularly in areas of interest, was important, as emphasised by Goss et al. (2018).

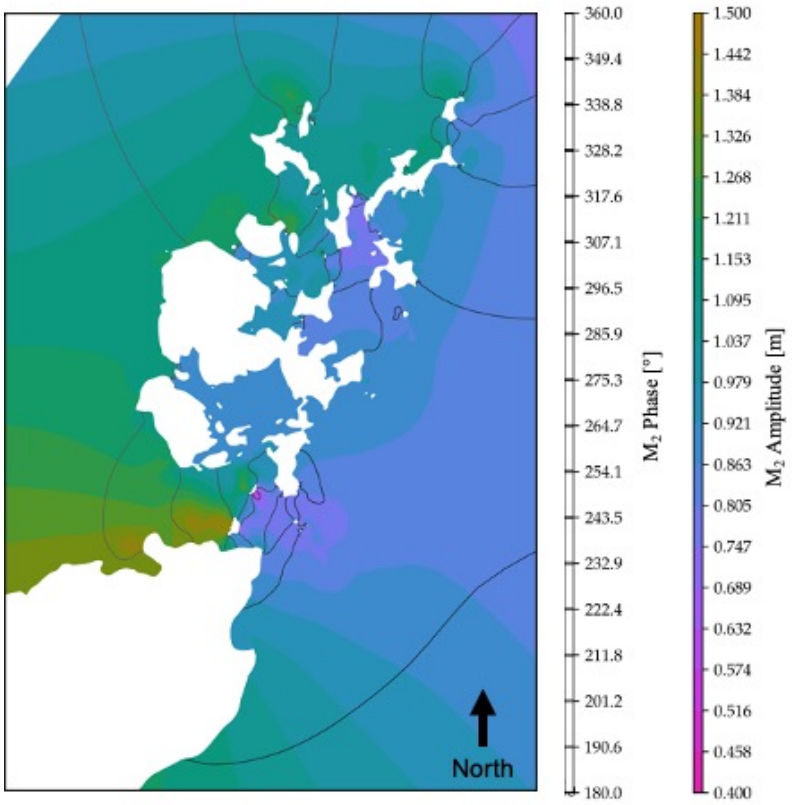

Figure 5.5: Co-tidal chart from the model used in this thesis demonstrating the M2 amplitude and phase across the domain.

One of the fundamental difficulties in tidal stream resource assessments is validating power output. Due to the status of industry tidal developments, there is limited data to assess against. Therefore, cases from previous modelling work by Adcock et al. (2013) were replicated to assess the validity of power predicted with the method of implementing turbines in *Thetis*. Adcock et al. (2013) solve the shallow water equations in discontinuous Galerkin ADCIRC (DG ADCIRC) (Kubatko et al., 2006) and represent turbines as line discontinuities in elevation. For undertaking this comparison, ADT is adopted, rather than BC-BEMT, to keep in line with the original study due to the interest in validating turbine implementation rather than turbine performance.

The mesh presented in Figure 5.6 illustrates the placement of the nine rows of turbines modelled for the comparison of results in Adcock et al. (2013). This study reproduces two cases from Adcock et al. (2013)—turbines in Row B1 with a blockage of 0.1 and

turbines in all nine rows with 0.4 blockage. The average power for each case is outlined in Table 5.3. Velocity data in the Pentland Firth was extracted from the same point in both models (illustrated in Figure 5.4 as model Node) and compared to further assess the validity of the *Thetis* model and the envelope of the flow rate is presented in Figure 5.7. The envelope of a signal demonstrates the boundary within which the signal is contained in the time domain and provides a clearer representation of the variation of the signal over time, calculated with the Hilbert transform (Ulrich, 2006). The results show good agreement considering the different turbine implementations, numerical schemes, bed friction representation, mesh and bathymetry data used in each model. This cross comparison gives us significant confidence that the turbines are capturing the correct fundamental physics with that of previous studies.

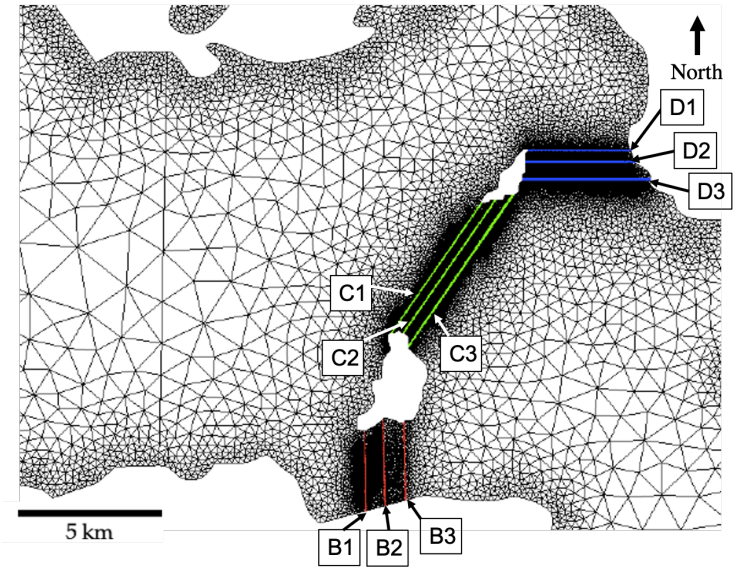

Figure 5.6: Mesh used to replicate Adcock et al. (2013) results with turbine row locations labelled according to Adcock et al. (2013).

Table 5.3: Comparison of results for two cases from Adcock et al. (2013).

		Average Power [GW]	
		DG ADCIRC	
Turbine Rows	Blockage	Adcock et al. (2013)	Thetis
Area B - 1 row	0.1	0.011	0.013
Areas B, C, D - 3 rows	0.4	1.94	2.24

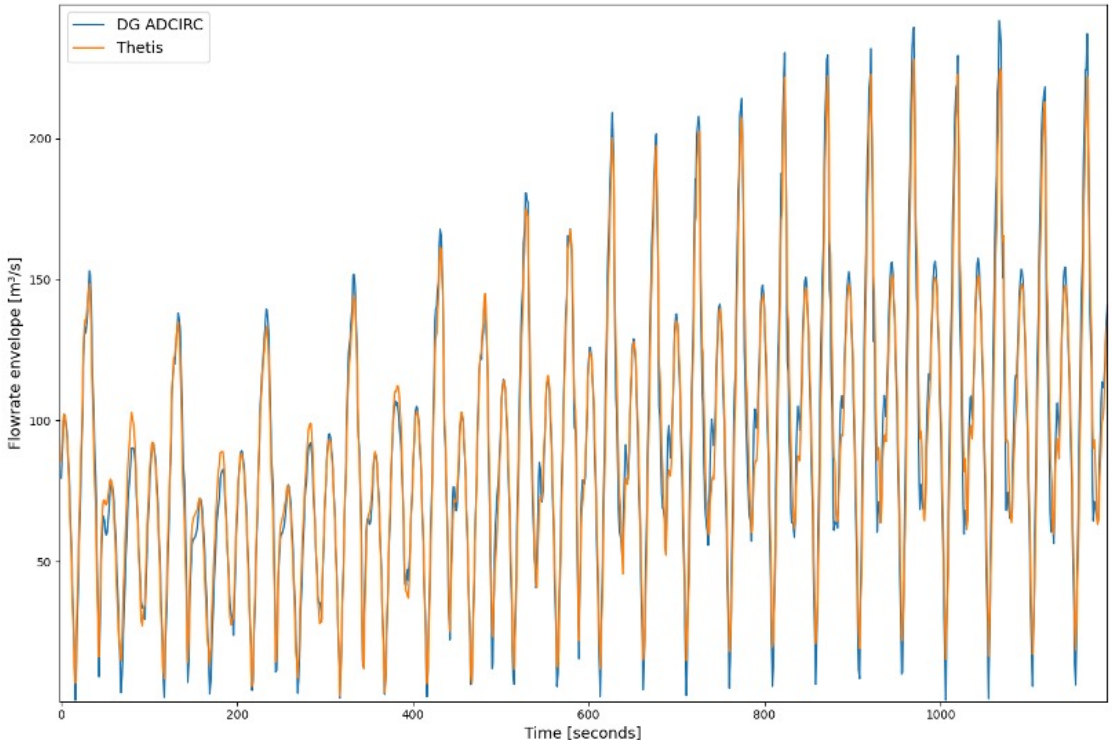

Figure 5.7: Envelope of the flow rate at a point in the model for the Adcock et al. (2013) DG ADCIRC model and in the *Thetis* model using in this study.

5.5 Heterogeneous Array Design Framework

The heterogeneous array design framework defines the turbine specifications for an array at any site based on site characteristics (flow velocity and bathymetry). The turbine specification refers to the diameter and rated speed of the turbines. The framework introduces heterogeneity of turbine specifications across a site as a whole, but deploys multiple homogeneous array areas within the array. This allows a compromise between uniformity of turbines, for ease of manufacturing, operation and maintenance, and heterogeneous turbine specifications to maximise utilisation of site area and power extraction.

Sixteen turbine specifications are considered in this framework; four rotor diameters (5 m, 10 m, 15 m and 20 m) and four rated speeds (1.5 m/s, 2.0 m/s, 2.5 m/s and 3.0 m/s). To ensure minimum blade tip to seabed (5 m) and blade tip to sea surface (8 m) clearances for bottom-fixed turbines according to the lowest astronomical tide outlined in Meygen (2012), the turbine diameter assigned to each array was assessed

against a bathymetry range presented in Table 5.4.

Table 5.4: Allowable turbine diameter based on minimum clearance requirements: 5 m blade tip to seabed and 8 m blade tip to sea surface, outlined in Meygen (2012).

Water Depth [m]	Turbine Diameter [m]
18 - 22	5
23 - 27	5, 10
28 - 32	5, 10, 15
> 33	5, 10, 15, 20

The framework for defining turbine specifications, developing the mesh and gathering data for the simulations is outlined in Figure 5.8 and input values are presented in Table 5.5. The extent of the area studied is specified and a grid of equally distributed coordinates, spaced l_s apart, are defined across the area, marking the centre of the square sub-array areas. The value of l_s should be determined based on the bathymetry resolution and the desired number of array areas to maintain computational efficiency. The bathymetry at each coordinate and at eight sample points around the coordinate, within the sub-array, are calculated. This allows any areas shallower than the minimum bathymetry to be excluded from having turbines deployed there because they would not comply with minimum clearances required for the smallest diameter turbine considered in the study (Table 5.4).

The distance from each coordinate to the coastline is calculated and turbines are not deployed to areas within a minimum distance, l_{min}, of the coast to avoid the width of the sub-channel being fully occupied or unrealistically placing turbines too close to the coast (Table 5.5). A similar proximity to the coast as the current MeyGen lease site is implemented (The Crown Estate, 2023, SAE Renewables, 2023). For the remaining coordinates, the minimum bathymetry across the sampled points are stored. Square areas with side length, l_s, are created around each stored coordinate. These represent the individual array areas in this study. A mesh is defined and the individual array area

subdomains are prescribed a unique ID to allow the assignment of different turbine specifications to each array area.

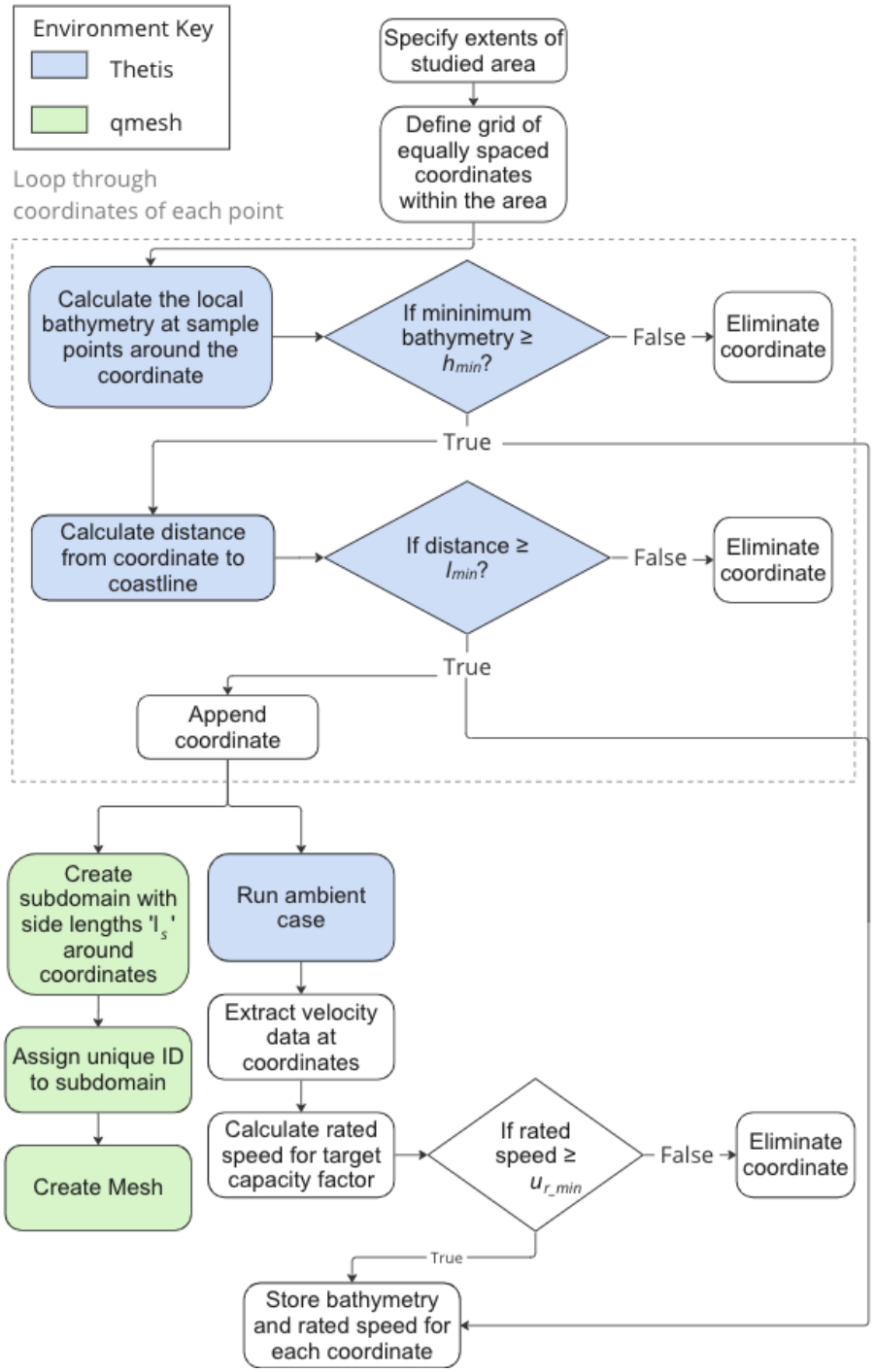

Figure 5.8: Flowchart explaining the method for creating the mesh and collecting data for assigning the turbine specifications in each array area.

Table 5.5: Inputs and values for meshing method used in this study.

Input	Value
Array area dimensions, l_s^2	300 x 300 m
Minimum deployment bathymetry, h_{min}	18 m
Minimum deployment distance from coastline, l_{min}	400 m
Minimum turbine rated speed, u_{r_min}	1.5 m/s

The rated speed is an important characteristic for turbine control and the turbine performance curve (Section 3.4.4) (Vogel et al., 2019, Wang and Adcock, 2019, Patel et al., 2023). It is the value of velocity above which, power is capped to the rated power up until the cut-off speed, where the turbine stops producing power. Capacity factor can indicate whether the rated speed is set too high or too low because the rated speed defines the rated power. A low capacity factor indicates a high rated speed, which can lead to a generator being oversized to accommodate peak velocities and subsequent spikes in power that occur over short periods of time. If the rated speed is too low, resulting in the capacity factor being too high, it indicates that high velocities occurring during the spring tide are not being fully exploited.

An ambient case, with no turbines, is simulated and velocity data is extracted from the stored coordinates of the remaining points. This simulation does not require use of the specific mesh created for homogeneous and heterogeneous cases, because it does not include any turbines. Therefore, it can be done as a parallel step to meshing by using a mesh without separate subdomains if mesh independence is achieved. A rated speed for each array is calculated, based on the ambient velocity data, to achieve a target capacity factor of 40% using the Newton-Raphson method. The target capacity factor is chosen based on the Verdant Power development, which has achieved a capacity factor of 0.42 over nine months of operation (Verdant Power, 2021, Coles et al., 2020). Any areas with a rated speed of less than 1.5 m/s is deemed to be not viable for energy extraction due to lack of sufficient power density. For the homogeneous diameter and

control cases, the modal value for rated speed across the array areas of homogeneous diameter is applied. A cut-in speed of 0.5 m/s and cut-out speed of 5 m/s is applied across turbines. The choice of cut-in and cut-out speeds were demonstrated to have significantly less impact on the power output of an array in Chapter 3.

The turbine specifications that are varied in this study are the diameter and rated speed (control) of devices within each sub-array. The homogeneous approach is split into two classifications; homogeneous in both turbine diameter and rated speed (homogeneous diameter and control), and homogeneous in turbine diameter only (homogeneous diameter). For the homogeneous diameter and control cases, arrays of 5 m, 10 m, 15 m or 20 m diameter turbines are deployed in allowable areas (Table 5.4) and the rated speed of turbines across the site is uniform, based on the modal value assigned to arrays considered in each case. The homogeneous diameter cases, consider the same diameters of turbines but the rated speed for each array varies across the entire site. For the heterogeneous case, all array areas are occupied by the maximum permissible diameter of turbine, and the rated speed of turbines in each array varies across the site. For cases with any aspect of heterogeneity, multiple turbine densities and turbine performance curves must be defined with each thrust curve represented as an additional momentum sink.

A number of assumptions are made on the placement of turbines. The seabed gradient and associated foundation issues are not considered. Additionally, space required for cabling and shipping lanes are not explicitly incorporated into the array design framework.

5.6 Results

Across the Inner Sound, a total of 81 sub-array areas were defined following the procedure outlined in Figure 5.8. The specification of turbines for each array area is presented in Figure 5.9. In this case study, no turbines were assigned a rated speed of 3 m/s despite

being considered as an option.

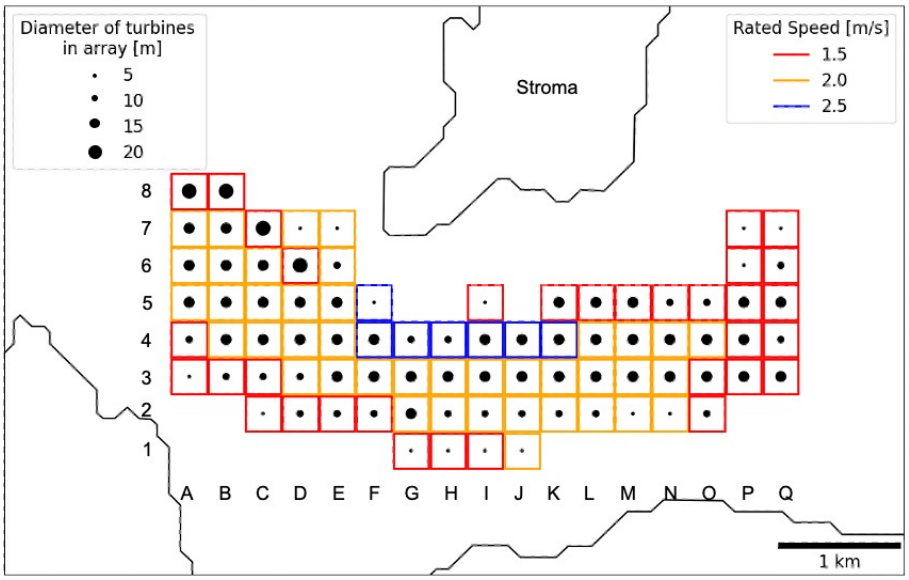

Figure 5.9: Individual array areas considered in the study. The maximum diameter of turbines allowable in each array indicated by the size of the inner black circle and the rated speed indicated by the edge colour.

In the heterogeneous case, 52% of array areas are occupied by 15 m diameter turbines (42 areas). The 10 m and 5 m diameter turbines occupy 20 and 15 array areas respectively. Four array areas in this study have bathymetry large enough to accommodate 20 m diameter turbines whilst meeting minimum clearance requirements.

For homogeneous cases, 5 m diameter turbines occupy all array areas that meet minimum siting constraints and as the diameter of turbines in each homogeneous case increases, the number of array areas occupied decreases due to diameter-specific bathymetry restrictions (as per Table 5.4). The results of the heterogeneous and homogeneous cases simulated for this study are summarised in Table 5.6. The power presented in Table 5.6, and throughout the results, is averaged over the 14-day spring-neap cycle and should not be taken as the maximum power output of the arrays. The power calculated in this study does not account for power take-off efficiency losses.

To consider the results presented in Table 5.6 in detail, the individual performance of array areas in the homogeneous diameter cases are presented in Figures 5.10 and 5.11.

Table 5.6: Overview of results for homogeneous diameter and control, homogeneous diameter and heterogeneous cases, all powers are averaged over the spring-neap cycle.

	Diameter [m]	Rated Speed [m/s]	Number of Turbines	Number of Array Areas	Total Swept Area [m^2]	Installed Capacity [MW]	Average Power [MW]	Capacity Factor	Average Power [MW] per Turbine	Average Power per Swept Area [kW/m^2]	Average Power per Thrust [kW/N] per Swept Area
Homo-geneous	5	2	6932	81	136110	300	80.96	0.27	0.0117	0.59	0.347
	10	2	1413	66	110977	250	72.69	0.29	0.0514	0.66	0.369
	15	2	438	46	77401	176	61.13	0.35	0.1396	0.79	0.418
	20	1.5	21	4	6597	6	2.81	0.44	0.1338	0.43	0.426
	5	1.5 - 2.5	6932	81	136110	260	79.45	0.33	0.0115	0.58	0.356
	10	1.5 - 2.5	1413	66	110977	220	69.70	0.34	0.0493	0.63	0.374
	15	1.5 - 2.5	438	46	77401	161	59.57	0.38	0.1360	0.77	0.421
Hetero-geneous	5 - 20	1.5 - 2.5	2134	81	136110	260	75.32	0.31	0.0353	0.55	0.344

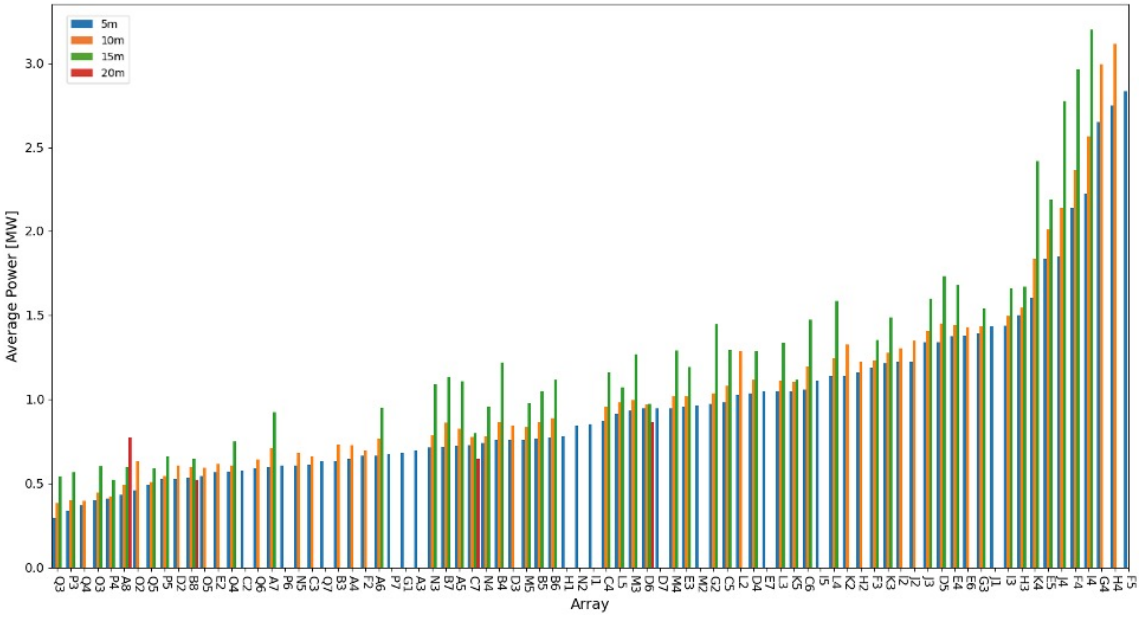

Figure 5.10: Average power for individual arrays in the homogeneous diameter cases, ordered according to increasing average power for the 5 m diameter case.

In Figure 5.10, results are arranged in order of increasing average power according to the 5 m homogeneous diameter case, which can be deployed in every feasible array area. The average power for each array is plotted to allow comparison of the power output based on the diameter of turbines placed in each area. For a heterogeneous array, resource spatial variability is demonstrated in Figure 5.12, which presents the average power, capacity factor and average power per swept area of each array area, and the specification of turbines that occupy each area.

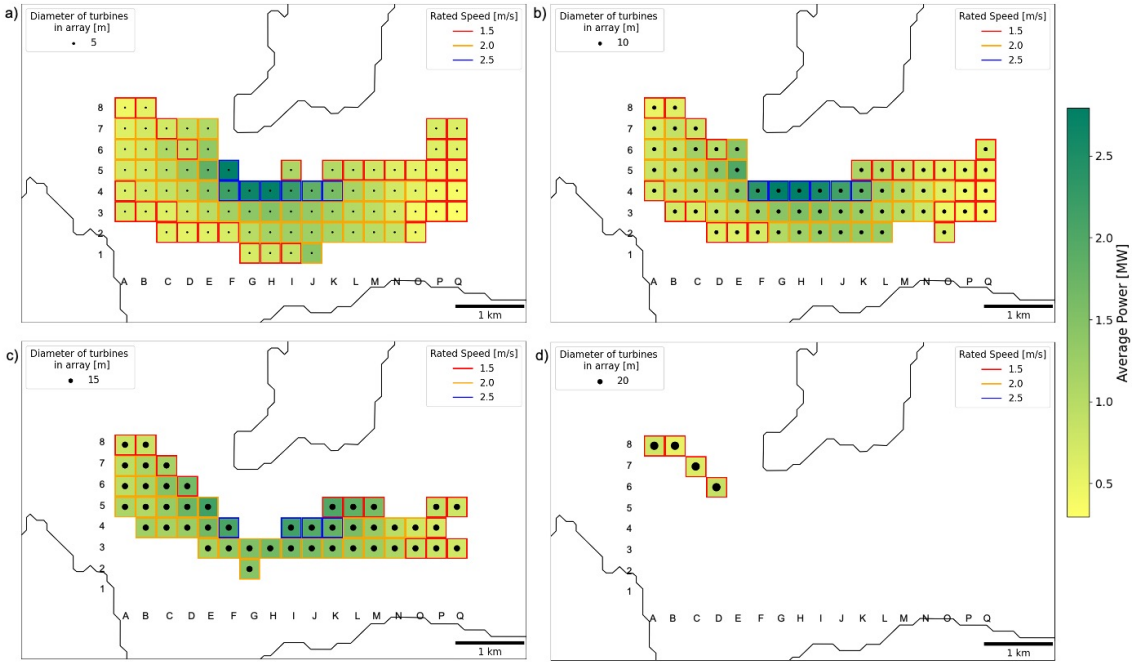

Figure 5.11: Average power for homogeneous diameter cases: a) 5 m, b) 10 m, c) 15 m and d) 20 m diameter. The rated speed of turbines in each array area is illustrated by the edge colour of the square and the diameter of the turbines is indicated by the size of the black circle.

The average power for each homogeneous case (both homogeneous diameter and homogeneous diameter and control) decreases with increasing diameter of turbine, whilst the capacity factor increases. Therefore, the greatest average power, for both homogeneous diameter and homogeneous diameter and control cases, is achieved when 5 m diameter turbines are deployed across the entire Inner Sound, with 79.45 MW and 80.96 MW for each case respectively. The high value in average power is mostly due to the large number of turbines deployed (almost 7000 turbines in total) and greatest capacity installed in the 5 m homogeneous case. This is attributed to the deployment of 5 m diameter turbines across all 81 sub-arrays, including areas where larger turbines are not allowed due to bathymetry constraints (Table 5.4).

In the 20 m diameter turbine array areas, control is uniform as they are assigned the same rated speed. The 20 m diameter turbine sub-arrays are situated in the same area, south west of Stroma (Figure 5.11), and the resource does not vary across these arrays as significantly as it does across the whole Inner Sound. The areas where 20 m diameter turbines are placed appear to have a low concentration of the resource because they are

all assigned rated speed of 1.5 m/s, which is the lowest value considered in this study. This highlights a trade-off between deploying larger turbines in deeper waters, which offer the necessary space whilst maintaining minimum clearance requirements, but consequently experience reduced flow velocities due to their increased depth. This decrease in flow speed and subsequent reduction in the concentration of the resource in these areas, due to conservation of mass, diminishes the potential power output, despite the advantage of accommodating larger turbines.

The eight array areas on the right hand side of Figure 5.10 (K4, E5, J4, F4, I4, G4, H4, F5) produce the most power on average for both the homogeneous diameter and heterogeneous cases. These array areas are located south of the island Stroma (Figure 5.11) demonstrating the concentration of the resource close to the narrowest constriction between Stroma and the mainland. All but one of the arrays have turbines operating at a rated speed of 2.5 m/s, which is the highest rated speed assigned in this case study. This indicates that in the ambient case the largest velocities occur in these areas as the flow passes the island, Stroma. Not allowing heterogeneous control and assigning the modal rated speed (to 2 m/s from 2.5 m/s) across the site leads to an increase in capacity factor and decrease in power because the turbine is being capped at a lower velocity for each array.

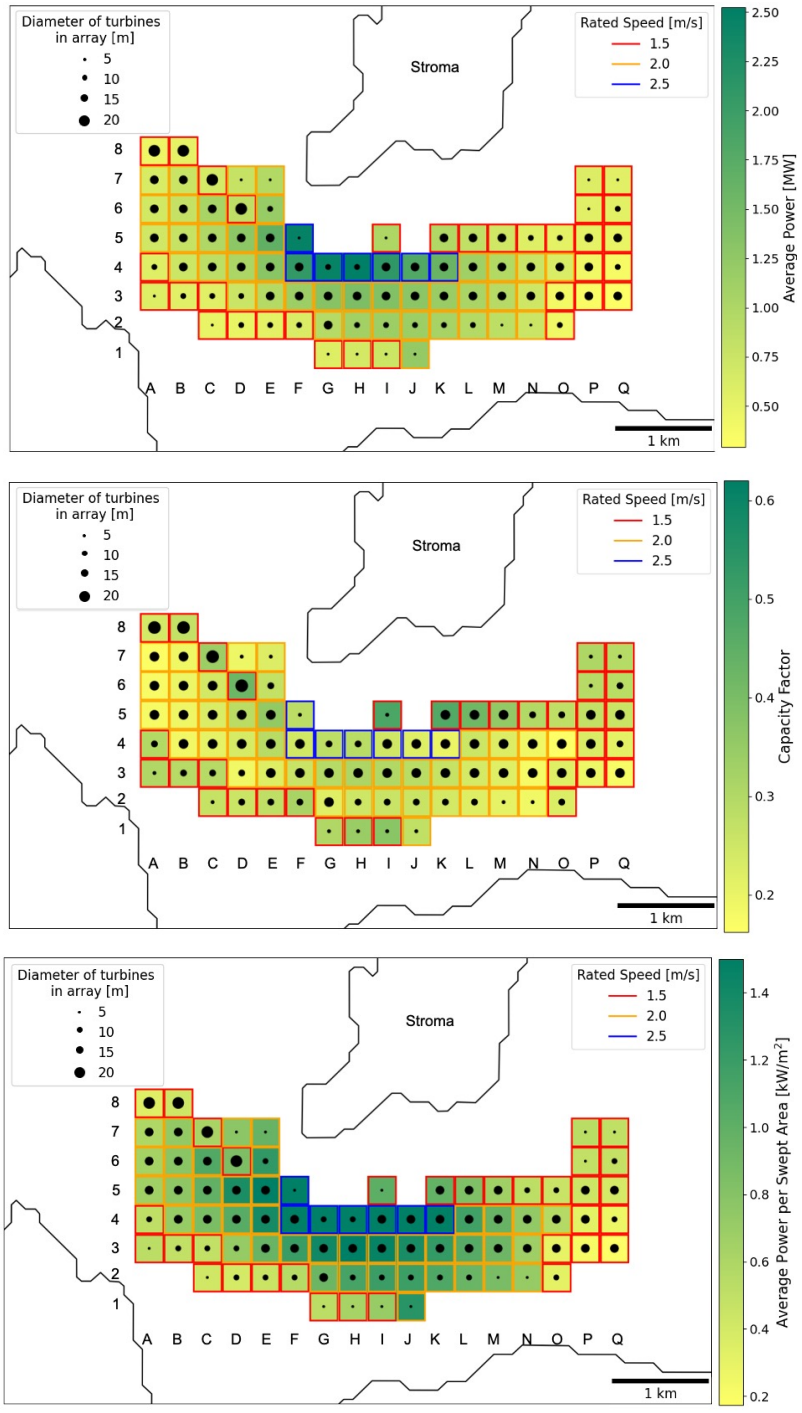

Figure 5.12: Average power, capacity factor and average power per swept area of arrays in the heterogeneous case. The rated speed of turbines in each array area is illustrated by the edge colour of the square and the diameter of the turbines is indicated by the size of the black circle.

The 15 m diameter turbines consistently demonstrate higher average power outputs compared to the 5 m and 10 m diameter turbines, across all permissible array areas (Figure 5.10). This occurs because there are fewer permissible array areas for 15 m

diameter turbines (the installed capacity is 62% of the 5 m case) and therefore less resistance on the flow due to turbines, which results in a smaller reduction in flow rate. The reduction in flow rate is evidenced by the decrease in capacity factor by 5 – 8% between the 15 m and 5 m homogeneous cases (discussed further in Section 5.7.2). The average power for the 15 m case compared to the 5 m case increases by more than 50% for some array areas, particularly those on the east and west sides of the overall area occupied by turbines. Arrays A5 and B4, located on the east side, and arrays P3 and Q3 on the west side are examples of arrays that experience this scale of increase in average power (Figure 5.11). These arrays are adjacent to areas designated for 5 m or 10 m diameter turbines. Consequently, in the homogeneous 15 m diameter turbine case these adjacent areas remain turbine-free, thus the flow rate is not reduced to the same extent as in other cases during ebb and flood due to the predominantly east-west flow in this channel.

5.7 Discussion

5.7.1 Array Composition Effects on Power Performance

The power per turbine and power per swept area are useful power performance indicators to consider when comparing arrays consisting of different number and size of turbines, but maintaining the same approximate blockage. The average power per turbine and power per swept area increases as diameter increases. The 5 m homogeneous cases have the lowest power per turbine and power per swept area compared to all the other larger diameter homogeneous cases with only 11.5 – 11.7 kW/turbine and 0.06 kW/m^2 because they have the greatest installed capacities and number of turbines, introducing greater resistance to the flow. The rated power of the 5 m turbine at rated speed of 2 m/s is approximately 40 kW. Deploying almost 7,000 turbines when each turbine only produces approximately 10 kW is not a feasible development strategy for a site, despite the seemingly high average power overall, considering the capital and operational costs associated with tidal turbines (Goss et al., 2021).

The highest performing array for the heterogeneous case in terms of power per swept area is array H4, with 1.76 kW/m^2 (Figure 5.12). The arrays that experience the least power per swept area are located on the south east of the studied array areas. Array Q3, located on the most south eastern corner of all the array areas, experiences the least power per swept area (0.23 kW/m^2). This array has a rated speed of 1.5 m/s, whereas the highest performing array has a rated speed of 2.5 m/s. The rated speeds are indicative of where the resource is concentrated based on ambient velocity data and the power per swept area reinforces this by mapping concentration of the resource across the Inner Sound.

Balancing performance, efficiency, and cost-effectiveness of an array is a key consideration for any tidal development. Large thrusts applied by turbines can be associated with increased costs and resistance to the flow but also the potential for greater power generation. Table 5.6 presents the average power per thrust per swept area for each case. Power per thrust is calculated by dividing the total instantaneous power and thrust of the array at each time-step and averaging over the spring-neap cycle. The power per thrust is divided by the swept area of the rotor. The metric of power per thrust is presented per swept area to give a more comparable metric between cases due to the different diameters of turbines in this study. The average power per thrust per swept area increases with increasing turbine diameter in the homogeneous cases. In contrast to the metrics of average power per turbine or average power per swept area, the homogeneous diameter and control cases have lower values for power per thrust compared to the homogeneous diameter cases for each turbine diameter. Although the average power per thrust per swept area is only marginally higher for the homogeneous diameter cases, compared to the homogeneous diameter and control cases, the result does indicate that allowing variable rated speed for the operation of turbines across a site is beneficial because it is a critical point in the performance curve for both power and thrust (Section 3.4.4).

5.7.2 Capacity Factor as an Indicator of Array Impact on Flow Characteristics

Although the rated speed was defined based on ambient velocity data to achieve a 40% capacity factor, a number of arrays in each case have capacity factors that are notably lower (Table 5.6 and Figure 5.12). The decrease in capacity factor is a result of array-induced flow adjustment compared to the ambient case, attributed to the thrust imposed on the flow due to turbines and the drag from the turbine support structures, when there are a large number of turbines present. The ambient case does not account for the impact of the flow due to the presence of an array and therefore, the rated speed specified for each array to achieve a 40% capacity factor will be either underestimated or overestimated depending on array interactions.

The flow rate, $Q(t)$, is evaluated across the transect presented in Figure 5.1 as,

$$Q(t) = \iint u(z, x, t)\mathrm{d}z\,\mathrm{d}x \tag{5.4}$$

where x is the distance along the transect, and z is the water depth, and $u(z, x, t)$ is the velocity normal to the transect (east-west). Figure 5.13 presents the flow rate across the transect during a spring cycle and neap cycle for the homogeneous diameter and heterogeneous cases and an ambient case with no turbines present. It is evident that cases with low capacity factors also have the lowest flow rates compared to ambient case. The rated speed is calculated based on ambient velocity, where resistance in the channel is lower due to no turbines being present. Therefore, the overall velocity in the channel is higher than when many turbines are installed. When the capacity factor decreases significantly below the target capacity factor, this indicates that the reduction in velocity due to the presence of turbines is large. Therefore, the array does not perform as well as expected based on ambient data and could lead to a rated speed that is too high being applied.

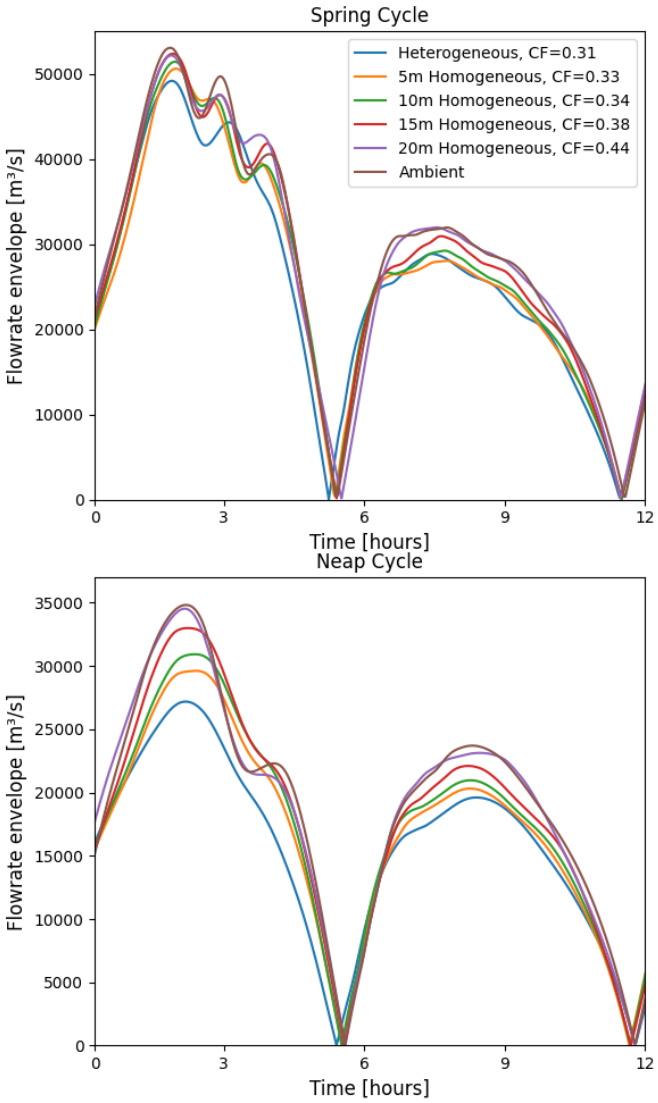

Figure 5.13: Envelope of the total flow rate across a transect of the channel during a spring cycle and neap cycle for the homogeneous diameter and heterogeneous cases and an ambient case with no turbines present. Capacity factor (CF) of each case is indicated in the key.

In cases where only diameter is kept homogeneous, the capacity factor of arrays decreases by 3-6% for each diameter of turbine compared to when control is kept homogeneous, with the exception of the 20 m diameter case where there is no variability in rated speed. The installed capacity of the homogeneous diameter and control cases is greater than the homogeneous diameter cases. Therefore, the power metrics are greater in the homogeneous diameter and control case compared to the homogeneous diameter cases for each diameter of turbine, with average power increasing up to 4% (Table 5.6). Considering the 5 m homogeneous cases, there is a 40 MW difference in

installed capacity between the homogeneous diameter and homogeneous diameter and control cases, however, the difference in average power is only 1.5 MW. Hence the decrease in capacity factor for the homogeneous diameter and control case.

The capacity factor deviates from the 40% target by up to 13% in the homogeneous diameter and control case and only 7% in the homogeneous diameter case. Whilst the introduction of resistance on the flow due to turbines does lead to a reduction in the capacity factor from the target value, Figure 5.14 presents the flow rate across the channel for both 5 m homogeneous cases, demonstrating the difference is minimal. Therefore, the reduction in capacity factor between the homogeneous cases is attributed to the rated speed being too high for certain areas. In the 5 m homogeneous diameter and control case, 40% of the arrays are operated with an increased rated speed (from 1.5 m/s to 2 m/s) and 9% of the arrays have rated speeds decreasing (from 2.5 m/s to 2 m/s) relative to the 5 m homogeneous diameter (Table 5.7). Therefore, more areas are experiencing an increase in rated speed, to a value that is too large with respect to the velocities in the areas, compared to the number of array areas that experience a decreased rated speed (which would result in higher capacity factors). Therefore, the overall effect is a decrease in capacity factor. This demonstrates that allowing heterogeneity in control is important because at any real site, the tidal resource does vary spatially. Tailoring the rated speed according to the spatial variability of the resource is beneficial in terms of capacity factor.

Table 5.7: Rated speed of turbines across array areas in the the homogeneous diameter and homogeneous diameter and control cases

	Homogeneous Diameter										Homogenenous Diameter and Control			
	5 m			10 m			15 m			20 m	5 m	10 m	15 m	20 m
Rated Speed [m/s]	1.5	2	2.5	1.5	2	2.5	1.5	2	2.5	1.5	2	2	2	1.5
Number of Areas	33	41	7	24	36	6	15	29	4	4	81	66	46	4

In the 5 m homogeneous cases, there are two arrays (H1 and I1) that experience a 21% change in capacity factor when the rated speed increases between the homogeneous

diameter and homogeneous diameter and control case, from 1.5 m/s to 2.0 m/s. The capacity factors of arrays H1 and I1 increase from 0.27 and 0.32 to 0.48 and 0.53 respectively. Therefore, the ideal rated speed for these arrays would likely be between 1.5 m/s and 2 m/s to achieve a capacity factor closer to 0.4. It is important to note that the effect of a 0.5 m/s change in rated speed on power generation is not equivalent between the values of 1.5 m/s – 2 m/s and 2.5 m/s – 3 m/s, due to the cubic relation of rated speed and power. Therefore, the change in capacity factor due to a 0.5 m/s increase in rated speed for arrays H1 and I1 cannot be directly compared to arrays with the same increase in rated speed to different values because the effects are non-linearly related to the rated power.

The installed capacity when all array areas are occupied with varied rated speed is 260 MW. This capacity is 65% of the 398 MW potential capacity that the Crown Estate awarded the lease agreement to MeyGen for the Inner Sound (SAE Renewables, 2023). The installed capacity in this study is low due to the conservative utilisation of the marine space based on the number of turbines placed in each array area. Therefore, the predicted average power over the spring-neap cycle, presented in this study should not be considered as the maximum potential of this site. The wind industry has taken the approach of increasing rotor diameter to achieve installed capacity targets with fewer turbines at sites, which reduces the cabling and foundation costs (Wiser et al., 2016). The heterogeneous approach helps achieve a high installed capacity by maximising the usage of the site with fewer turbines, compared to the homogeneous case, by deploying the maximum permissible diameter of turbine in each array area.

5.7.3 Homogeneous Diameter vs Heterogeneous

The advantages of allowing varied rated speeds across the Inner Sound has been discussed in the comparison between homogeneous diameter and homogeneous diameter and control cases (Section 5.7.2). Therefore, the subsequent discussion will focus on the difference between the homogeneous diameter and heterogeneous results.

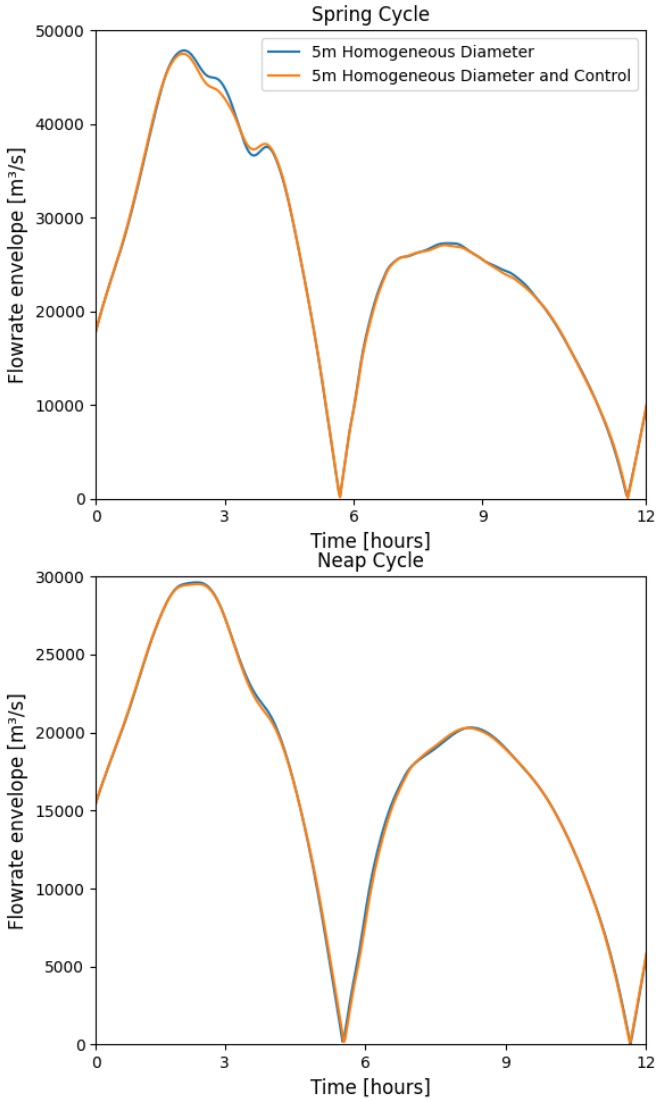

Figure 5.14: Envelope of the total flow rate across a transect of the channel during a spring cycle and neap cycle for the 5 m homogeneous diameter (rated speed = 1.5 – 2.5 m/s) and 5 m homogeneous diameter and control (rated speed = 2.0 m/s) cases.

Comparing the performance of homogeneous and heterogeneous arrays allows consideration of the sacrifices when only turbines of the same specification are deployed. The 5 m turbine diameter case is the highest yielding homogeneous diameter case in terms of average power and produces 5% more power on average than the heterogeneous case due to the greater drag acting on the flow introduced by larger turbines. The capacity factor between the cases only differs by 2%. Despite the apparent increased yield in average power, the discussion on power performance (Section 5.7.1) highlights the importance of comparing other metrics. As detailed in Section 5.7.1, as increasing diameters of turbines are implemented at a site, the power per turbine, power per swept area and power per thrust increases. In this instance, because the installed capacity is the same for both cases but the power is less for the heterogeneous case, the power per swept area is smaller. However, the average power per turbine is greater by 70% for the heterogeneous case. This metric is critical in terms of cost, and a higher value means better cost efficiency (Goss et al., 2021).

Having homogeneous turbines deployed at a site allows the exploitation of economies of scale for turbine manufacturing, which will be key in reducing levelised cost of energy (Milne, 2020). However, in this study, individual array areas are considered to be homogeneous, even in the heterogeneous cases. Therefore, economies of scale can still be utilised because numerous array areas consist of the same specification of turbines and supply chains for varying turbine specifications will be developed for other sites.

The heterogeneous array design maximises the utility of space at a site without compromising on the size of turbines deployed at a site. This approach minimises bathymetric constraints that restrict areas where turbines can be placed if a single diameter were considered. Heterogeneous arrays maximise the area of the lease site where turbines can be deployed, but are also critical for expanding the lease site without only considering small diameter turbines, which are less efficient in terms of power per turbine.

An advantage of increasing the installed capacity at a site is that costs can be distributed

across the turbines in the array due to economies of volume (Goss et al., 2021). As the installed capacity at a tidal site increases, the cost per unit of power effectively decreases because costs of installation and maintenance per turbine decreases as the number of turbines increases. For example, the costs of mobilising and demobilising vessels for offshore operations, installations, and maintenance diminish per turbine as the total number of turbines rises. The heterogeneous approach can help achieve economies of volume whilst being more power efficient than homogeneous cases with the same or greater installed capacity.

5.7.4 Further Considerations

The coarseness of bathymetry data introduces uncertainty due to under-resolved features at the site (Jordan et al., 2023). However, high-resolution data does not guarantee accuracy. The bathymetry resolution is required to be smaller than array resolution, therefore, the method presented in this study could be refined with the acquisition of accurate higher-resolution bathymetry data, enabling the division of array areas into smaller units. By considering the minimum bathymetry across the array area and due to the array resolution many array areas are only suitable for smaller diameter turbines. Only four array areas in this study are occupied by 20 m diameter turbines. Sites often have troughs across the sea bed, therefore it may be feasible to install 20 m turbines in some areas, if the array areas were smaller and the bathymetry was refined to identify these deeper areas. This refinement, however, necessitates a balance between allowing a certain degree of heterogeneity within an area without introducing too many arrays of different specifications and accommodating the highly variable bathymetry.

The velocity reduction of flow instigated by the introduction of resistance due to turbines is a key consideration at sites like the Pentland Firth, which is split into multiple streams (Adcock et al., 2013, Draper et al., 2014b). Figure 5.15 gives an initial indication of the effects, presenting the change in volume of flow through the Inner Sound for each case with respect to the ambient case. The volume of flow through the Inner Sound

channel during flood and ebb decreases for all cases when turbines are present, most significantly for the heterogeneous cases and least significant for the 20 m case. This observation aligns with expectations, as it mirrors the order of resistance due to turbines across the cases, consistent with the flow rate reductions discussed earlier (Figure 5.13). The net volume, calculated as the difference between ebb and flood volumes, does not exhibit a systematic increase or decrease trend across the various cases. The change in net volume demonstrates the effect on the tidal asymmetry at a site due to the presence of turbines, which has implications for the environment (Neill et al., 2009, 2014). Adcock et al. (2014) demonstrate implementing large arrays leads to significant modification of the flow and a reduction in asymmetry. However, the effect on tidal asymmetry across the cases in this study does seem to increase the asymmetry, except for the 20 m case. In this study the turbines only partially occupy the width of the channel unlike the study conducted by Adcock et al. (2014) where turbines occupy the full width. Therefore, in this study the change in net volume does not appear to correlate to the level of resistance introduced by turbines and the effects on tidal asymmetry based on the different cases are not as obvious.

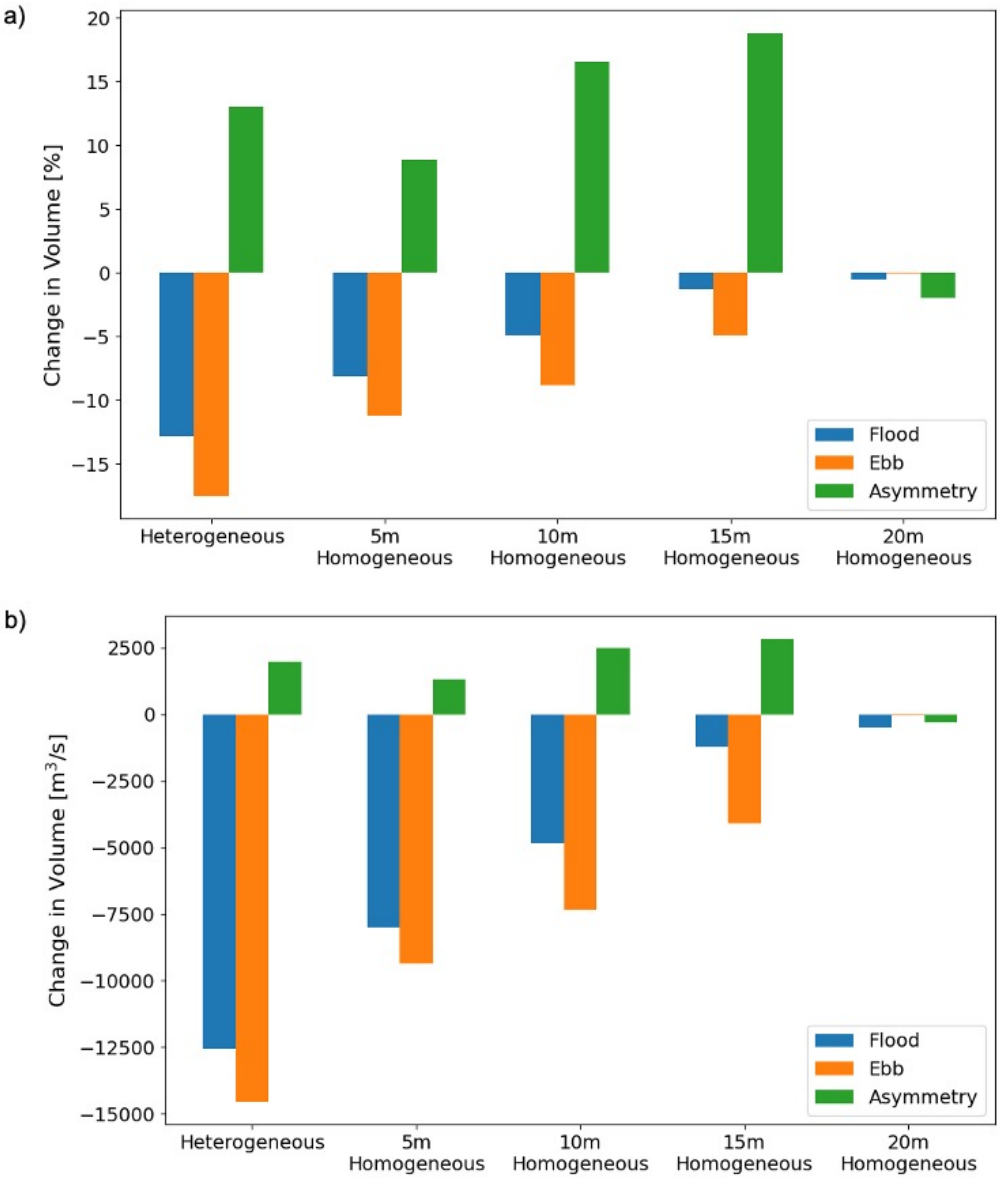

Figure 5.15: Volume a) percentage change and b) absolute change in flood, ebb and asymmetry (difference between flood and ebb) in the Inner Sound channel for homogeneous diameter and heterogeneous cases compared to an ambient case with no turbines present.

Quantifying the environmental impact of introducing resistance due to turbines on the flow at a site is complex and multi-faceted. Some studies have considered limiting the maximum permissible change in peak velocity, which could minimise sediment deposition effects (Neill et al., 2009, Haverson et al., 2018). However, it is a particularly limiting constraint for real tidal sites and does not necessarily demonstrate the environmental impact effectively (Patel et al., 2023). Figure 5.13 presents the flow rate for different deployment strategies and an ambient case, which could indicate the maximum reduc-

Table 5.8: Maximum change in amplitude and phase of the M_2 constituent for elevation for homogeneous diameter and heterogeneous cases with respect to the ambient case.

	Maximum change in amplitude [m]	Maximum change in phase [°]
Heterogeneous	0.048	0.097
5m Homogeneous	0.046	0.095
10 Homogeneous	0.050	0.060
15 Homogeneous	0.050	0.060
20 Homogeneous	0.021	0.025

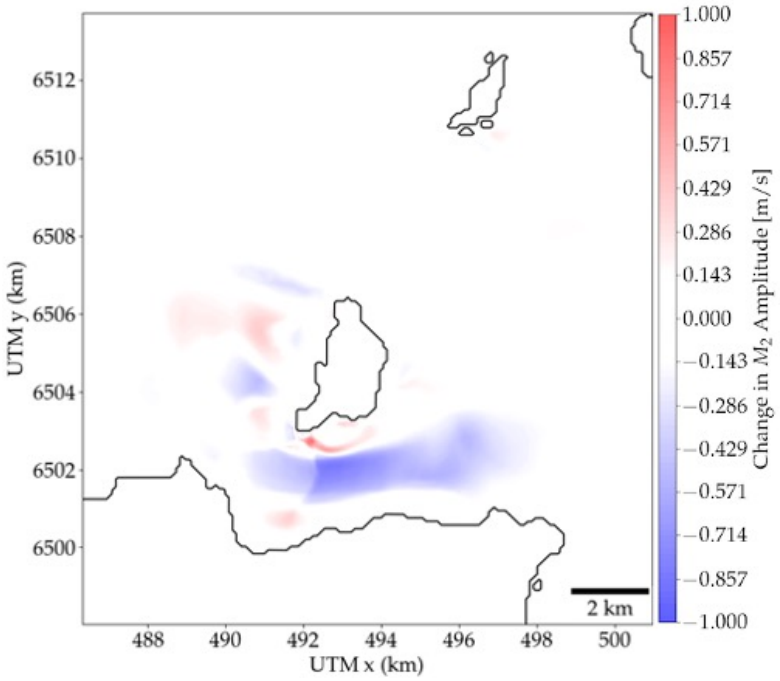

Figure 5.16: Change in amplitude of the M_2 constituent for current between the heterogeneous case and the ambient case.

tion in flow rate. However, when a phase difference occurs due to the introduction of turbines at a site, measuring the instantaneous difference in flow rate is not representative. Another environmental concern that needs to be monitored is the collision risk between turbines and marine animals. Ensuring arrays only partially occupy the width of the channel and avoiding excessively large blockages can help minimise this risk. Shared usage of the seabed through Crown Estate leasing and balancing usage priorities ensures turbines do not occupy the entire width of the channel allowing marine animals to navigate around the developed area, which is also necessary for navigation channels for boats (The Crown Estate, 2023). In this study, a minimum distance from the coastline where turbines could be placed was implemented to ensure turbines do not fully occupy the width of the channel.

The impact on the flow due to the presence of turbines is investigated by examining changes in amplitude and phase of the M_2 constituent for elevation and current. Table 5.8 presents the maximum difference in amplitude and phase, for elevation, between cases with turbines (homogeneous diameter and heterogeneous) and the ambient case. The maximum change in amplitude is 0.05 m and the maximum change in phase is 0.097° across the cases, which is minimal and demonstrates the affect of implementing turbines is negligible on elevation. Based on the principles presented in Garrett and Cummins (2005), the elevation should not change significantly due to the presence of turbines, but the current may vary. The change in amplitude of the M_2 constituent for current between the heterogeneous and ambient cases is presented in Figure 5.16, where positive values represent an increase in amplitude compared to the ambient case and negative values represent a decrease. The maximum change in amplitude for current is 0.91 m/s, which is an order of magnitude greater than the change for elevation. For the current, the greatest changes in amplitude occur directly south of Stroma. In this region, the area of lower amplitude is due to the presence of the overall array and the resistance on the flow due to turbines. The increased amplitude directly north and south of this region is the accelerated flow bypassing the array due to the resistance in the array occupied area with lower amplitude.

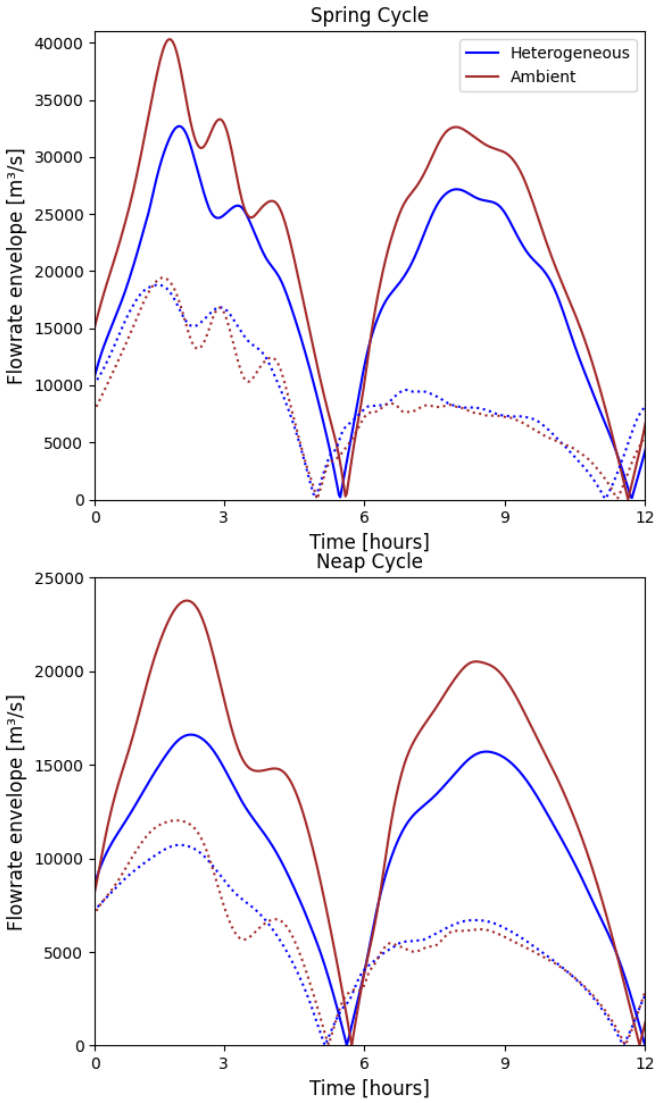

Figure 5.17: Envelope of the total flow rate across a transect of the channel, solid line representing the proportion of the transect occupied by the array and the dotted line representing the proportion of transect on either side of the array during a spring cycle and neap cycle for the heterogeneous and ambient cases.

Figure 5.17 presents the flow rate envelope across the transect presented in Figure 5.1. The portion of the transect occupied by turbines (solid line) is compared to the portion of transect on either side of the array (dotted line) for the heterogeneous and ambient cases. In the heterogeneous case, the flow through the portion of the transect occupied by the array is lower compared to the ambient case, but the unoccupied portions of the transect, which border the array see an overall increase in flow rate compared to the ambient case. The changes in velocity demonstrated in Figures 5.16 and 5.17 are expected when turbines are present due to the blockage effects that cause some increase

in flow that bypass the array. A similar effect is observed by Coles et al. (2020) in the Alderney Race and they suggest reducing the rated power during periods of high flow velocity so that the drag due to the turbines is limited. However, a reduction in rated speed (and hence rated power) would also lower the installed capacity and power output. Given the changes in current amplitude for the M_2 constituent from the ambient case are reasonable and there are no formal limitations, this is not a necessary approach.

5.8 Conclusion

This chapter explores bathymetry as a limiting practical constraint on the tidal stream energy resource and how it can shape array design. The conclusions of this case study of the Inner Sound are applicable to tidal sites in general because the resource and bathymetry will never be consistent across a real site and sites will have limited areas for tidal development. It has been shown that homogeneous diameter cases achieved better capacity factors, with regards to the 40% target, than homogeneous diameter and control cases. This highlights the importance of allowing heterogeneous control at a site. An inspection of the flow rate in the homogeneous diameter and homogeneous diameter and control cases demonstrates that the difference in capacity factor is primarily due to the misapplication of rated speed in the homogeneous control cases rather than the reduction in flow rate due to the increased installed capacity. Targeting a 40% capacity factor to define the rated speed of turbines across the array does have implications on the assessment of the resource but the conclusions that arise from comparing cases in this chapter will remain because the same target is applied across cases. However, the impact on the resource assessment is that a greater capacity factor target would be achieved by decreasing the rated speed and thus, less power would be extracted because power would be capped at a lower velocity. Increasing rated speed to achieve a lower capacity factor would result in a greater power output from the array. Implementing heterogeneous control of turbines also allows areas with a large concentration of the resource at a site to be identified. Identifying where the resource is concentrated at a

site is useful for guiding where lease sites should be defined, updated or expanded. In this case study, the areas primarily south of Stroma experience the greatest velocities and produce the most power and power per swept area. Expanding the lease site at the Inner Sound will allow the exploitation of the resource in these areas but will require heterogeneity in turbine diameter and rated speed to maximise the energy extraction and power performance. Comparing homogeneous and heterogeneous array configurations revealed that while homogeneous arrays may offer economies of scale in manufacturing and a 5% increase in power if small diameter turbines are deployed, heterogeneous arrays maximise the utility of the available space without compromising on deploying larger diameter turbines. The heterogeneous approach allows a balance between the power performance and power output of the array and addresses the issue of cost by considering sub-arrays of turbines with the same turbine specifications. The design framework for heterogeneous arrays offers a valuable tool for future tidal energy projects seeking to balance uniformity and power performance in array design. The study details the importance of not compromising on turbine size solely due to bathymetry constraints and utilising a heterogeneous rated speed of turbines across a site to exploit the spatial variability of the tidal resource.

Chapter 6

Impact of Real-world Constraints on the Tidal Stream Energy Resource in the Pentland Firth

In this chapter, a resource assessment is conducted of the Pentland Firth, considering the development of arrays in high resource areas across the site, in addition to the heterogeneous array in the Inner Sound from Chapter 5. In Section 6.1, the importance of developing multiple arrays through the review of other studies is presented and the need to strategically identify areas to develop within the practical limitations of a site is highlighted. Section 6.2 details the method for successively defining multiple arrays across a site through the extension and application of the heterogeneous array design framework developed in Chapter 5. Additionally, the assumptions for tidal support structure foundations are considered and their impact on support structure sizing and resistance to the flow. The results for the incremental development of the Pentland Firth are outlined in Section 6.3, presenting the evolving specification of turbines across the site as each array is defined and the performance of the arrays in each case. In Section 6.4, the results are contextualised by examining the flow rate across transects in areas of the site that coincide with each array to investigate the interaction between arrays. The incremental development of the site, seabed usage constraints and the implications of increased turbine density across the arrays are also discussed. Finally, the resource of the Pentland Firth is considered in the context of previous studies of the site and a range of strategic development options and subsequent resource quantification are examined.

6.1 Deployment of Multiple Arrays at a Site

The enhancement of an array's performance through micro-siting of turbines has been the subject of many studies, as discussed in Section 4.3. However, with limited areas suitable for tidal stream energy development, due to constraints on the resource (Figure

2.4), it is important to consider the interaction between independently developed arrays in close proximity. Zhang et al. (2022) highlight the risk of not successively developing distinct nearby arrays, which can lead to interactions with negative impacts on the power output of the array. They also emphasise that as the number of arrays increases, the aggregate environmental impact may not scale linearly.

Goss et al. (2018) investigated two contiguous arrays in the Alderney Race, developed by Alderney and France. They explored scenarios of collaborative, successive and independent developments. The study focused on the micro-siting of turbines and the competition effects between the arrays depending on the development strategy. The greatest power output is achieved when the arrays are developed collaboratively, although the power output between each scenario is similar. The array developed by France is found to have a greater impact on the array developed by Alderney and that a co-operative development would be more beneficial to Alderney. The effect of array interactions and consequences for independent developers are also highlighted by Waldman et al. (2019) in the context of policy implications.

One of the most notable sites for tidal stream energy in the UK is the Pentland Firth, a strait between the north coast of Scotland's mainland and the Orkney Islands. The strong currents in the area are due to the elevation phase difference between the east and west of the Pentland Firth, which is enhanced by tidal streaming due the area's topography (Neill et al., 2017). The area is divided into multiple streams due to the presence of two islands, Stroma and Swona. A number of studies have been conducted on the tidal stream energy resource at the Pentland Firth, with assessments ranging from 1 - 17.7 GW (Black and Veach, 2005, Salter and Taylor, 2007, Easton et al., 2012, Adcock et al., 2013, Draper et al., 2014a, O'Hara Murray and Gallego, 2017, De Dominicis et al., 2017). In 2010 four lease sties were agreed by the Crown Estate and leased to four different developers (The Crown Estate, 2023). Figure 6.1 presents planned lease sites in the Pentland Firth and Orkney for wave and tidal stream developments in

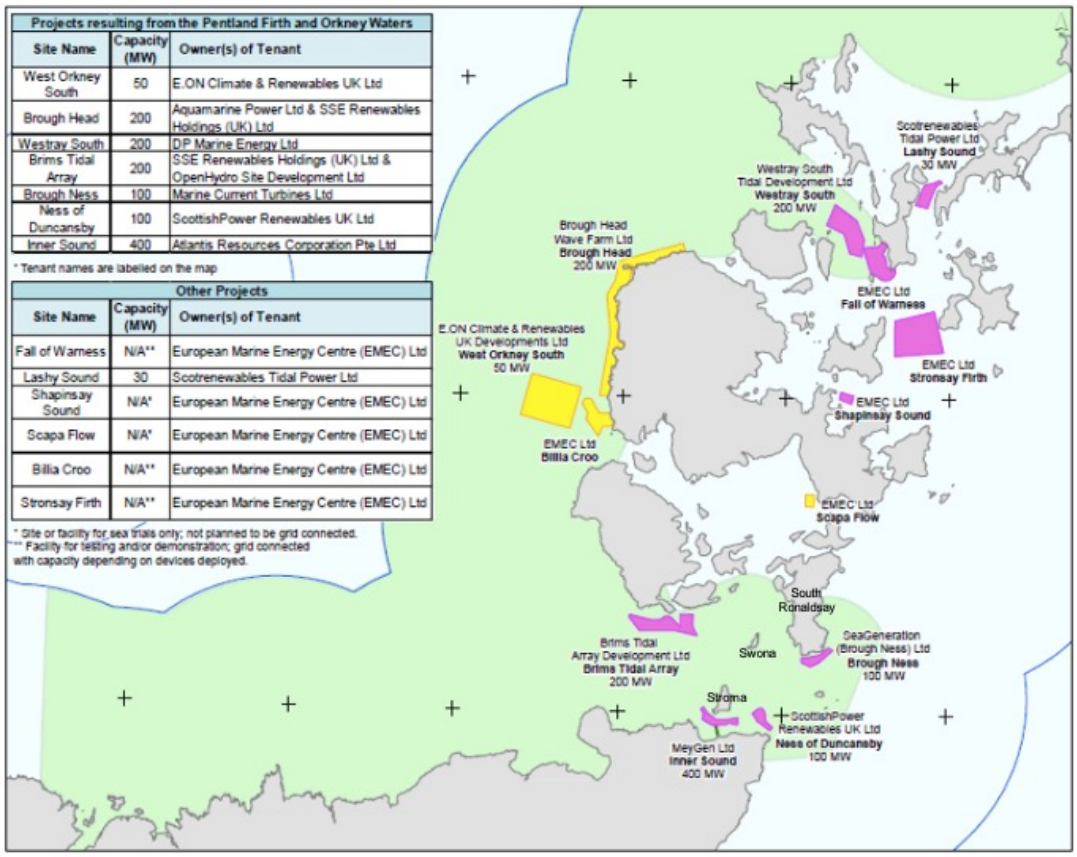

Figure 6.1: Planned lease sites for wave (yellow) and tidal stream (pink) developments in the Pentland Firth and Orkney in 2010 (Scottish Government, 2018).

2010. The development of these sites in isolation could prevent the optimal amount of energy being harnessed due to the impact of arrays on the hydrodynamics of a channel (Draper et al., 2014a,b). Of the four original lease sites in the Pentland Firth, three were discontinued after 2015, leaving the Meygen site in the Inner Sound as the only site being actively developed, with Phase 1 already operational (Meygen, 2012). The Ness of Duncansby lease has been reconsidered but has not progressed beyond the pre-planing stage. The original Crown Estate lease sites were outlined based on unrefined older modelling and have the potential to be updated as resource assessments are refined and seabed usage is re-prioritised. The study undertaken by Goss et al. (2018) highlights the need to carefully consider the development of independent arrays in order to maximise resource extraction for each developer.

Another study that investigates the interaction of multiple tidal stream developments in the Channel Islands was undertaken by Coles et al. (2017), looking at the Alderney Race

in conjunction with two other potential sites, the Casquets and Big Roussell. The upper bound estimate of the resource suggests the majority of the resource can be extracted in the Alderney Race. When power is extracted in the Alderney Race, the head difference and volume flux through the Casquets, a parallel site located 3 km away, increases as the flow increases around Alderney. This leads to constructive effects for power extracted in Casquets, when developed together with other sites. The third site, Big Roussel is located 40 km downstream of the Alderney Race and Casquets and experiences a reduction in extracted power when developed with the other sites. They find that during the ebb tide, the flow diverts around the Channel Islands when power is extracted in the Alderney Race and Casquets, leading to a volume flux reduction through Big Roussel compared to when power is extracted through Big Roussel alone. The study highlights the interaction between sites is highly dependent on their location relative to each other.

The interaction between four tidal arrays in the Pentland Firth is considered by Funke et al. (2016), through the implementation of a gradient-based optimisation method. Three of the arrays coincide with the Inner Sound, Ness of Duncansby and Brough Ness lease sites in Figure 6.1, and the fourth array is placed in Cantick Head, further east of the Brims Tidal Array development. They demonstrate that optimising the arrays individually and simultaneously leads to different outcomes for the resource. When the four sites are optimised individually the potential of each farm is overestimated. The Cantick Head and Brough Ness arrays have minimal differences when optimised individually or simultaneously because they are far enough apart that interference is minimised. However, the Inner Sound and Ness of Duncansby arrays lie directly behind each other in the direction of the flow and are in relatively close proximity. The optimisation of the Ness of Duncansby array is notably affected by the presence of the Inner Sound array, as the latter experiences more constrained flow due to the presence of Stroma.

A resource assessment of the Pentland Firth conducted by O'Hara Murray and Gallego

(2017) investigates arrays in three, 2 km wide areas of the Pentland Firth: the Inner Sound, the Outer Sound (between Stroma and Swona) and a third area between Swona and South Ronaldsy (Figure 6.1). They first consider a theoretical upper limit of the resource by considering all three areas with turbines distributed evenly across the channels and turbines modelled to span the entire water column in their 3-D model. In the second scenario, they acknowledge the deployment of 20 m diameter turbines is restricted by bathymetry. As a result, they avoid placing turbines in areas shallower than the turbine diameter to accommodate this practical constraint on the resource. The turbines are also modelled to only occupy a small fraction of the column in the second scenario, acknowledging that horizontal axis tidal turbines do not span the entire water column. They found that implementing the turbines across the entirety of all three areas generates the most power but leads to significant environmental effects. The power is reduced by 70% with the consideration of practical constraints in the second scenario but leads to a smaller reduction in flow rate through the Pentland Firth and the spatial extent of environmental impact, measured through the changes in M_2 elevation and current, is much smaller.

Draper et al. (2014a) highlight the ranging resource in the Pentland Firth depending on the development strategy of the site. They acknowledge that the resource cannot be described by a single value but instead by a range of values due to the interactions between developments in sub-channels of the Pentland Firth. Their findings indicate that developing sites in parallel sub-channels offers the advantage of increased power extraction for both sites, which is also observed in the study by Coles et al. (2017). However, when sites are developed in series, there is a disproportional decrease in power extraction for each site. Therefore, they emphasise the need to regulate individual developers to ensure optimal extraction of the resource. In a study of the inter-dependence of the resource extraction from sub-channels, Draper et al. (2014b) apply the electrical circuit analogy, discussed in Section 2.2. Using the analogy, they derive an equation to predict the power when placing turbines in parallel sub-channels. The formula demonstrated

reasonable agreement with a 2-D numerical model of the Pentland Firth, suggesting it as a suitable method to provide initial insight into the resource. However, the approach primarily considers energy extraction, which is an over-simplification of the real resource.

As the tidal energy sector continues to evolve, the deployment of multiple arrays in close proximity becomes increasingly common, leading to interactions between them. The studies outlined in this section have highlighted the importance of considering these effects in the development of sites. Other than studies that consider lease sites, the identification of the multiple arrays has not been strategic and very few studies consider the practical constraints on the resource. In this chapter, the development of multiple tidal stream arrays across the Pentland Firth, with the consideration of practical constraints on the resource, is investigated to assess and refine the assessment of the tidal stream resource in the Pentland Firth and inform the strategic development of the site.

6.2 Development of the Pentland Firth

The heterogeneous framework developed in Chapter 5 is extended and applied to identify key areas of the resource for extracting energy through multiple arrays at a site. The investigation of how the resource in the Pentland Firth responds to extraction through multiple arrays is important for guiding the next stages of marine spatial planning. The changing status of lease sites leads the way for identifying new areas to develop tidal stream arrays and update lease sites based on the best way to harness the resource. An investigation of how the resource and power yield of arrays respond to incremental development of the site provides insight into its development. This approach can inform the The Crown Estate and The Crown Estate Scotland's definition of lease sites, enabling independent developers to develop sites individually while minimising negative interference.

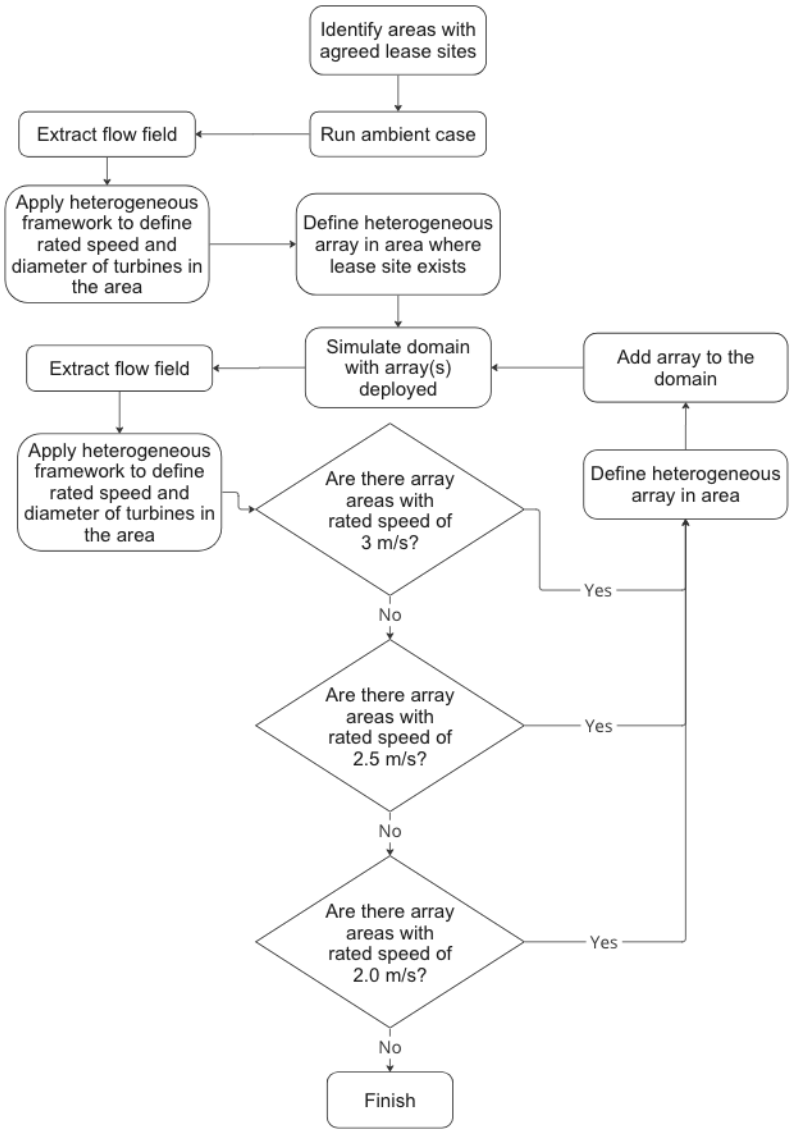

Figure 6.2: Extension and application of the heterogeneous framework for identifying multiple arrays at a site.

The approach undertaken for identifying multiple arrays across a site is presented in Figure 6.2. The heterogeneous array design framework, developed and outlined in Chapter 5, is applied across the Pentland Firth to identify additional areas to deploy arrays based on the concentration of the resource across the site. The framework defines the diameter and rated speed of the turbines based on bathymetry and flow field data. Successive arrays are defined using the flow field of the previous deployment strategy to account for effects of the increasing scale of development. The heterogeneous array modelled in the Inner Sound in Chapter 5 is considered as the first array, given the site's preeminent status. A minimum distance of 1.5 km between independent arrays is

maintained, a similar distance between the original Inner Sound and Ness of Duncansby lease sites (Figure 6.1).

6.2.1 Tidal Turbine Support Foundation

In shallow water environments (less than 100 m), the fastest currents, and majority of the energy, are usually assumed to be in the upper portion of the water column (Prandle, 1982, Goward Brown et al., 2017). Yang et al. (2013) modelled tidal stream energy extraction as a momentum sink in a 3-D model. They found that the energy yield of a turbine was highly dependent on the hub height in the water column and the maximum yield was achieved at the mid-depth. Therefore, the deployment of turbines with a hub height in the upper half of the water column has been seen as favourable for developers and turbines are designed to extract energy in the upper portion (Blunden and Bahaj, 2007, Goward Brown et al., 2017). However, turbine loads increase with the square of the flow speed, which poses challenges for turbine designers and developers (Adcock et al., 2021).

The Pentland Firth has depths up to 100 m, with an average of approximately 60 m across the area (Marine Scotland, 2016). The Inner Sound is the shallowest area of the site (Figure 5.1), with turbines being placed in depths no greater than 50 m in the scenarios presented in Chapter 5. However, other areas across the site are characterised by deeper bathymetry. While most large diameter turbines are bottom-fixed and smaller turbines are deemed more suitable for floating foundations, as detailed by Adcock et al. (2021) in a comprehensive overview of key rotor parameters, deploying bottom-fixed turbines in depths greater than 50 m with the aim of positioning the hub height in the upper half of the water column would require tall and thick support structures. The increasing size of support structures leads to an increase in thrust applied to the flow, which detrimentally impacts the resource due to the decrease in flow velocity, and also becomes uneconomical. Therefore, the option of a floating foundation is considered because the inversion of the support structure allows for its length to be

reduced, along with the diameter of the support structure, while still remaining in the upper portion of the water column. Consequently, all turbines in any array deployed in regions with an average depth greater than 50 m adhere to support structure dimensions pertaining to floating foundations; otherwise, support structures are sized in accordance with requirements for bottom-fixed turbines. The drag due to the vertical tower of the support structure is accounted for in both scenarios.

The minimum clearances for the rotor tip to seabed and sea surface for bottom-fixed turbines are taken according to guidance outlined by Meygen (2012), as presented in Section 5.3.1. For floating turbines, guidance for the rotor tip to sea surface clearance is taken from the Orbital O2 device, where the nacelle is positioned 14 m below sea surface for a 20 m diameter turbine, leaving approximately 4 m clearance between the blade-tip and sea surface (Orbital Marine, 2022, European Marine Energy Centre, 2023). The minimum rotor tip to seabed clearance remains according to Meygen (2012). The support structure height is the sum of the clearance between the rotor tip and the relevant surface (e.g., seabed for bottom-fixed and sea surface for floating) and the turbine radius.

There are certain effects on the performance of turbines with floating foundations that are not captured in the model, and acknowledged as a limitation. Floating turbines may experience motion induced by the platform on the sea surface (Adcock et al., 2021). The mobility of the floating platform can cause the turbine to tilt when the platform experiences pitching motion, which affects the performance of the turbine and is a problem in floating offshore wind turbines (Fang et al., 2020). Osman et al. (2020) examined the performance of a tidal turbine with a floating platform under the effects of surge motion and noted that the average power and thrust coefficients reduce in comparison to a turbine that does not experience surge motion. In some instances the rotor produced negative coefficients of power and thrust, acting as a propeller and unsteady loading on the rotor increases with the frequency and amplitude of the surge

motion oscillation. Additionally, the use of a depth-averaged model leads to a uniform velocity profile assumption, therefore, the velocity variation at different heights within the water column cannot be captured and does not reflect in the results. As an example, if a 20 m diameter turbine is placed in a 70 m depth area and a $\frac{1}{7}^{th}$ power law velocity profile was adopted, the difference in placing a turbine 15 m above the seabed and 55 m above the seabed, could lead to a 0.3 m/s change in velocity, which would translate to an even greater difference in power.

The purpose of considering floating foundations in this chapter is to reflect a sensible and realistic option for turbines, considering the practical constraints limiting the resource, to propose a development strategy for the site and assess the resource. Only the change in resistance on the flow due to the support structure size between the floating scenario compared to a bottom-fixed turbine is captured in the model. A comparison of the size of the support structure on the power output of an array in an idealised channel is undertaken to demonstrate the impact of their size on the resource.

An array of 20 m diameter turbines is modelled, with support structure sizes appropriate for bottom-fixed and floating turbines, whilst keeping the turbine in the upper portion of the water column, to quantify the effect on the power output of an array due to the resistance of the support structure. In the 80 m deep channel, the scenario with bottom-fixed turbines are modelled with a support structure length of 50 m (extremely large to position in upper portion of the water column) and for the floating turbines scenario the support structure length is 14 m (4 m clearance and 10 m turbine radius). The assumption of bottom-fixed turbines results in a 5% reduction in power output compared to the array featuring floating turbines due to the change in support structure size.

Having floating and bottom-fixed turbines brings an additional aspect of heterogeneity to the study, but in this case it is not heterogeneity within arrays as with the rated speed and turbine diameter, instead it is between arrays. This further emphasises the

need to compromise between homogeneity for the benefit of achieving economies of volume and heterogeneity in order to better harness the resource. Edwards et al. (2024) undertook a review of early-stage floating offshore wind platforms and highlighted that future trends indicate the competing priorities of developers will require a trade-off between standardisation and specialisation.

6.3 Results

Four arrays are sequentially defined across the Pentland Firth, in addition to Array 1 in the Inner Sound. The specification of turbines across the five arrays, defined through the extended heterogeneous framework, is presented in Figure 6.3. The turbines in Array 1 are assumed to be bottom-fixed because the average bathymetry across the array is less than 50 m and the turbines in Arrays 2–5 are assumed to be floating. The support structure sizes for each turbine reflect these assumptions. The turbines that make up Array 2, Array 4 and Array 5, are all homogeneous in diameter (20 m) because the areas have bathymetry deep enough to accommodate this size of turbine rotor and meet minimum clearance requirements. Array 3 primarily consists of 20m diameter turbines, although some 15 m diameter turbines are deployed in the north-eastern part of the array.

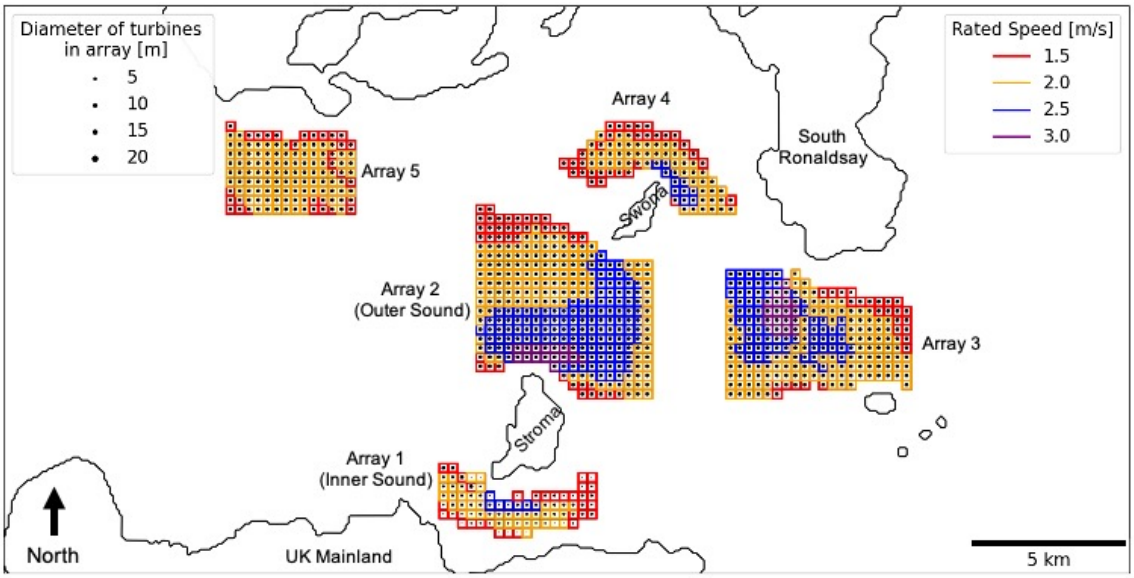

Figure 6.3: All arrays identified for the deployment of multiple arrays at a site through the extended heterogeneous framework (numbered in order of specification).

Five cases are defined, extending from the heterogeneous case discussed in Chapter 5. Each case is established with the addition of an array, following the sequential order of identification outlined in Section 6.3.1. With the deployment of each new array the number of turbines and total swept area increases in each case.

6.3.1 Defining Arrays

Figure 6.4 presents the available areas for development as arrays are deployed and the change of turbine specifications with the addition of each array is visible. Array 2 is situated north of the Inner Sound, between Stroma and Swona, selected on the basis that it is the only area with turbines operating at a rated speed of 3 m/s (Figure 6.4a), which indicates a high flow velocity and concentration of the resource.

When the heterogeneous framework is applied, based on the updated flow field, the change in turbine specifications across the available areas for development as the resource responds to the deployment of Arrays 1 and 2 can be seen in Figure 6.4b, in comparison to Figure 6.4a. Array 3 is defined around the area with turbines operating with rated speed of 3 m/s, located east of Array 2 (Figure 6.3).

Following the implementation of three arrays, there are no more areas with turbines specified to operate at rated speed of 3 m/s when the heterogeneous framework is re-applied (Figure 6.4c). From the remaining available areas for development, Array 4 is defined around the island Swona, with turbines operating at a maximum rated speed of 2.5 m/s. Subsequently, Array 5 is defined on the north-west side of the site, in an area where the maximum rated speed turbines are operating at 2 m/s.

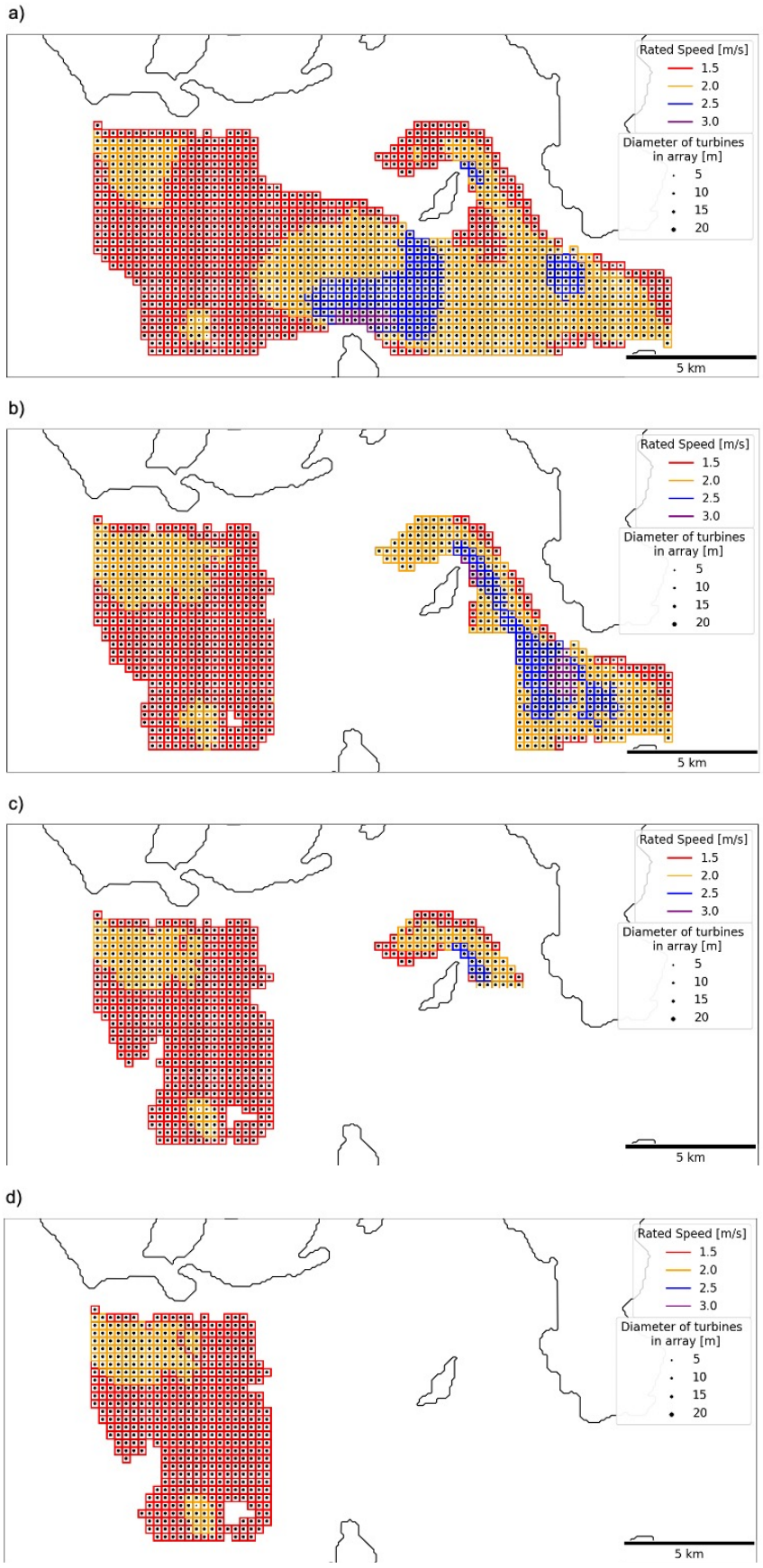

Figure 6.4: Specification of turbines within potential remaining array areas to define and deploy a) Array 2, b) Array 3, c) Array 4 and d) Array 5 as each additional array is deployed.

6.3.2 Incremental Development of the Pentland Firth

The average power and capacity factor of each array is presented in Table 6.1 for each case. In this chapter, as in Chapter 5, the average power is referring to the time-averaged power over the spring-neap cycle. Considering the varying turbine diameter and number of turbines across the arrays, assessing the average power per turbine and per swept area provides deeper insights into array performance and are presented for each array in each case in Table 6.1. The table also provides details on the number of array areas, swept area, number of turbines and installed capacity both individually and collectively.

The average power and capacity factor for each case are also presented in Figures 6.5 and 6.6 to visualise the distribution of the metrics spatially across the site and in context of the turbine specification in each case.

Deploying turbines beyond the Inner Sound (Array 2) results in a 15% increase in power for Array 1, averaged over the spring-neap cycle. The addition of Array 3 results in a minor decrease in the power yielded by Arrays 1 and 2 (2 and 4% respectively). When Array 4 and Array 5 are deployed, there is a minimal increase in power for Array 1 in comparison to the 3 Array case. The average power yield for Array 1 varies by less than 1% between the case with 3 Arrays and 5 Arrays. There is a 5% decrease in power yielded by Array 3 with the addition of Array 4 and 5. Array 4 also experiences a 5% decrease in power due to the presence of Array 5.

The average capacity factor of the arrays ranges from 31% to 45%, depending on the number of independent arrays deployed. Array 2 exhibits the highest power per swept area and power per turbine, along with the largest installed capacity among the arrays. Array 1 demonstrates the smallest power per turbine, power per swept area, and installed capacity.

Table 6.1: Overview of the size of arrays in each case and the average power, capacity factor, power per swept area and power per turbine for each array.

		Array 1	Array 2	Array 3	Array 4	Array 5	Overall
	Number of array areas	81	309	231	92	124	837
	Swept area [m^2]	136945	518397	388002	154514	208257	1406115
	Number of turbines	2134	1652	1260	492	663	6201
	Installed capacity [MW]	260	1670	830	320	400	3490
1 Array	Capacity factor	0.31	-	-	-	-	0.31
	Average power [MW]	75.32	-	-	-	-	75.32
	Power per swept area [kW/m^2]	0.55	-	-	-	-	0.55
	Power per turbine [kW/turbine]	35.30	-	-	-	-	35.3
2 Arrays	Capacity factor	0.38	0.47	-	-	-	0.45
	Average power [MW]	91.33	767.07	-	-	-	858.40
	Power per swept area [kW/m^2]	0.67	1.48	-	-	-	1.31
	Power per turbine [kW/turbine]	42.80	464.33	-	-	-	228.5
3 Arrays	Capacity factor	0.36	0.45	0.48	-	-	0.45
	Average power [MW]	89.89	739.02	347.56	-	-	1,176.47
	Power per swept area [kW/m^2]	0.66	1.43	0.90	-	-	1.13
	Power per turbine [kW/turbine]	42.12	447.35	275.84	-	-	235.6
4 Arrays	Capacity factor	0.37	0.45	0.47	0.39	-	0.44
	Average power [MW]	90.53	737.38	336.95	120.55	-	1,285.41
	Power per swept area [kW/m^2]	0.66	1.42	0.87	0.78	-	1.07
	Power per turbine [kW/turbine]	42.42	446.35	267.42	245.01	-	234.7
5 Arrays	Capacity factor	0.36	0.46	0.46	0.37	0.40	0.43
	Average power [MW]	90.15	741.89	330.25	113.97	154.28	1,430.54
	Power per swept area [kW/m^2]	0.66	1.43	0.85	0.74	0.74	1.02
	Power per turbine [kW/turbine]	42.24	449.09	262.11	231.64	232.69	233.4

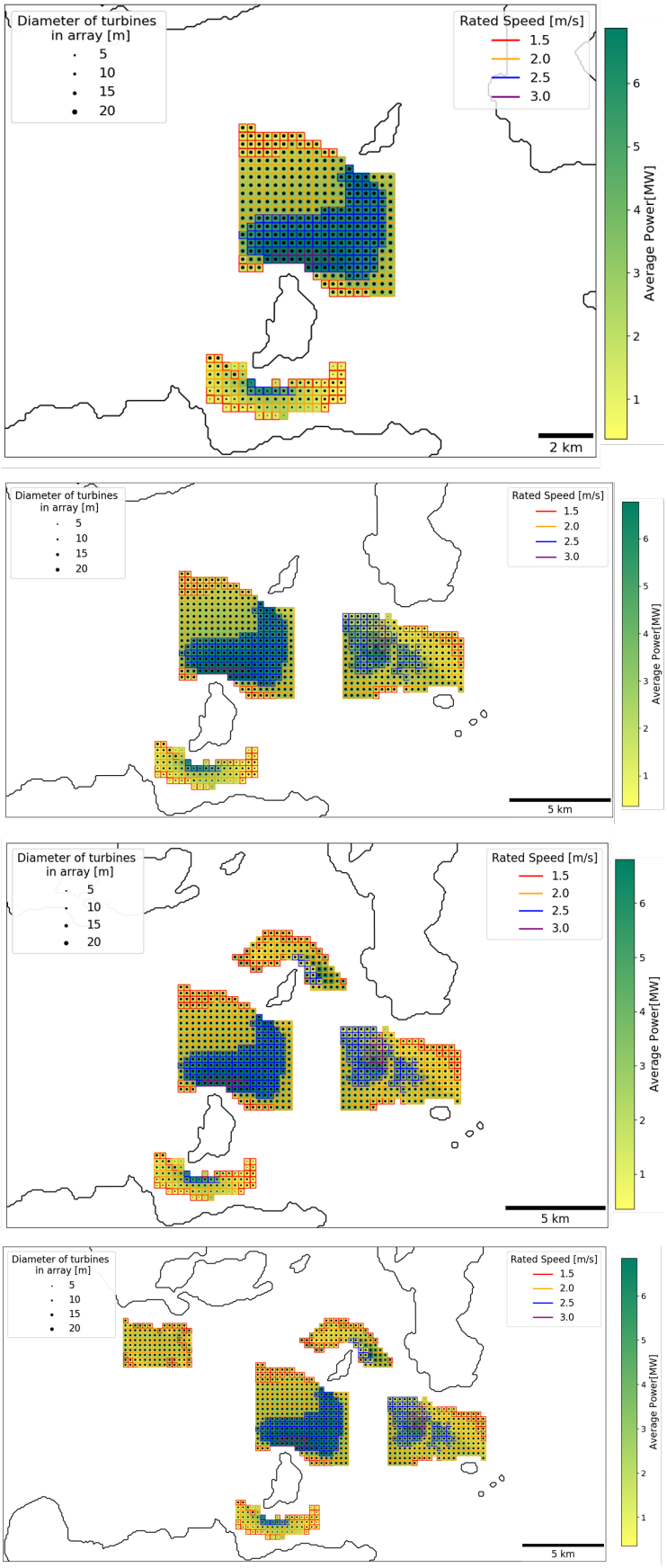

Figure 6.5: Average power over the spring-neap cycle of the arrays. The rated speed of turbines in each array area is illustrated by the edge colour of the square and the diameter of the turbines is indicated by the size of the black circle.

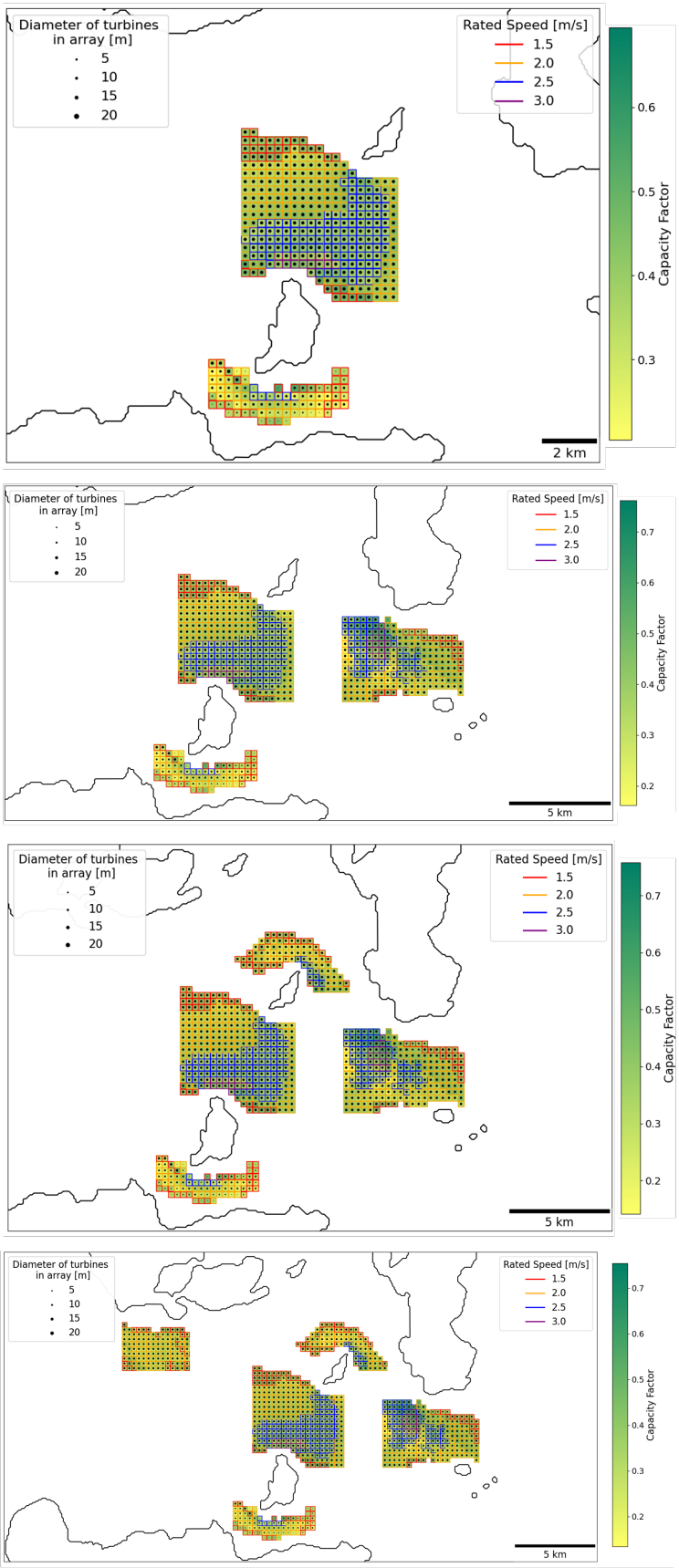

Figure 6.6: Capacity Factor of the arrays. The rated speed of turbines in each array area is illustrated by the edge colour of the square and the diameter of the turbines is indicated by the size of the black circle.

Figure 6.7a presents the total average power yielded by the arrays in each case against the total number of turbines deployed. Figure 6.7b illustrates the power per turbine for increasing number of turbines in each case. To assess the relative differences between each point on the curve in Figure 6.7a, the change in power divided by the change in the number of turbines between cases, essentially the gradient of the line between points on Figure 6.7a, is depicted in Figure 6.7c. The ratio of instantaneous power and instantaneous thrust (i.e., power per thrust) is proportional to the overall power for each case, therefore, the average power per thrust per turbine demonstrates the same trends as power per turbine.

As more turbines are deployed, through the inclusion of an additional array in each case, the total power output increases, evidenced in Figure 6.7a. As demonstrated in Figure 6.7b, the power per turbine increases to 230 kW per turbine, from 35 kW per turbine, with the addition of Array 2, and remains almost constant as arrays are added until there are 5 arrays, with a very small variation of 5 kW per turbine between the cases. When the change in power over the change in turbine is plotted (Figure 6.7c) between each case, it becomes evident that the gradient of the average power versus the number of turbines plot decreases at a progressively slower rate and becomes almost constant. This implies that power increases at the same rate, as more turbines are deployed in arrays across the site.

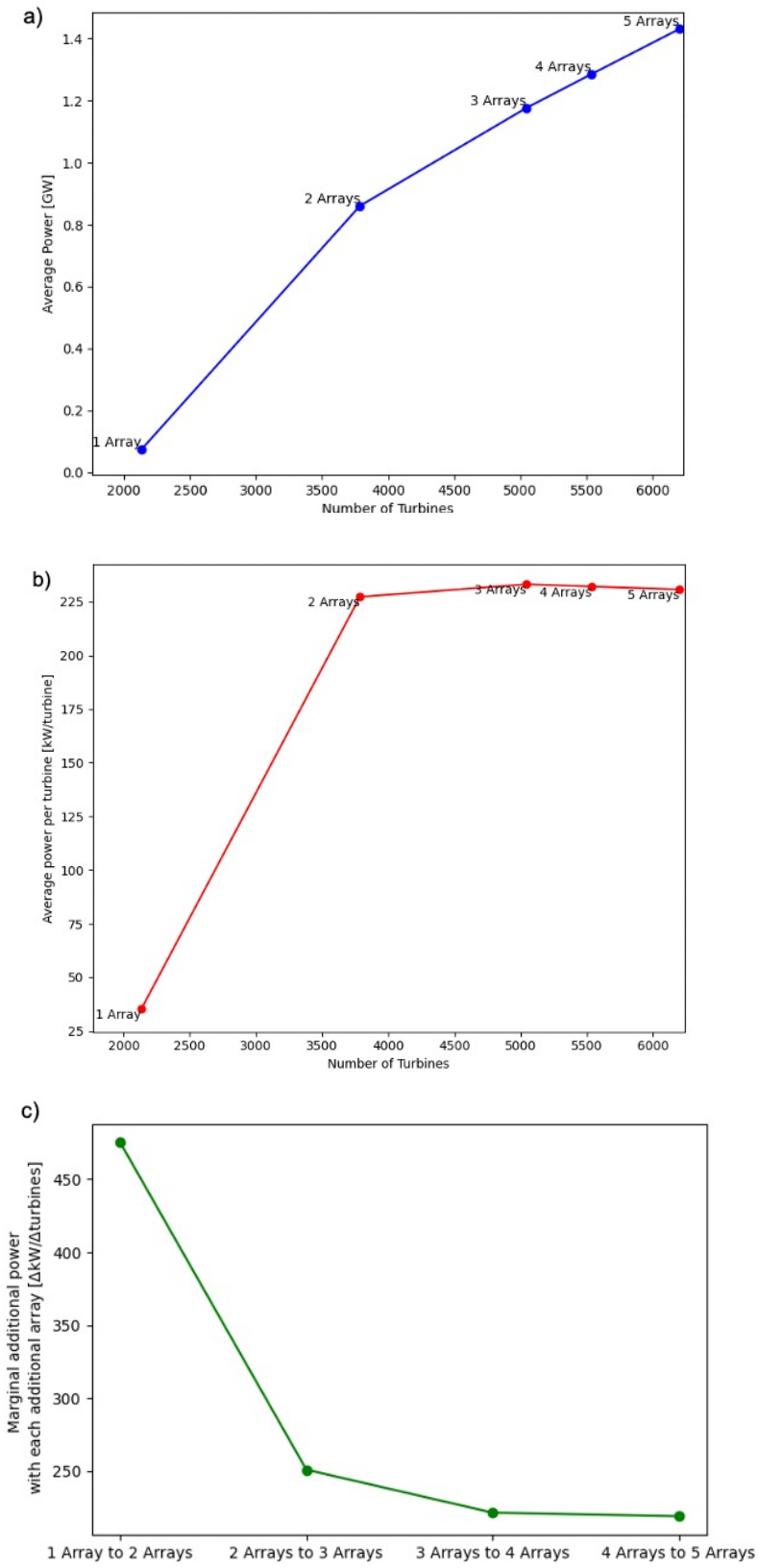

Figure 6.7: Relation between power and turbines a) average power vs number of turbines for each case b) average power per turbine vs number of turbines for each case c) marginal additional power with the addition of each array.

6.4 Discussion

6.4.1 Array Interactions

To evaluate the influence of energy extraction through turbines on flow dynamics and subsequent effects on the average power produced by each array, the flow rate across 5 transects illustrated in Figure 6.8 are considered. Table 6.2 presents the percentage change in flow rate amplitude for each case with respect to the ambient case across each transect. The relative changes in flow rate amplitude between cases is one way to demonstrate the impact of developing arrays in the Pentland Firth on the flow across the site.

When Array 1 is deployed, a 9.8% decrease in maximum flow rate is observed across Transect B, which is extended across the Inner Sound and in the same location as Array 1. The flow rate amplitude across Transect C increases by 0.7%. Transect C, positioned between Stroma and Swona, is located in the area identified to develop Array 2 due to concentration of the resource north of Stroma, indicated through the rated speed from the heterogeneous design framework (Figure 6.3.1a).

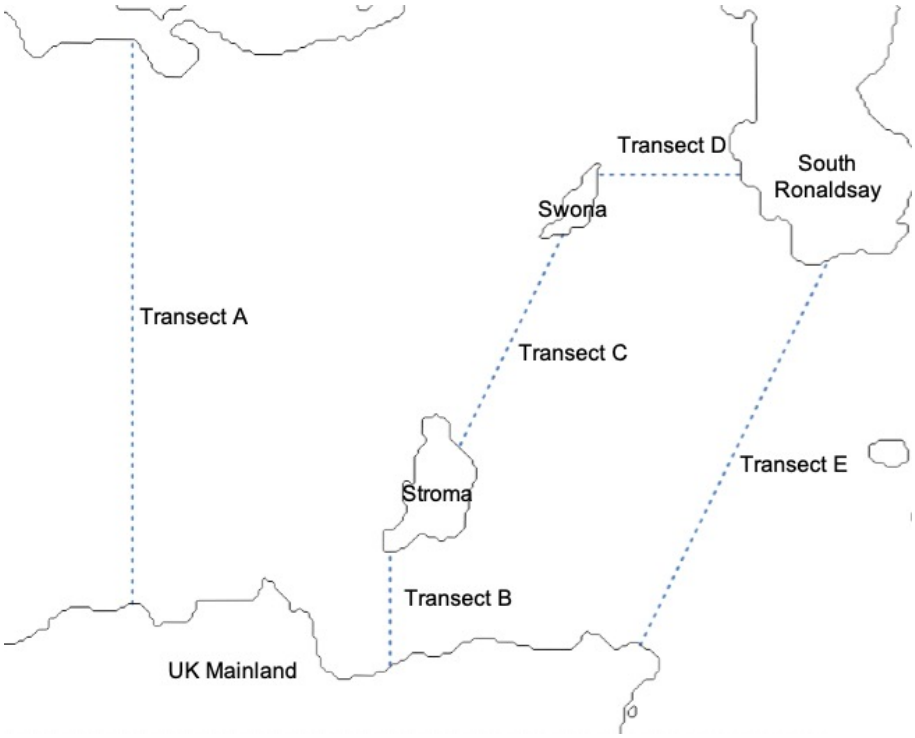

Figure 6.8: Transects across which the flow rate is evaluated.

Table 6.2: Percentage change in flow rate amplitude with respect to the ambient case. Values in bold are where the deployed arrays coincide with the transect in each case.

	Change in flow rate amplitude [%]				
Case	Transect A	Transect B	Transect C	Transect D	Transect E
1 Array	-2.9	**-9.8**	0.7	-6.0	0.1
2 Arrays	-3.4	**-7.1**	**-6.9**	-3.6	-2.1
3 Arrays	-5.2	**-8.1**	**-11.9**	-4.6	**-5.1**
4 Arrays	-5.6	**-6.5**	**-13.1**	**3.6**	**-5.4**
5 Arrays	**-5.5**	**-6.9**	**-13.9**	**-0.1**	**-7.3**

+15 +10 +5 0 -5 -10 -15

The extraction of energy through Arrays 1 and 2 results in a 3% increase in flow rate amplitude across Transect B, contributing to the 15% increase in power yielded by Array 1 compared to the case with 1 Array only. This illustrates the positive interaction between Array 1 and Array 2, which are situated in parallel sub-channels of flow, similarly observed in studies by Draper et al. (2014a,b), Coles et al. (2017). An 8% decrease in flow rate amplitude is observed across Transect C between the 1 Array and 2 Arrays cases and attributed to the presence of Array 2. Array 2 has a significantly large installed capacity of 1670 MW, which explains the significant decrease in flow rate due to the resistance imposed on the flow.

Comparing Figures 6.4a and 6.4b, it is evident that the deployment of Array 2 in combination with Array 1, results in an increased rated speed of turbines in the remaining areas for development on the east-side of the site. The increased resistance between Swona and Stroma leads to an increase in flow velocity around the north and east of Swona. Considering the change in flow rate amplitude across Transect D, which is located east of Swona, there is a 3% relative increase in flow rate amplitude between the 1 Array and 2 Arrays cases. This demonstrates the deployment of 2 Arrays also leads to a positive interaction across Transect D.

Conversely, Transects E and A, located in series with Array 2, experience a decrease in

flow rate amplitude across both transects following the deployment of Array 2. Despite the apparent relative decrease in flow rate amplitude across Transect E, Array 3 is defined in the north part of the transect where the rated speed of turbines increases due to the presence of Array 2. The area east of Array 2 appears to experience increased flow velocity due to the acceleration around Swona. However, the area east of Array 1 and south east of Array 2 experiences a decrease in flow velocity due to the combined negative interference of Arrays 1 and 2. The Ness of Duncansby lease lies in this area but the study suggests this is a relatively low resource area.

Array 4 is defined around the north and east side of Swona. When three arrays are deployed, the flow rate in this region decreases slightly, evidenced by a 1% decrease in flow rate across Transect D and lower rated speed specification of turbines across the site between Figures 6.4b and 6.4c. The flow rate amplitude across Transect D increases with respect to the ambient case. It is expected that the presence of an array in the area where the transect is located would relate to a decrease in flow rate relative to the ambient flow, therefore the results seems counter-intuitive. Figure 6.9 presents the change in amplitude for the M_2 constituent in each case relative to the ambient case. The plot reveals an increase in the M_2 velocity amplitude on the east side of Transect D, which is not occupied by the array. This indicates the increase in flow rate across Transect D is due to the bypassing flow velocity increasing. Across the other transects, the increase and decrease in flow rate amplitude relative to the 3 Arrays case reflects in the power yielded from the relative array coinciding over each transect.

The final array, Array 5, is positioned in the north-west of the site and comprises turbines with rated speeds of 1.5 m/s and 2.0 m/s. When all five arrays are deployed, the flow rate amplitude decreases by 13.9% across Transect C relative to the ambient case, marking the most significant decrease across all cases and transects. This reduction is primarily attributed to the presence of Array 2, which is situated in the same area as Transect C and is in series with two other arrays, Array 3 and Array 5. Consequently, the reduction

in flow velocity through Outer Sound is heightened, due to negative interference, as illustrated in Figure 6.9.

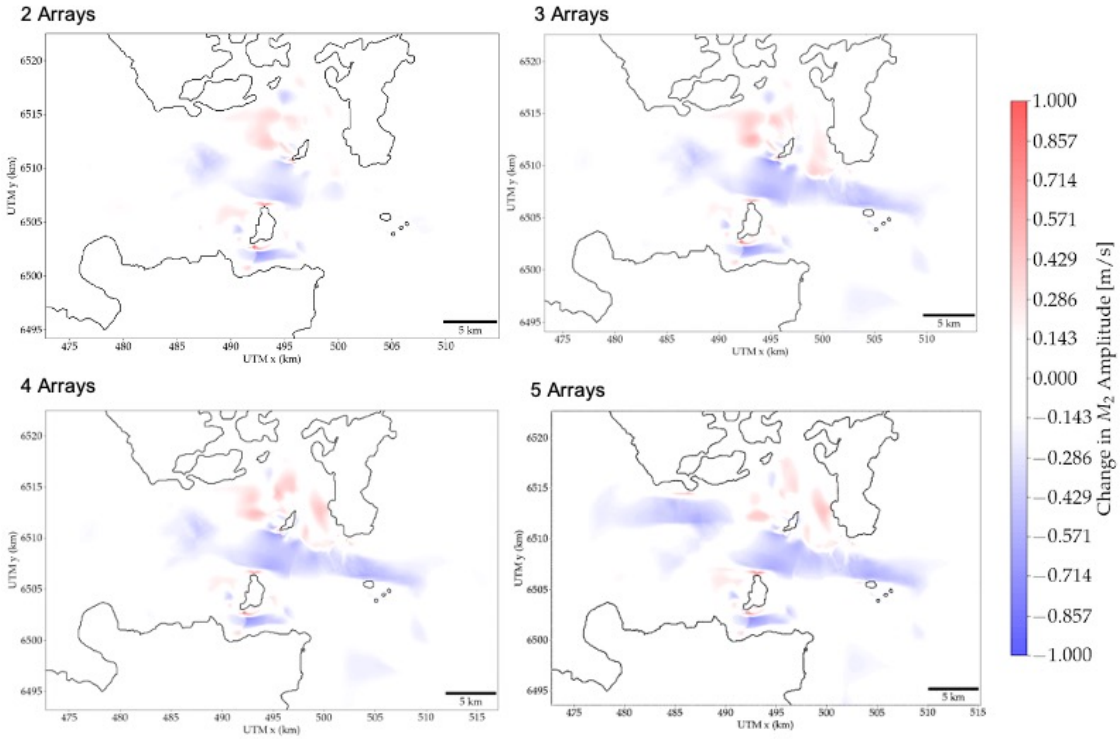

Figure 6.9: Change in amplitude of the M_2 constituent for current for each case with respect to the ambient case.

6.4.2 Pentland Firth Development

The cases presented in this chapter propose a gradual expansion of tidal developments across the Pentland Firth, which prioritises the need to harness tidal energy as a complementary renewable energy source to achieve net zero targets (Climate Change Committee, 2020). It is unlikely that the site will be developed all at once, and the method for identifying each array in this chapter demonstrates how the site can be incrementally developed as lease sites and seabed priorities evolve. Therefore, as every new array is defined sequentially, cases were run with the addition of each array. This allows the opportunity to consider how the resource responds to additional developments and the power yielded by the combination of arrays in each case if the site is developed in the same successive order, which is presented in Table 6.1.

Previous studies, as discussed in Section 6.1, have examined the dynamics of multiple

arrays across a site and found significant positive and negative interactions between arrays, dependent on whether they are arranged in parallel or series. However, in the arrays modeled in this chapter, while there are observable interactions between arrays in terms of power and flow rate amplitude across different areas of the site, their overall impact is not as significant. One notable exception is the effect on Array 1 when Array 2 is additionally deployed, which experiences a significant positive interaction. This is partly due to the installed capacity of the other 4 Arrays being more than half of Array 2, therefore imposing less resistance on the flow. Conversely, Arrays 2–4 only experience up to 6% fluctuation in power output between cases (Array 5 is not comparable because it is the last array to be deployed).

Table 6.3 details the number of arrays that are in parallel and series for each case. Array 2 is a critical array for the interactions between arrays because all positive and negative interference is due to the interaction with Array 2, which is centrally located in the site. In the 5 Arrays case, Array 2 is in series and parallel with 2 arrays respectively, therefore it is both experiencing and causing these effects. The significantly increased installed capacity of Array 2, in comparison to the other arrays, causes the interference to be enhanced.

Table 6.3: Combination of arrays in parallel and series for each case.

	Number of Arrays	
	Parallel	Series
1 Array	-	-
2 Arrays	2	0
3 Arrays	2	1
4 Arrays	3	1
5 Arrays	3	3

It has also been demonstrated in previous studies that increasing the number of turbines at a site, and therefore increasing the thrust imposed on the flow, leads to diminishing returns in power after a certain level of deployment (Draper et al., 2014a, Funke et al.,

2016, O'Hara Murray and Gallego, 2017). Vennell et al. (2015) emphasises that the energy available to an array is limited and therefore, the power per turbine will decrease with increasing numbers of turbines after a certain point. However, as demonstrated in 6.7a, in this study the power does not demonstrate diminishing returns as the overall resistance is increased through the addition of more arrays and turbines. A steep increase in power per turbine from the case with 1 Array to the case with 2 Arrays is apparent from Figure 6.7b. This occurs because Array 1 is made up of smaller diameter turbines. Therefore, to achieve the same capacity, more turbines are required compared to Arrays 2, 3, 4, and 5, which are made up primarily of 20 m turbines. The power per turbines remains almost constant after this point, rather than decreasing as in other studies, which highlights the benefit of identifying the arrays sequentially, based on the flow field of the previous deployment. As a result, the array specification adapts to how the resource is changing. Therefore, when multiple arrays are deployed, the rate of power per turbine remains constant up to the 5 Arrays being deployed (Figure 6.7b). The sequential identification of arrays, also contributes to the positive and negative interactions between arrays being less significant, because the resistance of the turbines in each array and the effect on the flow is accounted for in the definition of the next array, which minimises the effect without eliminating it. The change in power may diminish with a greater turbine density across the arrays. Therefore, a set of cases are considered to investigate the impact of increasing in turbine density for all five arrays, with the aim of testing the upper limit of power before diminishing returns are observed (Section 6.4.4).

6.4.3 Seabed Usage Constraints

A key factor for developing commercial tidal stream arrays is ensuring navigational channels and marine life passages are unobstructed, forming part of the decision for defining lease sites. The Scottish Government proposed 'Highly Protected Marine Areas' (HPMAs) to cover 10% of Scotland's marine areas by 2026 (Marine Scotland Science, 2022). The HPMAs were proposed to enable recovery of marine ecosystems

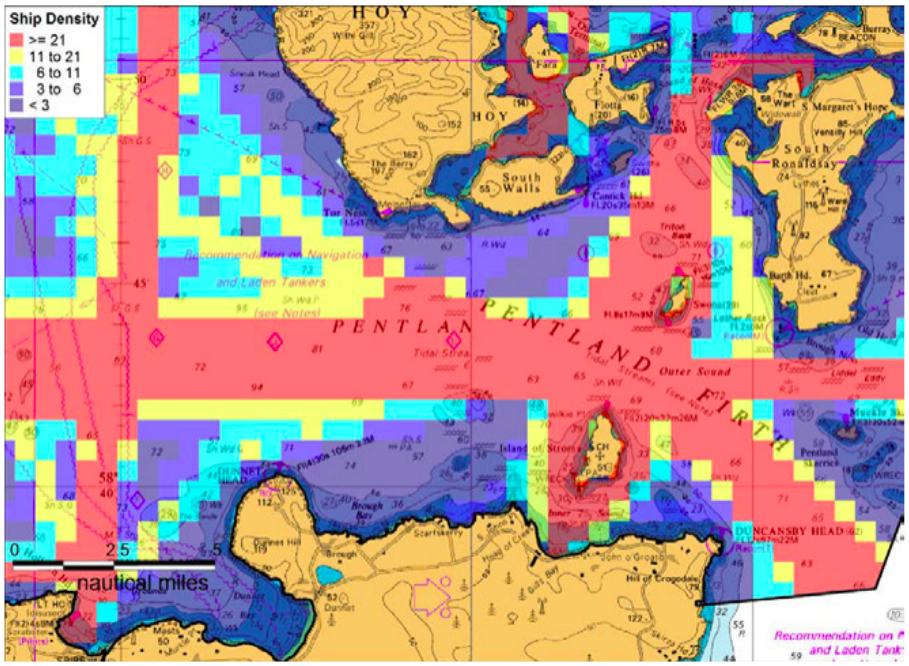

Figure 6.10: Ship density across the Pentland Firth from AIS Tracking (Marine Scotland, 2012).

and encourage a thriving environment. Under the proposal, any 'exploratory activity or construction of new infrastructure' for renewable energy would not be allowed in HPMAs. However, all shipping, including shipping associated with the development of renewable energy projects would be allowed. The proposal noted the need for offshore renewable energy and therefore, suggested that any existing agreements for renewable energy projects would be excluded when defining the HPMAs and remain unaffected. The Scottish Government conducted a consultation on the proposal, from December 2022 to April 2023, and received strongly divided responses. Therefore, as of November 2023, they are not implementing the policy for HPMAs (Scottish Government, 2023).

Despite HPMAs not being implemented, a significant seabed usage constraint for tidal stream energy developments that remains is the need to ensure navigation routes through the Pentland Firth. To inform the marine spatial planning pilot of the Pentland Firth and Orkney Waters (Marine Scotland, 2016), the Scottish Government conducted a shipping study to ensure future developments in the area do not impede on critical existing activities (Marine Scotland, 2012). The density of ships across the Pentland Firth is presented in Figure 6.10 (Marine Scotland, 2012).

While Figure 6.10 depicts multiple areas with high shipping density, the Outer Sound is a critical area for commercial ships (e.g., container ships) navigating north of the Scottish mainland. In the cases presented in this study, Array 2 occupies the majority of the Outer Sound (Figure 6.3), and leaves no navigation route. Therefore, a more practical case is presented where Array 2 is limited to accommodate a large shipping lane through the Outer Sound. This case allows 5 arrays to be developed across the Pentland Firth without significant rerouting of ships, which the Chamber of Shipping emphasised as a key concern in a shipping and navigation consultation undertaken by MeyGen (2012) regarding the Inner Sound lease site development. The navigation route is approximately 2.8 km in width, which is reasonable for the size of ship that passes through and the strong currents in the area (MeyGen, 2012, Marine Scotland, 2012). Jones et al. (2022) reported that 36% of the world's shipping carries energy products, which are predominantly fossil fuels. An energy transition to renewable sources will see the shipping of energy products fall, and could allow for the re-prioritisation of the seabed and reduce the number of large shipping lanes required. Figure 6.11 presents the update to Array 2 and the average power and capacity factor of the 5 arrays for the shipping channel accommodation case.

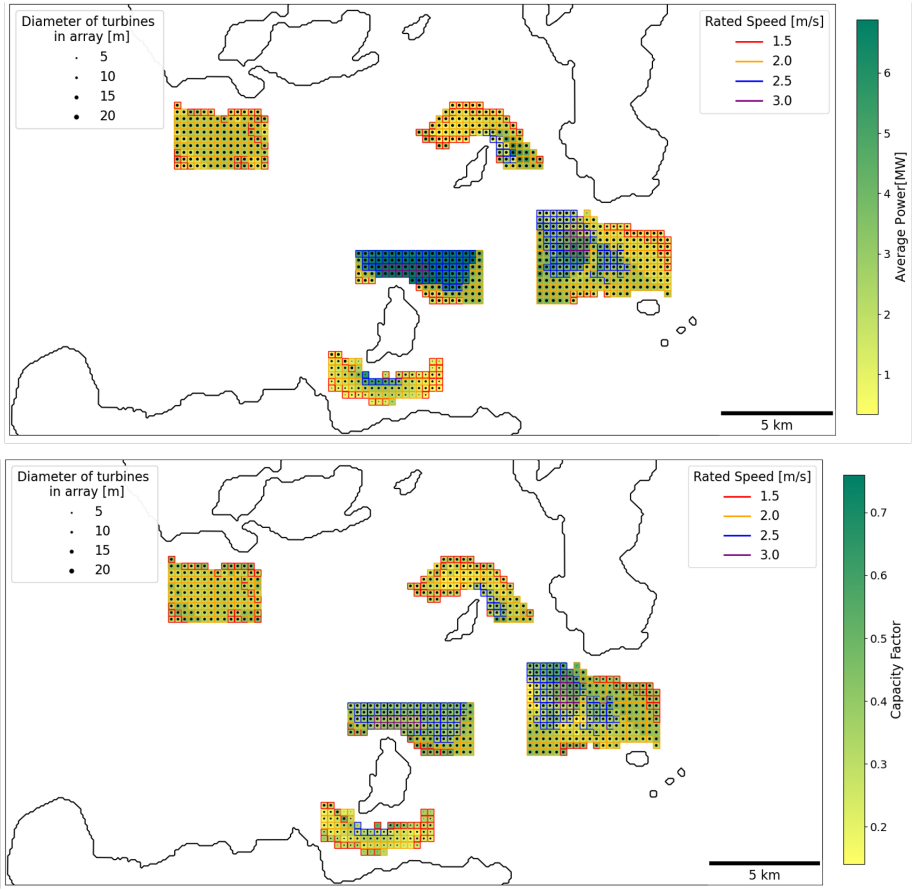

Figure 6.11: Average power and capacity factor of arrays in the shipping case. The rated speed of turbines in each array area is illustrated by the edge colour of the square and the diameter of the turbines is indicated by the size of the black circle.

Table 6.4 presents the average power, capacity factor and size of the arrays in terms of number of array areas, swept area, number of turbines and installed capacity for the 5 Arrays case and the case adapted for shipping. In comparison to the 5 Arrays case, the shipping case features only 38% of the number of array areas, turbines, and swept area in Array 2. Despite this reduction, the installed capacity of Array 2 in the shipping case is 47% of Array 2 in the 5 Arrays case. The areas of Array 2 that are retained in the shipping case are characterised by higher rated speeds and greater resource, compared to the north part of the Outer Sound. This strategic placement allows for the removal of more than half of Array 2 to accommodate ships in areas with lower flow velocity, while retaining turbines in regions with higher flow velocity that produce 50% of the power than an array more than double its size. As a result, the power per swept area and power

per turbine for Array 2 increases in the shipping case.

Table 6.4: Results for the 5 Arrays case and the Shipping case.

		Array 1	Array 2	Array 3	Array 4	Array 5	Overall
5 Arrays	Number of array areas	81	309	231	92	124	837
	Swept area [m^2]	136945	518397	388002	154514	208257	1406115
	Number of turbines	2134	1652	1260	492	663	6201
	Installed capacity [MW]	260	1670	830	320	400	3490
	Capacity factor	0.36	0.46	0.46	0.37	0.4000188	0.43
	Average power [MW]	90.15	741.89	330.25	113.97	154.28	1,430.54
	Power per swept area [MW/m^2]	0.66	1.43	0.85	0.74	0.74	1.02
	Power per turbine [MW/turbine]	42.24	449.09	262.11	231.64	232.69	233.4
Shipping	Number of areas	81	117	231	92	124	645
	Swept area [m^2]	136945	195934	388002	154514	208257	1083652
	Number of turbines	2134	625	1260	492	663	5174
	Installed capacity [MW]	260	780	830	320	400	2600
	Capacity factor	0.36	0.49	0.48	0.34	0.42	0.44
	Average power [MW]	87.89	371.49	344.25	103.82	163.79	1,071.25
	Power per swept area [kW/m^2]	0.64	1.90	0.89	0.67	0.79	0.99
	Power per turbine [kW/turbine]	41.19	594.39	273.21	211.02	247.05	207.0

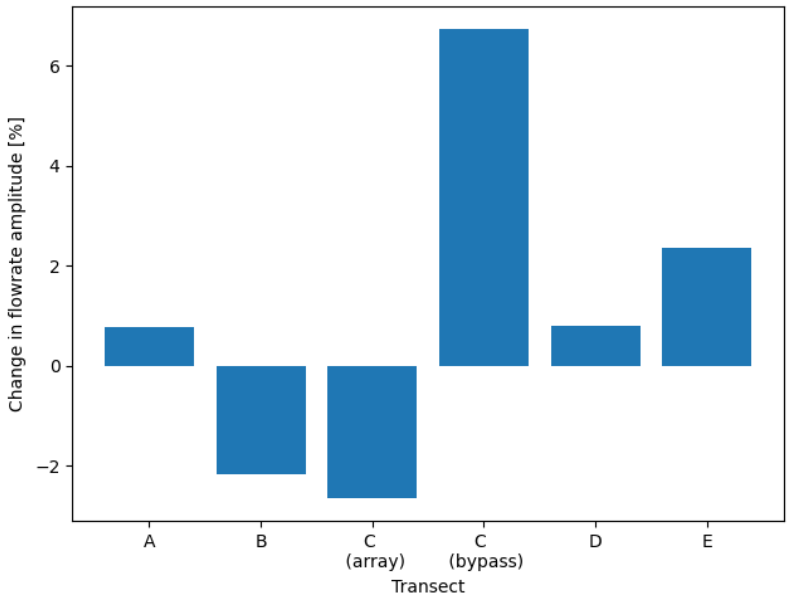

Figure 6.12: Percentage change in flow rate amplitude across five transects for the shipping case with respect to the 5 Arrays case. Transect C is presented in two portions, the portion occupied by Array 2 in the shipping case and the portion bypassing the array.

The adjustment to Array 2 for the shipping case impacts the interaction between arrays and the power produced by each, which is reflected in the change in flow rate amplitude across the five transects between the 5 Arrays case and the shipping case. Figure 6.12 presents the change in flow rate amplitude for the shipping case with respect to the 5 Arrays case. The flow rate across Transect C is evaluated separately over the portion that is occupied by Array 2 in the shipping case and the remaining proportion of the transect.

The adjustment made to Array 2 for the shipping case results in increased power for Arrays 3 and 5 by up to 4%, which are located across Transects E and A respectively. The flow rate amplitude across both transects also increases (up to 2.4%). In the 5 Arrays case, Arrays 3 and 5 are in series with Array 2, however, in the shipping case, they are no longer in direct obstruction of each other, which is why there is an increase in power for each of the arrays in the shipping case relative to the original case.

The power yielded by Array 1 and Array 4 decreases in the shipping case, with respect to the 5 Arrays case. The flow rate amplitude across Transect B, where Array 1 is located, decreases by 2.16% and the power produced by Array 1 also decreases by 3% in the shipping case. However, despite a small increase (less than 1%) in flow rate amplitude across Transect D, the power from Array 4, located over the transect, decreases by 9%. This is attributed to the fact that Array 4 partially coincides with Transect D, where the flow rate decreases, but the flow bypassing Array 4 experiences an increase in velocity, and this bypassing flow rate is enhanced when Array 2 is adjusted for the shipping case.

A similar effect is observed across Transect C for the shipping case because a portion of the transect is occupied by Array 2 and the other portion experiences the flow bypassing Array 2 with an increased velocity. This is demonstrated in Figure 6.12, where it can be seen that the flow rate amplitude across the bypass portion of Transect C increases by 6.72% in the shipping case compared to the 5 Arrays case and decreases by 2.64% in the array portion of Transect C. The envelope of the flow rate across the array and

bypass portion of Transect C is plotted in Figure 6.13. In the shipping case, the flow rate amplitude across the bypass portion is 19% greater than the flow rate amplitude through the array. Compared to the 5 Arrays case, where the 'bypass' portion is occupied by Array 2 and only experiences an 8% increase compared to the 'array' portion.

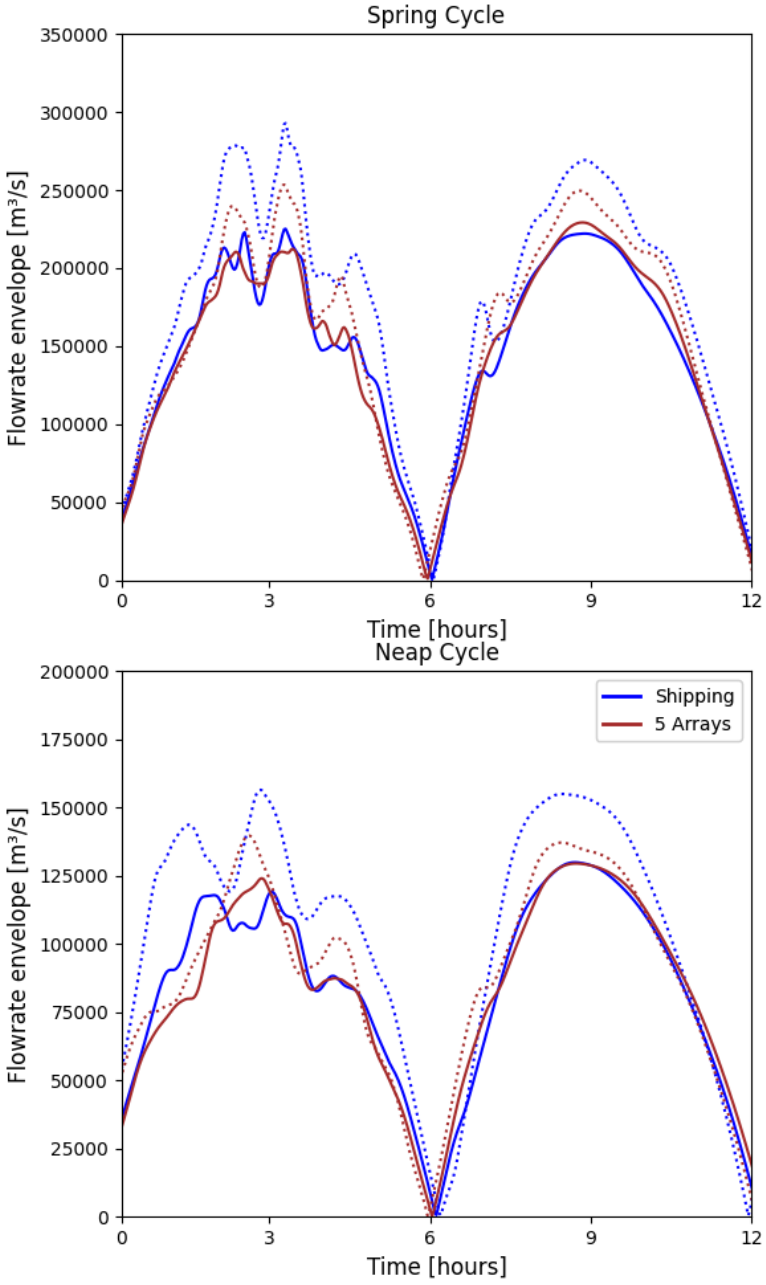

Figure 6.13: Envelope of the flow rate across Transect C for the shipping case and 5 Array case, solid line representing the proportion of the transect occupied by Array 2 in the shipping case and the dotted line representing the proportion of transect on north side of Array 2 during a spring cycle and neap cycle.

As discussed previously, the increase in flow rate bypassing Array 2 in the shipping case

causes the negative interference for Array 3 and 5, to be less significant in comparison to the 5 Arrays case. Similarly, the positive interference for Array 1 and 4, due to Array 2, are also diminished. This is because the flow in the parallel channels that the arrays are located in, do not experience as great an increase in flow velocity because the width of the Outer Sound is much less significantly blocked by Array 2 in the shipping case. Therefore, the flow rate through the bypass portion of Transect C increases. As discussed in Section 6.4.2, the interference between arrays is mostly dependent on Array 2 due to its positioning and significant installed capacity in the non-shipping cases. Reducing the capacity and spatial extent of Array 2 in the shipping case, demonstrates that it was the driving force for these interactions because they are diminished as the array is diminished (both in terms of installed capacity and occupation of the Outer Sound).

6.4.4 Turbine Density

To consider an alternative scale of development, the impact of increasing turbine density in all the arrays defined across the Pentland Firth is examined. This analysis aims to explore the extent of development that could take place across the Pentland Firth. Increasing the turbine density means the thrust imposed on the flow due to turbines also increases, therefore the power will only increase up to a certain point until too many turbines are deployed (Funke et al., 2016), which allows the upper limit of development to be investigated.

The 5 Arrays case is taken as the baseline case, where the turbine density for each array area is based on a 0.16 blockage (Section 5.3.1). The turbine density across each array is increased by 10% until 40% more turbines are deployed evenly across the arrays. The average power is plotted against the number of turbines and thrust imposed by the turbines in Figure 6.14.

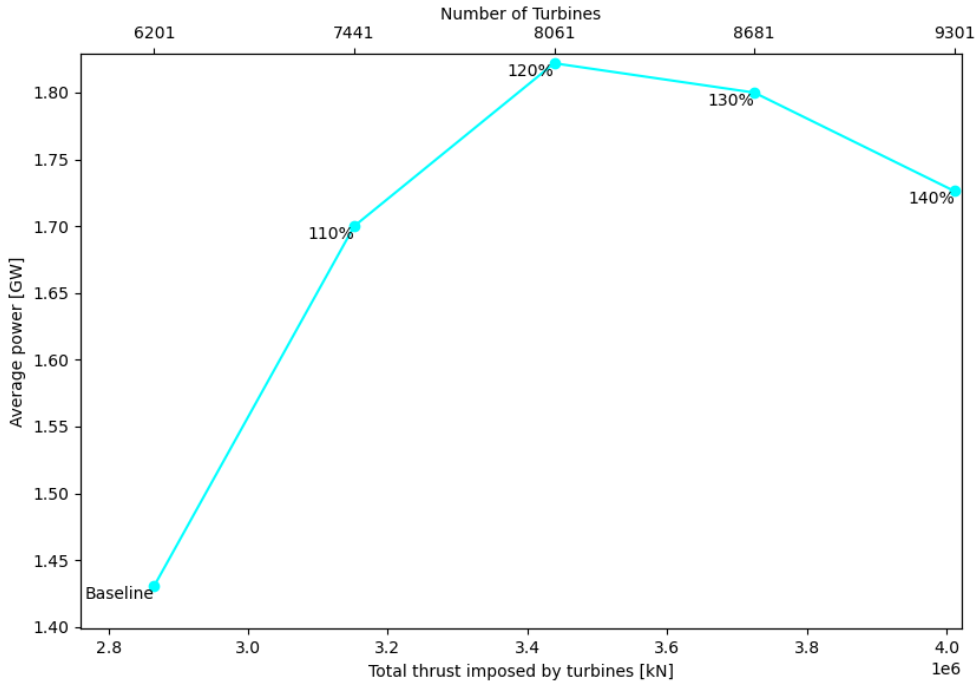

Figure 6.14: Average power with increasing thrust imposed by turbines as the turbine density across the 5 arrays increases up to 40%.

The average power increases as more turbines are deployed, reaching a peak with 8,000 turbines (20% increase), resulting in a power output of 1.82 GW. However, beyond this threshold, further increasing the turbine density leads to a decrease in power because of the significant thrust on the flow causing a significant decrease in velocity.

Table 6.5: Change in M_2 current amplitude and phase for the 5 Arrays case and the Shipping case with respect to an ambient case.

Turbine density	Change in M_2 current amplitude [m/s]	Change in M_2 current phase [°]
Baseline	0.97	3.05
110%	1.33	5.92
120%	1.46	7.83
130%	1.45	6.59
140%	1.49	11.37

It is important to consider the impact of the increasing thrust on the flow with increasing numbers of turbines at a site. Table 6.5 presents the maximum difference in M_2 current

amplitude and phase for each case of increasing turbine density and the ambient case with no turbines. The baseline case of 5 Arrays results in an maximum 0.97 m/s change in M_2 current amplitude and 3.05° change in phase. The change in current amplitude reaches a maximum of 1.49 m/s in the 140% case and exceeds 1 m/s in all cases with increased turbine density. This highlights the complexity of balancing maximising power yield without significantly affecting the natural environment of the site, and the maximum change in M_2 current indicates how the flow is being impacted. The preservation of the marine environment will always be a priority, therefore, significant changes in velocity across the site are unfavourable. It is unlikely that the maximum power yielded by the 120% turbine density case would be developed because of its potential negative impact on the natural environment.

6.4.5 The Pentland Firth Resource

The results from this study demonstrate the range of the practical resource in the Pentland Firth based on different development strategies and priorities. The maximum power yielded from the 5 arrays studied in this chapter is 1.82 GW (120% density case). However, if the change in M_2 current amplitude is to be within 1 m/s from the ambient case, the resource is restricted to 1.43 GW. In the case of shipping remaining a priority for seabed usage, the restriction of a navigation channel results in a 25% reduction in power output relative to not having this restriction and a minimal change in capacity factor. Installing bottom-fixed turbines, rather than floating turbines, across the Outer Sound could avoid needing to create a navigation channel through the array so that ships could pass over turbines, if the clearance is sufficient. However, this would lead to turbines being lower down in the water column, which would have implications on the power available to them (discussed in Section 6.2.1). Additionally, bottom-fixed turbines must still compete for seabed usage priorities (e.g. conflicting with bottom trawling).

Figure 6.15 presents the time-averaged flow velocity for an ambient case with the

arrays defined and proposed in this study, through the extension of the heterogeneous framework, and the original 2010 lease sites. Two of the arrays defined in this study are closely aligned to the original lease sites. The original lease sites are more conservative in their occupation of the seabed, however, they are missing key areas of the resource and were not defined with the consideration of the impact on the flow as the site is developed. The arrays proposed in this study have utilised the specification of rated speed across the site to define arrays sequentially and the interaction between arrays is accounted for in their definition, therefore, maximising extraction of the resource.

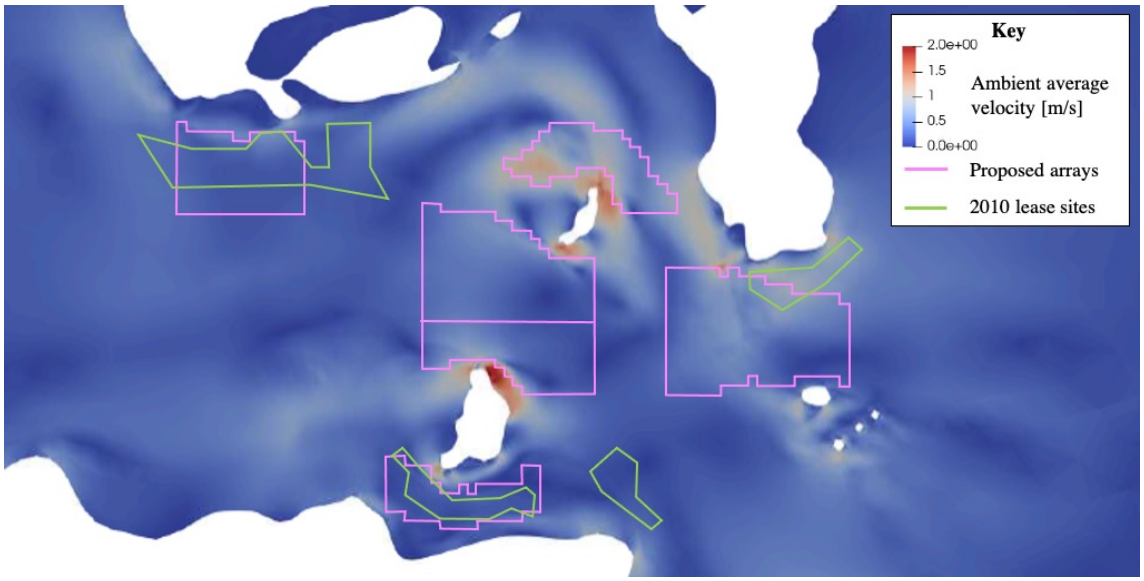

Figure 6.15: Time-average flow velocity [m/s] for the ambient case with The Crown Estate 2010 lease sites and the proposed arrays illustrated.

Table 6.6 outlines how constraints on the resource (presented in Figure 2.4) are incorporated in this study of the resource at the Pentland Firth. The technical constraints on the resource are accounted for through the use of BC-BEMT to more realistically represent the performance of tidal stream turbines in comparison to ADT. Additionally, the drag due to support structures is accounted for and assumptions for floating and bottom-fixed arrays are assumed to minimise support structure size, whilst maintaining the turbine hubs in the upper portion of the water column. However, there are limitations, including the assumption that the turbines are achieving optimal performance and experiencing 0.16 blockage, despite the difficulty in ascertaining the blockage each

turbine is experiencing at a real site (discussed in Section 5.3.1). Due to the relation between turbine density and blockage, and adoption of the continuous approach in this thesis (illustrated in Figure 4.1) the arrangement and micro-siting or individual turbines is not considered in this thesis. However, it should be noted that multiple levels of turbines, particularly for smaller turbine diameters, might be required to achieve 0.16 blockage in deep waters. The study does not account for the additional power yielded when a turbine rotor is placed higher in the water column, nor does it address challenges like foundation issues in terms of bed type and bed gradient for bottom-fixed turbines or the effects of motion on turbine performance on floating platforms. Despite these limitations, the study provides valuable initial insights into the resource.

Table 6.6: The incorporation of constraints limiting tidal stream energy in the assessment of the resource at the Pentland Firth.

Category	Constraint	Incorporation
Technical	Support structure	Floating and fixed foundation assumptions
	Turbine performance	BCBEMT for more realistic turbine representations
Practical	Bathymetry	Heterogeneity in turbine diameter
	Flow Velocity	Heterogeneity in rated speed
	Navigation channels	Shipping accommodation case
	Fishing	Not incorporated
Accessible	Institutional - Lease sites	Framework extended to propose new sites
	Public objection	Acknowledged through HPMAs
	Environmental constraints	Change in M_2 current amplitude
Viable	Economic viability	Consideration of economies of scale trade-offs
	Distance from mainland	Not incorporated
	Energy Storage	Not incorporated

The development of the heterogeneous array design framework in Chapter 5 was shaped by practical constraints, bathymetry and flow velocity. These constraints were used to define the diameter and rated speed of turbines across an array according to the spatially variable constraints. The practical constraints of navigation channels and fishing areas, are closely linked to the legislative and regulatory constraints that are categorised as

accessible. The categorisation of the resource was introduced by Sustainable Energy Ireland (2004), and used by O'Rourke et al. (2010) and Segura et al. (2017). Although it is not objective and the inter-dependency of constraints limiting the tidal resource makes their categorisation difficult, the categorisation is adopted to remain aligned with the literature. Fishing constraints are not explicitly incorporated into the study, however, they are considered as part of the Marine Spatial Planning consultation in the Pentland Firth and Orkney (Marine Scotland, 2016) and the definition of the original lease sites (Figure 6.1). Comparisons between proposed development areas from this study and previously defined lease sites indicate overlaps that might be feasible with fishing considerations (Figure 6.15). Commercial shipping is considered in a case to accommodate a navigation channel between Stroma and Swona. The effects of a shipping accommodation on the power yield of the array and overall development are demonstrated.

The evolving legislation regarding tidal stream energy development and leasing of the seabed poses challenges for accommodating accessible constraints in models. Nonetheless, this work offers considerations and suggestions to inform and account for such constraints. The institutional constraint of lease sites for the developing tidal stream energy in the Pentland Firth, agreed by the The Crown Estate and now managed by The Crown Estate Scotland, has undergone multiple changes with the exception of the Meygen Lease site. Therefore, in this study, lease sites are addressed by initially focusing on the Inner Sound, an actively developed area, and extending the heterogeneous framework to propose sites for development, based on concentration of the resource across the site and refined modelling. The proposed sites are compared in terms of their placement with the original lease sites to indicate how leases can be updated as seabed usage and renewable energy priorities evolve. While the consultation of public opinion and assessment of environmental impact through an EIA are beyond the scope of this study, the proposal of HPMAs was acknowledged and in absence of its implementation, environmental concerns are considered by examining changes in M_2 current amplitude

and considering a blockage of 0.16 to mitigate potential hazards to marine mammals. Environmental concerns are used to recommend that increasing the turbines density by 20% across all arrays would not be suitable due to adverse environmental effects, despite the increase in power (Section 4.10).

Finally, the constraints on the viable resource are mostly not accounted for in this study because considering the economic and commercial viability of tidal stream energy is challenging to do given the current stage of development of the sector and the need to have considered other constraints lower down in the pyramid before tackling these, which is the focus of this thesis. Although economic viability is not explicitly incorporated, the study considers the trade-off between standardisation for economies of scale and heterogeneity to improve the yield of arrays (Section 5.7.4). Furthermore, viable constraints such as energy storage and grid integration are not accounted for in this study. While a minimum distance to land is maintained, establishing a maximum distance to inhabited land may be necessary to facilitate grid integration.

In comparison with other resource assessments conducted in the Pentland Firth (Tables 2.1, 2.2), the range of the resource quantified in this study is in the same order of magnitude as O'Hara Murray and Gallego (2017), De Dominicis et al. (2018) and within the Adcock et al. (2013) upper bound assessment. However, this study not only provides an assessment of the tidal stream energy resource in the Pentland Firth, it has also informed the practical development of the site with the consideration of real-world constraints on the resource in a strategic way that can be replicated for the development of other sites.

6.5 Conclusion

The strategic and incremental development of a site, considering practical constraints on the resource and the response of the resource to the deployment of heterogeneous arrays, is detailed in this chapter. Utilising and extending the heterogeneous array de-

sign framework, introduced in Chapter 5, multiple arrays are successively identified at the site, showcasing another application of the methodology. The sequential definition of arrays incorporates the flow field of the previous deployment strategy within the heterogeneous framework, thereby minimising negative and positive interference effects between arrays, which have been significant in previous studies. The arrays are defined in areas of high resource and when compared to the lease sites from 2010, they highlight the areas where the resource would not have been exploited with the original leases. A total of 5 heterogeneous arrays are deployed across the Pentland Firth in this case study, with a combined installed capacity of 3.5 GW, yielding 1.43 GW. Array 2 is the largest array in terms of installed capacity, swept area, and number of turbines, driving both positive and negative interference effects for the other 4 arrays. The addition of each array in each case reveals that the power per turbine remains nearly constant after an initial increase from the power per turbine in Array 1 due to the specification of smaller diameter turbines. Exploring various limitations on the resource, such as shipping and environmental restrictions, demonstrates a potential power extraction range of 1.07–1.82 GW from the Pentland Firth. The range of development options investigated in this study demonstrates the potential power yield from the Pentland Firth as priorities evolve and how it can be developed by independent developers successively.

Chapter 7

Conclusion and Further Work

This thesis examines real-world constraints limiting the tidal stream energy resource in the UK, focusing on the Pentland Firth as the most notable site due to its development status. The limiting constraints on the resource are interrelated and challenging to incorporate in resource assessments due to their evolving nature, particularly legislative and technical advancements. However, integrating these constraints into assessments is crucial for characterising the resource, refining assessments and informing the realistic development of sites with an understanding of how the resource responds to energy extraction by arrays. A more refined assessment of the resource leads to reduced uncertainty and risk for developers, which helps to reduce cost, provide confidence for investors and inform government policies.

7.1 Contributions of the Thesis

In this thesis, the identification of parameters affecting tidal stream energy resource assessments has been undertaken to investigate their impact and importance in quantifying the resource, as well as the uncertainty introduced through their exclusion from models. The study highlighted the interdependence of parameters constraining resource assessments and difficulty of identifying individual key parameters. Instead, the influence of parameters on each other and the resource was analysed. A combination of site-based channel characteristics, turbine control and rotor design parameters and modelling assumptions were considered in the investigation. The study of channels with different geometries and dominant driving forces (inertia or drag) revealed distinct responses to the deployment of turbines, highlighting dynamic balance as a critical parameter in resource assessments. Furthermore, the thesis focuses on the UK, where tides are predominantly semi-diurnal and the investigation of sites spanning the semi-diurnal range suggests the number of constituents used to model sites should be

informed by the form factor of the site. The study of site-based channel characteristics illustrates how the application of the methods implemented in this thesis may be adapted for studies of alternative sites, beyond the case study of the Pentland Firth.

The technical constraints on the resource are investigated through the comparison of rotors designed for optimal performance in different blockages, the definition of characteristic points on a variable-speed, variable-pitch performance curve and the examination of different capping strategies. In the resource assessment conducted for the Pentland Firth, modelling assumptions regarding technical constraints are made according to the most probable strategies for tidal developers to best reflect the realistic development of a site. Therefore, power capping is adopted due to the complexity of combined power and thrust capping outweighing the benefits of support structure savings compared to power capping alone. Instead, support structure savings are made through floating and fixed turbine assumptions according to the average depth of the array. However, the investigation of the characteristic points in a performance curve underscores the significance of rated speed in harnessing the resource, which closely relates to the practical constraint on flow velocity at a site and the spatial variability of the resource in tidal energy.

The practical constraints of flow velocity and bathymetry are used to explore how variability of the resource at a site can inform array design by developing and applying a novel heterogeneous array design framework. The framework provides a new perspective on how arrays can be implemented in domains characterised by complex bathymetry and hydrodynamics, leading to a spatially variable resource, by utilising the constraints to define the turbine specifications of diameter and rated speed, rather than be limited by them. A key advantage in deploying heterogeneous arrays is the increase in power per swept area and power per turbine compared to a homogeneous array of small diameter turbines because fewer turbines are required to achieve the same installed capacity, which is a key benefit for developers. Heterogeneity emerges

as an important consideration for tidal stream energy developments due to the spatial variability of the resource and limited areas suitable for developments. The necessity of heterogeneity is underscored by the challenges facing future phases of development at the Meygen lease site, which has limited bathymetry. Whilst, modelling the Pentland Firth with 2 semi-diurnal constituents was appropriate for the purposes of this thesis, modelling the Pentland Firth with additional constituents would allow investigation of the resource over a longer time period than the spring-neap cycle. The variation over the nodal cycle is important for developers to consider for long-term forecasting and investment. Results from Chapter 3 indicate that from 2021 the tidal resource will enter a low resource period over the first half of the 18.6-year cycle. This is significant for investors and developers in their predictions of the resource and cost of tidal stream energy. Developments that occur in the next 10 years extract energy in the low and average part of the nodal cycle, which should be acknowledged when assessing the success of projects, particularly in terms of the net-zero strategy and prioritisation of the seabed.

The heterogeneous framework is extended to successively identify multiple independent arrays, in areas aside from existing and changing lease sites defined by the seabed leasing bodies, based on the evolving concentration of the resource across a site as each array is deployed. The positive and negative interference between arrays is minimised by strategically defining each new array based on the flow field of the previous deployment. Therefore, each array is defined with consideration of how the resource responds to the incremental development of the site. Five independent arrays are defined across the Pentland Firth through the heterogeneous framework, with the performance of arrays examined as each array is deployed to provide insight into the yield of a realistic and gradual development of the site, which could be undertaken by individual developers. The first array is developed in the Inner Sound due to its current lease site and development status. The overall power per turbine increases with the addition of another array and remains constant as further arrays are added. This underscores the

importance of considering the effects on the flow when defining each array to minimise array interference or avoid diminishing returns.

Multiple development options are explored to assess the range of development that could take place across the Pentland Firth based on different priorities. To accommodate shipping, the largest array, situated within a major commercial shipping channel, is adjusted by reducing the array size while retaining turbines in high-velocity areas. Despite the decrease in overall power production resulting from the reduced installed capacity, there is an increase in power per turbine and power per swept area, attributed to the turbines remaining in high-velocity areas. The upper limit to the scale of development in terms of turbine density is explored by increasing the number of turbines in each array in 10% increments across all five arrays. The average power increases with up to 20% more turbines before diminishing returns are observed due to the increasing thrust imposed on the flow by the number of turbines. Despite the peak in average power resulting from increased turbine density, a significant effect on the flow is observed, which implies such a scale of development will have subsequent impacts on the environment and marine habitat.

The heterogeneous array design framework can provide insight for leasing bodies and developers to identify high resource areas across a site for leasing and developing, and define rotor size and rated speed of turbines according to the bathymetry and flow characterisation across the site. The adaptability of the framework for evolving seabed priorities has been demonstrated and it is a useful tool for industry to realise the potential of tidal stream energy at sites, whilst understanding and minimising the impact of developments in close proximity.

The assessment of the resource to be within 1.07–1.82 GW based on a range of development options aligns with other evaluations of the resource magnitude at the Pentland Firth in the literature but proposes realistic development strategies that consider real-world constraints at a site. Furthermore, it provides a more refined assessment than

current upper bound and practical evaluations of the resource in the literature. The assessment of the resource in this thesis is dependent on the assumption of a target 40% capacity factor to define the rated speed of turbines in the heterogeneous framework. A different value of rated speed and capacity factor would result in a higher or lower power output of the array. However, the same target is used across all cases, which allows conclusions from the comparative analysis between cases to be transferable and the target value was chosen on the basis of an existing tidal development.

7.2 Future Work

A recommendation for future work is to extend the study of the Pentland Firth by modelling the site with a 3-D (layered) model, whilst incorporating limiting constraints on the resource. Previous adoption of constraints in resource assessments has been limited due to the complexities in accounting for them and understanding their importance. However, given the insights gained into the impact of real-world constraints on the resource and the demonstrated methods for accounting for them in the modelling of the Pentland Firth in this thesis, it is recommended to extend the research with a higher order model. A layered model enables a more accurate representation of the in-depth velocity profile, offering insights into the potential additional power that turbines in the upper portion of the water column could yield. This is particularly relevant to the proposal of floating and fixed turbines based on the average bathymetry across the array to minimise support structure sizes.

Furthermore, the research could be extended by applying the heterogeneous framework to other sites. A particular site of interest for tidal stream development is the Ramsey Sound, UK, which has an agreed lease with Cambrian Offshore Ltd. The site has prominent and complex bathymetric features including a semi-submerged rock, deep trench, and a rocky reef, which significantly influence the tidal dynamics (Haverson et al., 2018, Mackie et al., 2021). A high resolution and accurate characterisation of the bathymetry at such a site is critical and the heterogeneous framework could be

implemented with array areas of a smaller resolution to define turbine specifications across the array considering its complex bathymetry.

The heterogeneous framework is primarily designed to offer preliminary insights into how a site can be developed and assess the resource. While this thesis has primarily focused on resource assessment, the framework has the potential to be extended for micro-siting arrays and subsequent work at the turbine-scale. As developers move towards detailed planning and large scale deployment across a site, the arrangement of turbines within arrays and their interactions become crucial factors. The deployment of heterogeneous arrays in reality will necessitate the siting of individual turbines, taking into account factors such as seabed composition, bed gradients, and other complex considerations. In this context, the framework serves as a valuable tool for the initial identification of suitable areas for turbine deployment and definition of turbine specifications, but can be further extended to consider the arrangement of individual turbines within each array area.

Finally, two key areas in the pyramid of constraints that have been considered as beyond the scope of this work include environmental and viable constraints. In assessing the resource, it is crucial to incorporate the levels of the pyramid of constraints as additional layers of increasing complexity in models. Environmental constraints, categorised as an accessibility constraint, and viable constraints are towards the top of the pyramid. Therefore, it has been critical to address constraints lower in the pyramid before tackling those higher up, a step that has been undertaken in this thesis, leading to the potential of their incorporation in future work. For environmental constraints, it is evident that clearer legislative guidance is needed to formally incorporate them into resource assessments. Conducting an environmental impact assessment would be key to understanding the effects of developments on the marine environment, going beyond the commonly used metric of changes in velocity due to the presence of turbine, which may not fully capture these effects. Quantifying the impact of noise and sediment transport

could provide more insight to environmental effects. The viable resource of tidal stream energy is also constrained by economic factors and grid integration challenges. Evaluating the levelised cost of energy for tidal stream projects will be essential to assess their economic viability. Additionally, the framework would benefit from considering seabed usage required for cabling, which is crucial for offshore energy projects, and determining the most efficient methods for distributing electricity to the network.

References

T. A. A. Adcock and S. Draper. On the tidal stream resource of two headland sites in the English Channel: Portland Bill and Isle of Wight. In *International Conference on Offshore Mechanics and Arctic Engineering*, volume 45530, page V09AT09A003. American Society of Mechanical Engineers, 2014a.

T. A. A. Adcock and S. Draper. Power extraction from tidal channels–multiple tidal constituents, compound tides and overtides. *Renewable Energy*, 63:797–806, 2014b.

T. A. A. Adcock, A. G. L. Borthwick, and G. T. Houlsby. The open boundary problem in basin scale modelling of tidal energy extraction. In *Proceedings of the 9th European Wave and Tidal Energy Conference*, 2011.

T. A. A. Adcock, S. Draper, G. T. Houlsby, A. G. L. Borthwick, and S. Serhadlıoğlu. The available power from tidal stream turbines in the Pentland Firth. *Proceedings of the Royal Society A: Mathematical, Physical and Engineering Sciences*, 469(2157), 2013. ISSN 14712946. doi: 10.1098/rspa.2013.0072. URL `http://dx.doi.org/10.1098/rspa.2013.0072`.

T. A. A. Adcock, S. Draper, G. T. Houlsby, A. G. L. Borthwick, and S. Serhadlıoğlu. Tidal stream power in the Pentland Firth – long-term variability, multiple constituents and capacity factor. *Proceedings of the Institution of Mechanical Engineers, Part A: Journal of Power and Energy*, 228(8):854–861, 2014.

T. A. A. Adcock, S. Draper, and T. Nishino. Tidal power generation - a review of hydrodynamic modelling. *Proceedings of the Institution of Mechanical Engineers, Part A: Journal of Power and Energy*, 229(7):755–771, 2015.

T. A. A. Adcock, S. Draper, R. H. J. Willden, and C. R. Vogel. The fluid mechanics of tidal stream energy conversion. *Annual Review of Fluid Mechanics*, 53:287–310, 2021.

Admiralty Charts and Publications. *Admiralty Sailing Directions Channel Pilot*, volume NP 27. 1999.

C. Anderson. *Wind turbines: Theory and practice*. Cambridge University Press, 2020.

A. Avdis and J. Hill. *qmesh* Manual, 2017. URL `http://www.qmesh.org/`.

A. S. Bahaj and L. Myers. Analytical estimates of the energy yield potential from the Alderney Race (Channel Islands) using marine current energy converters. *Renewable energy*, 29(12):1931–1945, 2004.

A. S. Bahaj, L. E. Myers, M. D. Thomson, and N. Jorge. Characterising the wake of horizontal axis marine current turbines. In *Proceedings of the 7th European wave and tidal energy conference*, volume 9, 2007.

G. Bai, J. Li, P. Fan, and G. Li. Numerical investigations of the effects of different arrays on power extractions of horizontal axis tidal current turbines. *Renewable Energy*, 53: 180–186, 2013.

S. Balay, S. Abhyankar, M. F. Adams, S. Benson, J. Brown, P. Brune, K. Buschelman, E. Constantinescu, L. Dalcin, A. Dener, V. Eijkhout, J. Faibussowitsch, W. D. Gropp, V. Hapla, T. Isaac, P. Jolivet, D. Karpeev, D. Kaushik, M. G. Knepley, F. Kong, S. Kruger, D. A. May, L. C. McInnes, R. T. Mills, L. Mitchell, T. Munson, J. E. Roman, K. Rupp, P. Sanan, J. Sarich, B. F. Smith, S. Zampini, H. Zhang, H. Zhang, and J. Zhang. PETSc/TAO users manual. Technical Report ANL-21/39 - Revision 3.19, Argonne National Laboratory, 2016.

Black and Veach. Phase II UK Tidal Stream Energy Resource Assessment. Technical report, A report to the Carbon Trust's Marine Energy Challenge., 2005.

L. S. Blunden and A. S. Bahaj. Initial evaluation of tidal stream energy resources at Portland Bill, UK. *Renewable Energy*, 31(2):121–132, 2006.

L. S. Blunden and A. S. Bahaj. Tidal energy resource assessment for tidal stream generators. *Proceedings of the Institution of Mechanical Engineers, Part A: Journal of Power and Energy*, 221(2):137–146, 2007.

I. G. Bryden, S. J. Couch, A. Owen, and G. Melville. Tidal current resource assessment. *Proceedings of the Institution of Mechanical Engineers, Part A: Journal of Power and Energy*, 221(2):125–135, 2007.

J. A. Buck and S. D. Garvey. Analysis of force-capping for large wind turbine rotors. *Wind Engineering*, 39(2):213–228, 2015.

T. Burton, N. Jenkins, D. Sharpe, and E. Bossanyi. *Wind Energy Handbook*. John Wiley & Sons, 2011.

Cambrian Offshore Ltd. The Ramsey Sound Regeneration project, 2024. URL `https://cambrian-offshore.com/`.

A. R. Campbell, J. H. Simpson, and G. L. Allen. The dynamical balance of flow in the Menai Strait. *Estuarine, Coastal and Shelf Science*, 46(3):449–455, 1998.

B. Cao, R. H. J. Willden, and C. R. Vogel. Effects of blockage and freestream turbulence intensity on tidal rotor design and performance. In *Advances in Renewable Energies Offshore: Proceedings of the 3rd International Conference on Renewable Energies Offshore (RENEW 2018)*, pages 127–135, 2018.

Carbon Trust. UK tidal current resource and economics. Technical report, 2011. URL `https://www.marineenergywales.co.uk/wp-content/uploads/2016/01/CarbonTrustMarineResourceJune2011.pdf`.

D. E. Cartwright, A. C. Edden, R. Spencer, and J. M. Vassie. The tides of the northeast Atlantic Ocean. *Philosophical Transactions of the Royal Society of London. Series A, Mathematical and Physical Sciences*, 298(1436):87–139, 1980.

L. Chen. Design and operation of tidal arrays in channels. DPhil thesis, University of Oxford, 2019.

L. Chen, P. A. J. Bonar, C. R. Vogel, and T. A. A. Adcock. A note on the tuning of tidal turbines in channels. *Journal of Ocean Engineering and Marine Energy*, 5(1):85–98, 2019.

Climate Change Committee. The Sixth Carbon Budge; The UK's path to Net Zero, 2020. URL `https://www.theccc.org.uk/wp-content/uploads/2020/12/The-Sixth-Carbon-Budget-The-UKs-path-to-Net-Zero.pdf`.

D. Coles, A. Angeloudis, D. Greaves, G. Hastie, M. Lewis, L. Mackie, J. McNaughton, J. Miles, S. Neill, M. Piggott, et al. A review of the UK and British Channel Islands practical tidal stream energy resource. *Proceedings of the Royal Society A: Mathematical, Physical and Engineering Sciences*, 477(2255):20210469, 2021.

D. S. Coles, L. S. Blunden, and A. S. Bahaj. Experimental validation of the distributed drag method for simulating large marine current turbine arrays using porous fences. *International journal of marine energy*, 16:298–316, 2016.

D. S. Coles, L. S. Blunden, and A. S. Bahaj. Assessment of the energy extraction potential at tidal sites around the Channel Islands. *Energy*, 124:171–186, 2017.

D. S. Coles, L. S. Blunden, and A. S. Bahaj. The energy yield potential of a large tidal stream turbine array in the Alderney Race. *Philosophical Transactions of the Royal Society A*, 378(2178):20190502, 2020.

M. De Dominicis, R. O'Hara Murray, and J. Wolf. Multi-scale ocean response to a large tidal stream turbine array. *Renewable Energy*, 114:1160–1179, 2017.

M. De Dominicis, J. Wolf, and R. O'Hara Murray. Comparative effects of climate change and tidal stream energy extraction in a shelf sea. *Journal of Geophysical Research: Oceans*, 123(7):5041–5067, 2018.

D. Dehtyriov, A. M. Schnabl, C. R. Vogel, S. Draper, T. A. A. Adcock, and R. H. J. Willden. Fractal-like actuator disc theory for optimal energy extraction. *Journal of Fluid Mechanics*, 927:A40, 2021.

Department for Energy Security and Net Zero. Net zero strategy: Build back greener, 2022. URL `https://www.gov.uk/government/publications/net-zero-strategy`.

Department for Energy Security and Net Zero. UK energy in brief 2023, 2023. URL `https://www.gov.uk/government/statistics/uk-energy-in-brief-2023`.

Department for Energy Security and Net Zero and Department for Business, Energy and Industrial Strategy. Wave and tidal energy: Part of the UK's Energy Mix, 2013. URL `https://www.gov.uk/guidance/wave-and-tidal-energy-part-of-the-uks-energy-mix`.

Department of Trade and Industry. Atlas of UK Marine Renewable Energy Resources. Technical report, 2008.

D. N. Djama, J. Thiébot, S. Guillou, and N. Guillou. Blockage corrections for tidal

turbines—application to an array of turbines in the Alderney Race. *Energies*, 15(10): 3475, 2022.

S. Draper and T. Nishino. Centred and staggered arrangements of tidal turbines. *Journal of Fluid Mechanics*, 739:72–93, 2014. doi: 10.1017/jfm.2013.593.

S. Draper, G. T. Houlsby, M. L. G. Oldfield, and A. G. L. Borthwick. Modelling tidal energy extraction in a depth-averaged coastal domain. *IET renewable power generation*, 4(6): 545–554, 2010.

S. Draper, T. A. A. Adcock, A. G. L. Borthwick, and G. T. Houlsby. Estimate of the tidal stream power resource of the Pentland Firth. *Renewable Energy*, 63:650–657, 2014a. ISSN 09601481. doi: 10.1016/j.renene.2013.10.015.

S. Draper, T. A. A. Adcock, A. G. L. Borthwick, and G. T. Houlsby. An electrical analogy for the Pentland Firth tidal stream power resource. *Proceedings of the Royal Society A: Mathematical, Physical and Engineering Sciences*, 470(2161):20130207, 2014b.

R. Du Feu. *Advanced computational modelling of large-scale tidal energy systems: optimising the trade-off between environmental impacts and power generation*. PhD thesis, Imperial College London, 2019.

R. J. Du Feu, S. W. Funke, S. C. Kramer, D. M. Culley, J. Hill, B. S. Halpern, and M. D. Piggott. The trade-off between tidal-turbine array yield and impact on flow: A multi-objective optimisation problem. *Renewable Energy*, 114:1247–1257, 2017.

M. C. Easton, D. K. Woolf, and P. A. Bowyer. The dynamics of an energetic tidal channel, the Pentland Firth, Scotland. *Continental Shelf Research*, 48:50–60, 2012.

Edina Digimap Service. Bathymetry - Marine DEM 1 Arc Second, 2020. URL `https://digimap.edina.ac.uk/`.

M. Edmunds, R. Malki, A. Williams, I. Masters, and T. Croft. Aspects of tidal stream turbine modelling in the natural environment using a coupled BEM–CFD model. *International Journal of Marine Energy*, 7:20–42, 2014.

E. C. Edwards, A. Holcombe, S. Brown, E. Ransley, M. Hann, and D. Greaves. Trends

in floating offshore wind platforms: A review of early-stage devices. *Renewable and Sustainable Energy Reviews*, 193:114271, 2024.

G. D. Egbert and S. Y. Erofeeva. Efficient inverse modeling of barotropic ocean tides. *Journal of Atmospheric and Oceanic technology*, 19(2):183–204, 2002.

G. D. Egbert and R. D. Ray. Estimates of M2 tidal energy dissipation from TOPEX/Poseidon altimeter data. *Journal of Geophysical Research: Oceans*, 106(C10): 22475–22502, 2001.

European Marine Energy Centre. Tidal developers http://www.emec.org.uk/marine-energy/tidal-developers/, 2020. URL `http://www.emec.org.uk/marine-energy/tidal-developers/`.

European Marine Energy Centre. EMEC: European Marine Energy Centre, 2023. URL `https://www.emec.org.uk/about-us/our-tidal-clients/orbital-marine-power/`.

I. Fairley, P. Evans, C. Wooldridge, M. Willis, and I. Masters. Evaluation of tidal stream resource in a potential array area via direct measurements. *Renewable Energy*, 57: 70–78, 2013.

R. Falconer. An introduction to nearly horizontal flows, coastal, estuarial and harbour engineers reference book. *by MB Abbott and WA Price. Published in*, pages 2–6, 1993.

Y. Fang, L. Duan, Z. Han, Y. Zhao, and H. Yang. Numerical analysis of aerodynamic performance of a floating offshore wind turbine under pitch motion. *Energy*, 192: 116621, 2020.

J. Feng and W. Shen. Modelling wind for wind farm layout optimization using joint distribution of wind speed and wind direction. *Energies*, 8(4):3075–3092, 2015. ISSN 1996-1073. doi: 10.3390/en8043075. URL `http://dx.doi.org/10.3390/en8043075`.

P. L. Fraenkel. Power from marine currents. *Proceedings of the Institution of Mechanical Engineers, Part A: Journal of Power and Energy*, 216(1):1–14, 2002.

S. W. Funke, P. E. Farrell, and M. D. Piggott. Tidal turbine array optimisation using the adjoint approach. *Renewable Energy*, 63:658–673, 2014.

S. W. Funke, S. C. Kramer, and M. D. Piggott. Design optimisation and resource assessment for tidal-stream renewable energy farms using a new continuous turbine approach. *Renewable Energy*, 99:1046–1061, 2016.

A. Garanovic. UK supports 11 tidal energy projects with record capacity of over 50MW in latest CFD auction round, 2023. URL `www.offshore-energy.biz/uk-supports-11-tidal-energy`.

C. Garrett and P. Cummins. The power potential of tidal currents in channels. *Proceedings of the Royal Society A: Mathematical, Physical and Engineering Sciences*, 461 (2060):2563–2572, 2005.

C. Garrett and P. Cummins. The efficiency of a turbine in a tidal channel. *Journal of Fluid Mechanics*, 588:243–251, 2007.

C. Garrett and D. Greenberg. Predicting changes in tidal regime: the open boundary problem. *Journal of Physical Oceanography*, 7(2):171–181, 1977.

C. Geuzaine and J. F. Remacle. Gmsh Reference Manual, 2017.

H. Glauert. *The elements of aerofoil and airscrew theory*. Cambridge University Press, 1983.

E. González-Gorbeña, P. C. Rosman, and R. Y. Qassim. Assessment of the tidal current energy resource in São Marcos Bay, Brazil. *Journal of Ocean Engineering and Marine Energy*, 1:421–433, 2015.

L. Z. Goss, S. Warder, A. Angeloudis, S. C. Kramer, A. Avdis, and M. D. Piggott. Tidal modelling with Thetis: preliminary English Channel benchmarking. 2019.

Z. L. Goss, M. D. Piggott, S. C. Kramer, A. Avdis, A. Angeloudis, and C. J. Cotter. Competition effects between nearby tidal turbine arrays—optimal design for Alderney Race. *Advances in Renewable Energies Offshore, Lisbon, Portugal, 8–10 October*, pages 255–262, 2018.

Z. L. Goss, D. S. Coles, and M. D. Piggott. Identifying economically viable tidal sites within the Alderney Race through optimization of levelized cost of energy. *Philosophical Transactions of the Royal Society A*, 378(2178):20190500, 2020.

Z. L. Goss, D. S. Coles, S. C. Kramer, and M. D. Piggott. Efficient economic optimisation of large-scale tidal stream arrays. *Applied Energy*, 295:116975, 2021.

A. J. Goward Brown, S. P. Neill, and M. J. Lewis. Tidal energy extraction in three-dimensional ocean models. *Renewable Energy*, 114:244–257, 2017.

C. Greenwood, A. Vogler, and V. Venugopal. On the variation of turbulence in a high-velocity tidal channel. *Energies*, 12(4):672, 2019.

C. Haggett. Understanding public responses to offshore wind power. *Energy Policy*, 39 (2):503–510, 2011.

D. Haverson, J. Bacon, H. C. M. Smith, V. Venugopal, and Q. Xiao. Modelling the hydrodynamic and morphological impacts of a tidal stream development in Ramsey Sound. *Renewable Energy*, 126:876–887, 2018.

HM Government. 2050 Pathways Analysis. pages 1–252, 2010.

G. T. Houlsby, S. Draper, and M. L. G. Oldfield. Application of linear momentum actuator disc theory to open channel flow. 2008.

Hydrographic Office. *Admiralty tide tables. Volume 1A, United Kingdom English Channel to river Humber including Isles of Scilly, Channel Islands and European Channel ports.*, volume 1A. 2017.

IEC TS 62600-2015. Marine energy - Wave, tidal and other water current converters - Part 201: Tidal energy resource assessment and characterization. *International Electrotechnical Commission*, 2015.

L. Jie, B.-L. Lin, S. Jian, and Y.-L. Chen. Modelling hydrodynamic processes in tidal stream energy extraction. *Journal of Hydrodynamics, Ser. B*, 28(6):1058–1064, 2016.

C. Jones, S. Bullock, B. A. D. Tomos, M. Freer, A. Welfle, and A. Larkin. Shipping's role in the global energy transition. 2022.

K. R. Jones, C. J. Klein, B. S. Halpern, O. Venter, H. Grantham, C. D. Kuempel, N. Shumway, A. M. Friedlander, H. P. Possingham, and J. E. Watson. The location and protection status of Earth's diminishing marine wilderness. *Current Biology*, 28(15):2506–2512, 2018.

C. Jordan, D. Dundovic, A. K. Fragkou, G. Deskos, D. S. Coles, M. D. Piggott, and A. Angeloudis. Combining shallow-water and analytical wake models for tidal array micrositing. *Journal of Ocean Engineering and Marine Energy*, 8(2):193–215, 2022.

C. Jordan, A. Angeloudis, D. Coles, and F. Johnson. On tidal array layout sensitivity to regional and device model representation. In *Proceedings of the European Wave and Tidal Energy Conference*, volume 15, 2023.

E. Jump, A. Macleod, and T. Wills. Review of tidal turbine wake modelling methods: state of the art. *International Marine Energy Journal*, 3(2):91–100, 2020.

T. Kärnä, B. De Brye, O. Gourgue, J. Lambrechts, R. Comblen, V. Legat, and E. Deleersnijder. A fully implicit wetting–drying method for dg-fem shallow water models, with an application to the scheldt estuary. *Computer Methods in Applied Mechanics and Engineering*, 200(5-8):509–524, 2011.

T. Kärnä, S. C. Kramer, L. Mitchell, D. A. Ham, M. D. Piggott, and A. M. Baptista. Thetis coastal ocean model: discontinuous Galerkin discretization for the three-dimensional hydrostatic equations. *Geoscientific Model Development*, 11(11):4359–4382, 2018.

S. C. Kramer and M. D. Piggott. A correction to the enhanced bottom drag parameterisation of tidal turbines. *Renewable Energy*, 92:385–396, 2016.

S. C. Kramer, S. W. Funke, and M. D. Piggott. A continuous approach for the optimisation of tidal turbine farms. In *Proceedings of the 11th European Wave and Tidal Energy Conference Series, Nantes, France*, pages 6–11, 2015.

E. J. Kubatko, J. J. Westerink, and C. Dawson. hp discontinuous Galerkin methods for advection dominated problems in shallow water flow. *Computer Methods in Applied Mechanics and Engineering*, 196(1-3):437–451, 2006.

G. C. Larsen. From solitary wakes to wind farm wind fields a simple engineering approach. risø-r-1727 (en). *Technical report, DTU Wind Energy, Roskilde*, 2009.

M. Lewis, S. Neill, P. Robins, and M. Hashemi. Resource assessment for future generations of tidal-stream energy arrays. *Energy*, 83:403–415, 2015.

M. Lewis, R. O'Hara Murray, S. Fredriksson, J. Maskell, A. De Fockert, S. P. Neill, and P. E.

Robins. A standardised tidal-stream power curve, optimised for the global resource. *Renewable Energy*, 170:1308–1323, 2021.

D. J. MacKay. *Sustainable Energy-without the hot air*. Bloomsbury Publishing, 2016.

L. Mackie. *Modelling the interaction of tidal range power systems for renewable energy conversion*. PhD thesis, Imperial College London, 2022.

L. Mackie, P. S. Evans, M. J. Harrold, O. Tim, M. D. Piggott, and A. Angeloudis. Modelling an energetic tidal strait: investigating implications of common numerical configuration choices. *Applied Ocean Research*, 108:102494, 2021.

F. Maganga, G. Pinon, G. Germain, and E. Rivoalen. Wake properties characterisation of marine current turbines. In *3rd International Conference on Ocean Energy 2010, 6 October, Bilbao*, 2010.

Marine Scotland. Shipping Study of the Pentland Firth and Orkney Water. Technical report, A2765-MS-TN-1, 2012.

Marine Scotland. Pilot Pentland Firth and Orkney Waters Marine Spatial Plan. Regional Locational Guidance, 2016.

Marine Scotland Science. Scottish Highly Protected Marine Areas (HPMA), 2022. URL `https://consult.gov.scot/marine-scotland/scottish-highly-protected-marine-areas/`.

V. Martin. Digest of UK Energy Statistics (DUKES): electricity, 2023. URL `https://assets.publishing.service.gov.uk/media/64c23a300c8b960013d1b05e/DUKES_2023_Chapter_5.pdf`.

R. Martin-Short, J. Hill, S. C. Kramer, A. Avdis, P. A. Allison, and M. D. Piggott. Tidal resource extraction in the Pentland Firth, UK: Potential impacts on flow regime and sediment transport in the Inner Sound of Stroma. *Renewable Energy*, 76:596–607, 2015.

I. Masters, J. C. Chapman, M. R. Willis, and J. A. C. Orme. A robust blade element momentum theory model for tidal stream turbines including tip and hub loss corrections. *Journal of Marine Engineering & Technology*, 10(1):25–35, 2011.

J. McNaughton, B. Cao, A. Nambiar, T. Davey, C. R. Vogel, and R. H. J. Willden. Constructive interference effects for tidal turbine arrays. *Journal of Fluid Mechanics*, 943:A38, 2022.

Metoc. Tidal Power in the UK Research Report 1 - UK tidal resource assessment. Technical report, 2007. URL www.metoc.co.uk.

Meygen. Meygen Tidal Energy Project Phase 1 Environmental Statement. Technical report, 2012.

MeyGen, 2012. URL https://marine.gov.scot/sites/default/files/chapter_15_-_shipping_and_navigation.pdf.

C. Milne. Demystifying the cost of tidal energy, 2020. URL https://www.orbitalmarine.com/demystifying-the-cost-of-tidal-energy/.

I. A. Milne, R. N. Sharma, R. G. J. Flay, and S. Bickerton. Characteristics of the turbulence in the flow at a tidal stream power site. *Philosophical Transactions of the Royal Society A: Mathematical, Physical and Engineering Sciences*, 371(1985):20120196, 2013.

C. Molnar. Interpretable machine learning, Permutation Feature Importance https://christophm.github.io/interpretable-ml-book/feature-importance.html, 2021. URL https://christophm.github.io/interpretable-ml-book/feature-importance.html.

J. A. Morales. *Coastal geology, Chapter Tide Processes*. Springer Nature, 2022.

S. Muchala and R. H. J. Willden. Impact of tidal turbine support structures on realizable turbine farm power. *Renewable Energy*, 114:588–599, 2017.

L. Myers and A. Bahaj. Near wake properties of horizontal axis marine current turbines. In *Proceedings of the 8th European Wave and Tidal Energy Conference*, 2009.

L. E. Myers, B. Keogh, and A. S. Bahaj. Experimental investigation of inter-array wake properties in early tidal turbine arrays. In *OCEANS'11 MTS/IEEE KONA*, pages 1–8. IEEE, 2011.

NASA. Earth Data - Ocean, 2021. URL https://www.earthdata.nasa.gov/topics/ocean.

National Grid ESO, 2022. URL https://www.nationalgrideso.com/document/246851/download.

S. P. Neill, E. J. Litt, S. J. Couch, and A. G. Davies. The impact of tidal stream turbines on large-scale sediment dynamics. *Renewable Energy*, 34(12):2803–2812, 2009.

S. P. Neill, M. R. Hashemi, and M. J. Lewis. The role of tidal asymmetry in characterizing the tidal energy resource of Orkney. *Renewable Energy*, 68:337–350, 2014.

S. P. Neill, A. Vögler, A. J. Goward Brown, S. Baston, M. J. Lewis, P. A. Gillibrand, S. Waldman, and D. K. Woolf. The wave and tidal resource of scotland. *Renewable Energy*, 114:3–17, 2017.

T. Nishino and R. H. J. Willden. The efficiency of an array of tidal turbines partially blocking a wide channel. *Journal of Fluid Mechanics*, 708:596–606, 2012.

D. R. Noble, S. Draycott, A. Nambiar, B. G. Sellar, J. Steynor, and A. Kiprakis. Experimental assessment of flow, performance, and loads for tidal turbines in a closely-spaced array. *Energies*, 13(8):1977, 2020.

M. Nuernberg and L. Tao. Turbulence and wake effects in tidal stream turbine arrays. In *International Conference on Offshore Mechanics and Arctic Engineering*, volume 51319. American Society of Mechanical Engineers, 2018.

Ocean Energy Europe. Tidal current, 2023. URL https://www.oceanenergy-europe.eu/ocean-energy/tidal-energy/.

R. O'Hara Murray and A. Gallego. A modelling study of the tidal stream resource of the Pentland Firth, Scotland. *Renewable Energy*, 102:326–340, 2017. ISSN 18790682. doi: 10.1016/j.renene.2016.10.053.

R. O'Hara Murray and A. Gallego. Data review and the development of realistic tidal and wave energy scenarios for numerical modelling of Orkney Islands waters, Scotland. *Ocean & Coastal Management*, 147:6–20, 2017.

OpenTidalFarm. Tidal farm - Simulation and Optimisation Documentation, 2016. URL https://opentidalfarm.readthedocs.io/en/latest/examples/channel/channel.html.

Orbital Marine. O2 orbital marine, 2022. URL https://www.orbitalmarine.com/o2/.

M. Osman, R. H. J. Willden, and C. R. Vogel. The effects of surge motion on floating horizontal axis tidal turbines. *International Marine Energy Journal*, 3(2):45–54, 2020.

P. Ouro and T. Nishino. Performance and wake characteristics of tidal turbines in an infinitely large array. *Journal of Fluid Mechanics*, 925:A30, 2021.

F. O'Rourke, F. Boyle, and A. Reynolds. Tidal current energy resource assessment in Ireland: Current status and future update. *Renewable and sustainable energy reviews*, 14(9):3206–3212, 2010.

M. D. Patel, A. S. M. Smyth, A. Angeloudis, and T. A. A. Adcock. Investigation of low order parameters affecting tidal stream energy resource assessments. In *Proceedings of the 15th European Wave and Tidal Energy Conference*, 2023.

A. Phoenix and S. Nash. Optimisation of tidal turbine array layouts whilst limiting their hydro-environmental impact. *Journal of Ocean Engineering and Marine Energy*, 5: 251–266, 2019.

B. Polagye, B. Van Cleve, A. Copping, and K. Kirkendall. Environmental effects of tidal energy development. *Environmental Impact Assessment Review*, 32(1):133–139, 2011.

Policy and Innovation Group, University of Edinburgh. What are the UK power system benefits from deployments of wave and tidal stream generation?, 2023. URL https://supergen-ore.net/uploads/Supergen-ORE-Power-System-Benefits-Study-2023.pdf.

Power Technology. SeaGen Turbine, Northern Ireland, UK, 2020. URL https://www.power-technology.com/projects/strangford-lough/.

D. Prandle. The vertical structure of tidal currents and other oscillatory flows. *Continental Shelf Research*, 1(2):191–207, 1982.

D. T. Pugh. *Tides, surges and mean sea level*. John Wiley and Sons Inc., New York, NY, 1987.

R. C. T. Rainey. The optimum position for a tidal power barrage in the Severn estuary. *Journal of Fluid Mechanics*, 636:497–507, 2009.

F. Rathgeber, D. A. Ham, L. Mitchell, M. Lange, F. Luporini, A. T. T. McRae, G. Bercea, G. R. Markall, and P. H. J. Kelly. Firedrake: automating the finite element method by composing abstractions. *ACM Transactions on Mathematical Software (TOMS)*, 43(3): 1–27, 2016.

RenewableUK. UK Marine Energy Database (UKMED), 2015. URL https://www.renewableuk.com/page/UKMED2/UK-Marine-Energy-Database.htm.

SAE Renewables. Tidal Stream - MeyGen, 2023. URL https://saerenewables.com/tidal-stream/meygen/.

S. H. Salter. Correcting the under-estimate of the tidal-stream resource of the Pentland Firth. In *Proceedings of the 8th European Wave and Tidal Energy Conference, Uppsala, Sweden*, 2009.

S. H. Salter and J. R. M. Taylor. Vertical-axis tidal-current generators and the Pentland Firth. *Proceedings of the Institution of Mechanical Engineers, Part A: Journal of Power and Energy*, 221(2):181–199, 2007. ISSN 09576509. doi: 10.1243/09576509JPE295. URL https://journals.sagepub.com/doi/10.1243/09576509JPE295.

J. Schluntz and R. H. J. Willden. The effect of blockage on tidal turbine rotor design and performance. *Renewable Energy*, 81:432–441, 2015.

T. Schwedes, D. A. Ham, S. W. Funke, M. D. Piggott, T. Schwedes, D. A. Ham, S. W. Funke, and M. D. Piggott. An application: Optimising the layout of tidal turbine arrays. *Mesh dependence in PDE-constrained optimisation: an application in tidal turbine array layouts*, pages 79–107, 2017.

Scottish Government. Pilot Pentland Firth and Orkney Waters Marine Spatial Plan – Socio-Economic Baseline Review, 2018. URL https://www.gov.scot/publications/pilot-pentland-firth-orkney-waters-marine-spatial-plan-socio-economic/documents/.

Scottish Government. Scottish Highly Protected Marine Areas (HPMAs) con-

sultation, 2023. URL https://consult.gov.scot/marine-scotland/scottish-highly-protected-marine-areas/.

E. Segura, R. Morales, J. A. Somolinos, and A. López. Techno-economic challenges of tidal energy conversion systems: Current status and trends. *Renewable and Sustainable Energy Reviews*, 77:536–550, 2017.

S. Serhadlıoğlu. Tidal stream resource assessment of the Anglesey Skerries and the Bristol Channel. DPhil thesis, University of Oxford, 2014.

S. Serhadlıoğlu, T. A. A. Adcock, G. T. Houlsby, S. Draper, and A. G. L. Borthwick. Tidal stream energy resource assessment of the Anglesey Skerries. *International Journal of Marine Energy*, 3:e98–e111, 2013.

J. N. Sørensen. Aerodynamic aspects of wind energy conversion. *Annual Review of Fluid Mechanics*, 43:427–448, 2011.

J. N. Sørensen and W. Z. Shen. Numerical modeling of wind turbine wakes. *J. Fluids Eng.*, 124(2):393–399, 2002.

T. Stallard, R. Collings, T. Feng, and J. Whelan. Interactions between tidal turbine wakes: experimental study of a group of three-bladed rotors. *Philosophical Transactions of the Royal Society A: Mathematical, Physical and Engineering Sciences*, 371(1985): 20120159, 2013.

T. Stallard, T. Feng, and P. K. Stansby. Experimental study of the mean wake of a tidal stream rotor in a shallow turbulent flow. *Journal of Fluids and Structures*, 54:235–246, 2015.

P. Stansby and T. Stallard. Fast optimisation of tidal stream turbine positions for power generation in small arrays with low blockage based on superposition of self-similar far-wake velocity deficit profiles. *Renewable Energy*, 92:366–375, 2016.

P. K. Stansby. A mixing-length model for shallow turbulent wakes. *Journal of Fluid Mechanics*, 495:369–384, 2003.

P. K. Stansby. Limitations of depth-averaged modeling for shallow wakes. *Journal of Hydraulic Engineering*, 132(7):737–740, 2006.

X. Sun, J. P. Chick, and I. G. Bryden. Laboratory-scale simulation of energy extraction from tidal currents. *Renewable Energy*, 33(6):1267–1274, 2008.

Sustainable Energy Ireland. Tidal & current energy resources in Ireland. Technical report, Sustainable Energy Ireland, 2004.

G. Sutherland, M. Foreman, and C. Garrett. Tidal current energy assessment for Johnstone Strait, Vancouver Island. *Proceedings of the Institution of Mechanical Engineers, Part A: Journal of Power and Energy*, 221(2):147–157, 2007.

The Crown Estate. Tidal Stream Site Agreements (England, Wales & NI), The Crown Estate, 2023. URL `https://opendata-thecrownestate.opendata.arcgis.com`.

The Crown Estate Scotland. The Crown Estate Scotland, 2023. URL `https://www.crownestatescotland.com/`.

J. Thiébot, N. Guillou, S. Guillou, A. Good, and M. Lewis. Wake field study of tidal turbines under realistic flow conditions. *Renewable Energy*, 151:1196–1208, 2020a.

J. Thiébot, S. Guillou, and E. Droniou. Influence of the 18.6-year lunar nodal cycle on the tidal resource of the Alderney Race, France. *Applied Ocean Research*, 97:102107, 2020b.

J. Thiébot, N. Guillou, D. Coles, and S. Guillou. On nodal modulations of tidal-stream energy resource in north-western Europe. *Applied Ocean Research*, 121:103091, 2022.

T. Ulrich. Envelope calculation from the Hilbert transform. *Los Alamos Nat. Lab., Los Alamos, NM, USA, Tech. Rep*, 2006.

US Department of Commerce, National Oceanic and Atmospheric Administration. NOAA's national ocean service education, 2013. URL `https://oceanservice.noaa.gov`.

U.S Department of Energy. Marine energy resource assessment and characterization. URL `https://www.energy.gov/eere/water/marine-energy-resource-assessment-and-characterization`.

G. K. Vallis. *Essentials of atmospheric and oceanic dynamics*. Cambridge University Press, 2019.

R. Vennell. Tuning turbines in a tidal channel. *Journal of Fluid Mechanics*, 663:253–267, 2010.

R. Vennell. Estimating the power potential of tidal currents and the impact of power extraction on flow speeds. *Renewable Energy*, 36(12):3558–3565, 2011.

R. Vennell. Exceeding the Betz limit with tidal turbines. *Renewable Energy*, 55:277–285, 2013.

R. Vennell, S. W. Funke, S. Draper, C. Stevens, and T. Divett. Designing large arrays of tidal turbines: A synthesis and review. *Renewable and Sustainable Energy Reviews*, 41: 454–472, 2015.

V. Venugopal, T. Davey, H. Smith, G. Smith, L. Cavaleri, and L. Bertotti. Equimar deliverable D2. 2: Application of Numerical Models, 2010.

Verdant Power. The Roosevelt Island Tidal Energy (RITE) project, 2021. URL `https://www.verdantpower.com/rite/`.

C. R. Vogel. Theoretical limits to tidal stream energy extraction. DPhil thesis, University of Oxford, 2014.

C. R. Vogel and R. H. J. Willden. Multi-rotor tidal stream turbine fence performance and operation. *International Journal of Marine Energy*, 19:198–206, 2017.

C. R. Vogel, R. H. J. Willden, and G. T. Houlsby. Blade element momentum theory for a tidal turbine. *Ocean Engineering*, 169:215–226, 2018.

C. R. Vogel, R. H. J. Willden, and G. T. Houlsby. Tidal stream turbine power capping in a head-driven tidal channel. *Renewable Energy*, 136:491–499, 2019.

C. V. Vouriot, A. Angeloudis, S. C. Kramer, and M. D. Piggott. Fate of large-scale vortices in idealized tidal lagoons. *Environmental Fluid Mechanics*, 19:329–348, 2019.

S. Waldman, S. Weir, R. B. O. Murray, D. K. Woolf, and S. Kerr. Future policy implications of tidal energy array interactions. *Marine Policy*, 108:103611, 2019.

T. Wang and T. A. A. Adcock. Power and Thrust Capping of Tidal Stream Turbines: A Case Study of the Pentland Firth. In *International Conference on Offshore Mechan-*

ics and Arctic Engineering, volume 51319, page V010T09A002. American Society of Mechanical Engineers, 2018.

T. Wang and T. A. A. Adcock. Combined power and thrust capping in the design of tidal turbine farms. *Renewable Energy*, 133:1247–1256, 2019.

J. I. Whelan, J. M. R. Graham, and J. Peiro. A free-surface and blockage correction for tidal turbines. *Journal of Fluid Mechanics*, 624:281–291, 2009.

A. Wimshurst and R. H. J. Willden. Computational analysis of blockage designed tidal turbine rotors. In *Progress in Renewable Energies Offshore-Proceedings of 2nd International Conference on Renewable Energies Offshore, RENEW 2016*, pages 587–597, 2016a.

A. Wimshurst and R. H. J. Willden. Validation of an actuator line method for tidal turbine rotors. In *ISOPE International Ocean and Polar Engineering Conference*, pages ISOPE–I. ISOPE, 2016b.

R. Wiser, K. Jenni, J. Seel, E. Baker, M. Hand, E. Lantz, and A. Smith. Expert elicitation survey on future wind energy costs. *Nature Energy*, 1(10):1–8, 2016.

World Energy Council. World Energy Trilemma 2024, 2024. URL `https://www.worldenergy.org/assets/downloads/World_Energy_Trilemma_2024_Full_Report.pdf?v=1713438208`.

Z. Yang, T. Wang, and A. E. Copping. Modeling tidal stream energy extraction and its effects on transport processes in a tidal channel and bay system using a three-dimensional coastal ocean model. *Renewable Energy*, 50:605–613, 2013.

N. Yates, I. Walkington, R. Burrows, and J. Wolf. Appraising the extractable tidal energy resource of the UK's western coastal waters. *Philosophical Transactions of the Royal Society A: Mathematical, Physical and Engineering Sciences*, 371(1985):20120181, 2013.

J. Zhang, M. Cheng, Z. Chen, and X. Fu. Pitch angle control for variable speed wind turbines. In *2008 Third International Conference on Electric Utility Deregulation and Restructuring and Power Technologies*, pages 2691–2696. IEEE, 2008.

J. Zhang, C. Zhang, A. Angeloudis, S. C. Kramer, R. He, and M. D. Piggott. Interactions be-

tween tidal stream turbine arrays and their hydrodynamic impact around Zhoushan Island, China. *Ocean Engineering*, 246:110431, 2022.

Appendix A

The Crown Estate Lease Sites

Table A.1 presents leased and agreed to lease sites by The Crown Estate to developers in 2010 and the project statuses as of 2015 (RenewableUK, 2015).

Table A.1: Leased sites for tidal stream energy development in the UK (RenewableUK, 2015)

Property Name	**Project Status**	**Tenant Name**	**Lease Status**
Torr Head	In planning	Tidal Ventures Ltd.	Agreed
Portland Bill	In planning	Marine Current Turbines Ltd.	Agreed
Stronsay Firth	In planning	EMEC Ltd.	Agreed
Islay Demonstration Zone	In planning	EMEC Ltd.	Leased
Kyle Rhea	In planning	SeaGeneration (Kyle Rhea) Ltd.	Agreed
Isle of Islay (West Islay)	In planning	DP Marine Energy Ltd.	Agreed
North Devon Demonstration Zone	In planning	Wave Hub Ltd.	Leased
St David's Head	In development	Tidal Energy Developments South Wales Ltd.	Agreed
Fair Head	In development	Fair Head Tidal Energy Park Ltd.	Agreed
Lashy Sound	In development	Scotrenewables Tidal Power Ltd.	Agreed
Perpetuus Tidal Energy Centre	In development	Isle of Wight Council	Agreed
Mull of Kintyre	In development	Argyll Tidal Ltd.	Agreed
Brims Tidal Array	In development	Brims Tidal Array Ltd.	Agreed
Ness of Duncansby	In development	ScottishPower Renewables UK Ltd.	Agreed
Westray South	In development	Westray South Tidal Development Ltd.	Agreed
Brough Ness	In development	Sea Generation (Brough Ness) Ltd.	Agreed
Holyhead Deep	In development	Minesto UK Ltd.	Agreed
Mull of Galloway	In development	Marine Current Turbines Ltd.	Agreed
Strangford Lough Array	In development	Marine Current Turbines Ltd.	Agreed
West Anglesey Demonstration Zone	In development	Mentor Mon Cyf	Leased
Sound of Islay	Pre-construction	ScottishPower Renewables UK Ltd.	Agreed
Skerries	Pre-construction	Sea Generation (Wales) Ltd.	Agreed
Inner Sound	Under construction	MeyGen Ltd.	Leased
Bluemull Sound	Under construction	Nova Innovation Ltd.	Leased
Sanda Sound	Under construction	Oceanflow Development Ltd.	Leased
Ramsey Sound	Under construction	Tidal Energy Ltd.	Leased
Shapinsay Sound	Operational	EMEC Ltd.	Leased
Strangford Lough	Operational	Minesto UK Ltd.	Leased
Fall of Warness	Operational	EMEC Ltd.	Leased
SeaGen Strangford Lough	Operational	SeaGeneration Ltd.	Leased

Appendix B

Hydrodynamic Modelling Software

Table B.1 compares 2-D and 3-D hydrodynamic software tools.

Table B.1: Comparison of 2D and 3D hydrodynamic software [1,2,3]

		2D Software					3D Software					
		MIKE 21	TELEMAC-2D	DG ADCIRC	THETIS	DTOceanPlus	DELFT3D	MIKE 3 FM	TELEMAC-3D	ROMS	FVCOM
Access		Paid software	Open Source	Open Source	Open Source	Open Source	Open Source	Paid software	Open Source	Open Source	Open Source
Solver		Alternate direction implicit scheme or finite volume explicit Roe	Finite element of finite volume methods for solving Saint-Venant Equations	Runge-kutta discontinuous galerkin method to solve hyperbolic shallow water equations	Firedrake finite element partial differential equation solver	-	3D Navier Stokes equations with hydrostatic pressure approximation vertically, finite difference	3D incompressible RANS equations with hydrostatic pressure, finite volume	Finite volume	Second order finite difference	Finite volume, Hydrostatic pressure approach available
Turbulence	Horizontal	• Eddy Viscosity • Smagorinsky	• Constant viscosity • Elder model • k-ε • Smagorinksy	• Constant viscosity	• Constant viscosity • Smagorinksy	-	• Kappa Epsilon • k-L • Algebraic • Constant • Large Eddy Simulation	Horizontal: • Constant viscosity • Smagorinksy Vertical: • Constant • Logarithmic • k-ε	• Constancy viscosity • Elder model • k-ε • Smagorinksy	• User defined turbulence viscosity and diffusivity • Brunt-Vaisala frequency mix • Parameterization profile K • Generic Length	Horizontal: • Constant diffusion • Smagorinksky Vertical: • Mellor and Yamada • k-ε
Mesh	Horizontal	Regular or unstructured	Unstructured	Unstructured	Unstructured	Unstructured	Orthogonal–curvilinear	Unstructured	Unstructured	Structured	Unstructured
	Vertical						Z or sigma	Structured Z, sigma, combined	Sigma	Sigma	Sigma
Developer		DHI	EDF	University of North Carolina, Chapel Hill	Finnish Meteorological Institute, Durham University, University of Edinburgh, Imperial College London	DTOcean	Deltares Systems	DHI	EDF	Rutgers University and University of California	Massachusetts University and Woods Hole Oceanographics Institution
Areas		• Pentland Firth • Irish Coast • Ria of Avilés	• Norway • Portland Bill • Holy Head	• Pentland Firth • Anglesey Skerries	• Pentland Firth • Alderney Race • Ramsey Sound	• Ramsey Sound (DTOcean2.0)	• Pentland Firth • Orkney	• Gota Alv River • Caspian Sea • Ariake Sea • Jokor Strait	• Bay of Fundy • Brittany (Raz de Sein)	• Irish Sea • NW European Shelf	• New Jersey • Arctic Sea • Pentland Firth

[1]Source: Suárez-López, M. J., Espina-Valdés, R., Fernández Pacheco, V. M., Navarro Manso, A., Blanco-Marigorta, E., Álvarez-Álvarez, E. (2019). A review of software tools to study the energetic potential of tidal currents. Energies, 12(9), 1673.

[2]Source: Thetis Documentation, https://thetisproject.org/documentation.html

[3]Source: DTOceanPlus (2020) Deliverable D5.2 Site Characterisation - alpha version

Appendix C

Other UK Site-based Resource Assessments

C1 Ramsey Sound and Bishops and Clerks

Fairley et al. (2013) used Acoustic Doppler Current Profilers (ADCP) data to evaluate the maximum extractable power at Ramsey Sound, Bishops and Clerks and West Bishop (Table C.1). Fairley et al. (2013) note the values should not be taken as available power to the grid because once turbine efficiency and losses during transmission are considered, the value will be lower.

Table C.1: Ramsey Sound and Bishops and Clerks resource assessments (channel)

Reference	Method	Resource Assessment
Fairley et al (2013)	• Direct measurements from ADCP transects • Vennell (2011) approach for calculating maximum extractable power	• 7.2 MW (Ramsey Sound) • 21.8 MW (Bishops and Clerks) • 11 MW (West Bishop)

They evaluated maximum extractable power, $\overline{P}_{max}$, using Equation C.1 (Vennell, 2011),

$$\overline{P}_{max} = \frac{4}{3\pi} \frac{\rho C_F^{Peak}}{A^2} U_0^{Peak^3}, \tag{C.1}$$

where C_F^{Peak} is the optimal drag coefficient for the farm, A is the cross sectional area of the channel and U_0^{Peak} is peak velocity from direct measurements.

Evaluating power from direct measurements is not always feasible because it is expensive and time-consuming (Neill et al., 2014). Fairley et al. (2013) acknowledge that some data was not surveyed over a tidal cycle due to weather conditions. Higher temporal resolution data over a larger area would have been beneficial and velocity interpolation methods were not applicable due to non-uniform data. However, they propose the method is useful for estimating power potential with limited information and it is appropriate to assess sites for further measurements and investigations.

Ramsey Sound has significant bathymetric flow obstructions and at low water, geographical features (Horse Rock and The Bitches) emerge. This leads to a great difference in flux at high and low water because the maximum flux area is divided in two at the centre of Ramsey Sound. It is also noted that Ramsey Sound is a good location for an array based on the hydrodynamics but due to the limited area it would only be a viable site for a small array. The Bishops and Clerks channel shows the largest areas of maximum flux with a symmetric flow and Fairley et al. (2013) indicate that the area would be favourable for development. However, there are no lease sites West of Ramsey Sound, only North at St David's Head, presumably due to proximity to the mainland for grid integration.

C2 Anglesey Skerries

Serhadlıoğlu et al. (2013) assessed the resource at Anglesey Skerries (Table C.2). The study found it is more beneficial to arrange turbines in long rows than many rows in series. However, the area restrictions of lease sites will limit array layouts.

Table C.2: Anglesey Skerries resource estimate (headland)

Reference	Method	Resource Assessment
Serhadlıoğlu et al (2013)	• 2-D model • ADT - included as line sinks of momentum • Quadratic bed friction term Data Sources • BODC • Admiralty Charts Software • Discontinuous Galerkin ADCIRC	Maximum available power: • 17.2 MW (0.1 blockage, 0.35 optimum wake velocity coefficient) • 70 MW (0.3 blockage, 0.37 optimum wake velocity coefficient) • 145.3 MW (0.5 blockage, 0.46 optimum wake velocity coefficient)

C3 Orkney

Neill et al. (2014) used a 3-D model to investigate the impact of tidal asymmetry on the resource in Orkney (Table C.3). The study demonstrates asymmetry in velocity leads to significant asymmetry in power generated and affects turbulence properties. Turbulent velocity fluctuations can negatively impact the performance of a turbine and lead to excessive cyclic loading, which will cause fatigue and reduce the lifetime of a turbine. Losses due to energy extraction were not considered and the analysis was carried out based on undisturbed flow because only a single turbine was considered. Therefore, it is important to recognise that an array will have a significant effect on the flow. Adcock and Draper (2014a) state that modelling energy extraction as a constant drag resistance will reduce flow rate tidal asymmetry and the environmental impact of this should be considered.

Table C.3: Orkney resource assessment (channel)

Reference	Method	Resource Assessment
Neill et al (2014)	• Investigation of tidal symmetry on tidal energy resource • Generic length scale model for turbulence • Single Segen device to analyse asymmetry in power generation Data Sources • Admiralty tide tables • GEBCO bathymetry data - BODC • Boundary conditions – Aviso • Wind data – British Atmospheric Data Centre Software • ROMS	N/A Not intended as a resource assessment

C4 Portland Bill

Blunden and Bahaj (2006) produced a time-series velocity dataset using a 2-D model at Portland Bill. They presented the power output of a single turbine as an example of how the data could be used (Table C.4). However, they assume power generated is a fraction of kinetic energy, which is not accurate for resource assessments. The impact of the turbine on the flow is not considered. A large array would reduce flow speeds, and change the velocity profile and flow direction.

Table C.4: Portland Bill resource assessment (headland)

Reference	Method	Resource Assessment
Blunden and Bahaj (2006)	• 2-D model • Time-series of velocity was produced Data Sources • Validated with Admiralty Charts data Software • TELEMAC-2D	• 300 kW Mean power from a single turbine over spring cycle • 730 kW Peak power output
Adcock and Draper (2014)	• 2-D model • Discontinuous Galerkin method • ADT - included as line discontinuity Data Sources • Constituent data – le Provost database • Bathymetry – Seazone Ltd., GEBCO	• 21.9 MW (1 row, 0.25 blockage, 2.8 km from shore) • 36.6 MW (1 row, 0.25 blockage, 4 km from shore)

Adcock and Draper (2014b) studied the tidal stream resource at Portland Bill, evaluating the available power, which accounts for the energy lost due to mixing downstream of the turbines subtracted from the power extracted from the flow. The study did not consider losses associated with a real, deployed turbine. Therefore, Adcock and Draper (2014b) suggest the actual power that could viably be generated would be half of what is presented. The study suggests that the time-averaged viable power from each site would be in the order of magnitude of tens of MW.

C5 Irish Sea

Sustainable Energy Ireland (2004) carried out a resource assessment for The Republic of Ireland and Northern Ireland. O'Rourke et al. (2010) identified that the assessment needed updating based on developments in the tidal stream energy field including the installation of a 1.2 MW Seagen turbine, developed by Marine Current Turbines Ltd. at Strangford Lough (Power Technology, 2020). The performance of the turbine in practice highlighted the underestimation of the resource presented by Sustainable Energy Ireland (2004). O'Rourke et al. (2010) suggested a detailed 2-D model, with a finer mesh and over a smaller area, could provide a more accurate assessment of the theoretical resource. In addition, technical and practical limitations should be continually revised based on new developments of technology and better understanding of sites to ensure an up to date resource assessment.

Lewis et al. (2015) investigated the resource of the Irish Sea, using a 3-D hydrodynamic model to simulate velocities across the region. They quantify the resource based on the practical requirements (bathymetry and spring-tide velocity) of different generations of tidal energy devices, including future generations. First generation devices required a bathymetry range of 25 – 50 m and spring tide velocities in excess of 2.5 m/s. The second and third devices were defined as requiring bathymetry greater than 25 m and spring tide velocities in excess of 2 m/s and 1.5 m/s respectively. The kinetic energy over a 14.77 day Spring-Neap cycle in an undisturbed scenario is calculated to assess the resource. They acknowledge the overestimation of the power available using the kinetic flux method and the omission of resistance on the flow due to turbines in the model. Instead, the practical resource is estimated by applying the performance curve of the same Seagen device used in the O'Rourke et al. (2010) assessment of Strangford Lough.

Table C.5: Irish Sea and Strangford Lough (channel) resource assessment

Reference	**Method**	**Resource Assessment**
SEI (2004)	• 2-D model by RPS Kirk McClure Morton Data Sources • Validated with ADCP results • Admiralty Charts and Tidal Stream Atlases • Irish Coast Pilot • BODC • Marine Institute Data	130 GWh/year Viable energy (Strangford Lough)
O'Rourke et al (2010)	• 2-D model • Marine Current Turbines Ltd economic model Software • MIKE 21	• 150 GWh/year Viable energy • 400 GWh/year Practical resource (Strangford Lough)
Lewis et al (2015)	• 3-D model • Kinetic flux method • Marine Current Turbines Ltd Seagen turbine performance curve Software • ROMS regional ocean modelling system	Annual practical power available with finest mesh resolution: • 1st generation 24 GWh/year • 2nd generation 111 GWh/year • 3rd generation 182 GWh/year